

PHASE SEPARATION PHENOMENA
IN
CELLULOSE NANOCRYSTAL SUSPENSIONS
CONTAINING
DEXTRAN–DYE DERIVATIVES

by

Stephanie Christine Beck

A thesis submitted to the Faculty of Graduate Studies and Research of McGill University
in partial fulfillment of the requirements of the degree of Doctor of Philosophy

Department of Chemistry
McGill University
Montréal, Québec, Canada
May 1, 2007

© Stephanie Christine Beck, 2007



Library and
Archives Canada

Bibliothèque et
Archives Canada

Published Heritage
Branch

Direction du
Patrimoine de l'édition

395 Wellington Street
Ottawa ON K1A 0N4
Canada

395, rue Wellington
Ottawa ON K1A 0N4
Canada

Your file Votre référence

ISBN: 978-0-494-32145-4

Our file Notre référence

ISBN: 978-0-494-32145-4

NOTICE:

The author has granted a non-exclusive license allowing Library and Archives Canada to reproduce, publish, archive, preserve, conserve, communicate to the public by telecommunication or on the Internet, loan, distribute and sell theses worldwide, for commercial or non-commercial purposes, in microform, paper, electronic and/or any other formats.

The author retains copyright ownership and moral rights in this thesis. Neither the thesis nor substantial extracts from it may be printed or otherwise reproduced without the author's permission.

AVIS:

L'auteur a accordé une licence non exclusive permettant à la Bibliothèque et Archives Canada de reproduire, publier, archiver, sauvegarder, conserver, transmettre au public par télécommunication ou par l'Internet, prêter, distribuer et vendre des thèses partout dans le monde, à des fins commerciales ou autres, sur support microforme, papier, électronique et/ou autres formats.

L'auteur conserve la propriété du droit d'auteur et des droits moraux qui protègent cette thèse. Ni la thèse ni des extraits substantiels de celle-ci ne doivent être imprimés ou autrement reproduits sans son autorisation.

In compliance with the Canadian Privacy Act some supporting forms may have been removed from this thesis.

Conformément à la loi canadienne sur la protection de la vie privée, quelques formulaires secondaires ont été enlevés de cette thèse.

While these forms may be included in the document page count, their removal does not represent any loss of content from the thesis.

Bien que ces formulaires aient inclus dans la pagination, il n'y aura aucun contenu manquant.


Canada

In Copy 1 (Beck, Ph.D.), the following pages are intentionally blank:

pp. iii, viii, x, xii, xiii, xix, xxvii, xxxvi, xxxvii, xli, xlvii; and

pp. 52, 53, 60, 61, 84, 85, 122, 123, 129, 153, 157, 183, 187, 222, 223, 245.

This was done to keep the pagination in the Table of Contents consistent with the double-sided copy (Copy 2).

ABSTRACT

Sulfuric acid hydrolysis of native cellulose fibers produces stable suspensions of cellulose nanocrystals. Within a specific concentration range, the suspensions spontaneously form an anisotropic chiral nematic liquid crystal phase. This thesis examines the phase separation behaviour of these suspensions, alone and in the presence of added macromolecules. Initially, the effect of hydrolysis conditions on the nanocrystal and phase separation properties for hydrolyzed softwood pulp were investigated and compared to suspensions prepared from hardwood pulp. The macromolecules studied, blue dextrans of varying molecular weights and dye ligand densities, were synthesized and characterized with a number of techniques. The polyelectrolytic nature of these macromolecules was found to strongly influence their physico-chemical properties. Added blue dextran causes separation of an isotropic phase from highly concentrated, completely anisotropic suspensions. The observed phase separation was found to be associated with the charged dye molecules attached to the dextran. The partitioning behaviour of blue dextrans in biphasic aqueous suspensions of native cellulose nanocrystals was also studied with regard to the effect of total concentration of blue dextran, degree of dye substitution and dextran molecular weight on the blue dextran partition coefficient. Electrostatic and entropic contributions to the partition coefficient of blue dextran were discussed. Triphase isotropic–isotropic–nematic (I_1 – I_2 –N) equilibria are observed in suspensions containing both neutral dextrans and polyelectrolytic blue dextrans of varying molecular weight. Based on these results, phase diagrams for cellulose nanocrystal suspensions with different combinations of dextran and blue dextran are presented.

RÉSUMÉ

L'hydrolyse acide des fibres de cellulose par l'acide sulfurique donne une suspension stable de nanocristaux de cellulose. Dans une gamme de concentration donnée, la suspension présente spontanément une phase chirale nématique. Cette thèse étudie le phénomène de séparation de phase de telles suspensions qui peut se produire soit de façon naturelle soit par l'addition d'une seconde macromolécule. Initialement, les effets des conditions d'hydrolyse sur les nanocristaux et les propriétés de séparation de phase s'y rattachant pour les pâtes provenant de feuillus ont été étudiées et comparées aux suspensions préparées à partir de pâtes de résineux. Les macromolécules étudiées, des dextrans bleus à différents poids moléculaires et taux de colorant, ont été synthétisés et caractérisés à l'aide de différentes techniques physico-chimiques. La nature polyélectrolytique de telles molécules leur confère des propriétés physico-chimiques différentes par rapport au dextran. L'ajout de dextran bleu dans une suspension de cellulose très concentrée, anisotrope, induit une séparation de phase et l'obtention d'une phase isotrope, due principalement au caractère ionique du colorant. L'effet de partition du dextran bleu dans une suspension de nanocristaux de cellulose biphasique aqueuse a donc été étudiée en mettant l'attention tout particulièrement sur la concentration totale du dextran bleu, le degré de substitution du colorant et l'influence de la masse molaire. Les contributions entropiques et électrostatiques sur les coefficients de partition du dextran bleu sont aussi discutées. Un équilibre triphasique isotrope-isotrope-nématique (I_1-I_2-N) a été observé dans des suspensions contenant et le dextran bleu et le dextran et ce sur différentes masses molaires. A partir de ces résultats, différents diagrammes de phases ont été imaginés et discutés.

Contributions of Authors

CONTRIBUTIONS OF AUTHORS

Chapter 2 has been published in *Biomacromolecules* **2005**, 6, 1048–1054. Drs. Maren Roman and Derek Gray are co-authors of this article. Dr. Roman provided useful discussions regarding research ideas, performed the hydrolysis of the eucalyptus pulp and obtained the AFM images of the pulp fibre surfaces. Dr. Gray provided useful discussions regarding analysis of the results and editorial assistance in the writing of the article.

Chapter 3 is in preparation for submission to a scientific journal. Drs. David Viet and Derek Gray are co-authors of this article. Dr. Viet provided useful discussions regarding research ideas and analysis/interpretation of the results, and also performed some of the viscosimetric measurements. Dr. Gray provided useful discussions regarding analysis of the results and editorial assistance in the writing of the article.

Chapter 4 has been published in *Langmuir* **2006**, 22, 8690–8695. Drs. David Viet and Derek Gray are co-authors of this article. Dr. Viet provided useful discussions regarding research ideas and analysis/interpretation of the results. Dr. Gray provided useful discussions regarding analysis of the results and editorial assistance in the writing of the article.

Chapter 5 is in preparation for submission to a scientific journal. Drs. David Viet and Derek Gray are co-authors of this article. Dr. Viet provided useful discussions regarding research ideas and analysis/interpretation of the results. Dr. Gray provided useful discussions regarding analysis of the results and editorial assistance in the writing of the article.

A combination of Chapters 6 and 7 has been published in *Macromolecules* **2007**, *40*, 3429-3436. Drs. David Viet and Derek Gray are co-authors of this article. Dr. Viet provided useful discussions regarding research ideas and analysis/interpretation of the results. Dr. Gray provided useful discussions regarding analysis of the results and editorial assistance in the writing of the article. The AFM measurements were carried out by Tiffany Abitbol. Dr. Nilgun Ulkem also provided useful editorial assistance in preparing the manuscript.

I hereby give copyright clearance for the inclusion of the following article, of which I am a co-author, in the dissertation of Stephanie Beck:

“Effect of reaction conditions on the properties and behavior of wood cellulose nanocrystal suspensions”

Clara Roman

12/06/06

Dr. Maren Roman
Assistant Professor
Department of Wood Science and Forest Products
Virginia Tech
Blacksburg, VA 24061

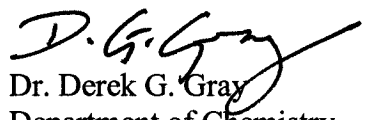
Date

I hereby give copyright clearance for the inclusion of the following articles, of which I am a co-author, in the dissertation of Stephanie Beck:

“Effect of reaction conditions on the properties and behavior of wood cellulose nanocrystal suspensions”

“Induced phase separation in low-ionic-strength cellulose nanocrystal suspensions containing high-molecular-weight blue dextrans”

“Triphase equilibria in cellulose nanocrystal suspensions containing neutral and charged macromolecules”



Dr. Derek G. Gray
Department of Chemistry
Pulp and Paper Building
McGill University
Montréal, Québec
H3A 2A7

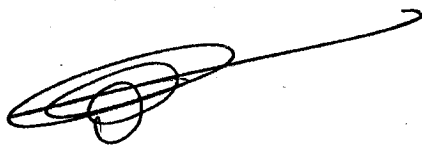
May 1, 2007

Date

I hereby give copyright clearance for the inclusion of the following articles, of which I am a co-author, in the dissertation of Stephanie Beck:

“Induced phase separation in low-ionic-strength cellulose nanocrystal suspensions containing high-molecular-weight blue dextrans”

“Triphase equilibria in cellulose nanocrystal suspensions containing neutral and charged macromolecules”



Dr. David Viet
Pulp and Paper Building
McGill University
Montréal, Québec
H3A 2A7

May 1, 2007

Date

Acknowledgements

ACKNOWLEDGEMENTS

To begin, I would like to thank Dr. Gray for his support, patience and encouragement throughout my thesis. I am grateful for the opportunities he gave me to do independent research and to attend conferences and communicate with others about my research. I am also indebted to Jean Bouchard for recommending Dr. Gray as a potential advisor; I'm glad I followed his advice.

Good research involves collaborating with others and sharing knowledge. During my thesis, I have worked with many people and have learned something from all of them. I would like to thank: Boel Nilsson for teaching me how to use the atomic force microscope and also how to say "cork borer" in Swedish (hint: it's pronounced "cork borer"!); Louis Godbout, for his quick response and good humour every time I came to tell him that the MilliQ water system needed fixing; Petr Fiurasek in the CSACS lab for showing me how to use the TGA and UV-visible spectrophotometer; Julie Boivin at l'Université de Montréal, for her skill in assisting with the measurements in Chapter 3; Dr. Petlicki for his kind help with dynamic light scattering measurements; and all the summer students for livening up the lab in the quiet summer months, especially Joshua Budman who made things very lively by blowing up the microwave...

Over the years, it has been my very great privilege and pleasure to work with a number of amazing postdocs and research associates. Thanks to Andrew Rodenhiser, for edifying discussions about spiders and goats at tea time; to Carl Bartels, for helpful discussions regarding polymers and viscosity; to Maren Roman, for giving me a model to aspire to and for being a good friend (I hope to see you at many conferences in the future); to Nilgun Ulkem, for her kind advice and words of encouragement when I was less than

optimistic, for keeping my banana plant alive, and for knowing where all the good equipment is; and to the Frenchmen in black, Greg Chauve and David Viet, who taught me how to make very strong coffee (but not to drink it!), the mysteries of Zen, and how to do good science while having fun in the lab. I would like to thank Greg for all his help with many experiments, even though they didn't make it into the thesis, for co-founding the Third Floor Lunch Club and for many batches of his famous home-made "croquants". David, with whom I have collaborated for the past two years, has been, as he put it, "a friend, boss, and postdoc," at the appropriate times. I am very grateful to him for his sense of humour, knowledge, advice and perspectives which he freely shared, and also for translating the abstract of this thesis. On a bien rigolé, merci beaucoup!

I would like to thank my fellow grad students and lab mates for putting up with the multitudes of vials containing various shades of blue that at times threatened to take over the lab. Thanks to Maggie, for bringing in goodies for group meetings and of course for being the Tea Queen and a great president of the Third Floor Tea Club, a tradition I am proud to be a part of. Thanks to Emily and Tiffany for being cool to chat with about life in grad school and life in general; Emily deserves a special mention for lending me her adorable cat Minnie on two occasions, and Tiffany for bringing in delicious cakes for the Tea Club when I was too busy writing up to even remember it was my birthday.

I would also like to acknowledge the staff of the Chemistry Department and of the Pulp and Paper Research Centre. Renee Charron and Chantal Marotte took good care of me, answered all my questions and made sure that my fees were paid on time. I could not have paid those fees without the financial support of several scholarships I would like to mention here: the Max Stern Recruitment Scholarship, NSERC PGS-A and PGS-B

scholarships, Sir James Lougheed Awards of Distinction, and the J.W. McConnell McGill Major Fellowship. I am grateful for the support of the Chemistry Department and the Departmental Chairs and Graduate Research Advisors. In the Pulp and Paper Building, I would like to thank Colleen McNamee for efficiently dealing with all the heating/cooling/leaking/fuming issues that cropped up but above all for her sense of humour and (very) dynamic personality. I would also like to mention Julie Taminiau for making the late lamented library a pleasant place to browse and for effortlessly finding that one crucial reference that wasn't online or in the university library. Thanks to M. Rebelo for always making sure I didn't slip on his freshly-mopped stairs and for opening the photocopy room after hours.

Throughout my life at grad school, I have participated in many activities organized by the CGSS or the members of my lab, including broomball, watching the World Cup final in a bar surrounded by rabid fans (*allez les bleus...*), going downhill skiing for the first and only time, and going curling, but the activity that most stands out is "Cottage Day" at Dr. Gray's lakeside cottage. I have been to more than my share of these annual escapes to the country and always had a wonderful time; I really appreciate Dr. Gray and his wife's generous hospitality. The Pulp and Paper Building Christmas Potluck lunch, organized by many volunteers, was always a highlight of the holiday season, with activities ranging from Christmas carol sing-alongs to Irish ceilidhs to treasure hunts to visits from Santa himself (although he bore a suspicious resemblance to Dr. van de Ven...). I am also grateful to Dr. Gray for supporting my desire to learn more than just chemistry when I decided to take Spanish classes (which more or less directly led to me meeting and marrying my husband, also during the thesis, so I am very grateful...). Gracias to Cathy,

Francisco, Soraya, Marino and Jocelyn for all the fun in Spanish class. Finally, merci to the members of the M.T.L. (you know who you are).

A special thanks to Mr. Wayne Wobick and Professor Viola Birss, my earliest mentors in chemistry, for encouraging my interest in this subject.

My thanks to whoever invented SciFinder for allowing me to get 90 % of my references without having to get up from the computer (which may or may not have been a good thing), to the aforementioned computer for not crashing and deleting all my data, to PhDcomics.com for many hours spent laughing at insightful and humorous depictions of the lives of all grad students everywhere, to J.R.R. Tolkien for the best book ever, to Junior the cat for his affectionate greetings whenever I would walk by, and to CSI: Miami and CSI: New York for coming on at 10 p.m. so I could still get my fix even when I worked late.

Above all, I have to thank my parents for their love, for always supporting me, and allowing me to move from Calgary to Montréal without feeling guilty. Many thanks for calling me back every time I phone and for partially financing all my trips back home. Special thanks to my twin sister and best friend Vickie for the hilarious e-mails, for the surprise parcels from Oxford, for the advice on how to get through a thesis in one piece, for excellent proofreading of almost the entire thesis, but especially for never, never asking when I was going to graduate. Finally, to my dear husband, José Agustín, thank you for your constant love and support, and also for taking care of such mundane things as washing the dishes while I was writing up.

Table of Contents

TABLE OF CONTENTS

Abstract.....	i
Résumé.....	ii
Contributions of Authors.....	v
Acknowledgements.....	xv
Table of Contents.....	xxi
List of Figures.....	xxix
List of Tables.....	xxxix
List of Symbols and Abbreviations.....	xlili

Chapter 1 Introduction: Phase Behaviour of Cellulose Nanocrystal Suspensions

1.1	Overview.....	1
1.2	Cellulose Nanocrystals.....	1
1.2.1	Chemical and supermolecular structure of cellulose.....	1
1.2.2	Cellulose nanocrystal suspensions.....	4
1.2.3	Characterization of cellulose nanocrystal suspensions.....	8
1.3	Liquid Crystalline Phases of Cellulose Nanocrystal Suspensions.....	10
1.3.1	Liquid crystals.....	10
1.3.2	Liquid crystalline phases of cellulose derivatives.....	13
1.3.3	Liquid crystalline phases of cellulose nanocrystals.....	13
1.3.3.1	Stability of colloidal suspensions.....	14
1.3.3.2	Onsager theory for the isotropic–nematic phase separation of neutral rodlike particles.....	16
1.3.3.3	Isotropic–chiral nematic phase separation of cellulose nanocrystal suspensions.....	20
1.3.3.4	Effect of the polyelectrolytic nature of cellulose nanocrystals on phase separation.....	22
1.3.3.5	Theoretical treatment of the phase separation of charged rodlike particles.....	23
1.4	Addition of Macromolecules to Cellulose Nanocrystal Suspensions.....	25

1.4.1	The depletion attraction.....	26
1.4.2	Theories of depletion attraction for spherical colloid + polymer coil mixtures.....	28
1.4.3	Theories of phase behaviour of rodlike colloid + polymer coil mixtures.....	29
1.4.4	Experimental mixtures of rodlike colloids and polymer coils.....	31
1.4.5	Partitioning of coiled or flexible macromolecules.....	32
1.5	Dye-Labeled Dextran in Cellulose Nanocrystal Suspensions.....	34
1.5.1	Properties and structure of dextran.....	34
1.5.2	Dextran derivatives.....	36
1.6	Motivation of Research and Outline of Thesis.....	37
1.7	References.....	41

<i>Introduction to Cellulose Nanocrystal Suspension Characterization Methods</i>	55
--	----

Chapter 2 Effect of Reaction Conditions on the Properties and Behaviour of Wood Cellulose Nanocrystal Suspensions

2.1	Introduction.....	63
2.2	Experimental Methods.....	66
2.2.1	Materials.....	66
2.2.2	Sulfuric acid hydrolysis of wood pulp.....	66
2.2.3	Gravimetric analysis.....	67
2.2.4	Atomic force microscopy (AFM).....	67
2.2.5	Phase separation behaviour.....	68
2.2.6	Conductometric titrations.....	69
2.2.7	Pitch measurement.....	69
2.3	Results and Discussion.....	70
2.3.1	Eucalyptus vs. black spruce cellulose suspensions.....	70
2.3.2	Effect of reaction time on softwood suspension properties.....	75
2.3.3	Effect of acid-to-pulp ratio on softwood suspension properties....	77
2.3.4	Chiral nematic pitch.....	78
2.4	Conclusions.....	80

2.5	References.....	81
<i>Introduction to the Characterization of Blue Dextran</i>		87
Chapter 3 Synthesis and Characterization of Blue Dextrans. A Comparative Study of the Physico-Chemical Properties for Various Molecular Weights and Dye Loadings		
3.1	Introduction.....	91
3.2	Experimental Methods.....	94
3.2.1	Chemicals.....	94
3.2.2	Preparation of blue dextrans.....	94
3.2.3	Thermogravimetric analysis (TGA).....	95
3.2.4	UV-visible spectroscopy.....	97
3.2.5	Viscosity measurements.....	98
3.2.6	Refractive index increments.....	100
3.2.7	Gel permeation chromatography (GPC).....	100
3.2.8	Dynamic light scattering (DLS).....	101
3.2.9	Static light scattering (SLS).....	102
3.3	Results and Discussion.....	102
3.3.1	Effect of reaction conditions on blue dextran properties.....	102
3.3.2	Viscosity.....	102
3.3.3	Refractive index increments.....	111
3.3.4	Gel permeation chromatography.....	111
3.3.5	Molecular weights.....	113
3.3.6	Hydrodynamic radii and radii of gyration.....	114
3.4	Conclusions.....	116
3.5	References.....	117
<i>Introduction to Cellulose-Dye Ligand Interactions</i>		125

Chapter 4 Induced Phase Separation in Low-Ionic-Strength Cellulose Nanocrystal Suspensions Containing High-Molecular-Weight Blue Dextrans

4.1	Introduction.....	131
4.2	Experimental Methods.....	133
4.2.1	Chemicals.....	133
4.2.2	Cellulose nanocrystal suspensions.....	133
4.2.3	Blue dextrans.....	134
4.2.4	Preparation of cellulose–dextran suspensions.....	136
4.3	Results and Discussion.....	137
4.3.1	Dextrans.....	137
4.3.2	Blue dextrans of increasing number density.....	140
4.3.3	Blue dextrans of increasing molecular weight.....	141
4.3.4	Blue dextrans of increasing ligand density.....	142
4.3.5	Blue dextran and Cibacron blue 3G-A.....	145
4.4	Conclusions.....	148
4.5	References.....	149
4.6	Appendix – Supporting Data.....	152

<i>Introduction to Partitioning in Biphase Systems</i>	155
--	-----

Chapter 5 Partitioning of Charged and Neutral Dextran-Dye Derivatives in Biphase Cellulose Nanocrystal Suspensions

5.1	Introduction.....	159
5.2	Experimental Methods.....	160
5.2.1	Materials.....	160
5.2.2	Cellulose nanocrystal suspensions.....	160
5.2.3	Preparation of blue dextrans.....	161
5.2.4	Acid hydrolysis of dextran T-2000.....	161
5.2.5	Characterization of blue dextrans.....	161
5.2.6	Preparation of cellulose suspensions containing dextran–dye conjugate.....	164

5.2.7	Determination of partition coefficients.....	164
5.3	Results and Discussion.....	165
5.3.1	Partition theory.....	165
5.3.2	Blue dextran partitioning.....	167
5.3.3	Effect of molecular weight on partition coefficient K	170
5.3.4	FITC-dextran partitioning.....	173
5.3.5	Increasing degree of dye substitution (DS).....	174
5.3.6	Increasing blue dextran concentration.....	176
5.3.7	Nonionic FITC-dextran vs. anionic blue dextran.....	176
5.4	Conclusions.....	179
5.5	References.....	180

<i>Introduction to Triphase Equilibria in Cellulose Nanocrystal + Dextran Systems</i>	185
---	-----

Chapter 6 Triphase Equilibria in Cellulose Nanocrystal Suspensions Containing Neutral and Charged Macromolecules.

6.1	Introduction.....	189
6.2	Experimental Methods.....	192
6.2.1	Chemicals.....	192
6.2.2	Cellulose nanocrystal suspensions.....	193
6.2.3	Blue dextrans.....	193
6.2.4	Preparation of cellulose–dextran suspensions.....	193
6.2.5	Characterization methods.....	194
6.3	Results.....	197
6.3.1	Triphase equilibrium.....	197
6.3.2	Phase separation mechanism.....	202
6.3.3	Cellulose nanocrystal fractionation.....	203
6.3.4	Dextran partitioning.....	203
6.4	Discussion.....	206
6.4.1	Triphase equilibrium.....	206

6.4.1.1	Blue-to-plain dextran ratio required to obtain I ₁ phase from I ₂ -N equilibrium.....	210
6.4.1.2	Effect of dextran molecular weight on phase equilibrium.....	210
6.4.2	Cellulose nanocrystal fractionation.....	212
6.4.3	Dextran partitioning.....	213
6.5	Conclusions.....	216
6.6	References.....	217

Chapter 7 Triphase Equilibria in Cellulose Nanocrystal Suspensions Containing Neutral and Charged Macromolecules. Phase Diagrams

7.1	Introduction.....	225
7.2	Experimental Methods.....	226
7.3	Results and Discussion.....	227
7.3.1	Phase diagram.....	227
7.3.2	Re-entrant phase behaviour.....	229
7.3.3	Effect of increasing blue dextran concentration.....	231
7.3.4	Effect of increasing dextran concentration.....	233
7.3.5	Effect of cellulose nanocrystal concentration.....	234
7.3.6	Blue-to-plain dextran ratio required to obtain I ₁ phase from I ₂ -N biphasic equilibrium.....	238
7.3.7	Effect of dextran molecular weight.....	239
7.3.8	Effect of blue dextran charge density.....	241
7.4	Conclusions.....	242
7.5	References.....	243

Chapter 8 General Conclusions

8.1	Conclusions.....	247
8.2	Original Contributions to Scientific Knowledge.....	249
8.3	Suggestions for Future Work.....	250

List of Figures

LIST OF FIGURES

Figure 1.1	Chemical structure of cellulose showing cellobiose repeat unit. The anhydroglucose residues adopt the energetically favourable chair conformation with the hydroxyl groups in the equatorial positions.	2
Figure 1.2	Hierarchical structure of native cellulose, from the molecular level to the supermolecular level. Cellulose is biosynthesized by assemblies of enzymes in the cell wall. The polymer chains instantly crystallize and aggregate to form microfibrils, which are held together by hydrogen bonding between the hydroxyl groups and oxygens of adjacent chains. A detail of the microfibril (circled area) is shown in Figure 1.3.	3
Figure 1.3	Cross-section of a microfibril composed of six elementary fibrils.	3
Figure 1.4	Each microfibril can be considered as a string of cellulose microcrystals linked by amorphous domains which act as structural defects.	5
Figure 1.5	Schematic representation of the surface cellulose chains in a nanocrystal, showing sulfate groups introduced by the action of sulfuric acid. Weak carboxylic acid groups are also shown.	7
Figure 1.6	Transmission electron micrographs of a) cotton whiskers and b) tunicate whiskers. Images obtained by Jean-Luc Putaux, CERMAV-CNRS, France.	9
Figure 1.7	Schematic diagram of the different types of liquid crystal structure.	11
Figure 1.8	A suspension of cellulose nanocrystals displaying an upper isotropic phase and a lower chiral nematic phase (helical packing of several nematic planes in which the rods are aligned on average with a vector). Half a pitch, $P/2$, is shown in the diagram.	12
Figure 1.9	Schematic representation of the total energy of interaction between two colloidal particles, according to DLVO theory.	15
Figure 1.10	Qualitative representation of the free energy of a dispersion of colloidal spheres as a function of the sphere density for the fluid (random) and solid (ordered) phases. At low particle densities, the fluid phase is energetically favoured, while above a critical density (dotted line), the solid phase becomes more stable and a phase transition occurs. Adapted from Baus et al. (1996).	16
Figure 1.11	Summary of the effects of added electrolyte on the phase separation behaviour of a suspension of cellulose nanocrystals at constant concentration.	25

Figure 1.12	The depletion mechanism. Free, non-adsorbing polymers are excluded from a shell of thickness R_g surrounding the colloidal particles of radius R . Initially, the osmotic pressure exerted on the colloids is uniform (top). As the colloids approach, the polymers cannot penetrate into the shaded volume. The osmotic pressure on the colloids becomes uneven (bottom), leading to an effective attraction between the particles.	27
Figure 1.13	Theoretical phase diagram for a mixture of rodlike particles and coiled polymer. The isotropic-nematic coexistence region is broadened by the addition of coiled polymer. As the coil density increases, the rod density in the isotropic phase decreases. The downward-sloping tie lines indicate that the coiled polymer partitions into the isotropic phase. The inset shows the region in which most experiments in this thesis are performed.	30
Figure 1.14	Schematic structure of native dextran showing α -(1,3) branching and α -(1,6)-linked backbone.	35
Figure 1.15	Solubility of dextrans in ethanol-water mixtures at 25°C. The M_w axis refers to the highest molecular weight dextran soluble in the given percentage composition of ethanol. Adapted from Basedow and Ebert (1979).	36
Figure 2-A	Principle of operation of the atomic force microscope (AFM).	55
Figure 2-B	Schematic diagram showing examples of tip-sample convolution originating from the relative sizes of the tip and the sample feature being measured.	56
Figure 2-C	Equipment used for conductometric titration of cellulose nanocrystals.	57
Figure 2-D	Conductometric titration curve for suspension of cellulose nanocrystals containing strong and weak acid groups at their surfaces.	58
Figure 2-E	Photomicrograph of the chiral nematic liquid crystal texture of a cellulose nanocrystal suspension viewed in a polarizing microscope. The nanocrystals lie parallel to the plane of the page in the light regions (—) and perpendicular in the dark regions (•).	59
Figure 2.1	Deflection mode AFM images taken in air showing microfibrils on the surface of a) eucalyptus pulp fibre, and b) black spruce pulp fibre. Scale bar = 0.5 μm .	70

Figure 2.2	Height mode AFM images of cellulose nanocrystals from a) eucalyptus pulp (E), b) black spruce pulp (S1), c) black spruce pulp (S2), and d) black spruce pulp (S3). Scale bar = 1 μm . The herringbone pattern seen in the background is an artifact.	72
Figure 2.3	Distribution of particle length of cellulose nanocrystals from suspensions a) E, b) S1, c) S2, and d) S3.	73
Figure 2.4	Phase separation diagrams for suspensions a) E, b) S1, c) S2, and d) S3. The region in which the volume fraction of the anisotropic phase, ϕ_{aniso} , lies between 0 and 1 is the biphasic region. To the left of the biphasic region, $\phi_{\text{aniso}} = 0$, and the suspensions are completely isotropic. To the right of the biphasic region, $\phi_{\text{aniso}} = 1$, and the suspensions are completely anisotropic.	74
Figure 2.5	Fingerprint texture in chiral nematic phase of 10 wt% eucalyptus suspension, viewed in polarizing microscope. Scale bar = 200 μm . Chiral nematic pitch $P = 17 \mu\text{m}$.	79
Figure 2.6	The effect of average cellulose nanocrystal length on the chiral nematic pitch P measured at 7 wt % cellulose suspension concentration.	79
Figure 3.1	Coupling of Cibacron blue 3G-A (I = R-Cl) with dextran (II) to give blue dextran (III), showing the random binding sites of the dye.	97
Figure 3.2	a) Absorption spectrum for blue dextran in water (0.266 mg/mL). b) Calibration curve of absorbance at 609 nm versus concentration c in mg/mL.	98
Figure 3.3	Differential refractive index as a function of blue dextran 2000 ₅₆ concentration at 690 nm.	101
Figure 3.4	Reduced viscosity η_{red} as a function of concentration c for blue dextran 2000 in solutions of increasing ionic strength.	104
Figure 3.5	Reduced viscosity η_{red} as a function of the concentration c for unmodified dextrans (open symbols) and blue dextrans (filled symbols) in 0.200 M NaCl (aq). Values were taken from the linear portion of the η_{red} vs c curve.	105
Figure 3.6	Intrinsic viscosity $[\eta]$ as a function of molar mass M_w for dextran T-2000 and blue dextran 2000 in 0.200 M NaCl (aq).	108
Figure 3.7	Reduced viscosity η_{red} as a function of the concentration c for blue dextran 2000 in solutions of increasing ionic strength.	109
Figure 3.8	Intrinsic viscosity $[\eta]$ of blue dextran 2000 as a function of $I^{-1/2}$.	109
Figure 3.9	Sample GPC chromatogram for blue dextran 2000 ₁₂ .	112

Figure 4-A	Molecular structure of Congo red (CR).	126
Figure 4-B	Molecular structure of Acid red 17 (AR17).	127
Figure 4-C	Molecular structure of Cibacron blue 3G-A (CB).	127
Figure 4.1	Schematic of idealized “nematic” nanocrystal distribution in the 13.8 wt% cellulose suspension. Separation between the cellulose rods $d \approx 20$ nm.	138
Figure 4.2	Induced phase separation caused by the addition of blue dextrans T-2000 of increasing ligand density to vials containing anisotropic cellulose nanocrystal suspension (13.8 wt%). Blue dextran partitions preferentially into the isotropic phase.	143
Figure 4.3	Volume fraction of upper isotropic phase as a function of time for phase separation of initially anisotropic samples (13.8 wt% nanocrystals) induced by adding blue dextrans 2000 with increasing ligand density. Samples: 2000-1 \blacklozenge ; 2000-2 \blacksquare ; 2000-3 \blacktriangle ; 2000-4 \times ; 2000-5 $+$.	144
Figure 4.4	Volume fraction isotropic phase as a function of ionic strength due to sulfonate groups on dye ligands for blue dextran 2000 (\blacklozenge) and on Cibacron blue 3G-A (\blacksquare).	146
Figure 5.1	Partition coefficients of blue dextran 2000 ₁₆₁ in ~ 10 wt% cellulose suspension. The line is the best fit to the data. Closed symbols were obtained in 10.1 wt% cellulose nanocrystal suspension; open symbols were obtained in 10.3 wt% cellulose nanocrystal suspension.	168
Figure 5.2	Natural logarithm of the measured partition coefficient K_{meas} as a function of $R_g^{5/3}$ for blue dextrans of different molecular weights. Radii of gyration of the dextrans were calculated using the equation $R_g = 0.66M_w^{0.43}$, which is valid over the M_w range 400 to 2700 kDa.	171
Figure 5.3	Structure of FITC-dextran. *FITC is assumed to associate randomly with any free hydroxyl group. ³³	174
Figure 5.4	Theoretical and experimental K values for blue dextrans and FITC-dextrans in cellulose nanocrystal suspension.	178

Figure 6-A	Cellulose nanocrystal suspensions containing identical concentrations of unmodified dextran T-2000 and blue dextran 2000 increasing in concentration from <i>b</i> to <i>h</i> . Sample <i>a</i> contains only dextran T-2000 and is designated I ₂ -N; sample <i>h</i> is designated I ₁ -N.	185
Figure 6.1	Sample of 8.7 wt% cellulose nanocrystal suspension containing blue dextran 2000 ($C_{\text{blue D}_x} = 8.3 \times 10^{-7} \text{ nm}^{-3}$) and dextran T-2000 ($C_{\text{D}_x} = 1.1 \times 10^{-5} \text{ nm}^{-3}$), showing separation into three phases: from top to bottom, I ₁ , I ₂ and N. Photos taken a) in incident light, and b) between partially crossed polars.	198
Figure 6.2	Photomicrographs of a) I ₁ , b) I ₂ and c) N phases of the sample in Figure 1. Taken at 10× magnification between 90° crossed polars with 530 nm full-wave retardation plate. Streaks and droplets are visible in b) due to ordering at the surface of the glass. Characteristic chiral nematic fingerprint texture with approximately 38 μm pitch is visible in c). Scale bar = 250 μm.	198
Figure 6.3	Schematic representation of the evolution of phase separation as typically observed in the three-phase coexistence region. (I) t_0 , initially uniform sample; (II) $t = 10\text{--}20$ min, droplets of I ₁ phase moving upwards (bicontinuous structure of I ₁ and I ₂ [*] phases); (III) $t = 1\text{--}3$ hours, well-defined I ₁ phase with metastable I ₂ [*] phase; (IV) $t = 48\text{--}96$ hours, final I ₁ -I ₂ -N coexistence.	202
Figure 6.4	TM-AFM images (height mode) of dilute samples from a triphasic cellulose nanocrystal suspension containing blue dextran 2000 and dextran T-2000: a) I ₁ phase showing polymer blobs on the mica; b) I ₂ phase showing nanocrystals; c) and d) N phase showing well-dispersed nanocrystals.	204
Figure 6.5	Type of phase behaviour shown by mixtures of rodlike colloids and flexible polymers as a function of the geometrical parameters L/D and σ/D . L is the rod length, D is the rod diameter and σ is the diameter of the polymer coil. "I ₁ -I ₂ -N" indicates a phase diagram with two isotropic phases and a nematic phase. Figure adapted from Lekkerkerker and Stroobants (1994).	207
Figure 6.6	Distribution of particle length L of cellulose nanocrystals for the a) I ₂ and b) N phases of a triphasic cellulose nanocrystal suspension containing blue dextran 2000 and dextran T-2000.	212

- Figure 7.1 Vials of triphasic I_1 – I_2 –N cellulose nanocrystal suspension (8.7 wt%) containing blue dextran 2000 (from left to right, 0.45 to $2.50 \times 10^{-6} \text{ nm}^{-3}$) and dextran T-2000 ($5.3 \times 10^{-6} \text{ nm}^{-3}$). The preferential partitioning of blue dextran into the I_1 phase is evident. The volume fraction of the I_1 phase increases from left to right as more blue dextran 2000 is added. 226
- Figure 7.2 Phase diagram for 8.7 wt% cellulose nanocrystal suspension containing blue dextran 2000 and dextran T-2000. Dotted line indicates equal number densities of dextran and blue dextran. The boundaries between the regions of the phase diagram are intended as a guide to the eye. Some data points have been omitted for clarity. Compositions of phases along the arrows are shown in Figures 7.4 to 7.6 below. 228
- Figure 7.3 Area of phase diagram showing re-entrant I_2 –N \rightarrow I_1 – I_2 –N \rightarrow I_2 –N phase behaviour for 8.7 wt% cellulose nanocrystal suspension containing blue dextran 2000 and dextran T-2000. The boundaries between the regions of the phase diagram are intended as a guide to the eye. 229
- Figure 7.4 Example of re-entrant I_2 –N \rightarrow I_1 – I_2 –N \rightarrow I_2 –N phase behaviour for 8.7 wt% cellulose nanocrystal suspension containing $8.2 \times 10^{-7} \text{ nm}^{-3}$ blue dextran 2000 and dextran T-2000 increasing from 0 to $2.0 \times 10^{-5} \text{ nm}^{-3}$ (concentrations correspond to arrow AB in Figure 7.2). As more dextran T-2000 is added, the N phase volume fraction decreases and the I_2 phase volume fraction increases; the I_1 phase increases and then decreases in volume fraction before disappearing. 230
- Figure 7.5 Example of phase behaviour for 8.7 wt% cellulose nanocrystal suspension with dextran T-2000 number density = $2.2 \times 10^{-5} \text{ nm}^{-3}$ and increasing blue dextran 2000 number density (concentrations correspond to arrow CD in Figure 7.2). 232
- Figure 7.6 Example of phase behaviour for 8.7 wt% cellulose nanocrystal suspension at blue dextran 2000 number density = $2.7 \times 10^{-6} \text{ nm}^{-3}$ and increasing dextran T-2000 number density (concentrations correspond to arrow EF in Figure 7.2). 234
- Figure 7.7 Relative volume fractions of the phases obtained when blue dextran 2000 and dextran T-2000 were added to a dilute nanocrystal suspension containing 6.3 wt% cellulose with $\phi_{\text{aniso}} = 0.29$. The number density of blue dextran is $8.3 \times 10^{-7} \text{ nm}^{-3}$ and the dextran T-2000 number density increases from 0 to $1.3 \times 10^{-5} \text{ nm}^{-3}$ (concentrations correspond to arrow GH in Figure 7.8). 235

Figure 7.8	Partial phase diagram for dilute biphasic (6.3 wt%; $\phi_{\text{aniso}} = 0.29$) cellulose suspension. The boundary between the regions of the phase diagram is intended as a guide to the eye.	235
Figure 7.9	Relative volume fractions of the phases obtained when blue dextran 2000 and dextran T-2000 ($C_{\text{blue Dx}} = 6.0 \times 10^{-6} \text{ nm}^{-3}$ and $C_{\text{Dx}} = 1.2 \times 10^{-5} \text{ nm}^{-3}$) were added to dilute cellulose suspensions (concentrations in wt% indicated).	237
Figure 7.10	Blue-dextran-to-dextran ratio required for the formation of I_1 - I_2 -N equilibrium in 8.7 wt% cellulose nanocrystal suspension.	239
Figure 7.11	Phase diagrams for 8.7 wt% cellulose nanocrystal suspension containing a) blue dextran 500 and dextran T-500; b) blue dextran 2000 and dextran T-500; and c) blue dextran 500 and dextran T-2000. The boundaries between the regions of the phase diagram are intended as a guide to the eye. Note: the phase diagrams are not on identical scales.	240

List of Tables

LIST OF TABLES

Table 2.1	Dimensions of cellulose nanocrystals from various sources.	64
Table 2.2	Experimental conditions: reaction time and acid-to-pulp ratios.	67
Table 2.3	Effect of reaction conditions on suspension properties.	73
Table 3.1	Preparation conditions and dye ligand densities for blue dextrans.	96
Table 3.2	Intrinsic viscosity $[\eta]$ and critical concentration C^* for unmodified and blue dextrans in 0.200 M NaCl (aq).	106
Table 3.3	Effect of increasing degree of dye substitution on intrinsic viscosity $[\eta]$ and critical concentration C^* for blue dextrans 2000 in 0.200 M NaCl (aq).	107
Table 3.4	Effect of ionic strength on intrinsic viscosity $[\eta]$ and critical concentration C^* for blue dextran 2000 ₁₆₁ .	110
Table 3.5	Refractive index increments dn/dc at 690 nm for blue dextrans of various molecular weights and dye loadings.	112
Table 3.6	Molecular weights and indices of polydispersity of blue dextrans.	113
Table 3.7	Experimental and literature values of R_H and R_g for unmodified and blue dextrans.	115
Table 3.8	The effect of ionic strength on R_H values of 0.4 g/L blue dextran 2000 ₁₆₁ .	116
Table 4.1	Preparation conditions and ligand densities for blue dextrans.	135
Table 4.2	Blue dextrans of increasing number density added to anisotropic suspension (13.8 wt% cellulose nanocrystals).	141
Table 4.3	Blue dextrans of increasing molecular weight added to anisotropic suspension (13.8 wt% cellulose nanocrystals).	142
Table 4.4	Blue dextrans 2000 of increasing ligand density added to anisotropic suspension (13.8 wt% cellulose nanocrystals).	143
Table 5.1	Properties of blue dextrans and FITC-dextrans.	163
Table 5.2	Partition coefficients of blue dextrans 2000 in 10.1 wt% cellulose nanocrystal suspension at two constant total dextran anhydroglucose monomer concentrations.	169

Table 5.3	Partition coefficients for blue dextrans 2000 in 10.1 wt% cellulose nanocrystal suspension at two constant dye concentrations.	170
Table 5.4	Partition coefficients for blue dextrans and FITC-dextrans of different molecular weight. Entries in italics denote blue dextrans of different molecular weights having similar DS values.	172
Table 5.5	Partition coefficients for FITC-dextrans.	173
Table 6.1	Molecular weights, polydispersities and radii of gyration of dextrans used.	193
Table 6.2	Preparation conditions and ligand densities of blue dextrans.	194
Table 6.3	Radii of hydration of unmodified dextrans and blue dextrans in 0.200 M NaCl (aq) obtained by dynamic light scattering.	196
Table 6.4	Minimum number densities of blue and unmodified dextrans required to obtain triphase equilibria in 8.7 wt% cellulose suspension, for dextrans of equal molecular weight.	199
Table 6.5	Minimum number densities of blue and unmodified dextrans required to obtain triphase equilibria in 8.7 wt% cellulose suspension, for dextrans of different molecular weight.	200
Table 6.6	Samples of 8.7 wt% cellulose suspension containing only unmodified dextran or only blue dextran, with dextran number density and ionic strength identical to those shown in Table 6.4.	201
Table 6.7	Partitioning of blue dextran in a triphasic 8.7 wt% cellulose nanocrystal suspension containing blue Dx 2000 ₁₆₁ ($C_{\text{blueDx 2000}} = 8.2 \times 10^{-7} \text{ nm}^{-3}$) and Dx T-2000 ($C_{\text{Dx T-2000}} = 1.1 \times 10^{-5} \text{ nm}^{-3}$).	205
Table 6.8	Concentrations of FITC-dextran 2000 (total $C_{\text{FITC-Dx}} = 2.28 \times 10^{-6} \text{ nm}^{-3}$) and blue dextran 2000 (total $C_{\text{blue Dx}} = 2.72 \times 10^{-6} \text{ nm}^{-3}$) in the three phases of a triphasic cellulose nanocrystal suspension (8.7 wt% total cellulose concentration).	205
Table 6.9	Theoretical and experimental values of the partition coefficients for FITC-dextran 2000 (total $C = 2.28 \times 10^{-6} \text{ nm}^{-3}$) and blue dextran 2000 (total $C = 2.72 \times 10^{-6} \text{ nm}^{-3}$) in triphasic 8.7 wt% cellulose nanocrystal suspension.	214
Table 7.1	Effect of cellulose nanocrystal concentration on dextran and cellulose number densities required to obtain triphase equilibrium.	236

List of Symbols and Abbreviations

LIST OF SYMBOLS AND ABBREVIATIONS

a	Mark-Houwink exponent
A_λ	Absorbance at wavelength λ
B_{rc}	Second virial coefficient of rod-coil interactions
c^*	Critical concentration of cellulose nanocrystals required for formation of anisotropic phase
c	Polymer concentration in g/mL
c_a	Concentration of blue dextran in anisotropic phase
c_i	Concentration of blue dextran in isotropic phase
C^*	Critical concentration for semi-dilute regime (viscosimetry)
C	Number density
C_a	Number density of rods in the anisotropic phase
C_i	Number density of rods in the isotropic phase
d	Distance between planes of rods
d_I	Concentration of blue dextran in isotropic phase
d_N	Concentration of blue dextran in nematic phase
D	Diameter of a rodlike particle
D_{eff}	Effective diameter of charged rods
dn/dc	Specific refractive index increment
e	Elementary charge
h	Twisting factor
h^2	Cross-sectional area of square rods
I	Ionic strength
k	Boltzmann's constant
k_H	Huggins constant
kT	Thermal energy
K	Partition coefficient
L	Length of a rodlike particle
M_n	Number-average molecular weight
M_w	Weight-average molecular weight

n	Average refractive index
P	Chiral nematic pitch
R	Radius of spherical colloidal particle
R_g	Radius of gyration
R_H	Hydrodynamic radius
T	Temperature
w	Weight percent cellulose concentration
ϕ_a	Volume fraction of rods in the anisotropic phase
ϕ_{aniso}	Volume fraction of anisotropic phase
ϕ_i	Volume fraction of rods in the isotropic phase
ϕ_{iso}	Volume fraction of isotropic phase
γ	Angle between rodlike particles
η	Solution viscosity
η_p	Polymer viscosity
η_s	Solvent viscosity
η_{red}	Reduced viscosity
η_{sp}	Specific viscosity
η_{rel}	Relative viscosity
$[\eta]$	Intrinsic viscosity
κ^{-1}	Debye screening length
λ	Wavelength
ρ	Density of cellulose in water
σ	Surface charge density of cellulose nanocrystals
$\sigma/2$	Radius of polymer coils
AFM	Atomic force microscopy
AGU	Anhydroglucose unit
AR17	Acid red 17 dye
ATPS	Aqueous two-phase system

CB	Cibacron blue 3G-A dye
CR	Congo red dye
DLS	Dynamic light scattering
DLVO Theory	Derjaguin, Landau, Verwey and Overbeek's theory
DMF	Dimethylformamide
DMSO	Dimethylsulfoxide
DP	Degree of polymerization
DS	Degree of substitution
Dx	Dextran
FITC	Fluorescein isothiocyanate
GPC	Gel permeation chromatography
HPC	Hydroxypropyl cellulose
I	Isotropic
I ₁	Dilute isotropic phase
I ₂	Concentrated isotropic phase
I _p	Index of polydispersity
IR	Infrared
MCC	Microcrystalline cellulose
MW	Molecular weight
N	Nematic, chiral nematic
NMR	Nuclear magnetic resonance
PBA	Poly- <i>p</i> -benzamide
PDMS	Polydimethylsiloxane
PEG	Polyethylene glycol
PEO	Polyethylene oxide
PIB	Polyisobutylene
PMMA	Polymethylmethacrylate
PS	Polystyrene
PTFE	Polytetrafluoroethylene
SLO Theory	Stroobants, Lekkerkerker and Odjik's theory
SLS	Static light scattering

S _N 1	Unimolecular nucleophilic substitution reaction
TEM	Transmission electron microscopy
TGA	Thermogravimetric analysis
THF	Tetrahydrofuran
TM-AFM	Tapping mode atomic force microscopy
TMV	Tobacco mosaic virus
UV	Ultraviolet

Chapter 1

Introduction:

Phase Behaviour of Cellulose Nanocrystal Suspensions

1.1 OVERVIEW

Cellulose whiskers or nanocrystals are obtainable by acid hydrolysis from a wide variety of low-cost renewable sources, are easily recyclable by combustion, and have reactive surfaces to which chemical groups can be grafted to tailor their chemical and physical properties. Together, these attributes make highly crystalline cellulose whiskers attractive for various applications, such as reinforcing materials in nanocomposites.^{1,2} Electrostatically-stabilized cellulose whiskers may also be used as a model system to verify theoretical models describing the phase separation in suspensions of rodlike polyelectrolytes, alone or with added macromolecules.

An initial background on the molecular and supermolecular structure of native cellulose and the historical development of cellulose nanocrystal production and characterization is essential to an understanding of their unique properties. Following this, the molecular structure and properties of blue dextran, the macromolecule most studied in cellulose nanocrystal suspensions, will be examined. Finally, the theoretical and experimental phase behaviour of colloidal suspensions containing added macromolecules will be discussed.

1.2 CELLULOSE NANOCRYSTALS

1.2.1 Chemical and supermolecular structure of cellulose

Cellulose is a linear polymer of β -(1,4)-D-glucose residues (Figure 1.1). Because the β -(1,4) linkage rotates the successive glucose units through 180° relative to each other, the cellulose repeat unit, called cellobiose, consists of two anhydroglucose residues.

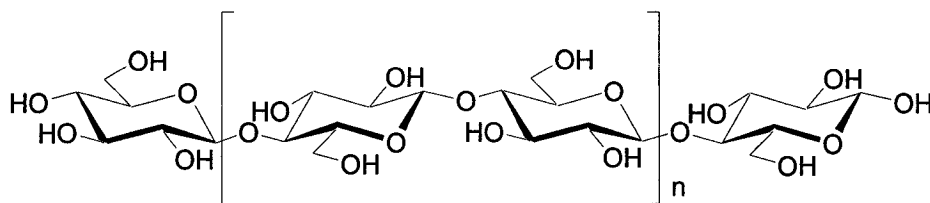


Figure 1.1. Chemical structure of cellulose showing cellobiose repeat unit. The anhydroglucose residues adopt the energetically favourable chair conformation with the hydroxyl groups in the equatorial positions.³

In nature, cellulose has a hierarchical structure, from the polymeric glucose chains to the microfibrils which make up the cell walls of plants (Figure 1.2). The molecular, crystallographic and supermolecular structures of cellulose, and their characterization, have been the subject of several recent reviews.⁴⁻⁷ However, we are mostly concerned with the elementary fibrils within the microfibrils. The rigidity of the cellulose molecule, coupled with strong intra- and intermolecular hydrogen bonding among the many hydroxyl groups along the cellulose chains,ⁱ means that the cellulose chains can pack closely to give areas of high crystallinity within the elementary fibril (Figure 1.3).⁸ According to the fringed micellar model, the elementary fibril also contains amorphous regions distributed randomly among the crystalline regions, or crystallites.⁹

Cellulose has six different interconvertible polymorphs (I, II, III_I, III_{II}, IV_I and IV_{II});⁴ in this thesis, only native cellulose (cellulose I) is studied. The crystal structure and morphology of native cellulose, in particular the crystallographic unit cell, have been the subject of much controversy over the years:¹⁰⁻¹⁴ Many inconsistencies existed among the

ⁱ The principal intramolecular hydrogen bond is between the hydrogen of the C3 hydroxyl group and the O5 oxygen of the adjacent ring; the principal intermolecular hydrogen bond lies between the hydrogen of the primary C6 hydroxyl group and the O3 oxygen.

early crystallographic studies and fibre X-ray diffraction studies were unable to account for all of the diffraction features recorded from algal cellulose I samples.¹⁵

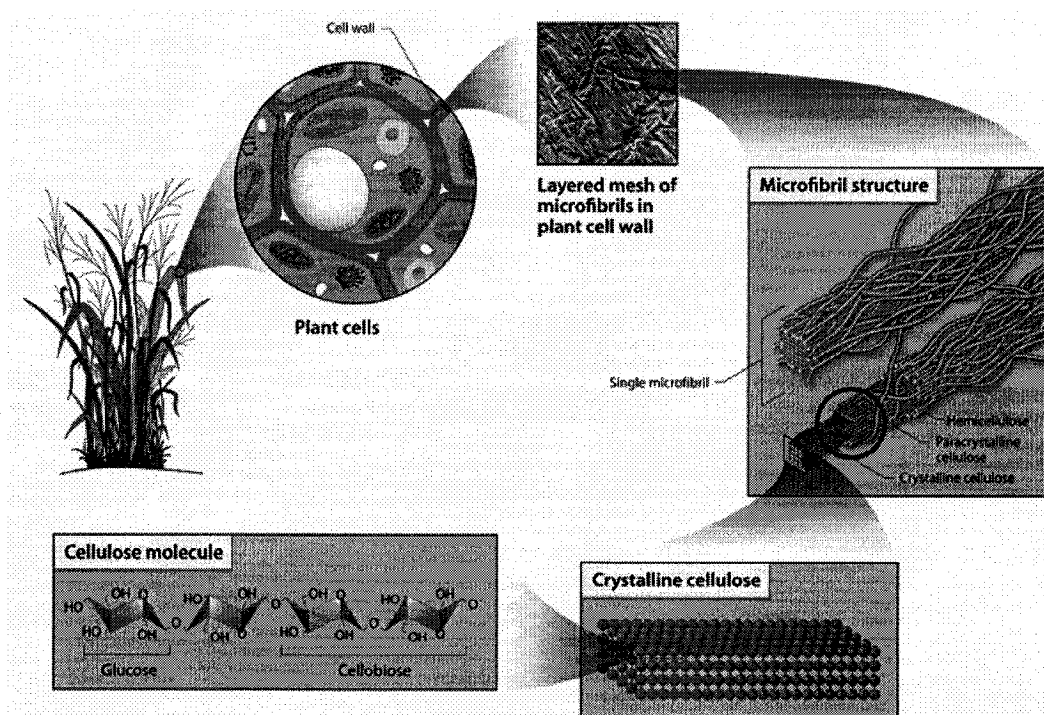


Figure 1.2. Hierarchical structure of native cellulose, from the molecular level to the supermolecular level.¹⁶ Cellulose is biosynthesized by assemblies of enzymes in the cell wall. The polymer chains instantly crystallize and aggregate to form microfibrils, which are held together by hydrogen bonding between adjacent chains to form fibrils.⁸ A detail of the microfibril (circled area) is shown in Figure 1.3.

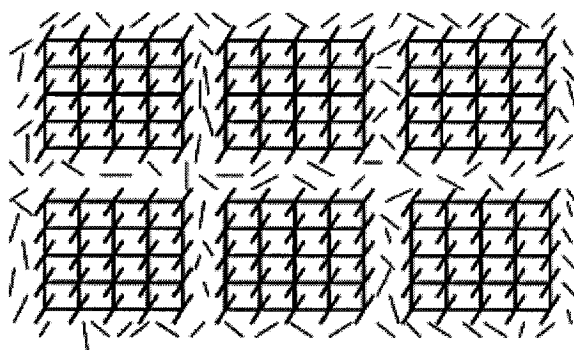


Figure 1.3. Cross-section of a microfibril composed of six elementary fibrils.⁸

The breakthrough in understanding native cellulose crystallography came in 1984, when Atalla and VanderHart showed by ^{13}C CP/MAS NMR that cellulose I was actually composed of two different crystal forms, cellulose I α and cellulose I β .^{17,18} An electron diffraction study on native algal cellulose several years later supported this model, suggesting a one-chain triclinic unit cell for cellulose I α and a two-chain monoclinic unit cell for I β , in both of which the molecular chains are arranged in parallel conformation.¹⁹ The I α phase is metastable and can be converted to the more stable I β form by annealing.^{20,21} Recent Synchrotron X-ray and fibre neutron diffraction studies have provided high-resolution coordinates for the atoms in the crystal structure of the polymorphs, as well as the positions of the hydrogen atoms involved in hydrogen-bonding.^{22,23}

The proportion of each crystal phase in a cellulose sample depends on the source of the cellulose; marine algae such as *Valonia* contain approximately two-thirds cellulose I α , while cellulose from higher plants, including wood and cotton cellulose, is mainly cellulose I β . Owing to its high degree of crystallinity, the crystallographic structure of *Valonia* cellulose has been extensively studied by several methods.²⁴⁻²⁹ Wood cellulose, on the other hand, is much less crystalline and has not been studied as much.

1.2.2 Cellulose nanocrystal suspensions

Cellulose microfibrils contain amorphous regions surrounding the crystalline regions and more or less randomly distributed along their length (Figure 1.3).^{30,31} The amorphous regions are what permit acid hydrolysis of cellulose to provide stable aqueous suspensions of insoluble colloidal cellulose particles. During acid hydrolysis, the amorphous regions act as structural defects (Figure 1.4), leading to transverse cleavage of

the microfibrils to give tiny monocrystalline fragments, “nanocrystals”, of cellulose.^{32,33} The less-dense amorphous regions have more rapid hydrolysis kinetics than the crystalline regions, as they are more susceptible to acid attack. In addition, the tight intermolecular hydrogen bonding of the crystalline regions effectively prevents the acid from penetrating into the crystal structure, making them less accessible to the acid. The resulting monocrystals have been (more-or-less interchangeably) called crystallites, microcrystals, nanocrystals, or whiskers.

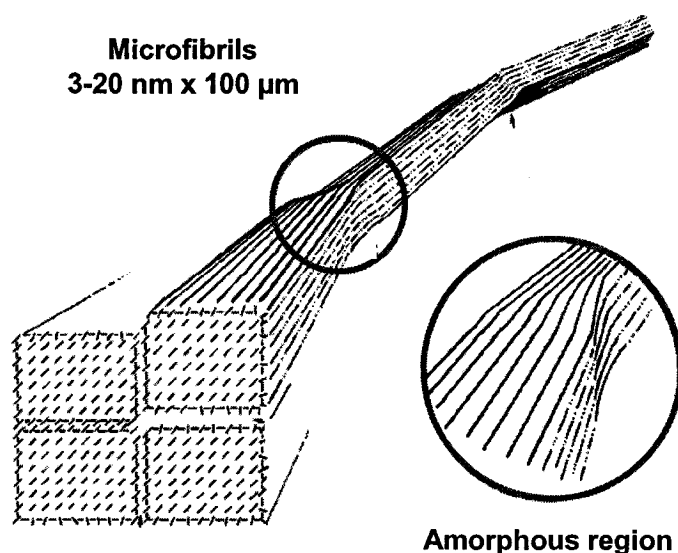


Figure 1.4. Each microfibril can be considered as a string of cellulose microcrystals linked by amorphous domains which act as structural defects.³⁴

Cellulose nanocrystals are rodlike in shape with an aspect ratio, L/D , where L is the length and D is the diameter, which can vary from 1 to 100. The degree of cellulose

crystallinity, degree of cellulose polymerization (DP)ⁱⁱ and the cross-sectional dimensions of the crystallites all depend on the cellulose source. For example, it is thought that cellulose chains have a DP of approximately 15 000 in cotton, and only 10 000 in wood.^{35,36} Cotton also has a higher degree of crystallinity than wood,^{35,37,38} rendering it less accessible to attack by acids.ⁱⁱⁱ Both factors tend to increase the L/D of cotton nanocrystals relative to wood nanocrystals, as well as the yield of nanocrystals per gram starting cellulose. Nanocrystal dimensions also depend, naturally, on the hydrolysis time, temperature, and acid concentration used to obtain them. Measured nanocrystal dimensions are also a function of the method used to measure them. For example, atomic force microscopy (AFM),^{24,39} transmission electron microscopy (TEM),⁴⁰ and light scattering^{41,42} all have inherent artifacts which affect the measured dimensions; see Chapter 2 for an example with AFM.

Rånby and co-workers were the first to discover that sulfuric acid-hydrolyzed cellulose fibers form stable suspensions of colloidal-sized crystals.⁴³⁻⁴⁵ The nanocrystals were found by electron microscopy to be approximately 50 nm long by 5–10 nm wide, which agreed with previous X-ray diffraction experiments.⁴⁶ Wood pulp and cotton were among the most widely-studied cellulose sources.^{47,48} The hydrolysis conditions for sulfuric acid and cotton cellulose have been optimized for yield and nanocrystal dimensions by Dong and co-workers.⁴⁹

The stability of the aqueous colloidal cellulose suspensions studied in this thesis is electrostatic in nature and is derived from sulfate ester groups randomly grafted onto the

ⁱⁱ The degree of polymerization also depends greatly on the purification process the cellulose has undergone.

ⁱⁱⁱ For this reason, all the suspensions studied in this thesis, apart from those in Chapter 2, are obtained from cotton cellulose.

cellulose nanocrystal surfaces by the sulfuric acid, imparting a negative charge to the nanocrystals (Figure 1.5).^{33,40,45,47,48,50-55} Hydrochloric acid has also been used to produce cellulose nanocrystals from bleached softwood kraft pulp.⁵⁴ In contrast to sulfuric acid, hydrochloric acid does not introduce charged surface groups, which means that HCl-prepared nanocrystal suspensions are not electrostatically stabilized. Post-sulfation of such nanocrystals by treatment with sulfuric acid⁵⁵ or by oxidation^{56,57} can provide similar levels of surface charge to sulfuric acid hydrolysis. All the cellulose suspensions studied in this thesis are produced by sulfuric acid hydrolysis; unless otherwise stated, the term “cellulose nanocrystals” will refer to nanocrystals obtained by this procedure.

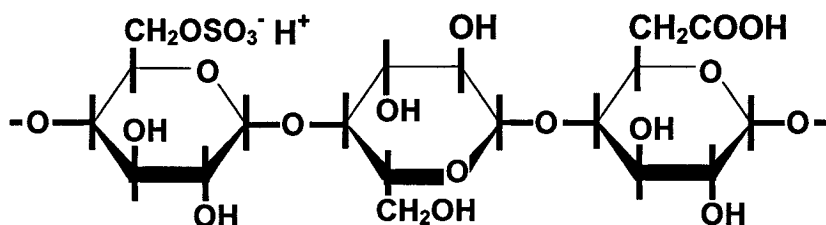


Figure 1.5. Schematic representation of the surface cellulose chains in a nanocrystal, showing sulfate groups introduced by the action of sulfuric acid. Weak carboxylic acid groups are also shown (see below).

Unmodified cellulose nanocrystals have polar hydrophilic surfaces and therefore form electrostatically stable suspensions in water. Dispersion in non-polar organic solvents is also possible if the nanocrystals are appropriately treated. Treatment methods include: coating the nanocrystals with surfactants such as Beycostat NA (to suspend them in

toluene and cyclohexane),⁵⁸ partial silylation of the nanocrystal surface (tetrahydrofuran, THF),⁵⁹ and grafting low molecular weight polyethylene glycol onto the surface (chloroform).⁵⁶ Redispersion of cellulose nanocrystals in polar organic solvents has also been achieved by partial surface silylation (acetone),¹ as well as in the absence of surfactants or chemical modification (dimethylformamide, DMF).⁶⁰ Recently, stable dispersions of unmodified cellulose nanocrystals were obtained in the dipolar aprotic solvents dimethylsulfoxide (DMSO) and DMF; a small amount of water appears to be critical to the suspension stability in this case.⁶¹

1.2.3 Characterization of cellulose nanocrystal suspensions

The stability of aqueous cellulose nanocrystal suspensions depends on the geometry and dimensions of the dispersed particles, their size polydispersity and surface charge. Transmission electron microscopy,⁶²⁻⁶⁴ atomic force microscopy,⁴⁰ and scattering techniques^{41,42} have been used to measure nanocrystal dimensions and polydispersity. It is possible to estimate the average length of the nanocrystals based on the residual degree of polymerization (DP):⁴⁵ Wood cellulose nanocrystals average 180–200 nm in length² and cotton nanocrystals average about 200–350 nm,³⁶ while Valonia (algal) and tunicate whiskers average greater than 1000 nm in length.^{2,24,36,62} Table 2.1 in Chapter 2 lists the lengths and cross-sectional dimensions of cellulose nanocrystals from various sources. As can be seen in Figure 1.6, cellulose nanocrystals tend to be quite polydisperse in length, due to the random nature of the acid hydrolysis, variation in hydrolysis conditions, and different percentages and distributions of amorphous regions in the cellulose microfibrils.^{2,51,65} The lateral dimensions have a much smaller distribution, presumably arising from the inaccessibility of the monocrystals to the acid.

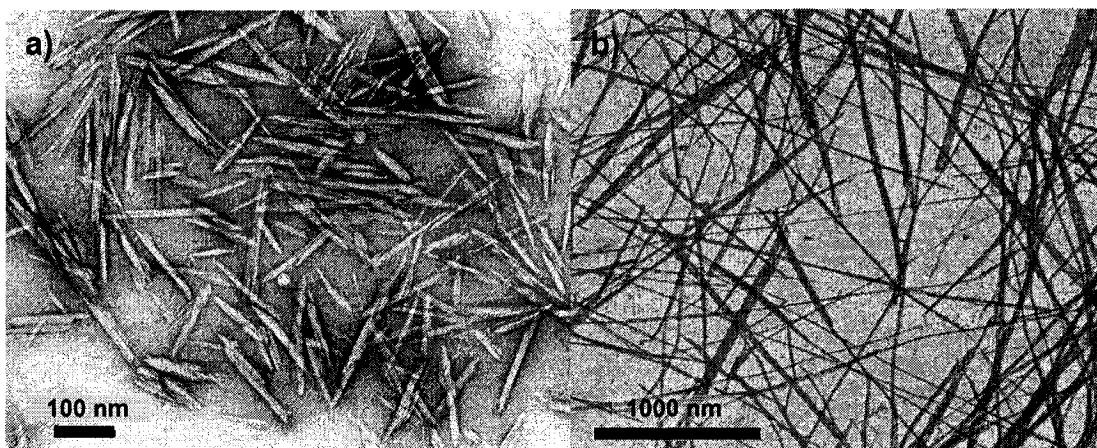


Figure 1.6. Transmission electron micrographs of a) cotton whiskers and b) tunicate whiskers. Images obtained by Jean-Luc Putaux, CERMAV-CNRS, France.

Conductometric titration and elemental analysis can be used to measure the sulfur content and surface charge density of the cellulose nanocrystals (see Chapter 2). Sulfur content depends on the hydrolysis conditions;^{40,49} typical values vary from 1 to 2 %.^{33,48} Typical charge densities, calculated based on average nanocrystal dimensions, vary from 0.2 to 0.3 e/nm², where e is the elementary charge. Araki et al. found a surface charge density of 0.155 e/nm² for nanocrystals prepared from wood pulp.^{54,55} Nanocrystals prepared by HCl hydrolysis exhibit negligible surface charge densities, as they contain only a few weak carboxylic acid groups.⁵²

The anisometry (axial ratio $\gg 1$) and appreciable surface charge of cellulose nanocrystals result in suspensions which have highly-sensitive phase separation behaviour, as discussed below. These attributes also influence their rheological behaviour such as viscosity and shear thinning;⁶⁶ the introduction of surface charge in particular reduces the viscosity relative to uncharged nanocrystals, due to self-ordering of the

ordered phase.⁵⁵ These properties, along with optical and orientation properties, and the use of nanocrystals in nanocomposites, are discussed in two recent reviews.^{67,68}

1.3 LIQUID CRYSTALLINE PHASES OF CELLULOSE NANOCRYSTAL SUSPENSIONS

Liquid crystalline behaviour of cellulose suspensions was first reported by Rånby in 1951.⁴⁵ However, it was not until more than four decades later that detailed study of this system was begun.⁴⁷ This section begins with an introduction to liquid crystal phases followed by a closer examination of the liquid crystalline behaviour of cellulose derivatives and cellulose nanocrystals.

1.3.1 Liquid crystals

Liquid crystals are an intermediate state of matter having the characteristics of both liquids (fluidity) and solids (some long-range order and anisotropy). They are typically formed by anisotropic molecules or particles that are rigid and rodlike.⁶⁹ Figure 1.7 illustrates the classification of liquid crystals according to the arrangement of the particles. Nematic liquid crystals possess orientational order, but no positional order, as the rods are free to slide or roll past each other. Smectic phases have a higher degree of positional order, as the rods are arranged in layers with their long axes perpendicular to the plane of the layers.

Chiral nematic liquid crystals possess a further degree of order compared to smectic and nematic textures. The rods are aligned parallel to each other and to the plane of the layer, each layer being rotated slightly with respect to the layers above and below it,^{iv} thereby giving the liquid crystal a long-range helical order. The pitch of the helix is

^{iv} Because the rods are free to move perpendicularly to the plane of the layer (i.e. they do not have any positional order in this direction), the term “pseudo-layer” or “quasi-nematic layer” is more appropriate.

defined as the distance required for the layers to make one full rotation about a line perpendicular to the layers (the chiral nematic or cholesteric axis).

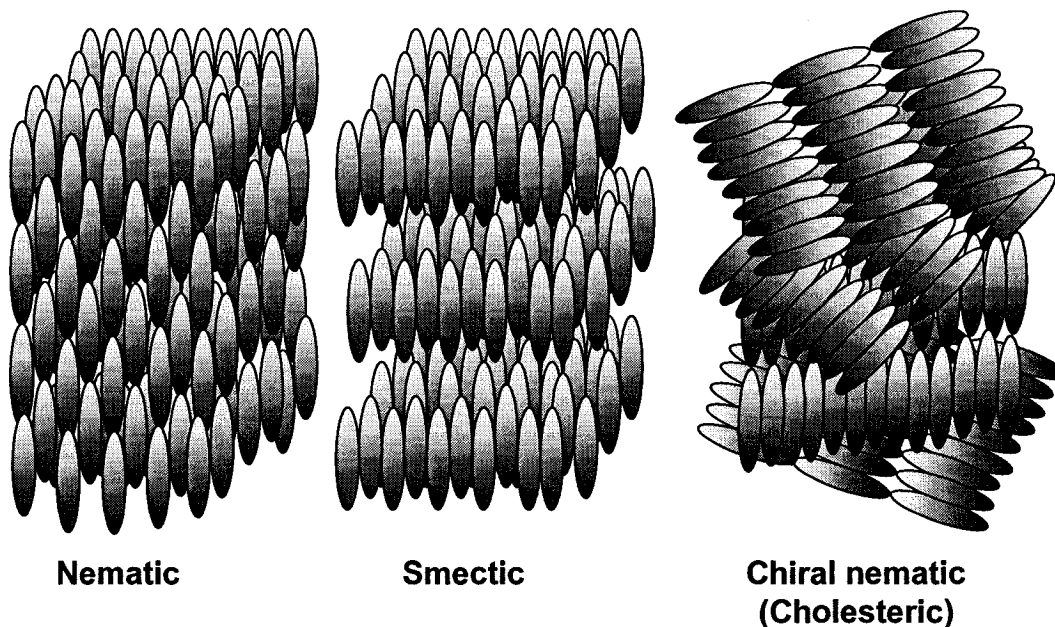


Figure 1.7. Schematic diagram of the different types of liquid crystal structure.

The phase transition from an isotropic liquid to an ordered liquid crystal can be effected by a change in temperature (thermotropic mesomorphism) or a change in concentration of the system (lyotropic mesomorphism).⁷⁰ Lyotropic colloidal liquid crystals were first recognized in the 1920s by Zocher, who investigated nematic textures in solutions of colloidal rodlike V_2O_5 particles.⁷¹⁻⁷³ Similar lyotropic isotropic–nematic transitions of colloidal particles were later reported by Langmuir for clay platelets⁷⁴ and Bawden et al. for tobacco mosaic virus (TMV) rods.^{75,76} More recently, the isotropic–nematic transition has been observed in systems of polytetrafluoroethylene (PTFE) whiskers,⁷⁷ other stiff

viruses such as fd bacteriophage and M13 virus,⁸⁶⁻⁸⁹ rodlike micelles of amphiphilic surfactants,⁷⁸ and colloidal boehmite rods.^{79,80}

Cellulose nanocrystal suspensions also form lyotropic liquid crystals. Figure 1.8 shows a suspension of cellulose nanocrystals which has formed a chiral nematic liquid crystal phase.

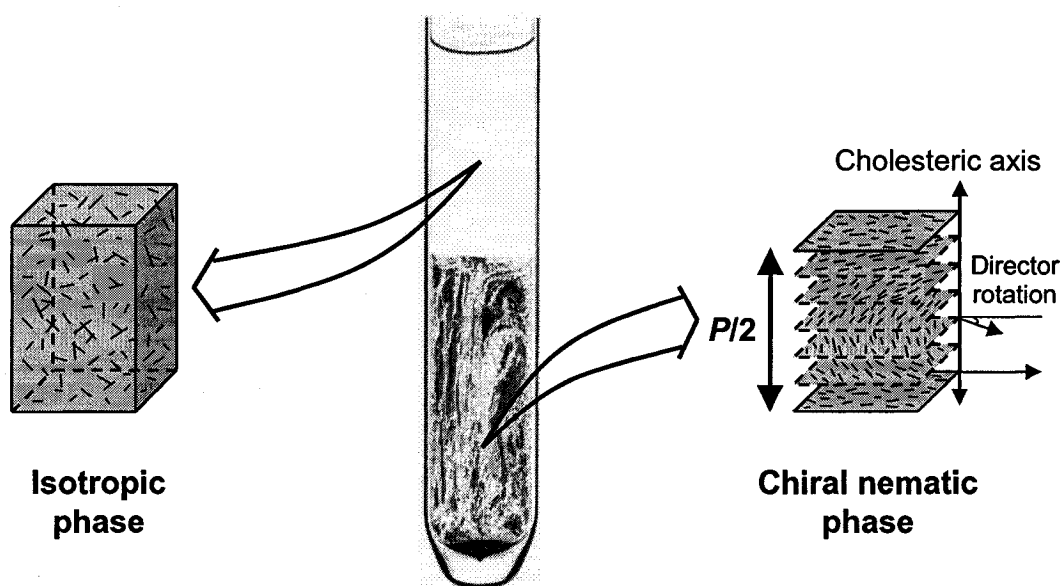


Figure 1.8. A suspension of cellulose nanocrystals viewed between crossed polarizers, displaying an upper isotropic phase and a lower chiral nematic phase (helical packing of several nematic planes in which the rods are aligned on average with a vector). Half a pitch, $P/2$, is shown in the diagram.

Chiral nematic cellulose nanocrystal liquid crystals form two optical “textures” which are identifiable when a sample is placed on a light microscope stage between two linear polarizers crossed at 90° . The birefringence (anisotropic refractive index; $\Delta n \approx 0.05$) of

the cellulose nanocrystals and the order of the liquid crystal allow light to pass through areas of the sample. The planar texture is observed when the cholesteric axis is parallel to the viewing direction; disclinations show up between crossed polars as dark lines against a coloured background.⁸¹ When the cholesteric axis is perpendicular to the viewing direction, a characteristic “fingerprint” texture is seen, in which dark and light lines alternate, the width of each line corresponding to one quarter of the chiral nematic pitch (Figure 2-E in Chapter 2).

1.3.2 Liquid crystalline phases of cellulose derivatives

Liquid crystalline properties of cellulose derivatives were discovered in 1976 by Werbowyj and Gray, who found that concentrated aqueous solutions of hydroxypropyl cellulose (HPC) appeared to form the helicoidal structure of a cholesteric liquid crystal.⁸² Acetoxypropyl cellulose was subsequently found to exhibit thermotropic cholesteric liquid crystal phases,⁸³ in contrast to the lyotropic HPC.⁸⁴ Other cellulose derivatives including ethyl cellulose and ether and ester derivatives of HPC in various solvents including water, methanol and acetic acid were studied. The handedness of the chiral nematic helices was found to vary with the substituents on the cellulose backbone,^{85,86} as well as with the solvent.⁸⁷

1.3.3 Liquid crystalline phases of cellulose nanocrystals

Liquid crystal phases of cellulose nanocrystals are easier to work with than molecular cellulose derivatives for several reasons. Because molecular cellulose derivatives are somewhat flexible, they do not behave as predictably as the rigid rodlike nanocrystals. In addition, concentrated solutions (55–70 % for HPC⁸²) of these polymers are required to obtain the liquid crystal phase, which makes handling the viscous solutions difficult.

Cellulose nanocrystals, in contrast, begin to form chiral nematic phases at concentrations of only 1–7 wt%, depending on their axial ratio.^{49,52,88}

In order to understand the liquid crystal phase behaviour of cellulose nanocrystals, it is necessary to understand how and why the phases form. It seems counterintuitive that randomly-distributed particles should spontaneously align to give an ordered phase, and even more counterintuitive that entropy should be the driving force behind this phenomenon. However, this is the case, as explained below.

1.3.3.1 Stability of colloidal suspensions

To model the stability of electrostatically stabilized colloids, Derjaguin, Landau, Verwey and Overbeek (DLVO) theory can be used. It combines the effects of van der Waals attractions, present for all particles, and the effects of electrostatic repulsions, determining the dominant force as a function of particle separation. The total potential energy of interaction between the colloids is the sum of the repulsion energy and the attraction energy, as shown in Figure 1.9. At very small interparticle separations, steep hard core repulsion is experienced, such as that exhibited by sterically stabilized colloids such as boehmite rods grafted with polyisobutylene (PIB).⁷⁹

The positive energy barrier between the secondary and primary minima prevents the colloidal particles from coming into contact and aggregating. A higher energy barrier arises when the particle surface potentials are larger, leading to more stable suspensions. If the surface charge is negligible, as for HCl-hydrolyzed nanocrystals, or excess ionic strength is present to screen the electrostatic double layer repulsions, the suspension becomes unstable and the particles precipitate or flocculate.

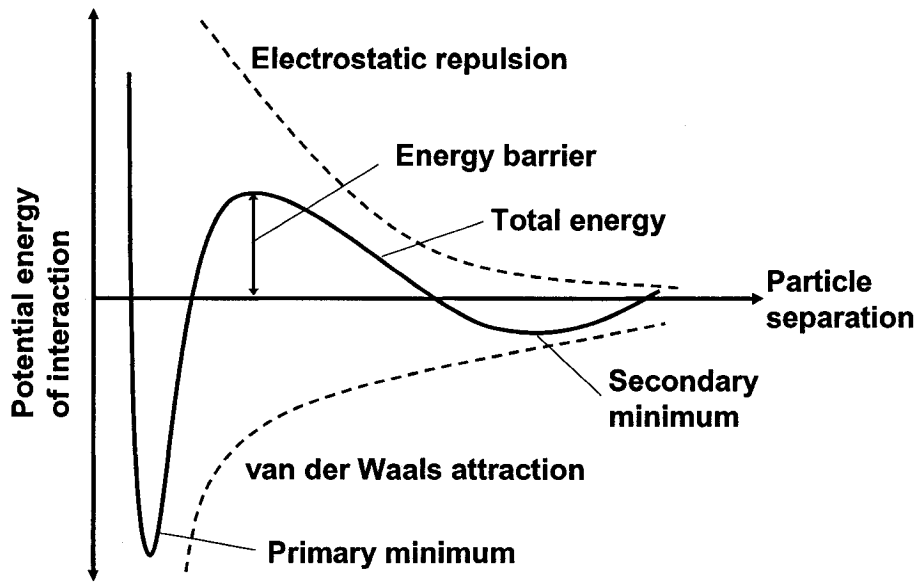


Figure 1.9. Schematic representation of the total energy of interaction between two colloidal particles, according to DLVO theory.

Even if they are electrostatically stabilized, the random behaviour of the colloidal particles is altered as their concentration in suspension increases. For N hard particles in a volume V , the free volume V_{free} available to the particles is only a fraction of the total volume because each particle excludes the other particles from a certain volume surrounding it. This reduces the total number of configurations available to the set of N particles and therefore lowers the system entropy. At a given density of colloidal particles, it can be demonstrated that if the excluded volume regions overlap, the free volume available to each particle increases, thereby increasing the entropy of the system and decreasing its free energy. In order to achieve this more thermodynamically favourable state, the system must phase shift to maximize the free volume.

The plot in Figure 1.10 shows qualitatively the calculated free energy for both the fluid phase and solid phase of a suspension of colloidal spheres as a function of the suspension

density. It can be seen that at low densities, the random fluid phase is favoured, while at high sphere densities, the close-packed solid phase is more stable.⁸⁹ The system thus undergoes a phase shift in order to maximize its free volume and hence its entropy.

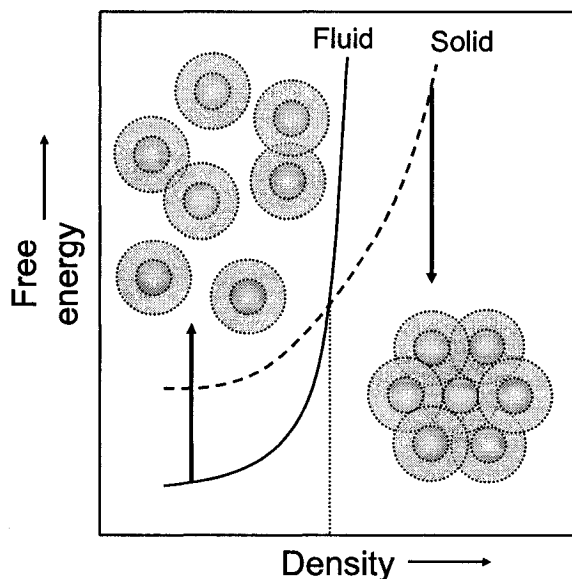


Figure 1.10. Qualitative representation of the free energy of a dispersion of colloidal spheres as a function of the sphere density for the fluid (random) and solid (ordered) phases. At low particle densities, the fluid phase is energetically favoured, while above a critical density (dotted line), the solid phase becomes more stable and a phase transition occurs. Adapted from Baus et al. (1996).⁸⁹

1.3.3.2 Onsager theory for the isotropic–nematic phase separation of neutral rodlike particles

Phase shifts are also observed in suspensions of rod-like particles for entropic reasons. The Onsager theory⁹⁰ is a cornerstone in the theory of liquid crystal phase formation for systems of long monodisperse rodlike particles. It accurately predicts an isotropic to

nematic transition, and although the predicted critical concentration of the phase transition is far from typical experimental values, it provides a simple explanation for the phase separation of dispersions of repulsive rodlike particles. The theory is based on the free energy of rigid rods in the limit of the second virial coefficient. The second virial coefficient was obtained by averaging the excluded volume over the equilibrium distribution of orientations at the minimum free energy. For a pair of rods with a high axial ratio ($L_1 \gg D_1 + D_2 \ll L_2$), the excluded volume is given by

$$L_1 L_2 (D_1 + D_2) \sin \gamma \quad (1.1)$$

where γ is the angle between the rods.

The angular dependence function of the excluded volume of a pair of long rods gives a maximum when the rods are oriented perpendicularly to each other, and a minimum when they are parallel. For charged rods, the potential of the average force ω between two cylindrical particles based on the Poisson-Boltzmann equation for electric potential is a minimum when the rods are oriented perpendicularly to each other and a maximum when they are parallel. The potential of average force between the rodlike particles at the equilibrium state must be calculated by summing over the total number of particles in the system. The free energy, osmotic pressure and chemical potential can then be found in terms of the average force.^v Assuming the forces to be pairwise additive, two-particle and three-particle interactions can be evaluated and used to correct the average force as first- and second-order correction terms (virial coefficients). The two-particle interaction term, β_1 , given by

^v In order for the isotropic and anisotropic phases to coexist, their chemical potential and osmotic pressure must be equal.

$$\beta_1 = \frac{1}{V} \int f_{12} d\tau_1 d\tau_2 \quad (1.2)$$

where τ is a volume element and V is the volume of the system, is equivalent to the excluded volume above (equation 1.1); the more complex three-particle interactions were approximated by Onsager, who limited the theory to dilute suspensions in which two-particle interactions predominate.⁹⁰ The free energy of the system can then be calculated using the virial coefficients.

The Onsager theory is somewhat restricted as it is accurate only in the limit of very long rods, i.e. $L/D \rightarrow \infty$, and low particle concentration. However, in this limit, excellent agreement between experiment and theory has been observed for suspensions of monodisperse rods.⁹¹

Another way of looking at the Onsager theory is to consider the entropy of the particles. The anisotropy of the rods means that in addition to positional or translational entropy of the spheres, the particles also have orientational entropy. When the ordered phase is formed, the system's orientational entropy is decreased (the density of particles is no longer uniform), but the gain in translational entropy more than offsets this loss. Thus, the phase transition is a purely entropic one, based on particle shape.^{vi} The critical concentration for phase separation is determined only by the axial ratio L/D :⁹⁰

$$\phi_i = 3.34 D/L \quad (1.3)$$

$$\phi_a = 4.48 D/L \quad (1.4)$$

where ϕ_i and ϕ_a are the volume fractions of the rods in the isotropic and anisotropic phases, respectively. That is, ϕ_i represents the critical concentration at which the nematic

^{vi} Attractive forces are therefore not required for ordered phase formation in these systems.

phase initially forms from an isotropic suspension and ϕ_a represents the (higher) concentration at which the suspension becomes completely anisotropic. Between these two concentrations, the suspension will separate into two phases.⁹⁰ As shown in Figure 2.4, this region spans a range of approximately 5–8 wt% for cellulose nanocrystals. It can be seen in equations 1.3 and 1.4 that longer rods decrease the critical concentration for anisotropic phase formation. That is, longer rods experience a larger excluded volume effect: Suspensions of boehmite rods with an axial ratio of 20 were found to phase separate, while rods of axial ratio 8 did not.⁸⁰ Fractionation of longer rods into the anisotropic phase was also predicted by Onsager,⁹⁰ and has been observed for cellulose nanocrystals.⁴⁰

Other theories such as the lattice-based theories of Flory and co-workers⁹²⁻⁹⁸ and DiMarzio,⁹⁹ also model the phase separation behaviour of liquid crystalline polymers, for example at higher densities and in length-bidisperse systems. However, these theories are qualitative and do not lead to the exact Onsager results for infinitely thin hard rods.

Experimentally, systems of sterically-stabilized rods are used to approximate hard-core rod-rod repulsions, for example the PIB-grafted boehmite particles mentioned above.⁷⁹ The slender fd virus, although it is highly charged, also leads to results in agreement with Onsager's theory when the double layer is taken into account.¹⁰⁰ In some systems, the particle length can be tailored to obtain bidisperse or polydisperse systems to examine the effect on the phase separation behaviour.⁷⁹ For example, broadening the particle length distribution introduces curvature into (and increases the range of) the biphasic coexistence region of the experimental phase diagram and increases the coexisting phase concentrations ϕ_i and ϕ_a with increasing particle concentration according to a lattice

theory of the phase separation of rodlike particles.¹⁰¹ Such curvature has been seen for sterically stabilized boehmite rods¹⁰² as well as cellulose nanocrystals.¹⁰³

It is worth noting that the free energy difference between a chiral nematic phase and a nematic phase is much smaller than the free energy difference between an isotropic phase and an anisotropic phase of rod-like particles.⁷⁰ Experimental data for chiral nematic liquid crystals can therefore be compared with theories developed for nematic phases.

1.3.3.3 Isotropic–chiral nematic phase separation of cellulose nanocrystal suspensions

After the hydrolysis conditions for obtaining cellulose nanocrystals were optimized,⁴⁰ Marchessault and co-workers in 1959 and Hermans in 1963 demonstrated that such suspensions displayed nematic liquid crystalline order.^{51,104} Marchessault reported macroscopic birefringence of cellulose whisker suspensions observed through crossed polarizers, due to the birefringence of the nanocrystals as well as to a flow anisotropy resulting from the alignment of the nanocrystals under shear.⁵¹ In 1992, Revol and co-workers showed that the suspensions in fact formed a cholesteric, or chiral nematic, liquid crystalline phase.⁴⁷

As the concentration of cellulose nanocrystals is increased, phase separation proceeds as follows: In dilute (isotropic) suspensions, spherical “droplets” of ordered nanocrystals called tactoids form and are visible by polarizing microscopy.⁴⁸ Order in dilute cellulose nanocrystal suspensions has also been observed using static and dynamic light scattering¹⁰⁵ and ultra-small-angle X-ray scattering, by which almost identical scattering profiles were found for the anisotropic and isotropic phases.¹⁰⁶ As the cellulose concentration increases, the tactoids coalesce to eventually give an anisotropic phase once a critical concentration has been reached. The ordered phase, as has been stated,

displays the optical characteristics of a chiral nematic liquid crystal.^{33,47,48,51,52} Interestingly, the concentrations of cellulose nanocrystals in the two phases do not differ greatly from each other, in contrast to similar coexisting phases of, e.g., ionic polymer latex particle dispersions.¹⁰⁷ A typical chiral nematic pitch for cotton nanocrystals is between 10–25 μm .⁴⁷

It is interesting to consider the self-ordering of rodlike cellulose nanocrystals to form a chiral nematic phase as opposed to a nematic phase when one remembers that there is no enthalpic advantage in forming the chiral nematic organization over the nematic. The molecular chirality of cellulose (section 1.2.1) cannot be transmitted between the rods because the distances separating them are too great, being on the order of 20–40 nm.^{108,109} The arrangement of charged groups in a spiral on the nanocrystal surface has also been ruled out.⁵⁶ Packing by chiral interaction of twisted rods in order to minimize excluded volume has been proposed:^{108,110} Although the nanocrystal separation prevents actual physical contact, the electrostatic double layer surrounding the rods may be thick enough to transmit the chiral twist if it is of the same order as the lateral dimensions of the rod.¹¹¹ A helicoidal organization of opposite handedness to the twist along the nanocrystals would be generated from this interaction. The formation of chiral nematic phases by PEG-grafted nanocrystals⁵⁶ and rodlike fd virus,¹¹² as well as surfactant-stabilized cellulose nanocrystals in nonpolar solvents⁵⁸ supports this hypothesis.

The order of liquid crystalline phases of cellulose nanocrystals can be enhanced by placing them in an applied magnetic field.¹¹³ Such ordered suspensions have been used as a medium in which to measure residual dipolar coupling of proteins by C' decoupled ^1H – ^{15}N IPAP-HSQC¹³ NMR.¹¹⁴

1.3.3.4 Effect of the polyelectrolytic nature of cellulose nanocrystals on phase separation

Interparticle electrostatic interactions have a large effect on the free energy of the system. They provide stability and promote order: The addition of salts screens the electrostatic charges, destroying the order of anisotropic cellulose nanocrystal suspensions¹⁰⁶ and causing them to flocculate.⁵² As Flory stated, "...the importance of electrical forces in bringing about separation of a dilute anisotropic phase from an even more dilute solution of highly anisotropic particles ... is clearly indicated, for the effect with (TMV) vanishes ... at salt concentrations exceeding 5×10^{-3} M. *The phase separation ... is not adequately explained by consideration of particle asymmetry alone.*"⁹²

According to Onsager's theory for neutral rods, the axial ratio determines the critical concentration for phase separation. Cellulose nanocrystals, while rodlike, are far from being infinitely long rods (typical axial ratios lie in the range 20–30 for cotton), and moreover are not electrostatically neutral owing to the charged sulfate groups on their surfaces. As previously stated, they also have quite large length distributions. It is therefore not surprising that the phase behaviour of this system agrees only qualitatively with Onsager's theory; the experimental critical concentration tends to be higher than the theoretical value.⁵² The critical concentration and the width of the biphasic coexistence region of suspensions of polyelectrolytic rodlike particles are also very sensitive to variables such as length polydispersity, axial ratio,^{vii} surface charge density, solution ionic strength and the nature of the counterions.^{54,55,113,115}

^{vii} The first two variables naturally apply to monodisperse neutral rods as well.

The stability and phase separation behaviour of polyelectrolytic cellulose nanocrystals is very sensitive to changes in inter-rod interactions such as electrostatic repulsion, steric interactions, hydrophobic and hydration forces.¹¹³ The nature (e.g. size, hydrophobicity) of the counterions associated with the sulfate groups is therefore also an important consideration. Inorganic counterions tend to increase the critical concentration – in other words, to decrease the tendency for ordered phase formation – in the order $\text{Na}^+ < \text{K}^+ < \text{Cs}^+$, most likely due to decreasing repulsive hydration forces as the hydration number and hydrated ion size decrease as one goes down the periodic table. For bulky organic counterions, the phase equilibrium is governed by a balance between hydrophobic attractions and steric repulsions.^{56,113}

1.3.3.5 Theoretical treatment of the phase separation of charged rodlike particles

As seen in section 1.3.3.2, Onsager took the electrostatic repulsion of charged particles into account by treating the double layer as part of the particle, with the effect of increasing the effective particle diameter.⁹⁰ However, the phase separation still could not be accurately predicted, despite taking the electrostatic double layer into account up to the second virial coefficient.

Other theories have been developed to predict the phase separation of rodlike polyelectrolytes.¹¹⁶⁻¹¹⁹ Stroobants, Lekkerkerker and Odjik's theory (SLO theory) of the phase equilibrium of charged rods modifies Onsager's equations to account for the increased effective rod diameter (D_{eff}) as well as a twisting effect h characterizing the electrostatic interactions between the charged rods: A perpendicular orientation between two rods minimizes the repulsion between them, while the larger effective diameter favours a parallel orientation to minimize the effect of the amplified excluded volume

and consequent increase in free energy. The magnitude of the twisting effect is given by h , which represents a balance between the electrostatic and entropic factors. The coexisting number densities C_i and C_a of the rods in the isotropic and anisotropic phases are given by the SLO theory by the following equations:¹²⁰

$$C_i = 3.290[(1 - 0.675h)b]^{-1} \quad (1.5)$$

$$C_a = 4.191[(1 - 0.730h)b]^{-1} \quad (1.6)$$

where h is the twisting factor and b is the second virial coefficient of the system. The values of h and b are given by

$$h = (\kappa D_{\text{eff}})^{-1} \quad (1.7)$$

$$b = \frac{\pi}{4} L^2 D_{\text{eff}} \quad (1.8)$$

where κ^{-1} is the Debye length (electrostatic double layer “thickness”) and L is the rod length. The effect of the increase in effective diameter due to the electrostatic double layer is to decrease C_i and C_a relative to analogous neutral rods. Dong et al. (1996) showed that particle dimensions and ionic strength govern the phase separation of cellulose nanocrystal suspensions.⁵² Ionic strength affects phase separation by screening out the electrostatic repulsions of the surface sulfate groups, thereby reducing the effective rod diameter. Increasing the sodium chloride concentration from 0.13 to 1.95 mM increased the critical concentration for phase separation from 6.5 to 9.0 wt% cellulose. The same effect can be observed by examining the volume fraction of anisotropic phase which decreases as salt is added. Figure 1.11 summarizes the effects of ionic strength on the phase separation behaviour of cellulose suspensions.

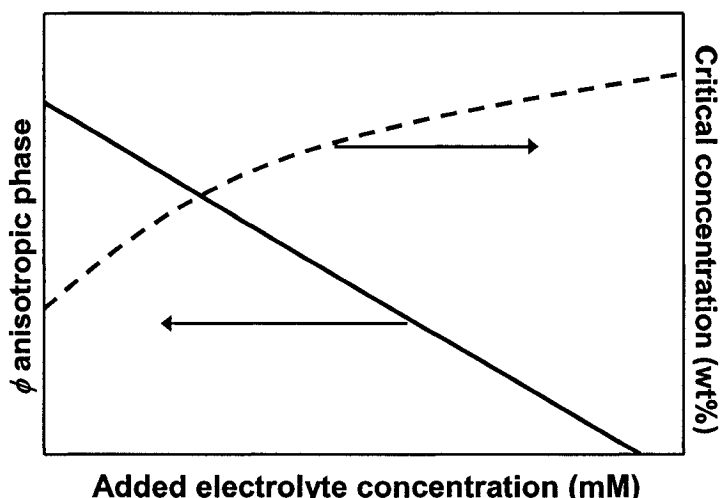


Figure 1.11. Summary of the effects of added electrolyte on the phase separation behaviour of a suspension of cellulose nanocrystals at constant concentration.

The chiral nematic pitch of the anisotropic phase also decreases as the solvent ionic strength increases, indicating a strengthening of chiral interactions, which are thought to be screened by the electrostatic double layer.⁵² Experimental results for cellulose and other systems are not in complete agreement with SLO theory, possibly because of factors such as difficulty in estimating the contribution of the polyionic particles to the ionic strength of the system.^{115,121}

1.4 ADDITION OF MACROMOLECULES TO CELLULOSE NANOCRYSTAL SUSPENSIONS

As discussed in the previous section, the stability of colloidal particles in suspension depends on the forces acting between them. DLVO theory of colloid stability examines the contributions of attractive van der Waals forces and electrostatic repulsion between charged particles. The balance between these forces determines whether the particles remain suspended or form reversible or irreversible aggregates or gels.

When a non-adsorbing macromolecule is added to a suspension of colloidal particles, a new attractive force develops and acts between the particles, although there is no direct interaction between any of the particles or the added macromolecule. The action of this force produces phenomena unaccountable for by DLVO theory alone. For example, for many years, X-ray crystallographers added polyethylene glycol (PEG) to protein suspensions to induce crystallization without having a complete theoretical understanding of the mechanism.^{122,123} Asakura and Oosawa^{124,125} and Vrij¹²⁶ explained this attractive force according to the depletion model described below.

1.4.1 The depletion attraction

When free, non-adsorbing polymer is added to a suspension of colloidal particles, a shell with thickness equal to the polymer's radius of gyration R_g is excluded to the centres of mass of ideal polymers in solution (Figure 1.12). When the colloids are far apart, a uniform osmotic pressure is exerted on the particles. When the colloids approach at distances less than $2R_g$, the excluded volumes overlap and the total free volume available to the polymers increases. As a result, the osmotic pressure is unbalanced and tends to drive the colloidal particles together; an *effective* attractive force acts on the particles. This lowering of the free energy is the driving force for depletion flocculation, or, under the right circumstances, for phase separation of the system. The range of the depletion attraction potential $U_{\text{dep}}(R)$ is determined by the radius of gyration R_g of the polymer, and its depth or strength is determined by the concentration of the macromolecules in solution:¹²⁵

$$U_{\text{dep}}(R) \approx \Pi_p V_{\text{ov}}(R) \quad (1.9)$$

where Π_p is the osmotic pressure of the polymer, and V_{ov} is the overlap volume of

neighbouring depletion layers. At low polymer concentrations, the mixing entropy dominates in binary macromolecule–colloid suspensions, but at higher concentrations, the translational entropy dominates, and phase separation occurs to minimize the free energy of the system. Adding a polymer thus shifts the system’s critical point to a more “accessible” location in its phase diagram. The net attractive potential is intensified when the polymer contains electric charges, because the osmotic pressure and molecular dimensions of polyelectrolytes are greater than those of analogous nonionic polymers.¹²⁵

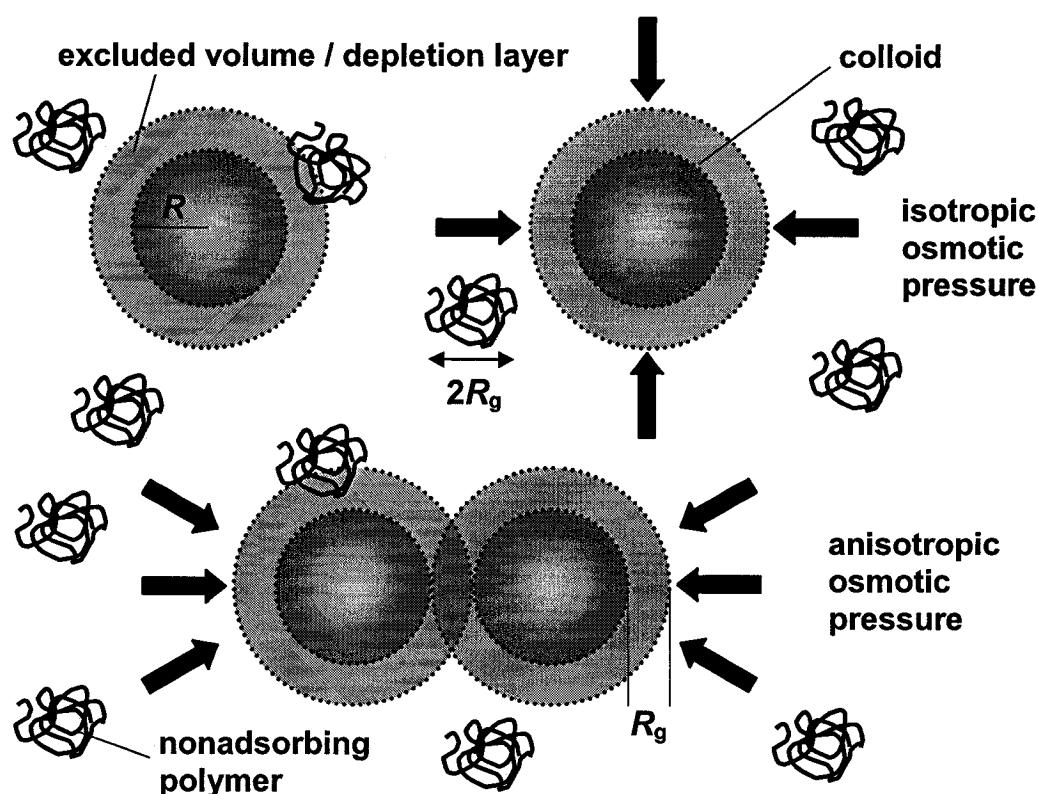


Figure 1.12. The depletion mechanism. Free, non-adsorbing polymers are excluded from a shell of thickness R_g surrounding the colloidal particles of radius R . Initially, the osmotic pressure exerted on the colloids is uniform (top). As the colloids approach, the polymers cannot penetrate into the shaded volume. The osmotic pressure on the colloids becomes uneven (bottom), leading to an effective attraction between the particles.

1.4.2 Theories of depletion attraction for spherical colloid + polymer coil mixtures

Following other workers' attempts to predict the phase diagrams of colloid-polymer mixtures using thermodynamic perturbation theory,^{127,128} Lekkerkerker and co-workers used a statistical mechanical model to treat the phase behaviour of a spherical colloid and nonadsorbing polymer mixture.¹²⁹ This approach has the advantage that it does not assume that the polymer concentration is the same in coexisting phases, which assumption directly contradicts experimental observations of polymer partitioning between the phases in polystyrene latex-dextran systems.^{130,131} The colloid particles are assumed to be hard spheres and the polymers are treated as freely interpenetrable coils. A phase diagram similar to that predicted by Flory (see section 1.4.3) was obtained, and three-phase gas-liquid-crystal coexistence was predicted for certain conditions.¹²⁹

Depletion attraction has been thoroughly verified experimentally. Direct measurements of the potential of mean force have been obtained for several model systems.¹³²⁻¹³⁴ It has been found through the study of these model colloid-polymer mixtures, for example nearly-hard-sphere particles of polymethyl methacrylate (PMMA) and random-coil polystyrene (PS) dispersed in simple hydrocarbon solvents,^{135,136} that the depletion-induced attraction is not sufficient in itself to cause the separation of a "vapor" phase from a "liquid" colloid phase.^{viii} The *range* of the attraction must be sufficiently long; that is, the polymer must be sufficiently large in comparison to the colloidal particles.

Additionally, there have been many experimental studies of depletion-driven phenomena, particularly of phase behaviour in model colloid systems such as polystyrene latex mixed with water-soluble polymers¹³⁸⁻¹⁴⁰ and PMMA mixed with PS in cis-

^{viii} These phases are "thermodynamically stable phases of dilute and dense disordered arrangements of diffusing particles"¹³⁷ and can be considered analogous to the isotropic and anisotropic phases of rodlike particles.

decalin.¹³⁵ It was found that the polymer–colloid size ratio is the key factor determining the topology of the phase diagram for the latter system. In fact, it has been shown that if a physical property of the polymer, such as shape or flexibility, differs enough from that of the colloid, bulk demixing can occur.¹⁴¹ Small rods have been used as depletion agents for much larger colloidal spheres, for example.¹⁴²

1.4.3 Theories of phase behaviour of rodlike colloid + polymer coil mixtures

Using a lattice-based theory, Flory examined the phase equilibria of athermal mixtures of rodlike solutes and random coiled chains in a solvent.⁹⁷ The diameters of all three components were considered equal and rods of axis ratio 10 to 100 were simulated. The length L and the diameter D of the rods, and the effective radius $\sigma/2$ of the polymer coils are related by $D/2 \ll L \sim \sigma/2$. For all axis ratios, addition of coils to the biphasic rod–solvent system increased the volume fraction of rodlike particles in the anisotropic phase^{ix} and broadened the isotropic–anisotropic coexistence region. The coils were found to partition almost exclusively into the isotropic phase, preferentially replacing the rodlike particles rather than the solvent. That is, the overall concentration of solute in the isotropic phase increased very little with addition of the coils to the binary system. For rods with the highest axis ratios (which therefore give results that most closely agree with Onsager theory), this partitioning occurred at relatively low concentrations of the rodlike particles.

Figure 1.13 shows a schematic drawing of a phase diagram of a system of rodlike particles and polymer coils. The downward slope of the isotropic phase boundary indicates that the rod density in the isotropic phase decreases as the polymer coil

^{ix} The loss of orientational entropy is more than offset by the gain in translational entropy.

concentration increases; this is because as the coils partition into the isotropic phase, the osmotic pressure in the isotropic phase increases; to balance this, cellulose rods migrate from the isotropic to the nematic phase, causing the widening of the biphasic region. The tie lines, which join the coexisting isotropic and nematic phases, slope downwards, indicating that the coiled polymer has a greater concentration in the isotropic phase.

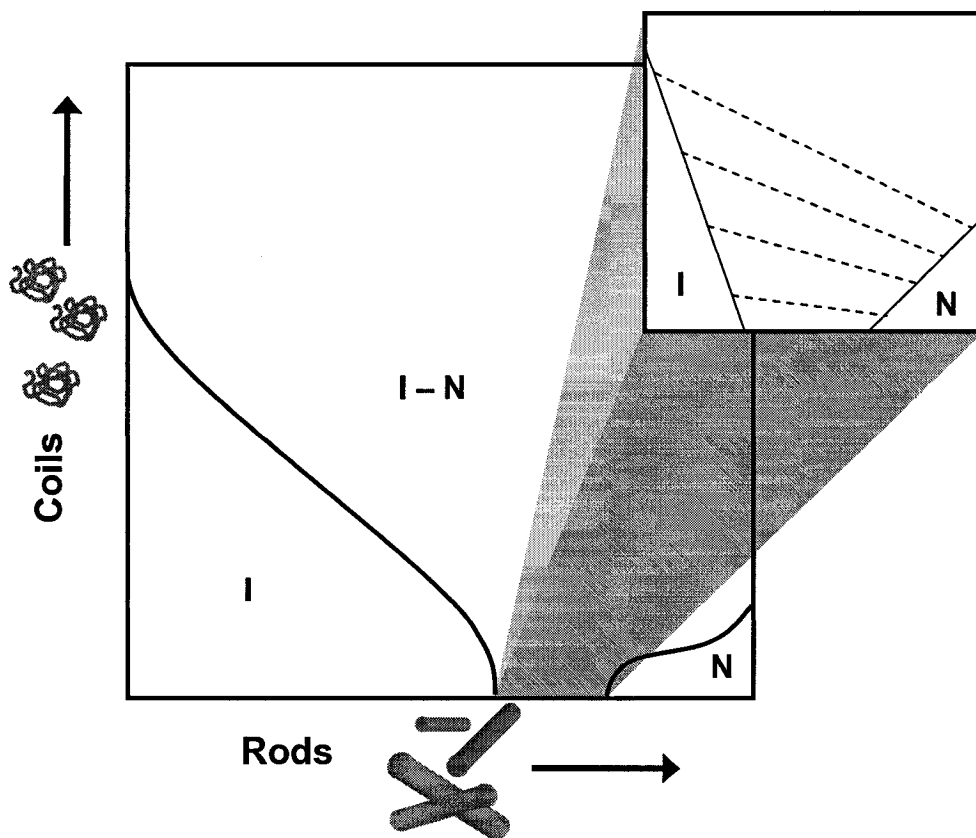


Figure 1.13. Theoretical phase diagram for a mixture of rodlike particles and coiled polymer. The isotropic-nematic coexistence region is broadened by the addition of coiled polymer. As the coil concentration increases, the rod density in the isotropic phase decreases. The downward-sloping tie lines indicate that the coiled polymer partitions into the isotropic phase. The inset shows the region in which most experiments in this thesis are performed.

A later theory¹⁴³ obtained the attractive depletion force by calculating the overlap of the excluded volume shells of a pair of hard rods and employing a virial expansion of the free volume available to the polymer, truncated at the second virial level. An expression for the free energy of the system was then obtained in terms of an orientational distribution function and calculated numerically. The isotropic-nematic phase transition is also widened by addition of the polymer, and the polymer is predicted to partition into the isotropic phase, albeit to a much lesser extent than predicted by Flory's theory. The dimensions of the particles in this theory are related by $\sigma/2 \sim D/2 \ll L$; like Onsager's theory, it is limited to very long hard rods as well as very low polymer concentrations.

Lekkerkerker and Stroobants¹⁴⁴ examined the phase behaviour of rodlike colloid and flexible polymer mixtures using the same statistical mechanical model as mentioned above.¹²⁹ However, their treatment is not limited to the second virial level and is valid for shorter rods and higher polymer concentrations.¹⁴⁴ At large L/D values, isotropic-nematic equilibria are predicted with the polymer partitioning into the isotropic phase as usual. Shorter rods, on the other hand, showed richer phase behaviour: a three-phase equilibrium consisting of two isotropic phases (dilute and concentrated) and a nematic phase was observed. An equilibrium consisting of one isotropic and two nematic phases was also predicted for longer rods and smaller polymer coils. The nature of the triphase equilibria depended on the relative values of L/D and σ/D .

1.4.4 Experimental mixtures of rodlike colloids and polymer coils

To a good approximation, sterically stabilized boehmite rods in cyclohexane can be considered as hard rods.¹⁰² Much work has been done examining their phase behaviour⁷⁹ as well as the partitioning behaviour of polydimethylsiloxane (PDMS) added to PIB-

grafted boehmite rods.^{103,145} Electrostatically stabilized boehmite rods have also been studied.⁸⁰ Other systems include rigid poly(*p*-benzamide) (PBA) plus semi-rigid X-500^x in dimethylacetamide / 3% LiCl,¹⁴⁶ rodlike poly(α ,1-glutamate) with triethylene glycol side chains plus polyethylene glycol in DMF,¹⁴⁷ and κ -carrageenan plus polysaccharides in solutions of 0.1 M NaI.¹⁴⁸ A preliminary investigation of aqueous cellulose nanocrystal suspensions plus blue dextran has also been carried out.¹⁴⁹

Mixtures of rodlike TMV and globular PEO have been found to exhibit rich phase behaviour, with the formation of isotropic, nematic, lamellar, and crystalline phases as a function of the constituents' concentration and the ionic strength.¹⁴¹ In addition, microphase separation may occur in mixtures having particular particle geometries or geometry relationships, leading to the coexistence of even more complex and numerous phases. For example, this occurs in binary mixtures of hard spheres at certain sphere diameter ratios,¹⁵⁰ and in mixtures of rods and spheres such as viruses and PS or PEO at certain rod length to sphere diameter ratios.¹⁵¹

1.4.5 Partitioning of coiled or flexible macromolecules

Two basic findings are common to all the theories of phase behaviour of rod-coil systems described above: Adding a coiled polymer to a system of rodlike particles causes a widening of the isotropic–nematic coexistence. Some degree of polymer partitioning also occurs, leading to rod-rich, coil-poor and coil-rich, rod-poor phases at equilibrium.

The extent of partitioning of flexible or coiled macromolecule between the isotropic and anisotropic phases of rodlike polymers or particles depends on the interplay among

^x This species has a conformation intermediate between that of a rodlike polymer and that of a random coiled polymer.¹⁴⁶

physical and chemical factors such as the relative geometries, chemical compatibility, and the concentrations of the two components. Some systems exhibit a total exclusion of the coiled species,¹⁴⁶ in line with predictions by Abe and Flory for systems of two rodlike particles which differ in length.⁹⁴ In other cases, appreciable quantities of coiled species remain in the anisotropic phase,¹⁴⁹ for example when the miscibility between the rods and coils is enhanced by flexible side chains on the rods.¹⁴⁷ Alternatively, there may be an even distribution of the coiled polymer throughout the system.¹⁴⁸ The charge on the polymer is also important, as ionic macromolecules tend to partition more evenly than neutral macromolecules, owing to the entropy of mixing of the counterions. It is important to remember that all else being equal, a higher concentration of added macromolecule will lead to greater partitioning into the isotropic phase.

A theory of partitioning for rigid-rod and flexible polymers has been proposed by Sear (1997).¹⁵² It is described in more detail in Chapter 5. In general, the partition coefficient depends on (a) the difference in the rod concentration between the two phases, (b) the second virial coefficient of rod-coil interactions and (c) the dimensions of the rods and coils. Characterization of both the system components is therefore important when predicting the partition coefficient. Experimental partition coefficients K for blue dextran in cellulose nanocrystal suspensions are several times larger than predicted by this theory, for reasons discussed in Chapter 5, although the theory does predict the correct order of magnitude of K .

1.5 DYE-LABELED DEXTRAN IN CELLULOSE NANOCRYSTAL SUSPENSIONS

Blue dextran has been studied as a coiled macromolecule added to suspensions of rodlike cellulose nanocrystals.¹⁴⁹

1.5.1 Properties and structure of dextran

The properties of dextran, a polymer of glucose with α -(1,6) linkages containing some α -(1,3) branching (Figure 1.14), have been thoroughly studied. Dextrans of commercial interest are obtained mainly from *Leuconostoc mesenteroides* NRRL B-512(F).¹⁵³ Values from 9×10^6 to 500×10^6 have been obtained for the molecular weight of native dextran.¹⁵⁴⁻¹⁵⁶ Dextran is soluble in water and other solvents such as DMSO, glycerol and ethylene glycol, and is insoluble in ethanol.¹⁵³ The solubility of dextran in ethanol–water mixtures depends on its molecular weight (Figure 1.15).¹⁵⁷ Its insolubility in ethanol is exploited in the fractional precipitation of clinical fractions of dextran having specific molecular weights,¹⁵³ and in the purification of blue dextrans (see Chapter 3). The α -(1,6)-linked polysaccharides are very flexible, in contrast with the rigidity and crystallinity of α -(1,4)-linked cellulose.¹⁵³ Dextrans with molecular weights between 2,000 – 10,000 Da behave as expandable coils in solution; above this molecular weight, they behave as though they were highly branched.

Periodate oxidation¹⁵⁸ and methylation analyses¹⁵⁹⁻¹⁶¹ indicate that the degree of dextran branching is approximately 5%. At lower molecular weights, the degree of branching is found to decrease slightly.¹⁶⁰ The average branch length is generally thought to be less than three glucose units, although conflicting data exist.^{160,162}

Partial acid hydrolysis of native dextran can be used to obtain dextran fractions of narrow molecular weight distribution, designated e.g. T-2000, where the “T” indicates

“technical grade” and the number indicates the molecular weight in kDa.^{163,164} Fractionation to give even narrower distributions of specific molecular weights can be achieved by ethanol fractionation, which precipitates the largest dextrans first,¹⁶⁵ or by size exclusion chromatography.¹⁶⁶

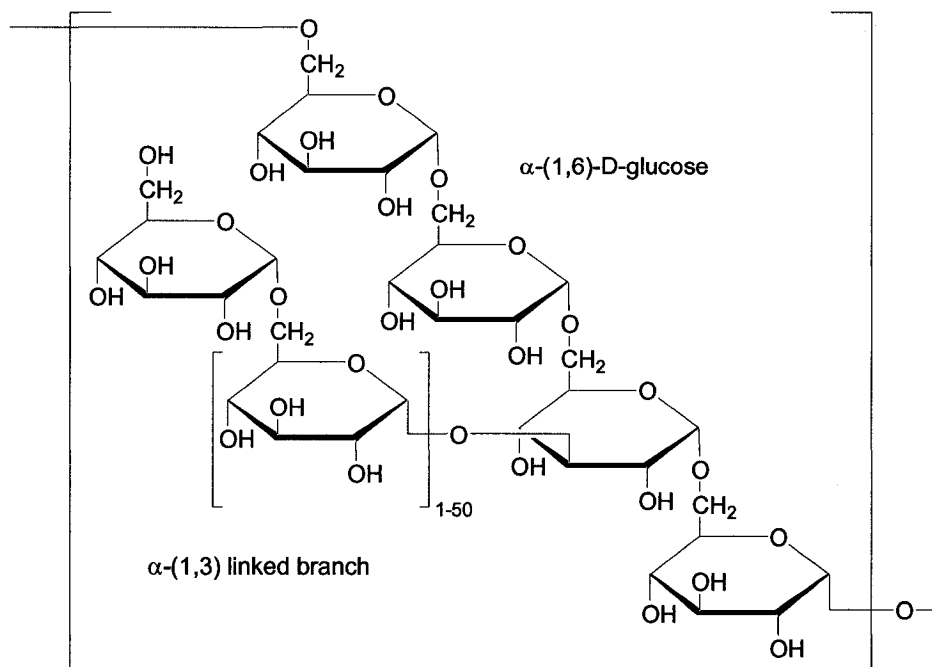


Figure 1.14. Schematic structure of native dextran showing α -(1,3) branching and α -(1,6)-linked backbone.

Unmodified dextran fractions have been used in a wide variety of biomedical applications, including plasma extenders,¹⁶⁷ centrifugation and organelle separation,¹⁶⁸ and inhibition of platelet aggregation.¹⁶⁹ Lower molecular weight dextrans are also used in a wide variety of applications involving aqueous two-phase systems, particularly dextran-PEG systems, for partitioning sub-cellular particles and macromolecules.¹⁷⁰

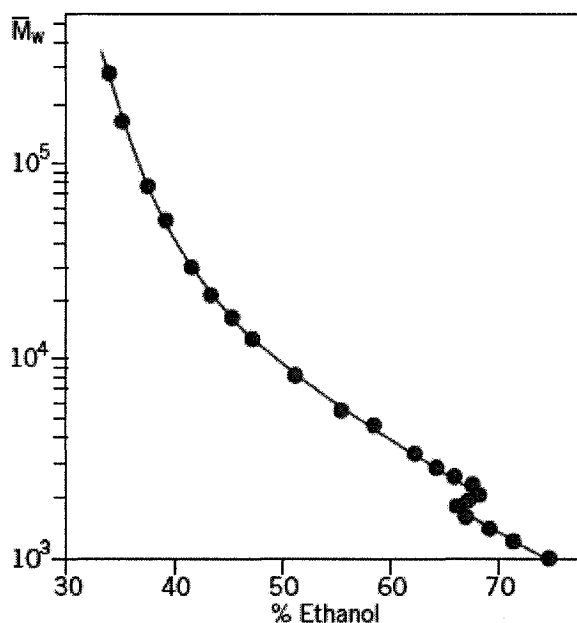


Figure 1.15. Solubility of dextrans in ethanol-water mixtures at 25°C. The M_w axis refers to the highest molecular weight dextran soluble in the given percentage composition of ethanol. Adapted from Basedow and Ebert (1979).¹⁵⁷

1.5.2 Dextran derivatives

The reactivity of dextran is derived mainly from the secondary, equatorially oriented hydroxyl groups, namely O2, O3 and O4.¹⁵³ Reactions of dextran include partial methylation,¹⁷¹ substitution with ethylene oxide,¹⁷² acylation with acetic anhydride in pyridine¹⁷³ or in aqueous alkali,¹⁵³ and sulfation.¹⁵³ More importantly for this thesis, the hydroxyl groups are also reactive to nucleophilic substitution reactions with halides in basic media, for example the chloride moiety of reactive dyes such as Cibacron blue 3G-A (Figure 3.1).¹⁷⁴ The product of this reaction is called blue dextran and is sold as a void volume marker for gel filtration columns. Dextran also reacts to give conjugates with other dyes including Reactive red 4, Reactive green 19, Rhodamine B isothiocyanate

and fluorescein isothiocyanate (FITC), all of which are commercially available. FITC-dextran, which is used as a macromolecular tracer in vascular permeability studies,¹⁷⁵ is also studied in this thesis.

Our particular interest in dye-labeled dextrans lies in their utility as visible macromolecules for quantification of the phase separation and partitioning phenomena that occur when they are added to aqueous suspensions of cellulose nanocrystals. The phase behaviour studies in this thesis are an extension of work begun by Edgar and Gray¹⁴⁹ using blue dextran to initially examine rod-coil systems. Blue dextran was chosen because the UV-visible absorption spectra of unmodified dextran and cellulose nanocrystals suspensions overlap; light scattering by the nanocrystals and absorption increases greatly at lower wavelengths, making it very difficult to detect variations in dextran concentration when measuring partitioning. The highly-coloured dyes also provide useful initial visible confirmation of partitioning.

1.6 MOTIVATION OF RESEARCH AND OUTLINE OF THESIS

As we have seen, studying systems of colloidal particles and added polymer can lead to insights which have greater relevance than just the physical chemistry or theoretical predictions. Colloidal suspensions frequently contain dissolved polymer additives which may be intended to stabilize them or to control their rheology, or at the other end of the spectrum, to de-stabilize and induce flocculation. In order to manipulate these systems to the desired end, we must understand the polymer-particle interactions and their effect on the macroscopic system properties. It is the goal of this thesis to gain an in-depth

comprehension of the factors controlling the interactions of dextran–dye ligands and native cellulose nanocrystals in aqueous suspension.

Apart from comparing experimental phase behaviour with theoretical predictions, it is essential to know the properties of nanocrystal suspensions on their own, to better understand the consequences of adding macromolecules. Cotton cellulose suspensions have been well-characterized.^{40,52,113} Chapter 2 instead looks at the less-investigated wood cellulose nanocrystals, comparing the properties of individual nanocrystals and their suspensions from softwood (black spruce) and hardwood (eucalyptus) sources. Atomic force microscopy is used to measure nanocrystal dimensions, and conductometric titration is used to measure the surface charge density of the nanocrystals. Bulk suspension properties are also examined and compared. The effect of reaction conditions on the nanocrystals is also considered, as it is important to be able to tailor the suspension to have the desired properties.

Just as it is important to characterize cellulose nanocrystal suspensions, it is also necessary to have an idea of the properties of the macromolecule being added to the suspension. In Chapter 3, blue dextrans are synthesized from Cibacron blue 3G-A dye and dextran. The physico-chemical properties of the resulting blue dextrans of varying molecular weights and degrees of substitution are then studied. Parameters such as hydrodynamic radii and radii of gyration, molecular weight and intrinsic viscosity are obtained by various methods such as light scattering, viscosimetry, and UV–visible spectroscopy. Together, such data can help elucidate properties and behaviour of these dextran–dye derivatives in solution.

The properties of cellulose nanocrystal suspensions and blue dextrans are united in Chapters 4 and 5. As an extension of previous work on the interactions of blue dextran and cellulose nanocrystals,¹⁴⁹ the phase separation induced by addition of blue dextran to anisotropic cotton cellulose nanocrystal suspensions is investigated in greater detail in Chapter 4: the effect of degree of dye substitution, dextran molecular weight, and the ionic nature of the dye ligand are all examined. In Chapter 5, the focus is on the partitioning of blue dextrans and FITC-dextrans between the isotropic and anisotropic phases of somewhat more dilute cellulose nanocrystal suspensions in which the isotropic and anisotropic phases coexist. Partitioning occurs to a lesser extent than in more concentrated cellulose suspensions, such as the (initially) anisotropic suspensions in Chapter 4; however, it is easier to work at lower cellulose concentrations because the equilibration times are much shorter due to the lower sample viscosity. Blue dextrans of decreasing molecular weight are obtained by acid hydrolysis, and the dependence of the extent of partitioning effects on dye substitution and molecular weight is determined. Partition coefficients of anionic blue dextrans and nonionic FITC-dextran are compared with each other and with theoretical predictions. The values of partition coefficients coincide nicely with those from the previous study.

Chapters 6 and 7 are an in-depth study of a phenomenon accidentally discovered while working on Chapter 5. When a certain concentration of an unmodified dextran along with a certain concentration of a blue dextran, is mixed with even a fairly dilute cotton cellulose nanocrystal suspension, an equilibrium among *three* phases results. In Chapter 6, the nature of the three phases is elucidated by optical microscopy, concentrations of cellulose in each phase are obtained by gravimetry, and blue dextran partitioning among

the phases is measured. Blue dextran partitioning is exaggerated compared to that observed in Chapter 5, with most of the blue dextran located in the upper isotropic phase. Phase diagrams for various combinations of unmodified and blue dextrans of different molecular weight, as well as cellulose nanocrystal concentration, are created and discussed in Chapter 7.

1.7 REFERENCES

- (1) Grunert, M.; Winter, W.T. *J. Polym. Environ.* **2002**, *10*, 27-30.
- (2) Favier, V.; Chanzy, H.; Cavaillé, J.Y. *Macromolecules* **1995**, *28*, 6365-6367.
- (3) Hon, D.N.-S. *Cellulose* **1994**, *1*, 1-25.
- (4) O'Sullivan, A.C. *Cellulose* **1997**, *4*, 173-207.
- (5) Kadla, J.F.; Gilbert, R.D. *Cellul. Chem. Technol.* **2001**, *34*, 197-216.
- (6) Brown, R.M., Jr. *J. Polym. Sci., Part A* **2004**, *42*, 487-495.
- (7) Atalla, R.H.; Isogai, A. in *Polysaccharides*; Dumitriu, S., eds.; Marcel Dekker, Inc.: New York, 2005, pp. 123-157.
- (8) Sarko, A.; Marchessault, R.H. *J. Polym. Sci., Part C: Polym. Symp.* **1969**, *28*, 317-331.
- (9) Mark, H. *J. Phys. Chem.* **1940**, *44*, 764-787.
- (10) Meyer, K.H.; Misch, L. *Helv. Chim. Acta* **1937**, *20*, 232-244.
- (11) Gardner, K.H.; Blackwell, J. *Biopolymers* **1974**, *13*, 1975-2001.
- (12) Sarko, A.; Muggli, R. *Macromolecules* **1974**, *7*, 486-494.
- (13) French, A.D. *Carbohydr. Res.* **1978**, *61*, 67-80.
- (14) Woodcock, C.; Sarko, A. *Macromolecules* **1980**, *13*, 1183-1187.
- (15) Honjo, G.; Watanabe, M. *Nature* **1958**, *181*, 236.
- (16) GTL Image Gallery, URL <http://genomics.energy.gov/gallery/gtl/detail.np/detail-36.html>.
- (17) Atalla, R.H.; VanderHart, D.L. *Science* **1984**, *223*, 283-285.
- (18) VanderHart, D.L.; Atalla, R.H. *Macromolecules* **1984**, *17*, 1465-1472.
- (19) Sugiyama, J.; Vuong, R.; Chanzy, H. *Macromolecules* **1991**, *24*, 4168-4175.

- (20) Sugiyama, J.; Okano, T.; Yamamoto, H.; Horii, F. *Macromolecules* **1990**, *23*, 3196-3198.
- (21) Yamamoto, H.; Horii, F. *Macromolecules* **1993**, *26*, 1313-1317.
- (22) Nishiyama, Y.; Langan, P.; Chanzy, H. *J. Am. Chem. Soc.* **2002**, *124*, 9074-9082.
- (23) Nishiyama, Y.; Sugiyama, J.; Chanzy, H.; Langan, P. *J. Am. Chem. Soc.* **2003**, *125*, 14300-14306.
- (24) Hanley, S.J.; Giasson, J.; Revol, J.-F.; Gray, D.G. *Polymer* **1992**, *33*, 4639-4642.
- (25) Baker, A.A.; Helbert, W.; Sugiyama, J.; Miles, M.J. *J. Struct. Biol.* **1997**, *119*, 129-138.
- (26) Baker, A.A. *High Resolution Atomic Force Microscopy of Polysaccharides*. Ph.D. thesis, University of Bristol: Bristol, 1998.
- (27) Finkenstadt, V.L.; Millane, R.P. *Macromolecules* **1998**, *31*, 7776-7783.
- (28) Sugiyama, J.; Imai, T. *Trends Glycosci. Glycotechnol.* **1999**, *11*, 23-31.
- (29) Baker, A.A.; Helbert, W.; Sugiyama, J.; Miles, M.J. *Biophys. J.* **2000**, *79*, 1139-1145.
- (30) Earl, W.L.; VanderHart, D.L. *Macromolecules* **1981**, *14*, 570-574.
- (31) Fink, H.P.; Philipp, B.; Paul, D.; Serimaa, R.; Paakkari, T. *Polymer* **1987**, *28*, 1265-1270.
- (32) Battista, O.A. *Ind. Eng. Chem.* **1956**, *48*, 333-335.
- (33) Marchessault, R.H.; Morehead, F.F.; Koch, M.J. *J. Colloid Sci.* **1961**, *16*, 327-344.
- (34) Rowland, S.P.; Roberts, E.J. *J. Polym. Sci., Part A* **1972**, *10*, 2447-2461.

- (35) Sjöström, E. *Wood Chemistry: Fundamentals and Applications*; 2nd ed.; Academic Press: New York, 1981.
- (36) Fengel, D.; Wegener, G. *Wood: Chemistry, Ultrastructure, Reactions*; Walter de Gruyter: New York, 1984.
- (37) Hermans, P.H. *Makromol. Chem.* **1951**, *6*, 25-29.
- (38) Krässig, H.A. *Cellulose: Structure, Accessibility and Reactivity*; Gordon and Breach Science Publishers: Yverdon, 1993, pp. 18-33.
- (39) Beck-Candanedo, S.; Roman, M.; Gray, D.G. *Biomacromolecules* **2005**, *6*, 1048-1054; Chapter 2 of this thesis.
- (40) Dong, X.M.; Revol, J.-F.; Gray, D.G. *Cellulose* **1998**, *5*, 19-32.
- (41) Terech, P.; Chazeau, L.; Cavaillé, J.Y. *Macromolecules* **1999**, *32*, 1872-1875.
- (42) de Sousa Lima, M.M.; Wong, J.T.; Paillet, M.; Borsali, R.; Pecora, R. *Langmuir* **2003**, *19*, 24-29.
- (43) Rånby, B.G. *Acta Chem. Scand.* **1949**, *3*, 649-650.
- (44) Rånby, B.G.; Ribi, E. *Experientia* **1950**, *6*, 12-14.
- (45) Rånby, B.G. *Discuss. Faraday Soc.* **1951**, *11*, 158-164.
- (46) Hengstenberg, J.; Mark, H. Z. *Kryst.* **1928**, *69*, 271-284.
- (47) Revol, J.-F.; Bradford, H.; Giasson, J.; Marchessault, R.H.; Gray, D.G. *Int. J. Biol. Macromol.* **1992**, *14*, 170-172.
- (48) Revol, J.F.; Godbout, L.; Dong, X.M.; Gray, D.G.; Chanzy, H.; Maret, G. *Liq. Cryst.* **1994**, *16*, 127-134.
- (49) Dong, X.M. *Chiral Nematic Ordered Suspensions of Cellulose Microcrystallites*. Ph.D. thesis, McGill University: Montreal, 1997.

- (50) Wise, L.E.; Murphy, M.; d'Addiecco, A.A. *Paper Trade J.* **1946**, 122, 35.
- (51) Marchessault, R.H.; Morehead, F.F.; Walter, N.M. *Nature* **1959**, 184, 632-633.
- (52) Dong, X.M.; Kimura, T.; Revol, J.-F.; Gray, D.G. *Langmuir* **1996**, 12, 2076-2082.
- (53) Revol, J.-F.; Godbout, L.; Gray, D.G.: United States Patent No. 5 629 05, 1997.
- (54) Araki, J.; Wada, M.; Kuga, S.; Okano, T. *Colloids Surf., A* **1998**, 142, 75-82.
- (55) Araki, J.; Wada, M.; Kuga, S.; Okano, T. *J. Wood Sci.* **1999**, 45, 258-261.
- (56) Araki, J.; Wada, M.; Kuga, S. *Langmuir* **2001**, 17, 21-27.
- (57) Isogai, A.; Kato, Y. *Cellulose* **1998**, 5, 153-164.
- (58) Heux, L.; Chauve, G.; Bonini, C. *Langmuir* **2000**, 16, 8210-8212.
- (59) Gousse, C.; Chanzy, H.; Excoffier, G.; Soubeyrand, L.; Fleury, E. *Polymer* **2002**, 43, 2645-2651.
- (60) Samir, M.A.S.A.; Alloin, F.; Sanchez, J.-Y.; El Kissi, N.; Dufresne, A. *Macromolecules* **2004**, 37, 1386-1393.
- (61) Viet, D.; Beck-Candanedo, S.; Gray, D.G. *Cellulose* **2006**, 13, 629-635.
- (62) Revol, J.-F. *Carbohydr. Polym.* **1982**, 2, 123-134.
- (63) Van Daele, Y.; Gaill, F.; Goffinet, G. *J. Struct. Biol.* **1991**, 106, 115-124.
- (64) Sassi, J.-F.; Chanzy, H. *Cellulose* **1995**, 2, 111-127.
- (65) Battista, O.A.; Smith, P.A. *Ind. Eng. Chem.* **1962**, 54, 20-29.
- (66) Orts, W.J.; Godbout, L.; Marchessault, R.H.; Revol, J.F. *ACS Symposium Series - Flow-Induced Structure in Polymers* **1995**, 597, 335-348.
- (67) de Sousa Lima, M.M.; Borsali, R. *Macromol. Rapid. Comm.* **2004**, 25, 771-787.
- (68) Samir, M.; Alloin, F.; Dufresne, A. *Biomacromolecules* **2005**, 6, 612-626.

- (69) Radel, S.R.; Navidi, M.H. *Chemistry*; 2nd ed.; West Publishing Company: New York, 1994, p. 563.
- (70) de Gennes, P.G.; Proust, J. *The Physics of Liquid Crystals*; 2nd ed.; Oxford University Press: Oxford, 1993, p. 110.
- (71) Zocher, H. *Z. Anorg. Allg. Chem.* **1925**, *147*, 91-110.
- (72) Freundlich, H. *J. Phys. Chem.* **1937**, *41*, 1151-1161.
- (73) Watson, J.H.L.; Heller, W.; Wojtowicz, W. *Science* **1949**, *109*, 274-278.
- (74) Langmuir, I. *J. Chem. Phys.* **1938**, *6*, 873-896.
- (75) Bawden, F.C.; Pirie, N.W.; Bernal, J.D.; Fankuchen, I. *Nature* **1936**, *138*, 1051-1052.
- (76) Bawden, F.C.; Pirie, N.W. *Proc. R. Soc. London, Ser. B* **1937**, *123*, 274-320.
- (77) Folda, T.; Hoffmann, H.; Chanzy, H.; Smith, P. *Nature* **1988**, *333*, 55-56.
- (78) Yu, L.J.; Saupe, A. *Phys. Rev. Lett.* **1980**, *45*, 1000-1003.
- (79) Buining, P.A.; Lekkerkerker, H.N.W. *J. Phys. Chem.* **1993**, *97*, 11510-11516.
- (80) Buining, P.A.; Philipse, A.P.; Lekkerkerker, H.N.W. *Langmuir* **1994**, *10*, 2106-2114.
- (81) Chilaya, G.S.; Lisetski, L.N. *Mol. Cryst. Liq. Cryst.* **1986**, *140*, 243-286.
- (82) Werbowyj, R.S.; Gray, D.G. *Mol. Cryst. Liq. Cryst.* **1976**, *34*, 97-103.
- (83) Tseng, S.-L.; Valente, A.; Gray, D.G. *Macromolecules* **1981**, *14*, 715-719.
- (84) Werbowyj, R.S.; Gray, D.G. *Macromolecules* **1984**, *17*, 1512-1520.
- (85) Gray, D.G. *Polymer Prepr.* **1996**, *37*, 485-486.
- (86) Guo, J.-X.; Gray, D.G. *Macromolecules* **1989**, *22*, 2086-2090.

- (87) Siekmeyer, M.; Zugenmaier, P. *Makromol. Chem. Rapid Comm.* **1987**, *8*, 511-517.
- (88) Kimura, F.; Kimura, T.; Tamura, M.; Hirai, A.; Ikuno, M.; Horii, F. *Langmuir* **2005**, *21*, 2034-2037.
- (89) Baus, M.; Coussaert, T.; Achrayah, R. *Physica A* **1996**, *232*, 575-584.
- (90) Onsager, L. *Ann. N.Y. Acad. Sci.* **1949**, *51*, 627-659.
- (91) Tang, J.; Fraden, S. *Liq. Cryst.* **1995**, *19*, 459.
- (92) Flory, P.J. *Proceedings of the Royal Society of London. Series A, Mathematical and Physical Sciences* **1956**, *234*, 73-89.
- (93) Flory, P.J.; Abe, A. *Macromolecules* **1978**, *11*, 1119-22.
- (94) Abe, A.; Flory, P.J. *Macromolecules* **1978**, *11*, 1122-1126.
- (95) Flory, P.J.; Frost, R.S. *Macromolecules* **1978**, *11*, 1126-1133.
- (96) Frost, R.S.; Flory, P.J. *Macromolecules* **1978**, *11*, 1134-1138.
- (97) Flory, P.J. *Macromolecules* **1978**, *11*, 1138-1141.
- (98) Flory, P.J. *Macromolecules* **1978**, *11*, 1141-1144.
- (99) DiMarzio, E.A. *J. Chem. Phys.* **1961**, *35*, 658-669.
- (100) Maret, G.; Dransfeld, K. *Strong and Ultrastrong Magnetic Fields and Their Applications*; Springer: Berlin, 1985, pp. 160-167.
- (101) Moscicki, J.K.; Williams, G. *Polymer* **1982**, *23*, 558-568.
- (102) van Bruggen, M.P.B.; Dhont, J.K.G.; Lekkerkerker, H.N.W. *Macromolecules* **1999**, *32*, 2256-2264.
- (103) van Bruggen, M.P.B.; Lekkerkerker, H.N.W. *Macromolecules* **2000**, *33*, 5532-5535.

- (104) Hermans, J. *J. Polym. Sci., Part C: Polym. Symp.* **1963**, 2, 129-144.
- (105) de Sousa Lima, M.M.; Borsali, R. *Langmuir* **2002**, 18, 992-996.
- (106) Furuta, T.; Yamahara, E.; Konishi, T.; Ise, N. *Macromolecules* **1996**, 29, 8994-8995.
- (107) Arora, A.K.; Tata, B.V.R. *Ordering and Phase Transitions in Charged Colloids*; VCH Publishers: New York, 1996, Ch. 6.
- (108) Orts, W.J.; Godbout, L.; Marchessault, R.H.; Revol, J.F. *Macromolecules* **1998**, 31, 5717-5725.
- (109) Beck-Candanedo, S.; Viet, D.; Gray, D.G. *Langmuir* **2006**, 22, 8690-8695; Chapter 4 of this thesis.
- (110) Straley, J.P. *Phys. Rev. A* **1976**, 14, 1835-1841.
- (111) Revol, J.-F.; Marchessault, R.H. *Int. J. Biol. Macromol.* **1993**, 15, 329-335.
- (112) Grelet, E.; Fraden, S. *Phys. Rev. Lett.* **2003**, 90, 198302-1 - 198302-4.
- (113) Dong, X.M.; Gray, D.G. *Langmuir* **1997**, 13, 2404-2409.
- (114) Fleming, K.; Gray, D.; Prasannan, S.; Matthews, S. *J. Am. Chem. Soc.* **2000**, 122, 5224-5225.
- (115) Fraden, S.; Maret, G.; Caspar, D.L.D.; Meyer, R.B. *Phys. Rev. Lett.* **1989**, 63, 2068-2071.
- (116) Stroobants, A.; Lekkerkerker, H.N.W.; Odijk, T. *Macromolecules* **1986**, 19, 2232-2238.
- (117) Lee, S.-D. *J. Chem. Phys.* **1987**, 87, 4972-4974.
- (118) Semenov, A.N.; Kokhlov, A.R. *Sov. Phys. Usp.* **1988**, 31, 988-1014.
- (119) Sato, T.; Teramoto, A. *Physica A* **1991**, 176, 72-86.

- (120) Odijk, T. *Macromolecules* **1986**, *19*, 2313-2329.
- (121) Strzelecka, T.E.; Rill, R.L. *Macromolecules* **1991**, *24*, 5124-5133.
- (122) McPherson, A. *Preparation and Analysis of Protein Crystals*; Krieger: Malabar, FL, 1982.
- (123) Weber, P.C. in *Macromolecular Crystallography*; Carter, J.C.W.; Sweet, R.M., eds.; Academic Press: New York, 1997; Vol. 276, pp. 13-22.
- (124) Asakura, S.; Oosawa, F. *J. Chem. Phys.* **1954**, *22*, 1255-1256.
- (125) Asakura, S.; Oosawa, F. *J. Polym. Sci.* **1958**, *33*, 183-192.
- (126) Vrij, A. *Pure Appl. Chem.* **1976**, *48*, 471-483.
- (127) Gast, A.P.; Hall, C.K.; Russel, W.B. *J. Colloid Interface Sci.* **1983**, *82*, 62.
- (128) Vincent, B.J.; Edwards, J.; Emmett, S.; Croot, R. *Colloids Surf.* **1988**, *31*, 267-298.
- (129) Lekkerkerker, H.N.W.; Poon, W.C.-K.; Pusey, P.N.; Stroobants, A.; Warren, P.B. *Europhys. Lett.* **1992**, *20*, 559-563.
- (130) Patel, P.D.; Russel, W.B. *J. Colloid Interface Sci.* **1989**, *131*, 192-200.
- (131) Robins, M.M. in *Microemulsions and Emulsions in Foods*; El-Nokaly, M.; Cornell, D., eds., 1991; Vol. 448, Ch. 17.
- (132) Richetti, P.; Kekicheff, P. *Phys. Rev. Lett.* **1992**, *68*, 1951-1954.
- (133) Sober, D.L.; Walz, J.Y. *Langmuir* **1995**, *11*, 2352-2356.
- (134) Verma, R.; Crocker, J.C.; Lubensky, T.C.; Yodh, A.G. *Phys. Rev. Lett.* **1998**, *81*, 4004-4007.
- (135) Ilett, S.M.; Orrock, A.; Poon, W.C.K.; Pusey, P.N. *Phys. Rev. E* **1995**, *51*, 1344-1352.

- (136) Poon, W.C.K. *J. Phys.: Condens. Matter* **2002**, *14*, R859-R880.
- (137) Poon, W. *Science* **2004**, *304*, 830-831.
- (138) Sperry, P.R.; Hopfenberg, H.B.; Thomas, N.L. *J. Colloid Interface Sci.* **1981**, *82*, 62-76.
- (139) Gast, A.P.; Russel, W.B.; Hall, C.K. *J. Colloid Interface Sci.* **1986**, *109*, 161-171.
- (140) Calderon, F.L.; Bibette, J.; Biais, J. *Europhys. Lett.* **1993**, *23*, 653-659.
- (141) Adams, M.; Fraden, S. *Biophys. J.* **1998**, *74*, 669-677.
- (142) Koenderink, G.H.; Vliegenthart, G.A.; Kluijtmans, S.G.J.M.; van Blaaderen, A.; Philipse, A.P.; Lekkerkerker, H.N.W. *Langmuir* **1999**, *15*, 4693-4696.
- (143) Warren, P.B. *J. Phys. I* **1994**, *4*, 237-244.
- (144) Lekkerkerker, H.N.W.; Stroobants, A. *Il Nuovo Cimento* **1994**, *16D*, 949-962.
- (145) Buitenhuis, J.; Donselaar, L.N.; Buining, P.A.; Stroobants, A.; Lekkerkerker, H.N.W. *J. Colloid Interface Sci.* **1995**, *175*, 46-56.
- (146) Bianchi, E.; Ciferri, A.; Tealdi, A. *Macromolecules* **1982**, *15*, 1268-1272.
- (147) Inomata, K.; Ohara, N.; Shimizu, H.; Nose, T. *Polymer* **1998**, *39*, 3379-3386.
- (148) Ramzi, M.; Borgström, J.; Piculell, L. *Macromolecules* **1999**, *32*, 2250-2255.
- (149) Edgar, C.D.; Gray, D.G. *Macromolecules* **2002**, *35*, 7400-7406.
- (150) Eldridge, M.D.; Madden, P.A.; Frenkel, D. *Nature* **1993**, *365*, 35-37.
- (151) Adams, M.; Dogic, Z.; Keller, S.L.; Fraden, S. *Nature* **1998**, *393*, 349-352.
- (152) Sear, R.P. *J. Phys. II* **1997**, *7*, 877-886.
- (153) de Belder, A.N. *Dextran*; Amersham Biosciences: Piscataway, NJ, 2003, 62 pp.
- (154) Bovey, F.A. *J. Polym. Sci.* **1959**, *35*, 167-182.

- (155) Senti, F.R.; Hellman, N.N.; Ludwig, N.H.; Babcock, G.E.; Tobin, R.; Glass, C.A.; Lamberts, B.L. *J. Polym. Sci.* **1955**, *27*, 527-546.
- (156) Antonini, E.; Bellelli, L.; Bruzzesi, M.R.; Caputo, A.; Chiancone, E.; Rossi-Fanelli, A. *Biopolymers* **1964**, *2*, 27-34.
- (157) Basedow, A.M.; Ebert, K.H. *J. Polym. Sci., Part C: Polym. Symp.* **1979**, *66*, 101-115.
- (158) Rankin, J.C.; Jeanes, A. *J. Am. Chem. Soc.* **1954**, *76*, 4435-4441.
- (159) Van Cleve, J.W.; Schaefer, W.C.; Rist, C.E. *J. Am. Chem. Soc.* **1956**, *78*, 4435-4438.
- (160) Lindberg, B.; Svensson, S. *Acta Chem. Scand.* **1968**, *22*, 1907-1912.
- (161) Jeanes, A.; Seymour, F.R. *Carbohydr. Res.* **1971**, *74*, 31-40.
- (162) Larm, O.; Lindberg, B.; Svensson, S. *Carbohydr. Res.* **1971**, *20*, 39-48.
- (163) Wolff, I.A.; Mehlretter, C.L.; Mellies, R.L.; Watson, P.R.; Hofreiter, B.T.; Patrick, P.L.; Rist, C.E. *Ind. Eng. Chem.* **1954**, *46*, 370-377.
- (164) Zief, M.; Brunner, G.; Metzendorf, J. *Ind. Eng. Chem.* **1956**, *48*, 119-121.
- (165) Sigma-Aldrich, Dextran Product No. D9260, D4626, D4133, D1662, D4751, D3759, D1390, D1537, D4876, D5251, D1037, D5376, and D5501. Product Information, 1997.
- (166) Granath, K.A.; Flodin, P. *Makromol. Chem.* **1961**, *48*, 161-171.
- (167) Reynolds, J.E.F. *Martindale: The Extra Pharmacopoeia*; 30th ed.; Royal Pharmaceutical Society: London, 1993, pp. 650-651.
- (168) Harris, R.; Ukaejiofo, E.O. *Brit. J. Haematol.* **1970**, *18*, 229.
- (169) Gelin, L.E.; Ingelman, B. *Acta Chir. Scand.* **1961**, *122*, 294.

- (170) Albertsson, P.-Å. *Partition of Cell Particles and Macromolecules*; 3rd ed.; Wiley-Interscience: New York, 1986, 323 pp.
- (171) Norrman, B. *Acta Chem. Scand.* **1968**, 22, 1381.
- (172) de Belder, A.N.; Norrman, B. *Carbohydr. Res.* **1968**, 10, 391-394.
- (173) de Belder, A.N. *Carbohydr. Res.* **1968**, 8, 1-6.
- (174) Sigma-Aldrich, Blue Dextran Molecular Weight 2,000,000 Product No. D5751. Product Information, 1997.
- (175) Sigma-Aldrich, Fluorescein Isothiocyanate Dextran Product No. FD-2000S. Product Information, 1997.

Introduction to Cellulose Nanocrystal Suspension

Characterization Methods

In the following chapter, the properties of wood cellulose nanocrystals and aqueous suspensions thereof are examined with respect to the hydrolysis conditions used to produce them. Several characterization methods are employed: Atomic force microscopy (AFM) and conductometric titration determine the average dimensions and surface charge density of the cellulose nanocrystals, which influence the suspension behaviour, while phase diagrams and optical microscopy offer information on the properties of the suspension as a whole. A brief description of each method follows.

The atomic force microscope employs a probe tip mounted on a sensitive cantilever-type spring. As the tip is scanned across the surface of the sample, the force interaction between the sample and the tip causes the cantilever to deflect according to Hooke's law. The resulting vertical and horizontal displacement is measured by detecting the deflection of a laser beam reflected off the rear side of the cantilever (Figure 2-A), and translated into a three-dimensional image of the sample.

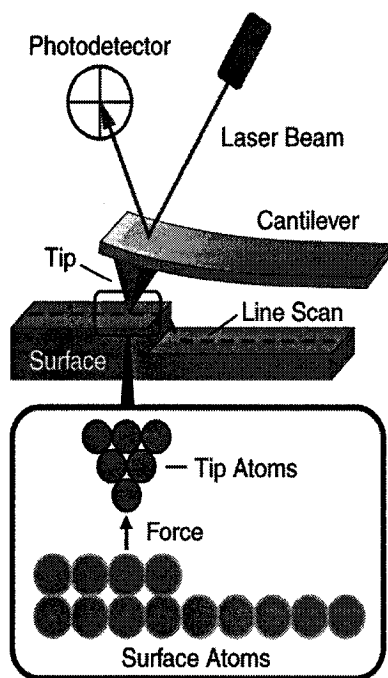


Figure 2-A. Principle of operation of the atomic force microscope (AFM).

One of the great advantages of AFM is the minimal sample preparation required as compared to electron microscopy. A drop of dilute suspension is dried onto a freshly-cleaved mica surface, which has been coated with positively charged poly-L-lysine to which the nanocrystals stick, reducing the clusters or clumps of nanocrystals that form when the surface tension of the drying water droplet pulls them together. This results in more representative samples in which many individual nanocrystals can be imaged.

Tip-sample convolution (Figure 2-B) can create image artifacts which interfere with accurate measurement, particularly in the x-y plane. In order to avoid these artifacts as much as possible, nanocrystal length is measured at the top of the cross-section (asterisk in Figure 2-B), while the diameter is measured vertically, assuming the nanocrystal is a cylinder or has a square cross-section.

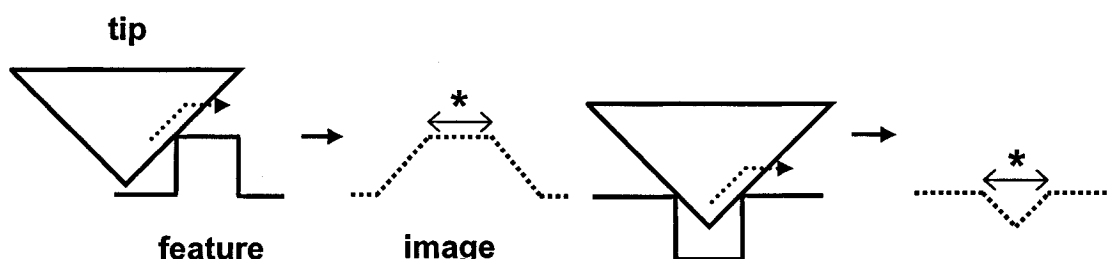


Figure 2-B. Schematic diagram showing examples of tip-sample convolution originating from the relative sizes of the tip and the sample feature being measured.

Apart from the surface sulfate ester groups introduced during sulfuric acid hydrolysis, cellulose nanocrystals may also contain carboxylic acid groups which can arise from the oxidation of the C6 hydroxyl group. Conductometric titration is a simple and accurate method used to quantify the surface charge on the cellulose nanocrystals. A dilute

suspension of nanocrystals in the acid form will contain -COOH and -OSO_3^- groups and the associated H^+ counterions. The conductance of the suspension will depend mainly on the hydrogen and hydroxyl ions present; however, conductometric titrations of polyelectrolytes must be carried out in the presence of a neutral salt (1 mM NaCl) to avoid the Donnan equilibrium.¹ Figure 2-C shows the set-up for a conductivity titration. A typical titration curve for nanocrystals containing both surface carboxylate and sulfate groups is shown in Figure 2-D.

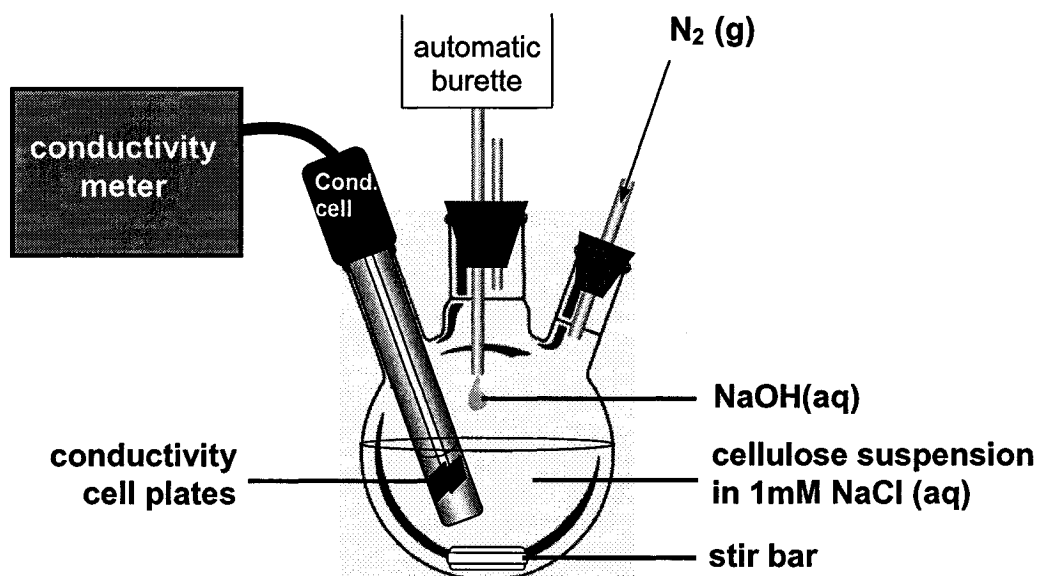


Figure 2-C. Equipment used for conductometric titration of cellulose nanocrystals.

Initially, the measured conductance decreases as the H^+ ions dissociated from the sulfate esters (strong acid) are neutralized by the hydroxyl anions from the NaOH until the first equivalence point is reached. The weaker carboxylic acid groups are then

¹ Neale, S.M.; Stringfellow, W.A. *Trans. Faraday Soc.* **1937**, *31*, 881-889; and Grignon, J.; Scallan, A.M. *J. Appl. Polym. Sci.* **1980**, *25*, 2829-2843.

neutralized by the NaOH; the conductance remains relatively constant because there is a small concentration of H^+ ions in equilibrium with the carboxylic acid as it is titrated. Past the second equivalence point, the conductance again increases as excess NaOH is added. The equivalence points are determined by extrapolation of the linear portions of the titration curve.

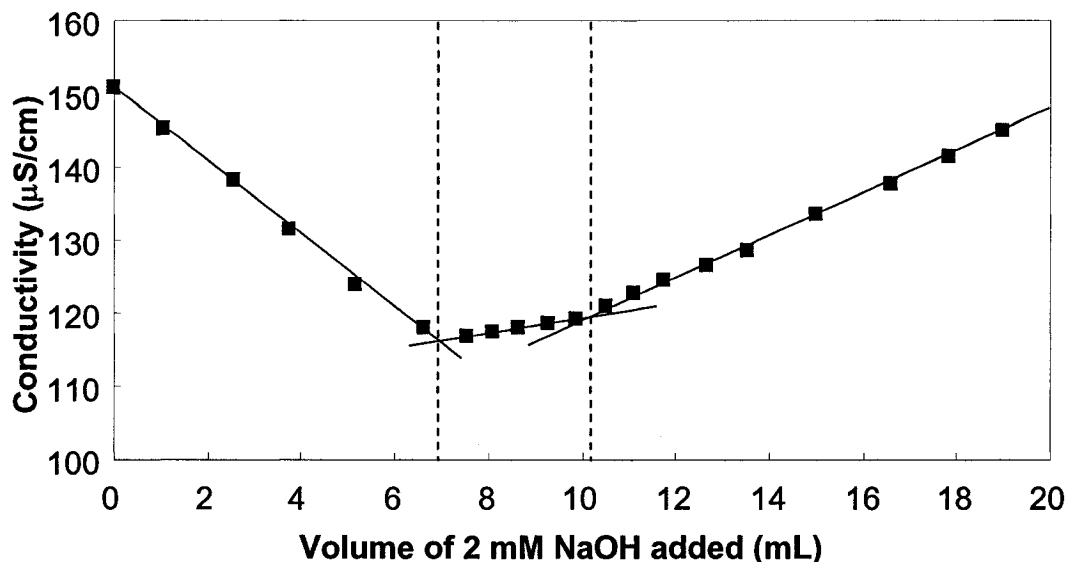


Figure 2-D. Conductometric titration curve for suspension of cellulose nanocrystals containing strong and weak acid groups at their surfaces.

Conductometric titration can be used to determine the sulfur content of the nanocrystals, their surface charge density (using cellulose nanocrystal dimensions measured by AFM), and the amount of NaOH required to convert the suspension to the sodium form, in which all the counterions are Na^+ and the suspension pH is neutral.

Phase diagrams (see Figure 2.4 in Chapter 2) show the critical concentration at which the chiral nematic phase first forms as well as the concentration range over which the isotropic–chiral nematic phase coexistence occurs for a given suspension. This can

provide corroboration of parameters such as nanocrystal length, on which the critical concentration is inversely dependent, length polydispersity, which tends to broaden the coexistence region, as well as ionic strength and the nature of the counterion.² In addition, phase diagrams are a useful and simple way of comparing one suspension with another.

Optical microscopy takes advantage of the birefringence of cellulose to measure the pitch of the chiral nematic liquid crystalline phase of a biphasic sample (Figure 2-E). The pitch gives an indication of the strength of the chiral interaction between the nanocrystals, which in turn depends on factors such as the cellulose concentration, nanocrystal surface charge density and the ionic strength of the suspension.

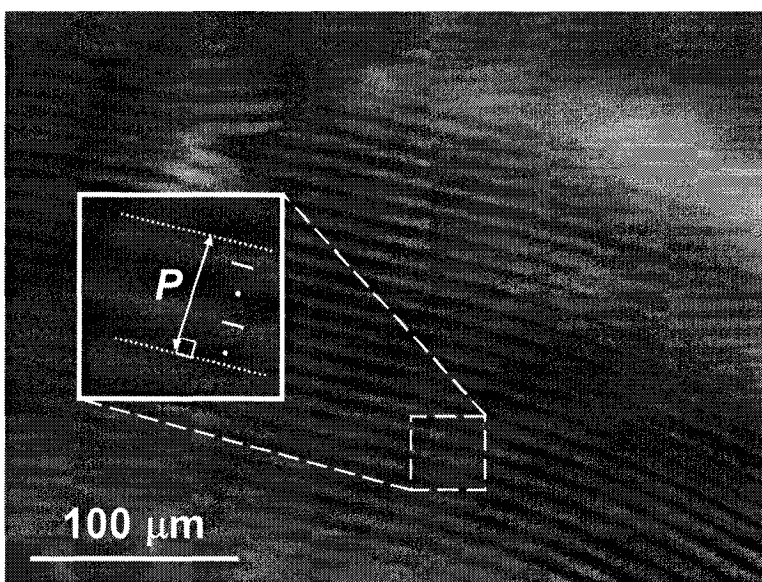


Figure 2-E. Photomicrograph of the chiral nematic liquid crystal texture of a cellulose nanocrystal suspension viewed in a polarizing microscope. The nanocrystals lie parallel to the plane of the page in the light regions (—) and perpendicular in the dark regions (•).

² Onsager, L. *Ann. N.Y. Acad. Sci.* **1949**, *51*, 627-659.

Chapter 2

Effect of Reaction Conditions on the Properties and Behaviour of Wood Cellulose Nanocrystal Suspensions

Reproduced with permission from
Beck-Candanedo, S.; Roman, M.; Gray, D.G. *Biomacromolecules* **2005**, *6*, 1048-1054.
Copyright 2005 American Chemical Society.

2.1 INTRODUCTION

Acid hydrolysis of cellulose fibres yields highly crystalline rodlike particles through selective degradation of the more accessible material. The cellulose nanocrystals that result from this degradation are of colloidal dimensions, and when stabilized they form aqueous suspensions, the properties and applications of which are reviewed in a recent article.¹

Rånby and Ribi were the first to produce stable suspensions of colloidal-sized cellulose crystals by sulfuric acid hydrolysis of wood and cotton cellulose.^{2,3} The nanocrystals were found to be approximately 50–60 nm long by 5–10 nm wide, which agreed with previous X-ray diffraction experiments as well as electron microscopy investigations of cellulose fibres.³ The first electron microscopy images of the cellulose nanocrystals themselves were obtained in 1953.⁴ Marchessault and co-workers in 1959 and Hermans in 1963 demonstrated that such cellulose nanocrystal suspensions displayed liquid crystalline order.^{5,6} However, it was not until several decades later that Revol and co-workers showed that the aqueous cellulose nanocrystal suspensions in fact formed a stable chiral nematic liquid crystalline phase.⁷

Using acid hydrolysis, native cellulose suspensions have been prepared from a variety of sources, including bacterial cellulose,^{8,9} microcrystalline cellulose,¹⁰ sugar beet primary cell wall cellulose,¹¹ cotton,¹² tunicate cellulose,¹³ and softwood pulp (mostly black spruce).^{7,14} The hydrolysis conditions are known to affect the properties of the resulting nanocrystals. For example, a longer reaction time leads to shorter nanocrystals.¹² Different acids also affect the suspension properties: hydrochloric acid hydrolysis yields cellulose rods with minimal surface charge,¹⁰ while the use of sulfuric acid provides highly stable aqueous suspensions, due to the esterification of surface

hydroxyl groups to give charged sulfate groups.² Above a critical concentration, the rodlike shape of the charged cellulose nanocrystals leads to the formation of anisotropic liquid crystalline phases, which have been extensively studied.^{5,7,12,14-17}

Nanocrystal size, dimensions, and shape are also determined to a certain extent by the nature of the cellulose source. The degree of crystallinity of the cellulose within the organism as well as the dimensions of the microfibrils vary widely from species to species.^{18,19} Thus, algal and tunicate cellulose microfibrils, which are highly crystalline,²⁰⁻²³ yield nanocrystals up to several micrometers in length. In contrast, wood microfibrils, which have lower crystallinity (50–83 %)²⁴⁻²⁶ yield much shorter nanocrystals.²⁶ Table 2.1 lists the nanocrystal dimensions for various cellulose sources; cross sectional dimensions are similar to those of the microfibril. Microfibril dimensions are similar for tunicate,^{13,22} bacterial,^{27,28} and algal cellulose,^{29,30} while cotton and wood microfibrils are smaller.^{14,26}

Table 2.1. Dimensions of cellulose nanocrystals from various sources.

Cellulose type	Length	Cross-section
Tunicate ^a	100 nm – several μ m	10-20 nm
Bacterial ^b	100 nm – several μ m	5-10 nm by 30-50 nm
Algal (<i>Valonia</i>) ^c	> 1000 nm	10 to 20 nm
Cotton ^d	200 - 350 nm	5 nm
Wood ^e	100 - 300 nm	3-5 nm diameter

^a References 13 and 22. ^b References 27 and 28. ^c References 29 and 30. ^d Reference 26. ^e References 14, 26; this work.

There are of course important differences between the cell wall structures of hardwoods and softwoods; native softwood tracheids tend to be longer (3–4 mm) than hardwood tracheids (0.5–1.5 mm), as well as somewhat wider ($\sim 35\ \mu\text{m}$ vs. $\sim 20\ \mu\text{m}$, respectively).²⁶ Data on the difference between the dimensions of softwood and hardwood microfibrils is less accessible. It is generally accepted that in wood the cellulose molecules initially form long crystalline elements with cross-section dimensions around 2–5 nm (sometimes called elementary fibrils or protofibrils) that aggregate into larger microfibrils with lateral dimensions in the tens of nanometers. Determining the exact dimensions of cellulose microfibrils is complicated by the specific limitations of the different analytical methods used. For example, in this study, we observed microfibril widths on the surface of pulp fibres of $\sim 70\ \text{nm}$, which corresponds with previous atomic force microscopy (AFM) results from Hanley and Gray,³¹ and also with electron microscopy results.³² However, a much smaller cross-sectional dimension of about 3–5 nm has been observed for wood microfibrils by electron diffraction³³ and AFM measurements.^{14,26,31,34} In the case of AFM, tip/sample broadening represents the main limitation, resulting in an overestimation of microfibril dimensions.

In the present study we compare the properties of cellulose nanocrystals obtained by hydrolysis of a softwood (black spruce) pulp to those of nanocrystals produced from a hardwood (eucalyptus) pulp. To our knowledge, the properties and behaviour of hardwood cellulose nanocrystal suspensions have not previously been examined in detail. We also examine the effects of reaction time and acid-to-pulp ratio for suspensions of black spruce nanocrystals. Nanocrystal dimensions and surface charge are measured, and the phase separation behaviour and liquid crystalline properties investigated.

2.2 EXPERIMENTAL METHODS

2.2.1 Materials

Bleached softwood (black spruce, *Picea mariana*) sulfite pulp (Temalfa 93) was provided by Tembec Inc., Temiscaming, Québec. Bleached hardwood (eucalyptus, *Eucalyptus* spp.) ECF pulp was provided by Cenibra S.A., Brazil. Sulfuric acid (95-98 %) for hydrolysis was purchased from Fisher Scientific. Sodium hydroxide, sodium chloride and sulfuric acid volumetric standards for titration were purchased from Aldrich. All water used was purified (Millipore Milli-Q purification system).

2.2.2 Sulfuric acid hydrolysis of wood pulp

Suspensions of cellulose nanocrystals were prepared as follows. Wood pulp was ground in a Wiley mill (Thomas-Wiley Laboratory Mill Model 4, Thomas Scientific, U.S.A.) to pass through a 20-mesh screen. Hydrolysis was performed at 45 °C, using 64 wt% sulfuric acid at various acid-to-pulp ratios for varying times (see Table 2.2 for details). Immediately following hydrolysis, suspensions were diluted tenfold to stop the reaction. The suspensions were then centrifuged, washed once with water, and re-centrifuged. The resulting precipitate was placed in Spectrum Spectra/Por® regenerated cellulose dialysis membranes having a molecular weight cut-off of 12 000–14 000 Da and dialyzed against water for several days until the water pH remained constant. To achieve colloidal cellulose particles, suspensions were sonicated for 7 minutes at 60 % output control (Vibracell sonicator, Sonics & Materials Inc., Danbury, CT, U.S.A.), while cooling in an ice bath to avoid overheating. Finally, suspensions were allowed to stand over a mixed bed resin (Sigma-Aldrich) for 24 to 48 hours and then filtered through hardened ashless filter paper (Whatman, 541). The final aqueous suspensions were approximately 1 %

concentration by weight; concentration was increased by evaporation at ambient conditions.

Table 2.2. Experimental conditions: reaction time and acid-to-pulp ratios.

Sample	Pulp source	Reaction time	Acid-to-pulp ratio
E	Eucalyptus	25 min	8.75 mL/g
S1	Black spruce	25 min	8.75 mL/g
S2	Black spruce	45 min	8.75 mL/g
S3	Black spruce	45 min	17.5 mL/g

2.2.3 Gravimetric analysis

The concentration of cellulose in the samples was determined by weighing aliquots of the samples before and after the evaporation of water (typically, by heating for 10 to 15 minutes in an oven at 105 °C).

2.2.4 Atomic force microscopy (AFM)

The size distribution of the cellulose nanocrystals was determined by AFM. Original cellulose suspensions were diluted to about 10^{-3} to 10^{-4} % concentration by weight, and filtered through a 0.45- μm membrane (Schleicher & Schuell, NH, U.S.A.). A 20- μL drop of 0.1 % w/v solution of poly-L-lysine (Ted Pella, Inc.) was placed on a $\sim 1 \text{ cm}^2$ piece of freshly cleaved mica for 3 minutes and then washed off with water and the mica dried. A 10- μL drop of suspension was allowed to stand on the mica for 1 minute and then rinsed off with water and dried. The mica was attached to an AFM specimen disc and analyzed. Images were obtained using a NanoScope IIIa Atomic Force Microscope (Digital

Instruments), using an NP tip (Digital Instruments) having a nominal spring constant of 0.12 N/m. Tips have a nominal radius in the range of 20 to 60 nm (given by the manufacturer). Samples were scanned in contact mode under ambient conditions at 2 Hz with scan sizes ranging from 5 to 10 μm using the J piezoelectric scanner (Digital Instruments). Particle diameters were determined using the section analysis tool provided with the AFM software (Digital Instruments, Version 4.32r1). Since the nanocrystals are assumed to be cylindrical in shape, the height of the nanocrystals was taken to be equivalent to the diameter, to compensate for image widening due to the convolution of the tip and the particle. Length measurements were obtained from printouts of several height mode AFM images for each sample. The uncertainty in the AFM length measurements is about 4–7 nm, and the uncertainty in the diameter measurements is about 0.2–0.5 nm. Samples of black spruce and eucalyptus pulp fibres were prepared for AFM as follows: pulp sheets were uniformly dispersed in distilled water ($\sim 0.3\%$ w/v) by prolonged vigorous stirring. The slurry was then filtered through a 200-mesh screen. The mini-handsheet was then removed and pressed between blotting paper and Teflon disks, to yield a flat surface. When the sheet was almost dry, it was pressed with a warm steel disk between Teflon disks. Sections of the mini-handsheets were glued to metal pucks for examination on the AFM.

2.2.5 Phase separation behaviour

Samples of increasing cellulose concentration were prepared from a concentrated “stock” suspension by dilution with water. Suspensions were allowed to stand for 48 hours to equilibrate completely. The volume fraction of the anisotropic phase was determined by measuring the height of the lower phase in each cylindrical vial.

2.2.6 Conductometric titrations

The sodium hydroxide (0.002 N) used in the conductometric titrations was standardized against carefully diluted volumetric standard sulfuric acid. A Contiburette® $\mu 10$ automatic burette (Ing. CAT, Staufen, Germany) was used for all titrations. Titrations were performed with mechanical stirring and under a flow of nitrogen, using an Orion conductivity cell 018010 (cell constant $K = 0.987 \text{ cm}^{-1}$) attached to a Fisher Scientific accumet® pH meter 50. Sulfur content and surface charge density calculations were made using the dimensions determined by AFM, assuming a cylindrical shape and a density of 1.6 g/cm^3 for the cellulose nanocrystals.

2.2.7 Pitch measurement

The chiral nematic pitch of the liquid crystalline phase was determined for each sample at a variety of total cellulose concentrations. An aliquot of each suspension was placed in a rectangular cross-section glass capillary tube having an optical path length of 0.4 mm (VitroCom Inc., NJ, U.S.A.). Photomicrographs were taken using a polarized light microscope (Nikon Microphot-FXA) and the chiral nematic pitch was measured directly from the spacing of the fingerprint texture in the images, where the distance between the lines is equivalent to one half the full pitch.

2.3 RESULTS AND DISCUSSION

The effects of varying cellulose source, reaction time, and acid-to-pulp ratio were investigated for suspensions of wood cellulose nanocrystals.

2.3.1 Eucalyptus vs. black spruce cellulose suspensions

Figure 2.1 shows AFM deflection images of eucalyptus and black spruce pulp fibre surfaces before acid hydrolysis. For both starting materials, the cellulose microfibrils are clearly visible. The microfibril width is on the order of 70 nm and appears to be slightly ($\leq 10\%$) larger for black spruce than for eucalyptus. These dimensions may be influenced by AFM tip broadening artifacts, but are in accord with the dimensions of aggregates of elementary fibrils.²⁶

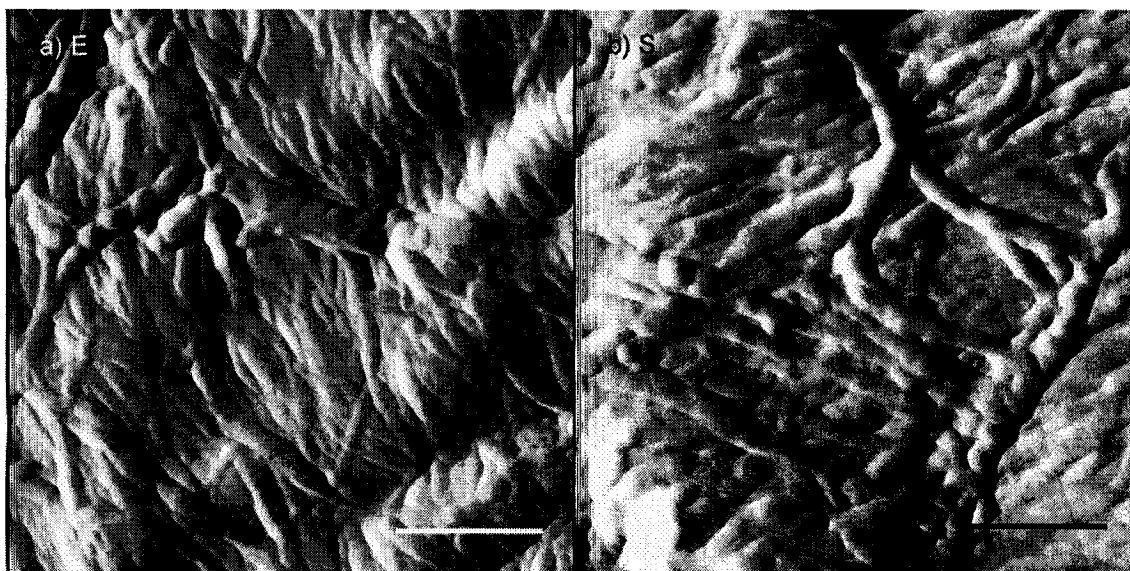


Figure 2.1. Deflection mode AFM images taken in air showing microfibrils on the surface of a) eucalyptus pulp fibre, and b) black spruce pulp fibre. Scale bar = 0.5 μm .

Images taken of the nanocrystals, produced from the two pulps by sulfuric acid hydrolysis, are shown in Figure 2.2, parts a and b. The images were used to determine the distribution of nanocrystal dimensions. Tip artifacts remain a problem in quantifying the widths of the rods, and the different apparent widths of the nanocrystals in Figure 2.2 may be due to the fact that different tips were used to image the black spruce and the eucalyptus samples. To eliminate the effect of tip radius on width measurements, we measured the heights of the nanocrystals, which are not subject to peak broadening artifacts, and assumed the nanocrystals to be cylindrical in shape (see Table 2.3 below). The cross-sectional dimensions of the nanocrystals clustered around 5 nm for both wood species. This is clearly smaller than the apparent size of the microfibril aggregates observed on the pulp fibre surfaces, but close to the dimensions of microfibrillar material observed in fines generated by beating spruce kraft fibres.³¹

The distribution of particle lengths in suspensions E and S1 was obtained from image analysis and is shown in Figure 2.3, parts a and b. The samples show a similar mean particle length, and length polydispersity. The number average particle length was 147 ± 7 nm for the eucalyptus cellulose, and 141 ± 6 nm for the black spruce.

As shown in Table 2.3, the two suspensions are essentially identical in terms of nanocrystal dimensions and surface charge, which suggests that these properties are controlled by reaction conditions such as time, temperature, and acid-to-pulp ratio, all of which were identical for the two samples. Differences in microfibril structure and size do not appear to affect the suspension properties, implying that the basic unit of wood cellulose organization is the same for the two species.

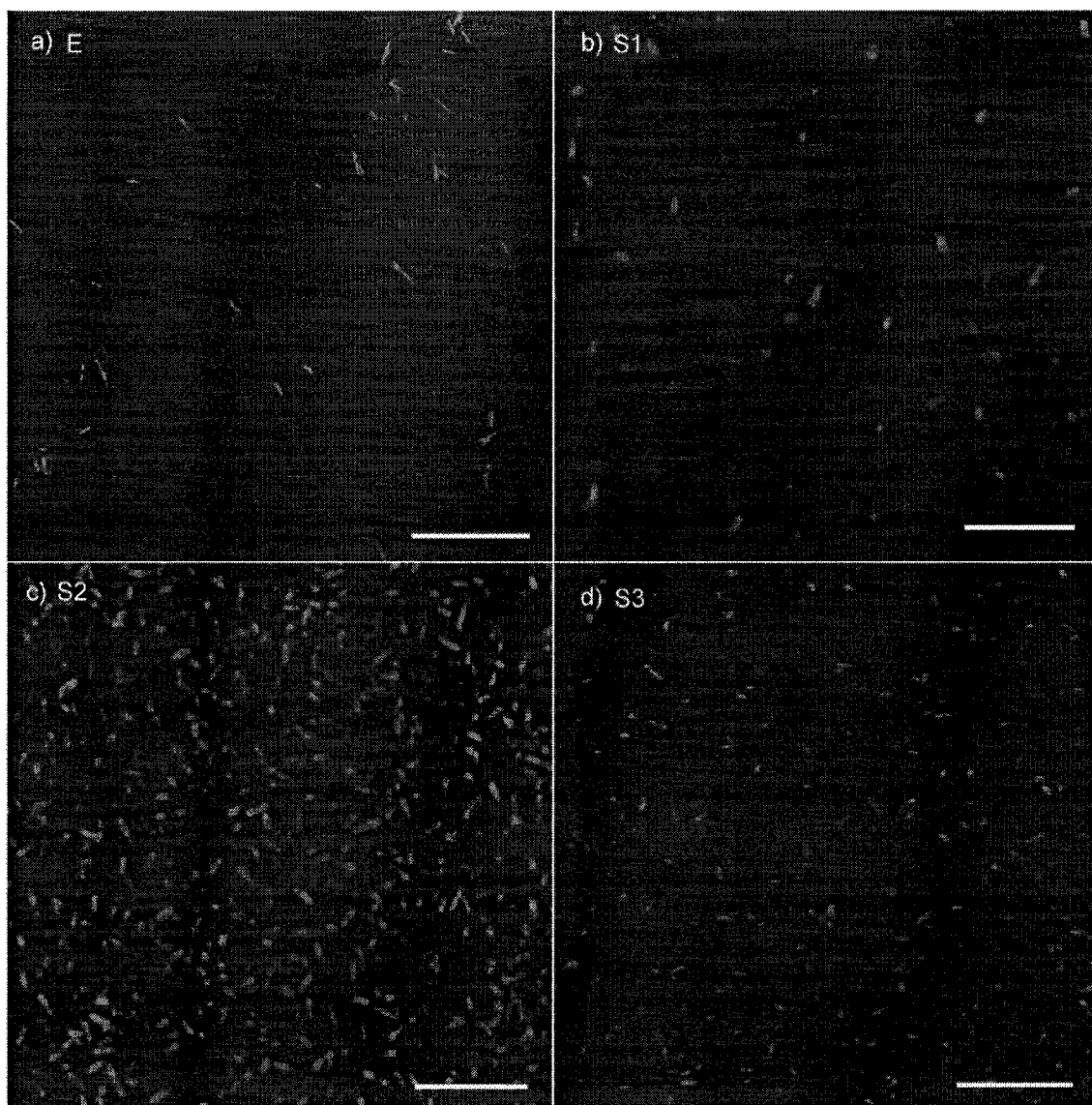


Figure 2.2. Height mode AFM images of cellulose nanocrystals from a) eucalyptus pulp (E), b) black spruce pulp (S1), c) black spruce pulp (S2), and d) black spruce pulp (S3). Scale bar = 1 μm . The herringbone pattern seen in the background is an artifact.

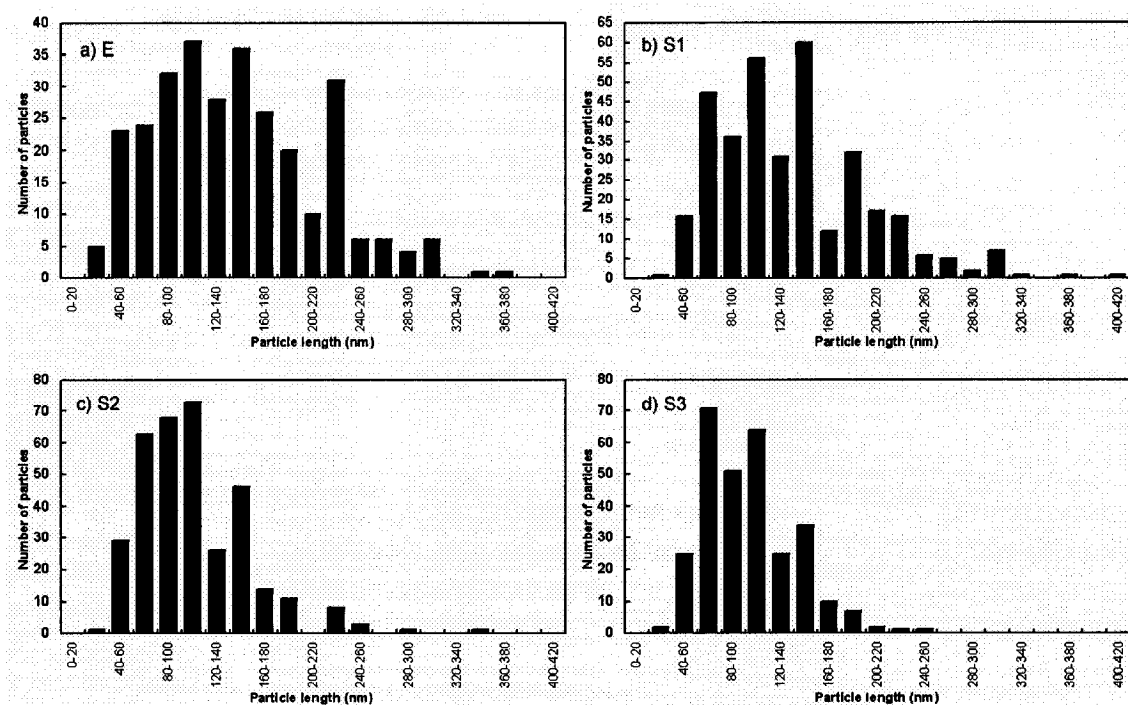


Figure 2.3. Distribution of particle length of cellulose nanocrystals from suspensions a) E, b) S1, c) S2, and d) S3.

Table 2.3. Effect of hydrolysis conditions on suspension properties.

	E	S1	S2	S3
Nanocrystal length, L	147 ± 7 nm	141 ± 6 nm	120 ± 5 nm	105 ± 4 nm
Standard deviation in L	65 nm	60 nm	45 nm	36 nm
Nanocrystal diameter, D	4.8 ± 0.4 nm	5.0 ± 0.3 nm	4.9 ± 0.3 nm	4.5 ± 0.3 nm
Axial ratio, L/D	30.6	28.2	24.5	23.3
Sulfur content	0.80 ± 0.03 S %	0.89 ± 0.06 S %	1.06 ± 0.02 S %	$(0.86 \pm 0.02$ S %) ^a
Surface charge density, σ	0.29 ± 0.01 e/nm ²	0.33 ± 0.02 e/nm ²	0.38 ± 0.01 e/nm ²	-- ^a
Critical concentration, c^*	4.6 wt%	4.8 wt%	5.3 wt%	6.9 wt%
Chiral nematic pitch, P^b	21 μ m	18 μ m	10 μ m	7 μ m

^a See text for explanation. ^b Measured at a total cellulose concentration of 7 wt%.

The eucalyptus and black spruce suspensions do not differ noticeably in the value of the critical cellulose concentration, c^* , required for the formation of an anisotropic liquid crystalline phase. Figure 2.4, parts a and b, shows the phase separation diagrams of the two suspensions. The biphasic range is also essentially the same for the two pulps. Phase separation of rod-like particles is governed by the axial ratio and the surface charge of the rods, with a decrease in either variable tending to increase the critical concentration for anisotropic phase formation.^{15,35} These properties are also nearly identical for the two suspensions; there are no differences that can be attributed to the wood species.

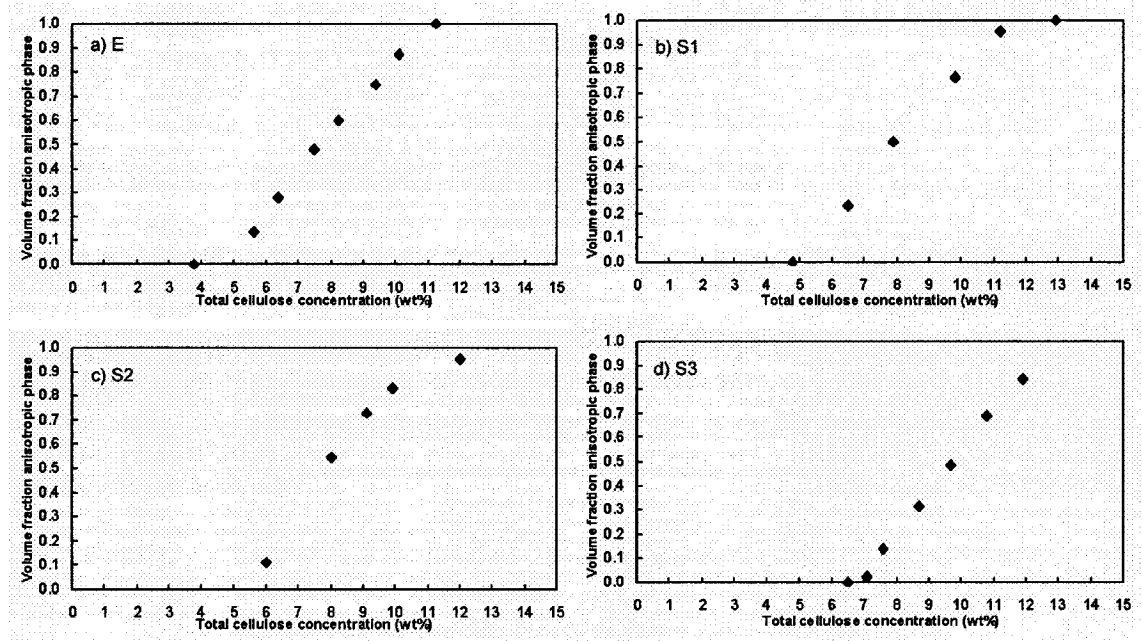


Figure 2.4. Phase separation diagrams for suspensions a) E, b) S1, c) S2, and d) S3. The region in which the volume fraction of the anisotropic phase, ϕ_{aniso} , lies between 0 and 1 is the biphasic region. To the left of the biphasic region, $\phi_{\text{aniso}} = 0$, and the suspensions are completely isotropic. To the right of the biphasic region, $\phi_{\text{aniso}} = 1$, and the suspensions are completely anisotropic.

2.3.2 Effect of reaction time on softwood suspension properties

Reaction time is one of the most important parameters to consider in the acid hydrolysis of wood pulp. Too long a reaction will digest the cellulose completely to yield its component sugar molecules; too short a reaction will yield only large undispersable fibres and aggregates. There exists a fairly narrow range of reaction time which yields the desired suspension of well-dispersed colloidal nanocrystals. Within this range, the reaction time must be optimized to obtain the largest yield possible.

Black spruce pulp was subjected to 25- or 45-minute hydrolysis using an acid-to-pulp ratio of 8.75 mL/g (S1 and S2, respectively). Figure 2.2, parts b and c, shows AFM images of the nanocrystals. The distribution of particle lengths in S2 is shown in Figure 2.3c. Suspension S2 shows a smaller mean particle length (120 ± 5 nm) than S1 (141 ± 6 nm), as well as a narrower, less polydisperse length distribution, attributable to the longer hydrolysis time.

Table 2.3 shows that at the longer reaction time, suspension S2 has a higher sulfur content. The production of shorter, less polydisperse rods with higher sulfur content at longer reaction times is consistent with previous literature results.^{12,36} As expected from the larger sulfur content, the surface charge density σ of the nanocrystals, calculated using the sulfur content and the nanocrystal dimensions, appears to increase with increasing reaction time for this acid-to-pulp ratio. Suspension S1 has a surface charge density of 0.33 ± 0.02 e/nm², which is smaller than the value of 0.38 ± 0.01 e/nm² obtained for S2.

Figure 2.4, parts b and c, shows the phase separation diagrams for suspensions S1 and S2. Increasing the reaction time from 25 to 45 minutes causes an increase in the critical concentration for the formation of anisotropic phase, from 4.8 wt% to 5.3 wt%.

According to Onsager's phase separation theory for uncharged rods, c^* decreases with increasing axial ratio (L/D).¹⁵ However, due to the charged surface sulfate esters, the rod-like cellulose nanocrystals are polyelectrolytic in nature. The electrostatic interactions between the rods result in an increase in effective diameter and a twisting factor that governs particle orientation.^{37,38} Thus, the interparticle forces are not only governed by the axial ratio, but also by the ionic strength³⁸ and the nature of the counterions.³⁹ Phase separation behaviour and therefore critical concentration is very sensitive to variation in particle geometry and electrostatic interactions.³⁸ For example, Dong et al. found that longer hydrolysis times result in a rapid decrease in the critical concentration; more extensive hydrolysis generates cellulose rods with larger axial ratios (due to the breaking up of coarse aggregates of cellulose), as well as increased total surface charge.¹² In addition, theory predicts that the polydispersity plays a role in determining the critical concentration: The narrower length distribution of suspensions resulting from longer hydrolysis times increases the critical concentration.⁴⁰ The effect of reaction time on the critical concentrations of suspensions S1 and S2 can therefore be summarized as follows.

(1) Suspension S2 has a narrower length distribution and smaller average particle length and a slightly smaller axial ratio than S1. These factors would increase the value of c^* for S2, as observed.

(2) However, suspension S2 has a higher total surface charge (measured as sulfur content), as well as surface charge density, which would decrease the value of c^* for S2.

Based on our observations of S1 and S2, rod dimensions and geometry appear to influence critical concentration to a greater extent than surface charge in this case.

2.3.3 Effect of acid-to-pulp ratio on softwood suspension properties

Black spruce pulp was subjected to 45-min hydrolysis using acid-to-pulp ratios of 8.75 mL/g and 17.5 mL/g (suspensions S2 and S3, respectively). AFM images of the nanocrystals are shown in Figure 2.2, parts c and d.

The distribution of particle lengths in suspension S3 is shown in Figure 2.3d. Suspensions S2 and S3 show comparable mean particle lengths, the higher acid-to-pulp ratio affording a smaller mean length (120 ± 5 nm for S2 and 105 ± 4 nm for S3) as well as smaller polydispersity (Table 2.3).

The effect of acid-to-pulp ratio on suspension properties has not been thoroughly investigated in the literature; it has been found in this lab that larger volumes of the 64 wt% acid used tend to hydrolyze a given amount of pulp faster, and thus yield shorter rods for a given reaction time. This is somewhat unexpected, as in all cases, the acid is in excess relative to the pulp. The effect is not large, as shown in Table 2.3: doubling the acid-to-pulp ratio resulted in a decrease in rod length of about 12.5 % for a reaction time of 45 min. A recent study found the sulfur content of bacterial cellulose to increase with acid-to-cellulose ratio and hydrolysis time.⁹ Acid-to-pulp ratio was not seen to have a well-defined effect on sulfur content of the wood cellulose suspensions (see below); suspension S3 has a lower sulfur content than S2 (0.86 vs. 1.06 S %). However, it should be noted that the sulfur content listed for S3 in Table 2.3 was obtained using a different batch of suspension produced under the same reaction conditions as the suspension which was used for all other measurements.

The phase separation diagrams for suspensions S2 and S3 are shown in Figure 2.4, parts c and d. Doubling the acid-to-pulp ratio leads to an increase in the critical

concentration (from 5.3 to 6.9 wt%). The smaller mean rod length and the lower total surface charge of the rods would also tend to increase the critical concentration of S3.

When comparing suspensions S3 and S1, it can be seen that the combination of longer reaction time and higher acid-to-pulp ratio yields a suspension having a smaller mean rod length and narrower length distribution (i.e., smaller polydispersity), as expected. Because the critical concentration of S3 is significantly larger than that of S1, it follows that the decreases in length polydispersity affect the critical concentration to a greater extent than do decreases in average rod length under the conditions used.

2.3.4 Chiral nematic pitch

Figure 2.5 shows the fingerprint texture of the chiral nematic phase of a eucalyptus suspension. The chiral nematic pitch measured from the fingerprint texture in photomicrographs of the suspensions decreased with increasing cellulose concentration. For example, when S1 concentration was increased from 7 wt% to 13 wt%, pitch decreased from $\sim 20\ \mu\text{m}$ to $\sim 10\ \mu\text{m}$. This decrease in pitch with increasing concentration of chiral rods has been observed in several chiral rod systems. There are however few reports of the effect of rod length or charge on the liquid crystal chiral nematic pitch P . We measured the chiral nematic pitch at a total cellulose concentration of 7 wt% for all suspensions, which have varying average nanocrystal lengths. The pitch was found to increase with increasing rod length (Figure 2.6), in accord with an observation of Grelet and Fraden on mutant virus fd suspensions.⁴¹ Thus, the longer rods show less tendency to form the twisted chiral nematic structure, presumably because at the same volume fraction of rods in the suspension, longer rods show a greater tendency to align in a parallel (untwisted) arrangement. The suspensions show a similar tendency to align and increase the pitch when the ionic strength is decreased.³⁸ The pitch found for suspensions

E and S1 was close to that found for the sodium form of cotton cellulose nanocrystals by Dong and Gray at similar total cellulose concentrations.³⁹

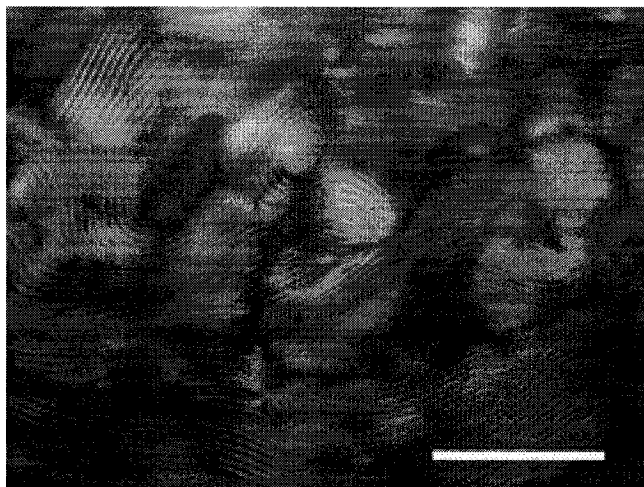


Figure 2.5. Fingerprint texture in chiral nematic phase of 10 wt% eucalyptus suspension, viewed in polarizing microscope. Scale bar = 200 μm . Chiral nematic pitch $P = 17 \mu\text{m}$.

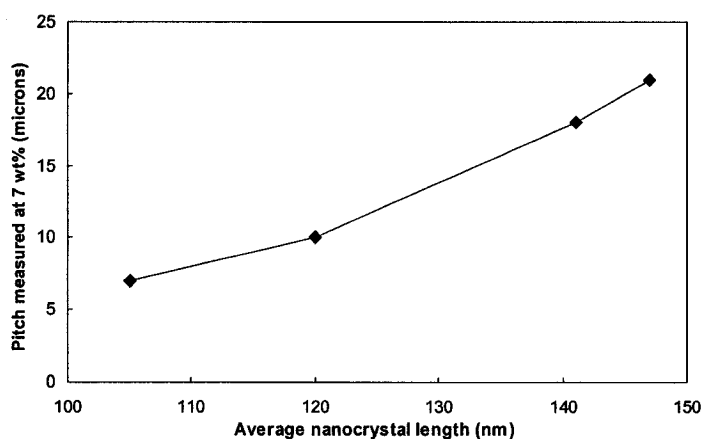


Figure 2.6. The effect of average cellulose nanocrystal length on the chiral nematic pitch P measured at 7 wt% cellulose suspension concentration.

2.4 CONCLUSIONS

The properties of colloidal eucalyptus cellulose suspensions produced by sulfuric acid hydrolysis are essentially identical to those of similarly prepared black spruce cellulose suspensions. For black spruce pulp, longer hydrolysis times lead to shorter cellulose rods with narrower particle length distribution; the effect on sulfur content and surface charge is less clear. Higher acid-to-pulp ratio decreases nanocrystal dimensions to some extent at the reaction time of 45 minutes. At the shorter reaction time of 25 minutes, the effect of acid-to-pulp ratio on critical concentration and rod dimensions may be more apparent. An effect of the reaction conditions on cellulose nanocrystal surface charge and sulfur content was not apparent. The surface charge of nanocrystals is highly sensitive to heat, as an increase in temperature can cause de-esterification of the sulfate groups on the surface of the crystals. Although we cooled the suspensions in an ice bath during sonication, an increase in temperature, in particular local temperature, cannot be completely ruled out. Surface charge and sulfur content of the cellulose may therefore be controlled by factors other than hydrolysis conditions. Chiral nematic pitch decreases with increasing cellulose concentration and decreasing nanocrystal length.

2.5 REFERENCES

- (1) de Sousa Lima, M.M.; Borsali, R. *Macromol. Rapid. Comm.* **2004**, *25*, 771-787.
- (2) Rånby, B.G. *Acta Chem. Scand.* **1949**, *3*, 649-650.
- (3) Rånby, B.G.; Ribí, E. *Experientia* **1950**, *6*, 12-14.
- (4) Mukherjee, S.M.; Woods, H.J. *Biochim. Biophys. Acta* **1953**, *10*, 499-511.
- (5) Marchessault, R.H.; Morehead, F.F.; Walter, N.M. *Nature* **1959**, *184*, 632-633.
- (6) Hermans, J. *J. Polym. Sci., Part C: Polym. Symp.* **1963**, *2*, 129-144.
- (7) Revol, J.-F.; Bradford, H.; Giasson, J.; Marchessault, R.H.; Gray, D.G. *Int. J. Biol. Macromol.* **1992**, *14*, 170-172.
- (8) Araki, J.; Kuga, S. *Langmuir* **2001**, *17*, 4493-4496.
- (9) Roman, M.; Winter, W.T. *Biomacromolecules* **2004**, *5*, 1671-1677.
- (10) Araki, J.; Wada, M.; Kuga, S.; Okano, T. *J. Wood Sci.* **1999**, *45*, 258-261.
- (11) Dinand, E.; Chanzy, H.; Vignon, M.R. *Food Hydrocolloids* **1999**, *13*, 275-283.
- (12) Dong, X.M.; Revol, J.-F.; Gray, D.G. *Cellulose* **1998**, *5*, 19-32.
- (13) Favier, V.; Chanzy, H.; Cavaillé, J.Y. *Macromolecules* **1995**, *28*, 6365-6367.
- (14) Araki, J.; Wada, M.; Kuga, S.; Okano, T. *Colloids Surf., A* **1998**, *142*, 75-82.
- (15) Onsager, L. *Ann. N.Y. Acad. Sci.* **1949**, *51*, 627-659.
- (16) Revol, J.F.; Godbout, L.; Dong, X.M.; Gray, D.G.; Chanzy, H.; Maret, G. *Liq. Cryst.* **1994**, *16*, 127-134.
- (17) Araki, J.; Wada, M.; Kuga, S.; Okano, T. *Langmuir* **2000**, *16*, 2413-2415.
- (18) Battista, O.A.; Coppick, S.; Howsmon, J.A.; Morehead, F.F.; Sisson, W.A. *Ind. Eng. Chem.* **1955**, *48*, 333-335.

- (19) Marchessault, R.H.; Morehead, F.F.; Koch, M.J. *J. Colloid Sci.* **1961**, *16*, 327-344.
- (20) Belton, P.S.; Tanner, S.F.; Cartier, N.; Chanzy, H. *Macromolecules* **1989**, *22*, 1615-1617.
- (21) Sassi, J.-F.; Chanzy, H. *Cellulose* **1995**, *2*, 111-127.
- (22) Terech, P.; Chazeau, L.; Cavaillé, J.Y. *Macromolecules* **1999**, *32*, 1872-1875.
- (23) de Sousa Lima, M.M.; Borsali, R. *Langmuir* **2002**, *18*, 992-996.
- (24) Hermans, P.H. *Makromol. Chem.* **1951**, *6*, 25-29.
- (25) Sjöström, E. *Wood Chemistry: Fundamentals and Applications*; 2nd ed.; Academic Press: New York, 1981.
- (26) Fengel, D.; Wegener, G. *Wood: Chemistry, Ultrastructure, Reactions*; Walter de Gruyter: New York, 1984.
- (27) Tokoh, C.; Takabe, K.; Fujita, M.; Saiki, H. *Cellulose* **1998**, *5*, 249-261.
- (28) Grunert, M.; Winter, W.T. *J. Polym. Environ.* **2002**, *10*, 27-30.
- (29) Revol, J.-F. *Carbohydr. Polym.* **1982**, *2*, 123-134.
- (30) Hanley, S.J.; Giasson, J.; Revol, J.-F.; Gray, D.G. *Polymer* **1992**, *33*, 4639-4642.
- (31) Hanley, S.J.; Gray, D.G. *J. Pulp Pap. Sci.* **1999**, *25*, 196-200.
- (32) Jayme, G.; Koburg, E. *Holzforschung* **1959**, *13*, 37-43.
- (33) Fink, H.P.; Hofmann, D.; Purz, H.J. *Acta Polym.* **1990**, *41*, 131-137.
- (34) Harada, H.; Kishi, A.; Sugiyama, J. *Structure of cellulose microfibrils in wood*: Proceedings of the International Symposium on Wood Pulping Chemistry, Tsukuba, Japan, 1983, pp. 6-10.
- (35) Odjik, T. *Macromolecules* **1986**, *19*, 2313-2329.

- (36) de Sousa Lima, M.M.; Wong, J.T.; Paillet, M.; Borsali, R.; Pecora, R. *Langmuir* **2003**, *19*, 24-29.
- (37) Stroobants, A.; Lekkerkerker, H.N.W.; Odjik, T. *Macromolecules* **1986**, *19*, 2232-2238.
- (38) Dong, X.M.; Kimura, T.; Revol, J.-F.; Gray, D.G. *Langmuir* **1996**, *12*, 2076-2082.
- (39) Dong, X.M.; Gray, D.G. *Langmuir* **1997**, *13*, 2404-2409.
- (40) Moscicki, J.K.; Williams, G. *Polymer* **1982**, *23*, 558-568.
- (41) Grelet, E.; Fraden, S. *Phys. Rev. Lett.* **2003**, *90*, 198302-1 - 198302-4.

Introduction to the Characterization of Blue Dextran

Determining the properties of a cellulose nanocrystal suspension is essential to understanding its behaviour when mixed with a macromolecule. However, knowledge of the properties of the macromolecule itself can be equally important in interpreting its effect on the resulting phase separation phenomena. Blue dextran is at the core of the phase separation studies performed in this thesis. Because the dye ligands in blue dextran clearly contribute to the observed phase behaviour when it is mixed with cellulose nanocrystal suspensions, it was thought necessary to characterize these macromolecules in greater detail. In the following chapter, the physico-chemical properties of a range of blue dextrans are investigated. A brief introduction to some of the characterization methods is presented here.

Dextrans are hygroscopic and can absorb up to 10–20 % moisture at 50 % relative humidity.¹ Thermogravimetric analysis (TGA) was therefore used to quantify the dextran and blue dextrans' moisture content in order to obtain accurate concentrations of dextran solutions, important in the measurement of viscosity and dn/dc (see below).

The viscosity of dilute solutions of polymers can be used to measure their hydrodynamic dimensions and molecular weights via the intermolecular interactions in the solvent: the intrinsic viscosity of random coil polymers is related to the volume occupied by a single molecule in the solution (i.e., the radius of gyration).² Blue dextrans' polyelectrolytic nature greatly modifies their viscosity behaviour as compared to unmodified dextrans. The lack of data in the literature made viscosity experiments essential, as, for example, information regarding the dilution regime is provided by the critical concentration C^* .

¹ Fakes, M.G.; Dali, M.V.; Haby, T.A.; Morris, K.R.; Varia, S.A.; Serajuddin, A.T. *PDA J. Pharm. Sci. Technol.* **2000**, *54*, 144-149.

² Hiemenz, P.C. *Polymer Chemistry: The Basic Concepts*; Marcel Dekker, Inc.: New York, 1984, p 583.

Gel permeation chromatography (GPC) was performed to determine the purity of blue dextrans synthesized in this lab. A high ionic strength solvent (0.8 M aqueous NaNO_3) was used to screen the charges of the blue dextran and prevented the dextran–dye derivatives from interacting with and sticking to the column, which contain macroporous copolymer beads with an extremely hydrophilic “neutral” polyhydroxyl functionality.³

Light scattering detection coupled to the GPC was used to obtain both number- and weight-average molecular weights, as well as radii of gyration. A differential refractive index detector was used to obtain values of the specific refractive index increment dn/dc (the change in solution refractive index versus the change in concentration of the blue dextran). Calculating the “instantaneous” concentrations and molecular weights by light scattering is only possible knowing dn/dc , which may be obtained by one of two means. First, normalizing the concentration chromatogram based on the accurately-known mass of polymer injected allows the concentration c eluted from the GPC to be calculated. The term dn/dc is then found based on c and the calibration of the infrared (IR) detector in volts per Δn . Alternatively, the dn/dc term may be found in published tables or from previous characterizations of similar polymers. Calibration of the IR detector can then be performed using polymer standards having precisely-known dn/dc values. The second option was not available to us, as the blue dextrans had not been previously characterized. The value of dn/dc depends on the wavelength at which it is measured, particularly at shorter wavelengths. In theory, the dn/dc found at 633 nm by multi-angle light scattering will differ from that measured by IR refractometry at 900 nm; however, the discrepancies are small in this wavelength range.

³ *Polymer Laboratories Aqueous GPC / SEC columns*, URL <http://www.polymerlabs.com/gpc/aqueous.htm>

Chapter 3

Synthesis and Characterization of Blue Dextrans.

**A Comparative Study of the Physico-chemical Properties for
Various Molecular Weights and Dye Loadings**

3.1 INTRODUCTION

Dextran, a polymer of α -D-(1,6)-linked anhydroglucose containing $\sim 5\%$ α -(1,3) branching, produced by strains of *Leuconostoc mesenteroides* bacteria, has been used in clinical applications such as plasma extenders and centrifugation.¹⁻⁵ Blue dextran, a soluble dextran complex consisting of the triazinyl dye Cibacron blue F3GA covalently bound to high molecular weight (2000 kDa) dextran,⁶ was developed for use as a visible marker for void volume in gel filtration chromatography columns.^{7,8} Further, certain proteins were found to elute in the void volume of the gel filtration column when they were co-chromatographed with blue dextran, allowing them to be separated from other proteins of similar molecular weight. It was established in 1968 that the dye ligand was responsible for binding to these proteins.⁹⁻¹¹ This phenomenon has been widely exploited in protein purification by affinity chromatography,¹¹⁻¹³ the low cost, high affinity and high protein-binding capacity of various triazine dyes making them attractive and useful as substitutes for more specific coenzymes.^{7,13} Initially, blue dextran was bound to various supports; later the dye alone was conjugated directly to matrices such as agarose and cross-linked dextran gels to improve the column capacity and reduce leakage of the dye into the eluate.^{14,15} Triazine dyes are also used to immobilize or link other affinity ligands to matrices for affinity gel filtration.⁷ The need for a means of selecting the dye having optimal affinity for a particular protein was recognized in 1990,¹⁶ and within two years, rational design allowed ligands to be “designed specifically to interact with the protein to be purified.”¹⁷ More recently, blue dextran and other dextran derivatives such as FITC-dextran have been used as easily-visualized macromolecules in studies of demixing (phase separation) and partitioning phenomena for systems of rodlike colloidal particles.¹⁸⁻²⁰

Blue dextran preparation methods are adapted from those used to couple dyes to support matrices such as cross-linked dextran and agarose.^{13,21,22} The dye–dextran coupling occurs as a nucleophilic substitution reaction between the chlorine moiety of the triazine dye and the hydroxyl groups of the dextran substrate.²³ Dextran is dissolved in water, and a base (typically Na_2CO_3 , NaOH ,¹³ or Na_3PO_4 ^{9,22}) and the dye are added. The mixture is then heated (25–90 °C) for a period of hours to days.¹³ Precipitation of the dextran with ethanol followed by redissolution in water is repeated several times; other purification steps, such as dialysis or treatment with diethylaminoethyl cellulose as an anion exchanger, may also be used to remove unbound dye.²² The addition of sodium chloride to the dye/dextran mixture prior to the addition of base, essential for optimal coupling of the dye to a cross-linked matrix, is not necessary for the free dextran polymer.¹³ Reaction conditions significantly affect the degree of dye substitution which may be obtained with both cross-linked dextran gels and dextran itself.^{7,13,22,24,25} Mayes et al. found that increasing the reaction time led to higher dye ligand density on the dextran.²⁴ Reaction completion times decrease with increasing temperature; for monochlorotriazinyl dyes such as Cibacron blue, coupling takes 3 to 5 days at room temperature, as compared to 2 hours at 60 °C.¹³ Optimum base concentrations also vary from 0.10 M Na_2CO_3 to 0.05–0.20 M NaOH for monochlorotriazinyl dyes.^{13,26,27} Blue dextran is produced commercially, but the effect of altering the reaction conditions on the properties of the dextran–dye conjugate has not been assessed.

The physico-chemical properties of dextrans have been thoroughly studied. The molecular weight distribution of native and fractionated dextrans,^{28,29} as well as the radius of gyration^{30,31} have been obtained by light scattering and other methods such as

size exclusion chromatography.^{32,33} Branching and dextran structure have been studied by several methods,³⁴⁻³⁷ yielding conflicting data which suggest branches shorter than 3 glucose units^{38,39} or as long as 50 units.^{28,40} Viscosity behaviour of dextrans in various solvents has been explored for a variety of molecular weight fractions.^{28,29,32,41} Dextran derivatives such as dextran sulfates have also been characterized.⁴²

Perhaps not surprisingly given their principal use as bound ligands for affinity chromatography, blue dextrans have been characterized mainly with regard to degree of dye substitution.²⁴ The dextran concentration in a solution can be determined by polarimetry or dry weight measurements combined with spectroscopy, while the dye concentration is determined by UV-visible spectrometry.^{22,24} Care must be taken to avoid conditions leading to dye-stacking in solution, which causes a concentration-dependent red-shift for Cibacron blue.⁷ The optical properties of blue dextran have also been exploited in order to test an optical detection system for molecular weight measurement of dye-labeled polysaccharides by analytical ultracentrifugation, during which study the molecular weight of blue dextran 2000 was verified.⁴³ However, no in-depth studies of the physico-chemical properties of blue dextran 2000 have been performed, as noted by Ohta et al.⁴⁴ While dextran properties such as branching and polydispersity remain unchanged upon binding the dye ligands to the dextran chain, it is reasonable to assume that the nature of the attached dye can significantly affect the physico-chemical properties of the polymer. The bound aromatic sulfonate dye introduces both hydrophobic and ionic elements into the dextran macromolecule, which will alter its properties and behaviour in solution as compared to unmodified dextrans. This chapter examines the effect of Cibacron blue dye ligands on the physico-chemical properties of blue dextrans of nominal molecular weights ranging from 70 to 2000 kDa. It presents a first step towards the

optimization of the tailored synthesis of blue dextrans of different molecular weights and provides an initial look at their physico-chemical properties in solution. An understanding of the effect of dye ligands on the properties of blue dextrans may ultimately provide insight into their interactions (electrostatic, hydrophobic and steric) with other polyelectrolytes such as cellulose nanocrystals with surface sulfate groups. It is hoped that this data will be useful in elucidating the effect of charged and uncharged dextrans on the phase behaviour of aqueous cellulose nanocrystal suspensions.^{18,20}

3.2 METHODS AND MATERIALS

3.2.1 Chemicals

Dextrans T-70, T-110, T-500, T-2000 (nominal $\bar{M}_w = 70\,000, 106\,000, 532\,000$ and $2\,000\,000$, respectively, manufacturer's data) were purchased from Pharmacia Fine Chemicals (Sweden). Blue dextran 2000 ($\bar{M}_w \approx 2\,000\,000$ with 0.1 mmol Reactive blue 2 dye per gram of dextran bonded randomly via an ether linkage to the polymer backbone⁶) was purchased from Aldrich. Cibacron blue 3G-A (CB, 55 % dye content) was purchased from Aldrich and used without further purification; see Figure 3.1 for the structure. Sodium chloride (ACS reagent grade) was purchased from Fisher Scientific. Sodium carbonate (ACS reagent grade) was purchased from Anachemia. All reactions were performed using water purified with a Millipore Milli-Q purification system.

3.2.2 Preparation of blue dextrans

Blue dextrans of various molecular weights and degree of dye substitution (Table 3.1) were prepared using methods adapted from Mayes et al.²⁴ and Tang et al.⁴⁵ (Figure 3.1). A typical preparation is as follows: A solution of 4 g of dextran T-2000 in 120 mL of

water was mixed with solutions of 0.8 g of Cibacron blue 3G-A (55 % dye content) in 40 mL of water and 0.2 g of Na_2CO_3 in 40 mL of water. The mixture was shaken in a water bath at 45 °C. After around 75 h, the free reactive dye is consumed²⁴ and another 0.8 g of CB was added. To precipitate the dextran–dye conjugate, an equal volume of ethanol was added to the mixture, which was allowed to stand at –20 °C for at least 60 min. The precipitate was then spun down and rinsed with ethanol. Following resuspension in 40 mL of water, the dextran was dialyzed (Spectrum Spectra/Por membrane, molecular weight cutoff 12 000–14 000) against distilled water to remove any traces of unreacted dye and salt. Cleavage of the chromophore from the dextran chain has not been found to occur in aqueous solution;^{46,47} this was confirmed by gel filtration using Bio-Gel P-30 size exclusion polyacrylamide gel (nominal exclusion limit 40 kDa, Bio-Rad Laboratories), which indicated the absence of unreacted or free dye. Solutions of the blue dextrans were filtered through glass microfiber filters (Ahlstrom, 0.7 μm pore size). The final product was lyophilized and stored as a solid. Final yields were comparable to literature values.²⁴

3.2.3 Thermogravimetric analysis (TGA)

Moisture contents of the dextrans and dextran–dye conjugates were determined by thermogravimetric analysis (TA Instruments TGA Q500). The dextrans contained 10.5–11.5 % water by mass, and the blue dextrans contained 9–15 % water by mass. All dextran concentrations were calculated taking moisture contents into account.

Table 3.1. Preparation conditions and dye ligand densities for blue dextrans.

Dextran	Reaction time (h)	Dye/Dx ratio (mol:mol)^a	[Na₂CO₃] (M)	Dye ligand density (DS/AGU^b, 10⁻⁴)	Yield (%)
Blue Dx 2000₁₆	21.5	300	0.010	16	46
Blue Dx 2000₃₀	48.0	300	0.010	30	60
Blue Dx 2000₃₆	96.5	300	0.010	36	46
Blue Dx 2000₅₆	144.5	300	0.010	56	48
Blue Dx 2000₁₆₁	n/a ^c	n/a ^c	n/a ^c	161	n/a ^c
Blue Dx 2000₇	48	150	0.018	7	22
Blue Dx 2000₈	48	300	0.018	8	40
Blue Dx 2000₁₅	48	600	0.018	15	19
Blue Dx 2000₁₂	48	300	0.036	12	72
Blue Dx 2000₁₇	48	300	0.072	17	87
Blue Dx 2000₁₉	48	300	0.126	19	84
Blue Dx 500₁₁	24.0	300	0.008	11	39
Blue Dx 110₂₃	24.0	300	0.040	23	28
Blue Dx 70₆₆	144.0	10	0.189	66	47

^a Initial ratio. ^b Degree of substitution per anhydroglucose repeat unit. ^c Commercially available blue dextran 2000 (Aldrich).

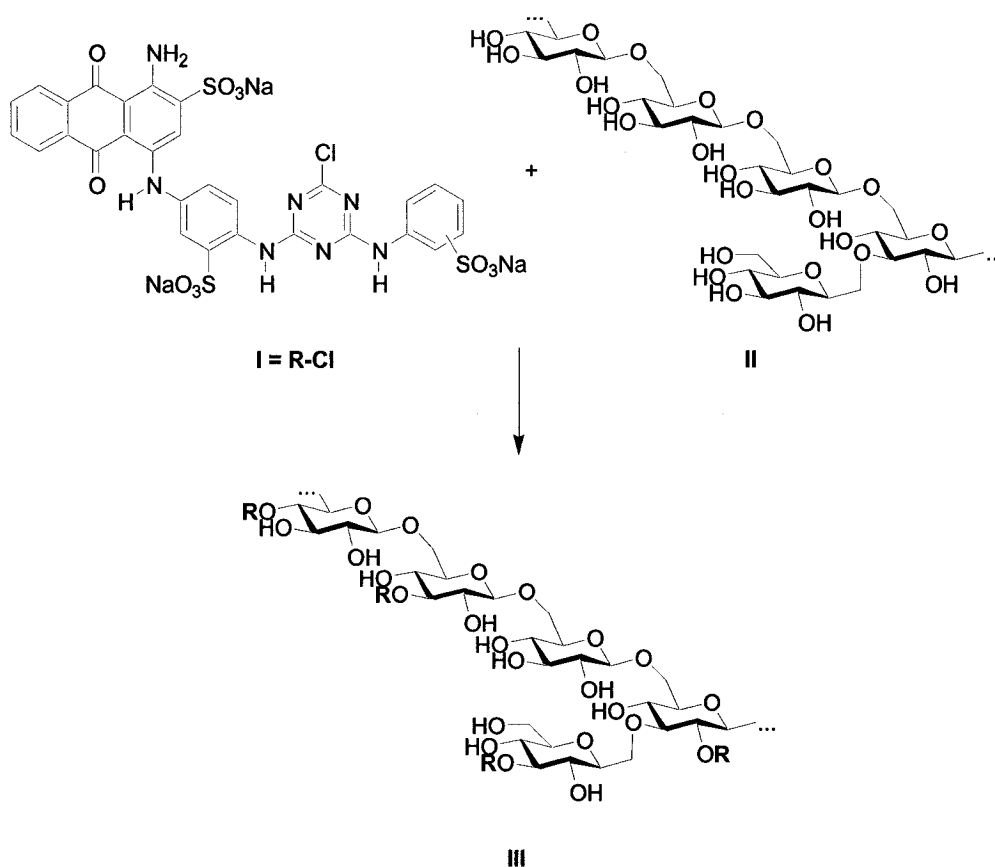


Figure 3.1. Coupling of Cibacron blue 3G-A (I = R-Cl) with dextran (II) to give blue dextran (III), showing the random binding sites of the dye.⁶

3.2.4 UV–visible spectroscopy

The dye content of the dextran–dye conjugates was determined from UV–visible spectra (Figure 3.2a) measured with a Varian Cary 300 Bio spectrophotometer. A calibration curve was obtained from solutions of commercially-available blue dextran 2000 (Figure 3.2b). Adherence to the Beer-Lambert law was established. The molar extinction coefficient for blue dextran 2000 at 609 nm was found to be $8870 \text{ M}^{-1}\text{cm}^{-1}$. The extinction coefficient at 620 nm was $8970 \text{ M}^{-1}\text{cm}^{-1} = 0.823 \text{ g}^{-1}\text{dm}^3\text{cm}^{-1}$, which agrees well with the value of $0.812 \text{ g}^{-1}\text{dm}^3\text{cm}^{-1}$ found by Champ et al. for commercially available blue dextran 2000.⁴⁷ The ligand density was estimated from absorbance

measurements at 609 nm for solutions of the dextran–dye conjugates, and calculated in terms of the degree of substitution (DS) per anhydroglucose (AGU) repeat unit. Absorbance measurements in dilute aqueous solution and in 6 M HCl (aq)^{24,48} have shown that negligible intramolecular dye stacking occurs at dye ligand densities comparable to those reported in this chapter.

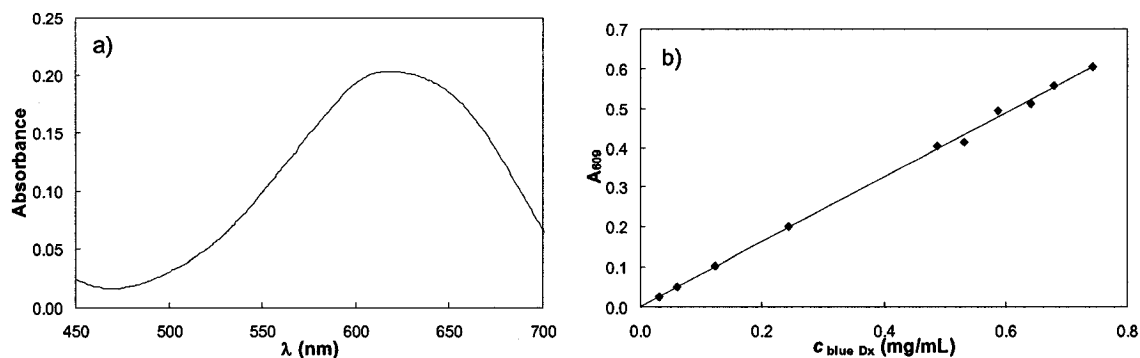


Figure 3.2. a) Absorption spectrum for blue dextran in water (0.266 mg/mL). b) Calibration curve of absorbance at 609 nm versus concentration c in mg/mL.

Blue dextran samples are denoted by their molecular weight followed by a subscript number indicating the degree of dye substitution per anhydroglucose repeat unit. However, according to convention, commercially available blue dextran 2000 purchased from Aldrich will be referred to as “blue dextran 2000” in the text, except where necessary for clarity.

3.2.5 Viscosity measurements

Viscosity measurements were carried out in a capillary viscometer of Cannon-Fenske type at a constant temperature of 25 ± 0.01 °C. Solvent flow times were on the order of 10 seconds; the kinetic energy correction was performed. Each data point is the average of at least three trials. Samples contained from 3×10^{-4} to 2×10^{-2} g/mL polymer and were filtered with a $0.45 \mu\text{m}$ membrane prior to analysis.

If the viscosity of the solution η is defined as the sum of the solvent viscosity η_s and the viscosity due to the dissolved polymer η_p , the specific viscosity of the polymer in the solvent is given by equation 3.1:⁴⁹

$$\eta_{sp} = \frac{\eta_p}{\eta_s} = \frac{\eta - \eta_s}{\eta_s} \quad (3.1)$$

The reduced viscosity η_{red} is calculated dividing the specific viscosity η_{sp} by the concentration c of the polymer in g/mL:⁴⁹

$$\eta_{red} = \frac{\eta_{sp}}{c} = \frac{\eta - \eta_s}{\eta_s \cdot c} = \frac{\eta_{rel} - 1}{c} \quad (3.2)$$

The Huggins equation,

$$\eta_{red} = \frac{\eta_{sp}}{c} = [\eta] + k_H \cdot [\eta]^2 \cdot c \quad (3.3)$$

allows us to calculate the intrinsic viscosity $[\eta]$, which gives an indication of the hydrodynamic volume of the polymer coils, by plotting η_{red} against concentration and extrapolating to $c = 0$. The slope of the plot yields the empirical Huggins constant k_H , which is a measure of the intermolecular interactions for a given polymer-solvent system.⁴⁹

The transition from the dilute regime, where polymer coils interact mainly with the solvent, to the semi-dilute regime, where the polymer coils interpenetrate and intermolecular interactions dominate the solution flow properties, is denoted by the critical concentration C^* . At this point the solution volume is completely filled with polymer coils. Assuming the polymer coils behave as non-draining coils in solution (Einstein's ideal viscosity correlation), the critical concentration can be calculated from the intrinsic viscosity:⁴⁹

$$C^* = \frac{2.5}{[\eta]} \quad (3.4)$$

Other authors have experimentally determined the constant in the numerator to be 1.2 for unmodified dextrans of molar mass 10–500 kDa.⁴¹ In this chapter, the ideal viscosity value of 2.5 will be used to estimate C^* for both blue and unmodified dextrans. Branching of the dextrans will hinder draining somewhat, particularly at lower molecular weights. Blue dextrans will likely have more “non-draining” character owing to osmotic effects of the charged ligands, some of which will be located in the interior of the dextran coil.

The intrinsic viscosity and the molar mass M of a polymer are related by the Kuhn-Mark-Houwink-Sakurada relation

$$[\eta] = K \cdot M^a \quad (3.5)$$

where K and a are constant for a given polymer/solvent system at a particular temperature and must be determined experimentally. The exponent a is an indication of the solvent quality.⁴⁹

3.2.6 Refractive index increments

Specific refractive index increments, dn/dc , were measured at 690 nm by injecting 2-mL samples of blue dextrans (0.05–0.60 mg/mL) in 0.8 M NaNO₃ and 0.01 M NaH₂PO₄ solution containing 0.2 % NaN₃ (pH 7) into a Wyatt Optilab rEX IR detector (Figure 3.3).

3.2.7 Gel permeation chromatography (GPC)

Blue dextrans (1 mg/mL) were dissolved in the eluent (pH 7, 0.8 M NaNO₃ and 0.01 M NaH₂PO₄ containing 0.2 % NaN₃) and filtered using 0.45-μm membranes. Samples (100 μL) were injected onto a GPC column (300×75 mm PL aquagel-OH mixed 8 μm, 100–1×10⁷ Da separation, Polymer Laboratories) at a flow rate of 1.0 mL/min using a Merck Hitachi AS-2000A autosampler and Waters 510 HPLC pump. The column was

coupled to a Wyatt Optilab rEX IR detector and Wyatt Technology Corporation DAWN EOS light scattering detector. Data were analyzed with Astra v5.3.0 18 software (Wyatt Technology Corporation).

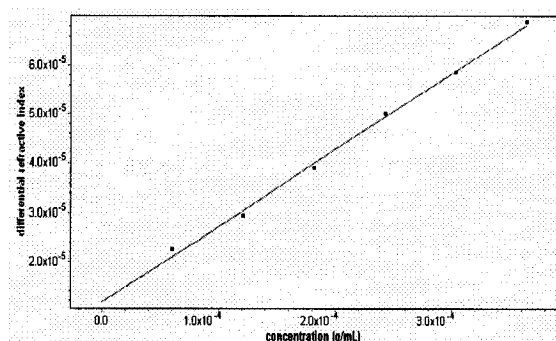


Figure 3.3. Differential refractive index as a function of blue dextran 2000₅₆ concentration at 690 nm.

3.2.8 Dynamic light scattering (DLS)

Hydrodynamic radii (R_H) were determined by dynamic light scattering. Solutions of dextrans and blue dextrans (0.2 to 1.0 g/L) were prepared in 0.200 M NaCl (aq). The solutions and solvents were clarified by filtration through a nylon filter of pore size 0.2 μm (Millipore); samples were filtered directly into the light scattering cells. Light scattering measurements were made at 21–22 °C on a Brookhaven Research BI-200SM laser light scattering goniometer and BI-2030AT digital correlator, using a polarized incident beam of wavelength 632.8 nm from a He-Ne laser (35 mW total power). DLS measurements were made at a 90° angle with sample times of 20 μsec over a duration of 15–30 seconds. Results are the average of 5 or more measurements. The data were analyzed with BI-2030AT software.

3.2.9 Static light scattering (SLS)

Molecular weights (\bar{M}_w, \bar{M}_n), radii of gyration (R_g) and indices of polydispersity (I_p) were determined using a Wyatt Technology Corporation DAWN EOS light scattering detector (690 nm) coupled to the GPC column (Tables 3.6 and 3.7) Data were analyzed with Astra v5.3.0 18 software (Wyatt Technology Corporation). Refractive index increments dn/dc obtained offline using the Wyatt Optilab rEX IR detector were used in the molecular weight calculations.

3.3 RESULTS AND DISCUSSION

3.3.1 Effect of reaction conditions on blue dextran properties

According to Mayes et al.,²⁴ for a given set of initial reaction conditions, increasing the reaction time increases the degree of dye substitution of the final product, despite the decrease in the rate of dye loading as the free dye reacts with both the dextran and the hydroxyl group of the solvent water. Not unexpectedly, increasing the initial dye-to-dextran molar ratio from 150:1 to 600:1 also increases the degree of dye substitution somewhat (Table 3.1). Higher base concentrations appear to significantly increase the yield of blue dextran obtained (Table 3.1).

3.3.2 Viscosity

In water, blue dextran 2000 shows typical polyelectrolyte behaviour (Figure 3.4). As polymer concentrations decrease from high to intermediate values (13 to 1 mg/mL), η_{red} levels off and then increases with further decreasing concentration. At very low polymer concentrations η_{red} decreases again. This rheological behaviour has been seen for other polyelectrolytes.^{50,51} The sharp increase in reduced viscosity is attributed to expansion of

the polyelectrolyte coils caused by gradually increasing dissociation of the ionic groups (dye ligands). Increasing coulomb repulsions result in an expansion of the coil and increase its hydrodynamic volume, leading to the maximum in η_{red} observed at low polymer concentration. At concentrations below this maximum η_{red} , the polymer is in a dilute state even for nearly fully expanded polyelectrolyte coils, which reduces intermolecular interactions to such an extent that the reduced viscosity decreases again.⁴⁹ Although it is not shown, at high concentrations (greater than those shown in Figure 3.4), the reduced viscosity η_{red} should again increase with increasing polymer concentration.

At increasing ionic strengths, the shielding of inter- and intramolecular coulomb forces by the additional counterions attenuates the increase of η_{red} , until at 0.200 M sodium chloride the blue dextran behaves as a neutral polymer. Viscosity measurements were performed in 0.200 M NaCl (aq) solutions to allow the extrapolation of the reduced viscosity to $c \rightarrow 0$.

It is important to note that although the dye ligands contain ionic groups which tend to improve the polymer-solvent interactions, their aromatic rings also impart a hydrophobic character to the blue dextrans. Hydrophobic association in hydrophobically modified polyelectrolytes, such as anionic polyvinyl alcohol (PVA⁻) or polymethacrylic acid/ethyl acrylate (MAA/EA), has been found to reduce the polyelectrolyte effect and lower the values of the reduced viscosity at low polymer concentrations, suggesting that the chains are less expanded.^{52,53} A similar phenomenon may occur in blue dextran, with the result that the overall structure may be more tightly coiled than an unmodified dextran of the same molecular weight.

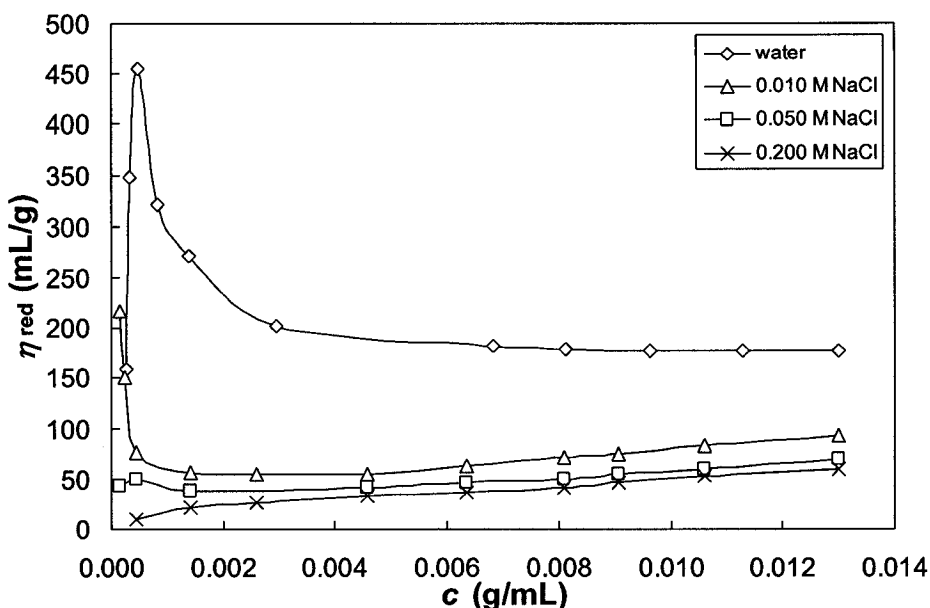


Figure 3.4. Reduced viscosity η_{red} as a function of concentration c for blue dextran 2000 in solutions of increasing ionic strength.

All viscometric measurements were performed in the dilute regime at concentrations clearly below C^* , such that polymer-solvent interactions determine the flow properties. Experiments were performed at relative viscosities $\eta_{rel} = \eta_s/\eta$ between 1.2 and 2.0 to ensure accurate data. Over the concentration range studied, both unmodified and blue dextrans showed decreasing η_{red} with decreasing polymer concentration (Figure 3.5). This confirms that the 0.200 M ionic strength was sufficient to suppress the chain expansion which would occur during dilution of the polymer due to a large increase in intramolecular coulombic repulsion forces between the increasingly dissociated sulfonate groups. The slopes of the plots increased with dextran molecular weight; plots of η_{red} vs. c are steeper for blue dextrans than for unmodified dextrans of a given molecular weight. The decrease in intrinsic viscosity $[\eta]$ and the increase in critical concentration C^* with

decreasing molecular weight (Table 3.2) is attributed to the smaller coil size of the lower molecular weight polymers; dynamic light scattering data supports this conclusion.

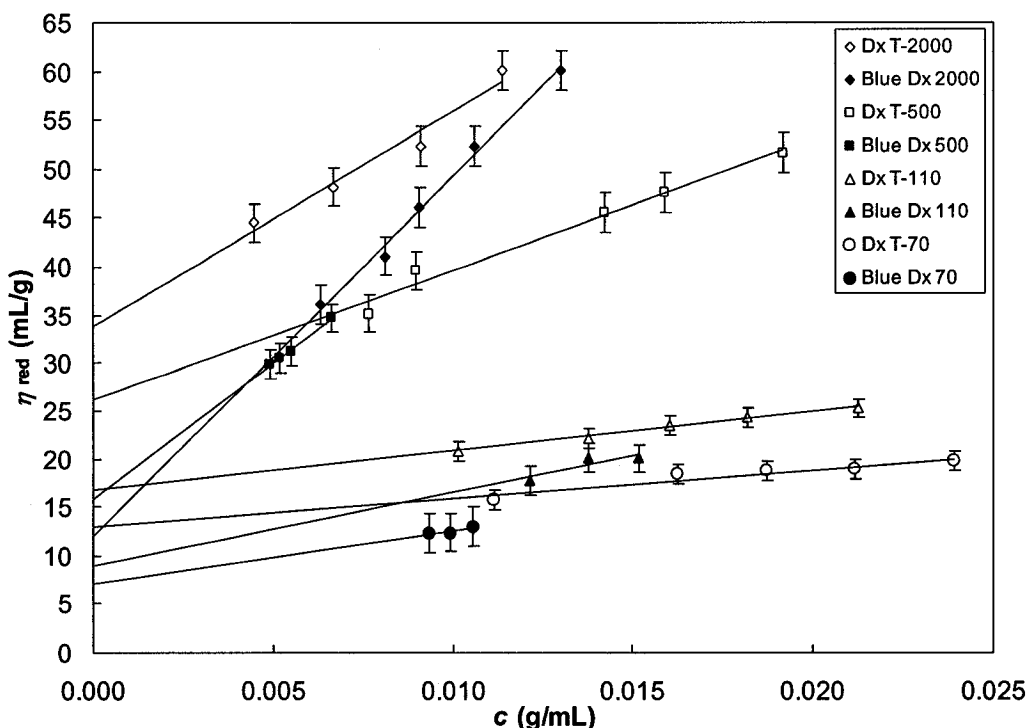


Figure 3.5. Reduced viscosity η_{red} as a function of the concentration c for unmodified dextrans (open symbols) and blue dextrans (filled symbols) in 0.200 M NaCl (aq). Values were taken from the linear portion of the η_{red} vs. c curve.

The differences in the parameters (smaller $[\eta]$ and larger C^* values for blue dextrans) shown in Table 3.2 indicate that blue dextrans experience poorer polymer-solvent interactions than their unmodified counterparts. This phenomenon can be explained by the presence of hydrophobic association of the aromatic dye ligands in the blue dextran structure. The effect is particularly noticeable in the most highly substituted blue dextran 2000, which contains the most aromatic rings and therefore shows a large decrease in intrinsic viscosity $[\eta]$ as compared to dextran T-2000, for example. For a given dextran

molecular weight, the critical concentration values are higher for blue dextrans because they are more tightly coiled, so a higher concentration is needed before the coil overlap point is reached.

These results differ from those obtained for branched and linear dextran sulfates, where the intrinsic viscosity *increased* upon sulfation and with increasing sulfation (see below).⁴² However, sulfate groups are not hydrophobic and the intrinsic viscosity is likely governed by the coil expansion caused by repulsion of the charged sulfate groups.

Table 3.2. Intrinsic viscosity $[\eta]$ and critical concentration C^* for unmodified and blue dextrans in 0.200 M NaCl (aq).

Dextran	$[\eta]$ (mL/g)	C^* (g/mL)
Dextran T-2000	34	0.07
Dextran T-500	26	0.10
Dextran T-110	17	0.15
Dextran T-70	13	0.20
Blue dextran 2000 ₁₆₁	12	0.21
Blue dextran 500 ₁₁	16	0.16
Blue dextran 110 ₂₃	9	0.28
Blue dextran 70 ₆₆	7	0.36

Viscosity data taken in 0.200 M NaCl (aq) for blue dextrans 2000 with different degrees of substitution support this hypothesis (Table 3.3). Critical concentration values increase with increasing degree of dye substitution, which would not be expected if only the ionic groups on the dye ligands affected the viscometric behaviour. Blue dextran

2000₈, with the lowest DS (and therefore the lowest degree of hydrophobicity) has the highest intrinsic viscosity and the lowest critical concentration. Blue Dx 2000₁₆ has similar $[\eta]$ and C^* values to those of dextran T-2000, suggesting that at low degrees of substitution, the ionic character and coulombic repulsion of the dye ligands dominates over the effect of hydrophobicity and causes coil expansion (cf. blue dextran 2000₈), while at higher dye substitutions, the coils shrink due to the hydrophobic nature of the dye molecules.

Table 3.3. Effect of increasing degree of dye substitution on intrinsic viscosity $[\eta]$ and critical concentration C^* for blue dextrans 2000 in 0.200 M NaCl (aq).

Dextran	Dye ligand density (DS per AGU, 10^{-4})	$[\eta]$ (mL/g)	C^* (g/mL)
Dextran T-2000	0	34	0.07
Blue dextran 2000 ₈	8	36	0.07
Blue dextran 2000 ₁₆	16	34	0.07
Blue dextran 2000 ₃₀	30	33	0.08
Blue dextran 2000 ₃₆	36	28	0.09
Blue dextran 2000 ₅₆	56	26	0.10
Blue dextran 2000 ₁₆₁	161	12	0.21

The value of $[\eta]$ was found to decrease with decreasing dextran molecular weight M_w . A plot of $[\eta]$ against M_w shows behaviour somewhat resembling that of branched polymers (Figure 3.6). Branched polymers are denser than linear polymers of the same molar mass and therefore have lower intrinsic viscosities.⁴⁹ The effect is more important

at higher molar masses, where the intrinsic viscosity of branched polymers levels into a plateau. Similar behaviour has been observed for dextran and dextran sulfates.^{28,42}

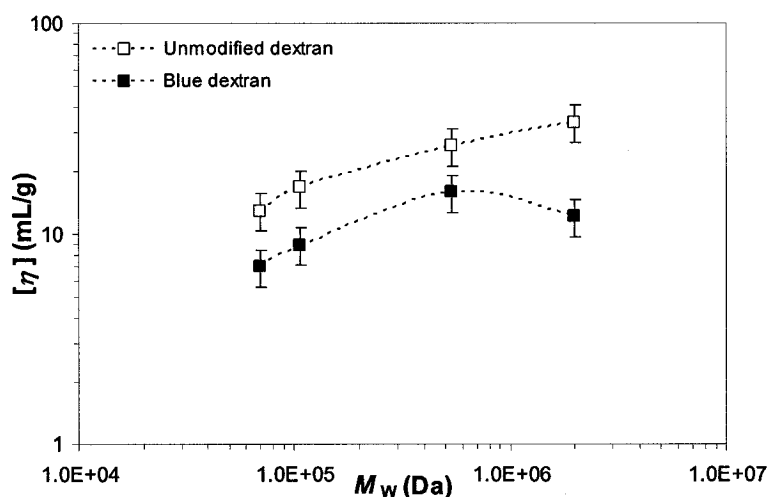


Figure 3.6. Intrinsic viscosity [η] as a function of molar mass M_w for dextran T-2000 and blue dextran 2000 in 0.200 M NaCl (aq).

That the ionic groups on the dye ligands do play a role in the viscosity behaviour of blue dextran is shown by the effect of increasing the ionic strength of the solvent (Figure 3.7). The hydrodynamic volume of each blue dextran coil will depend on the electrostatic interactions (and hydrophobic associations) present, which are sensitive to the solvent ionic strength. The intrinsic viscosity of blue dextran 2000 decreases monotonically with increasing ionic strength (Table 3.4), indicating a decreasing coil expansion due to further shielding of the coulomb repulsion forces between the ionic sulfonate groups of the dye ligands.^{54,55} A concurrent increase in the critical concentration with increasing ionic strength is consistent with this finding. Ohta et al. also observed a decrease in the “charge effect” upon increasing the solution ionic strength.⁴⁴ The intrinsic viscosity was found to be proportional to $I^{1/2}$ (Figure 3.8), in agreement with the literature.^{56,57} Hydrodynamic radii of blue dextran 2000 in solutions

of increasing ionic strength obtained by dynamic light scattering (see Table 3.8) support these data.

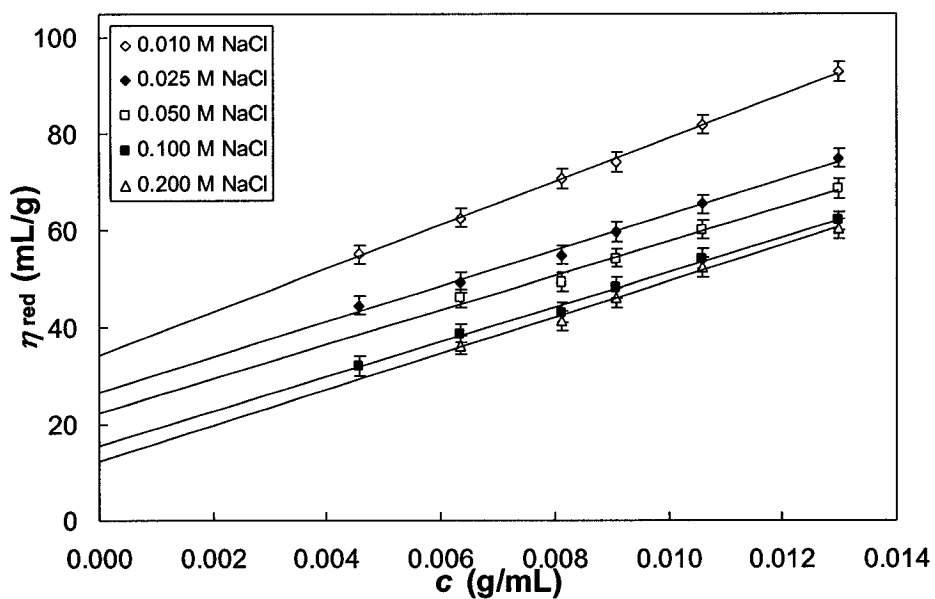


Figure 3.7. Reduced viscosity η_{red} as a function of the concentration c for blue dextran 2000 in solutions of increasing ionic strength.

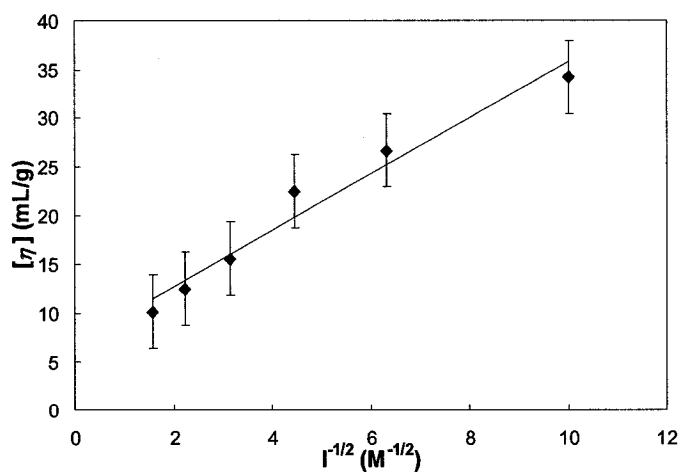


Figure 3.8. Intrinsic viscosity $[\eta]$ of blue dextran 2000 as a function of $I^{1/2}$.

It is interesting to note that increasing the degree of dye substitution of blue dextran 2000 in 0.200 M NaCl solution has an effect of similar magnitude on the intrinsic viscosity and critical concentration to that of increasing the ionic strength of solutions of blue dextran 2000₁₆₁ (compare Tables 3.3 and 3.4). Specifically, increasing the dextran 2000 dye substitution from 16×10^{-4} to 56×10^{-4} in 0.200 M NaCl and increasing the ionic strength from 0.010 M to 0.025 M for blue dextran 2000₁₆₁ both result in similar values of $[\eta]$ and C^* .

Table 3.4. Effect of ionic strength on intrinsic viscosity $[\eta]$ and critical concentration C^* for blue dextran 2000₁₆₁.

Ionic strength (M)	$[\eta]$ (mL/g)	C^* (g/mL)
0.010	34	0.07
0.025	27	0.09
0.050	23	0.11
0.100	16	0.16
0.200	12	0.21

Values of the Huggins constant k_H are greater than 2 for all samples, as reported for a number of polyelectrolyte systems.^{54,56,58} Some authors propose that the Huggins constant can be much greater than 0.5 in cases of association or aggregation.⁵⁹ The 5- μ M dye concentration required for aggregation of free dye in solution²⁴ suggests that *intermolecular* dye stacking or aggregation is possible at the blue dextran concentrations used for the viscosity measurements. However, the absorbance behaviour of blue dextran solutions at dye ligand concentrations up to 70 μ M is linear, implying that no aggregation

occurs at these concentrations. In addition, the solutions of blue dextran are at concentrations below C^* , which should inhibit aggregation owing to the minimal polymer-polymer interactions.

3.3.3 Refractive index increments

The refractive index increments dn/dc of the blue dextrans lie in the range 0.120 to 0.175 at 690 nm (Table 3.5). It has been found that the dn/dc of unmodified dextran increases with increasing molecular weight over a wide range of values.^{30,60} For example, aqueous solutions of dextrans of molecular weight 80–7400 kDa have been found to have dn/dc values of 0.150–0.154 at 436 nm.³⁰ According to the Cauchy equation, the dn/dc for dextran at 690 nm should be slightly lower;⁶¹ the high salt content of the solvent will also tend to reduce the dn/dc below the typical values of ~ 0.150 , owing to the increase in the solvent refractive index.⁶² Table 3.5 shows that increasing dye substitution increases the refractive index increment, which may explain the anomalously high value obtained for blue dextran 70₆₆. The refractive index increments were used in the molecular weight calculations from the GPC data.

3.3.4 Gel permeation chromatography

Ethanol precipitation/centrifugation and exhaustive dialysis were used to purify blue dextrans and remove unreacted dye and residual sodium carbonate. GPC chromatograms confirm the purity of the samples; peaks are sharp, indicating the absence of any unreacted dextran (Figure 3.9).

Table 3.5. Refractive index increments dn/dc at 690 nm for blue dextrans of various molecular weights and dye loadings.

Dextran	Dye ligand density (DS per AGU, 10^{-4})	dn/dc ^a
Blue dextran 2000 ₁₂	12	0.124
Blue dextran 2000 ₃₆	36	0.138
Blue dextran 2000 ₅₆	56	0.153
Blue dextran 2000 ₁₆₁	161	0.157
Blue dextran 110 ₂₃	23	0.118
Blue dextran 70 ₆₆	66	0.173

^a In pH 7 0.80 M NaNO₃ and 0.01 M NaH₂PO₄ (aq) with 0.2 % NaN₃.

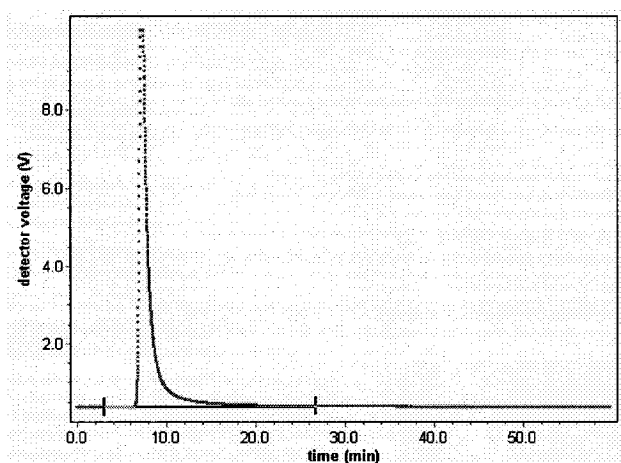


Figure 3.9. Sample GPC chromatogram for blue dextran 2000₁₂.

3.3.5 Molecular weights

Molecular weights were calculated for the blue dextrans using nominal weight-average molecular weights for unmodified dextrans and dye loadings from UV-visible spectroscopy (see Table 3.1):

$$\bar{M}_w^{calc} = \bar{M}_w^{Dx} [1 + M_{CB} (DS/M_{AGU})] \quad (3.6)$$

where \bar{M}_w^{calc} is the calculated molecular weight, \bar{M}_w^{Dx} is the nominal molecular weight for unmodified dextran, $M_{CB} = 840.12$ Da is the molecular weight of the Cibacron blue dye, DS is the degree of dye substitution per anhydroglucose unit of the blue dextran and $M_{AGU} = 162.2$ Da is the molecular weight of the anhydroglucose repeat unit.

The molecular weights and indices of polydispersity of the blue dextrans were determined by GPC-LS. Table 3.6 presents the theoretical molecular weights together with the weight- and number-average molecular weights and indices of polydispersity of several blue dextrans. Masses calculated by GPC-LS are in agreement with the theoretical molecular weights. The molar mass distribution is very narrow, as indicated by the indices of polydispersity.

Table 3.6. Molecular weights and indices of polydispersity of blue dextrans.

Dextran	\bar{M}_w^{calc} (kDa)	\bar{M}_w^{GPC} (kDa)	\bar{M}_n^{GPC} (kDa)	Ip
Blue dextran 2000 ₅₆	2 060	2 100 ± 20	1 800 ± 90	1.16
Blue dextran 110 ₂₃	107	130 ± 5	130 ± 7	1.03
Blue dextran 70 ₆₆	72	65 ± 3	52 ± 3	1.25

3.3.6 Hydrodynamic radii and radii of gyration

The hydrodynamic radii of unmodified and blue dextrans were determined by DLS in 0.010–0.200 M NaCl solutions. Blue dextrans were found to have larger radii of hydration than the unmodified dextrans owing to coulomb repulsion between the ionic dye ligands; values decrease with decreasing dextran molecular weight (Table 3.7). Our R_H value for dextran T-2000 (37.7 nm) is somewhat larger than the value found by Nordmeier for dextran T-2000 in deionized water at 25 °C (27 nm); values for the smaller dextrans are comparable to literature values.⁶³ Overall, the hydrodynamic radii of the blue dextrans and unmodified dextrans lie in the same range, except for blue dextran 110, which shows a much larger radius. This may be because the blue dextran R_H values were measured using 0.2 g/L solutions and were not extrapolated to zero concentration due to limited sample amounts.

Increasing the solution ionic strength from 0.010 to 0.200 M resulted in a decrease of about 5 nm of the hydrodynamic radius of blue dextran 2000 (Table 3.8). The increased shielding of electrostatic repulsions between the dye ligand sulfonate groups would contribute to the observed coil shrinkage. No specific trend in the hydrodynamic radius was observed among blue dextrans 2000 of increasing DS (Table 3.7).

The radii of gyration of the blue dextrans were obtained with a static light scattering detector in 0.8 M NaNO₃ and 0.01 M NaH₂PO₄ (aq). Blue dextrans exhibit larger values of R_g as compared to their unmodified counterparts. Because particles with physical dimensions $R_g \ll \lambda/20$ ($R_g < 10$ nm for 690 nm incident radiation) scatter light isotropically, molecular size data cannot be obtained for these species.⁶⁴ Blue dextran 70 falls into this category (R_g of dextran T-70 = 8.3 nm⁶⁵); its radius of gyration could not be

determined. Values of R_g for the unmodified dextrans are comparable to literature values.^{30,66}

Table 3.7. Experimental and literature values of R_H and R_g for unmodified and blue dextrans.

Dextran	Dye ligand density (DS per AGU, 10^{-4})	R_H (nm) ^a	R_g (nm)
Blue dextran 2000 ₁₆₁	161	40.2 ± 0.8	--
Blue dextran 2000 ₅₆	56	36.9 ± 0.9	40.8 ± 2.0 ^b
Blue dextran 2000 ₃₆	36	35.1 ± 1.1	--
Blue dextran 2000 ₁₆	16	37.9 ± 0.8	--
Blue dextran 2000 ₁₅	15	46.2 ± 0.8	--
Blue dextran 2000 ₁₂	12	40.8 ± 1.0	--
Dextran T-2000	0	37.7 ± 0.8	34 ^c
Blue dextran 500 ₁₁	11	18.4 ± 0.7	--
Dextran T-500	0	17.8 ± 0.3	19.8 ^{c,d}
Blue dextran 110 ₂₃	23	30.7 ± 3.1	16.3 ± 1.6 ^b
Dextran T-110	0	7.7 ± 1.3	9.7 ^c
Blue dextran 70 ₆₆	66	< 10 ^e	< 10 ^e
Dextran T-70	0	< 10 ^e	8.3 ^c

^a Measured at 0.2 g/L by DLS in 0.200 M NaCl (aq). ^b Measured by GPC-SLS in 0.80 M NaNO₃ and 0.01 M NaH₂PO₄ (aq) with 0.2 % NaN₃. ^c Fishman et al.⁶⁵ ^d Nordmeier et al.³⁰ ^e Isotropic scatterer; dimensions too small for measurement by light scattering.

Table 3.8. The effect of ionic strength on R_H values of 0.4 g/L blue dextran 2000₁₆₁.

Dextran	Dye ligand density (DS per AGU, 10^{-4})	[NaCl] (M)	R_H (nm)
Blue dextran 2000	161	0.200	40.2 ± 0.8
		0.100	41.7 ± 1.0
		0.050	43.0 ± 1.0
		0.025	43.7 ± 0.5
		0.010	45.4 ± 0.9

3.4 CONCLUSIONS

Blue dextrans of varying molecular weights and dye ligand densities have been synthesized and characterized. The ionic dye ligands turn dextran into a polyelectrolyte and have a significant effect on the physico-chemical properties of the polymer. The viscosity behaviour of the blue dextrans demonstrated their polyelectrolytic nature as compared to the unmodified dextrans. Increasing solvent ionic strength decreased the coil expansion, as shown by the decrease in intrinsic viscosity and increase in critical concentration. Specific refractive index increments were higher for blue dextrans than for unmodified dextrans. Purity of the blue dextrans was confirmed by gel permeation chromatography, which showed the absence of unreacted dextrans and low sample polydispersity. Molecular weights determined by static light scattering compared favourably with theoretical values calculated from the dextran molar mass and dye loading from UV-visible spectroscopy. Hydrodynamic radii and radii of gyration were found by light scattering.

3.5 REFERENCES

- (1) de Belder, A.N. *Dextran*; Amersham Biosciences: Piscataway, NJ, 2003, 62 pp.
- (2) Reynolds, J.E.F. *Martindale: The Extra Pharmacopoeia*; 30th ed.; Royal Pharmaceutical Society: London, 1993, pp. 650-651.
- (3) Minor, A.H.; Burnett, L. *N.Y. State J. Med.* **1953**, *53*, 547.
- (4) Boyum, A. *Scan. J. Clin. Lab. Invest.* **1968**, *21*, 31.
- (5) Harris, R.; Ukaejiofo, E.O. *Brit. J. Haematol.* **1970**, *18*, 229.
- (6) Sigma-Aldrich, Blue Dextran Molecular Weight 2,000,000 Product No. D5751. Product Information, 1997.
- (7) Dean, P.D.G.; Watson, D.H. *J. Chromatogr., Chromatogr. Rev.* **1979**, *165*, 301-319.
- (8) Subramanian, S. *CRC Crit. Rev. Biochem.* **1984**, *16*, 169-205.
- (9) Andrews, A.T.; Harris, D.P.; Wright, G.; Pyle, D.L.; Asenjo, J.A. *Biotechnol. Lett.* **2000**, *22*, 1349-1353.
- (10) Kopperschläger, G.; Freyer, R.; Diezel, W.; Hofmann, E. *FEBS Lett.* **1968**, *1*, 137-141.
- (11) Haeckel, R.; Hess, B.; Lauterborn, W.; Wuster, K.H. *Hoppe-Seyler's Z. Physiol. Chem.* **1968**, *349*, 699-714.
- (12) Kopperschläger, G.; Diezel, W.; Freyer, R.; Liebe, S.; Hofmann, E. *Eur. J. Biochem.* **1971**, *22*, 40-45.
- (13) Lowe, C.R.; Pearson, J.C. *Methods Enzymol.* **1984**, *104*, 97-113.
- (14) Travis, J.; Pannell, R. *Clin. Chim. Acta* **1973**, *49*, 49-52.

- (15) Travis, J.; Bowen, J.; Tewksbury, D.; Johnson, D.; Pannell, R. *Biochem J.* **1976**, *157*, 301-306.
- (16) Stellwagen, E. *Methods Enzymol.* **1990**, *182*, 343-357.
- (17) Lowe, C.R.; Burton, S.J.; Burton, N.P.; Alderton, W.K.; Pitts, J.M.; Thomas, J.A. *Tibtech* **1992**, *10*, 442-448.
- (18) Edgar, C.D.; Gray, D.G. *Macromolecules* **2002**, *35*, 7400-7406.
- (19) Dogic, Z.; Purdy, K.R.; Grelet, E.; Adams, M.; Fraden, S. *Phys. Rev. E* **2004**, *69*, 051702-1 - 051702-9.
- (20) Beck-Candanedo, S.; Viet, D.; Gray, D.G. *Langmuir* **2006**, *22*, 8690-8695;
Chapter 4 of this thesis.
- (21) Böhme, H.-J.; Kopperschläger, G.; Schulz, J.; Hofmann, E. *J. Chromatogr.* **1972**, *69*, 209-214.
- (22) Johansson, G.; Andersson, M. *J. Chromatogr.* **1984**, *303*, 39-51.
- (23) Stead, C.V. *Dyes Pigm.* **1982**, *3*, 161-171.
- (24) Mayes, A.G.; Moore, J.D.; Eisenthal, R.; Hubble, J. *Biotechnol. Bioeng.* **1990**, *36*, 1090-1096.
- (25) Mayes, A.G.; Eisenthal, R.; Hubble, J. *Biotechnol. Bioeng.* **1992**, *40*, 1263-1270.
- (26) Atkinson, A.; Hammond, P.M.; Hartwell, R.D.; Hughes, P.; Scawen, M.D.; Sherwood, R.F.; Small, D.A.P.; Bruton, C.J.; Harvey, M.J.; Lowe, C.R. *Biochem. Soc. Trans.* **1981**, *9*, 290-293.
- (27) Atkinson, A.; McArdell, J.E.; Scawen, M.D.; Sherwood, R.F.; Small, D.A.P.; Lowe, C.R.; Bruton, C.J. in *Affinity Chromatography and Related Techniques*; Gribnau, T.C.J.; Visser, J.; Nivard, R.J.F., Eds.; Elsevier: Amsterdam, 1982, p. 399.

- (28) Senti, F.R.; Hellman, N.N.; Ludwig, N.H.; Babcock, G.E.; Tobin, R.; Glass, C.A.; Lamberts, B.L. *J. Polym. Sci.* **1955**, *27*, 527-546.
- (29) Antonini, E.; Bellelli, L.; Bruzzesi, M.R.; Caputo, A.; Chiancone, E.; Rossi-Fanelli, A. *Biopolymers* **1964**, *2*, 27-34.
- (30) Nordmeier, E.; Xing, H.; Lechner, M.-D. *Makromol. Chem.* **1993**, *194*, 2923-2937.
- (31) Ioan, C.E.; Aberle, T.; Burchard, W. *Macromolecules* **2001**, *34*, 326-336.
- (32) Granath, K.A. *J. Colloid Sci.* **1958**, *13*, 308-328.
- (33) Granath, K.A.; Flodin, P. *Makromol. Chem.* **1961**, *48*, 161-171.
- (34) Jeanes, A.; Wilham, C.A. *J. Am. Chem. Soc.* **1950**, *72*, 2655-2657.
- (35) Rankin, J.C.; Jeanes, A. *J. Am. Chem. Soc.* **1954**, *76*, 4435-4441.
- (36) Van Cleve, J.W.; Schaefer, W.C.; Rist, C.E. *J. Am. Chem. Soc.* **1956**, *78*, 4435-4438.
- (37) Covacevich, M.T.; Richards, G.N. *Carbohydr. Res.* **1977**, *54*, 311-315.
- (38) Lindberg, B.; Svensson, S. *Acta Chem. Scand.* **1968**, *22*, 1907-1912.
- (39) Larm, O.; Lindberg, B.; Svensson, S. *Carbohydr. Res.* **1971**, *20*, 39-48.
- (40) Bovey, F.A. *J. Polym. Sci.* **1959**, *35*, 167-182.
- (41) Rotureau, E.; Dellacherie, E.; Durand, A. *Eur. Polym. J.* **2006**, *42*, 1086-1092.
- (42) Pasika, W.M.; Cragg, L.H. *J. Polym. Sci.* **1962**, *57*, 301-310.
- (43) Errington, N.; Harding, S.E.; Rowe, A.J. *Carbohydr. Polym.* **1991**, *17*, 151-154.
- (44) Ohta, K.; Yamaguchi, K.; Jikumaru, N.; Kawahara, K. *J. Chromatogr.* **1985**, *350*, 292-295.
- (45) Tang, M.; Zhang, R.; Bowyer, A.; Eisenthal, R.; Hubble, J. *Biotechnol. Bioeng.* **2004**, *87*, 791-796.

- (46) Huglin, M.B.; Yip, D.C.F. *Makromol. Chem., Rapid Commun.* **1987**, *8*, 237-242.
- (47) Champ, S.; Xue, W.; Huglin, M.B. *Macromol. Chem. Phys.* **2000**, *201*, 931-940.
- (48) Chambers, G.K. *Anal. Biochem.* **1977**, *83*, 551-556.
- (49) Kulicke, W.-M.; Clasen, C. *Viscosimetry of Polymers and Polyelectrolytes*; Springer-Verlag: Berlin, 2004, 120 pp.
- (50) Cohen, J.; Priel, Z. *Macromolecules* **1989**, *22*, 2356-2358.
- (51) Vink, H. *Polymer* **1992**, *33*, 3711-3716.
- (52) Ng, W.K.; TAm, K.C.; Jenkins, R.D. *Eur. Polym. J.* **1999**, *35*, 1245-1252.
- (53) Knudsen, K.D.; Lauten, R.A.; Kj  niksen, A.-L.; Nystr  m, B. *Eur. Polym. J.* **2004**, *40*, 721-733.
- (54) Goring, D.A.I.; Rezanowich, A. *J. Colloid Sci.* **1960**, *15*, 472-482.
- (55) Moan, M.; Wolff, C. *Makromol. Chem.* **1974**, *175*, 2881-2894.
- (56) Pals, D.T.F.; Hermans, J.J. *Rec. Trav. Chim.* **1952**, *71*, 433.
- (57) Noda, I.; Tsuge, T.; Nagasawa, M. *J. Phys. Chem.* **1970**, *74*, 710-719.
- (58) Trivedi, H.C.; Patel, R.D. *Angew. Makromol. Chem.* **1985**, *141*, 11-18.
- (59) Bohdanecky, M.; Kovar, J. *Viscosity of Polymer Solutions*; Elsevier: Amsterdam, 1982; Vol. 2.
- (60) Basedow, A.M.; Ebert, K.H.; Ruland, U. *Makromol. Chem.* **1978**, *179*, 1351-1353.
- (61) Huglin, M. *Light Scattering from Polymer Solutions*; Academic Press: New York, 1972, pp. 165-331.
- (62) Vink, H.; Dahlstr  m, G. *Makromol. Chem.* **1967**, *109*, 249-252.
- (63) Nordmeier, E. *J. Phys. Chem.* **1993**, *97*, 5770-5785.
- (64) Wyatt, P.J. *Anal. Chim. Acta* **1993**, *272*, 1-40.

- (65) Fishman, M.L.; Damert, W.C.; Phillips, J.G.; Barford, R.A. *Carbohydr. Res.* **1987**, *160*, 215-225.
- (66) Ioan, C.E.; Aberle, T.; Burchard, W. *Macromolecules* **2000**, *33*, 5730-5739.

Introduction to Cellulose–Dye Ligand Interactions

High-molecular-weight blue dextran has been found to induce the separation of an isotropic phase from a completely ordered cellulose nanocrystal suspension,¹ while an unmodified dextran of similar dimensions does not. The distinct properties imparted to blue dextran by the sulfonated triazine dye Cibacron blue 3G-A (CB), characterized in the previous chapter, account for this disparity. In the following chapter, the effect of these properties on the induced phase separation behaviour in anisotropic cellulose suspensions caused by blue dextrans is further elucidated. The effect of free dye molecules having various charges has also been studied;² anionic dyes which do not (strongly) adsorb on cellulose surfaces were found to induce phase separation at low concentrations. A brief background on the physical interactions between dyes and cellulose surfaces is given below.

Reactive dyes are dyes that react with hydroxyl groups in cellulose to form covalent bonds. It is believed that the reaction proceeds in two steps: the adsorption of the planar portion of the dye molecule, followed by the reaction of the dye with the hydroxyl group of the glucose monomer.³ More recent experiments and theoretical studies have been performed to determine the mechanisms of dye-cellulose interactions. Several factors including ionic strength, solvent conditions and molecular weight are thought to affect the interparticle forces, but the mechanisms and driving force for the adsorption processes are still being debated. Several types of interactions have been reported, including electrostatic, van der Waals, hydrogen-bonding, and hydrophobic interactions.⁴ While it has been suggested that van der Waals forces are more important than hydrogen

¹ Edgar, C.D.; Gray, D.G. *Macromolecules* **2002**, *35*, 7400-7406.

² Beck-Candanedo, S.; Viet, D.; Gray, D.G. *Cellulose* **2006**, *13*, 629-635.

³ Zollinger, H. *Senryo To Yakuhin* **1968**, *13*, 349-360.

⁴ Yamaki, S.B. et al. *Langmuir* **2005**, *21*, 5414-5420.

bonding, these forces are all strongly distance-dependent: the dye core must be able to closely approach the cellulose surface to ensure a good enthalpy of binding.⁵ The number and relative position of the sulfonate groups, which are thicker than the conjugated aromatic core, control the distance between the core and the cellulose surface and therefore the binding enthalpy of the dye.⁵

Congo red (CR, Figure 4-A) is a direct diazo dye known to physically adsorb strongly onto cellulose surfaces.⁴ The adsorption is thought to be based on hydrogen bonds with azo and amino groups, and electrostatic interactions with sulfonate groups.

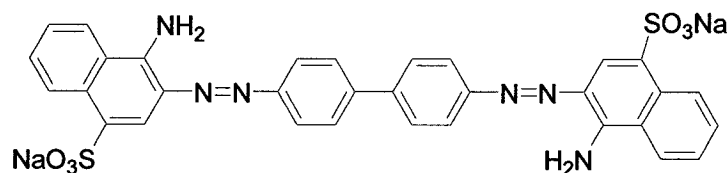


Figure 4-A. Molecular structure of Congo red (CR).

Acid dyes are negatively-charged species which can dye tissues by ionic bonding and are thought to adsorb onto cellulose from acid solution by hydrogen bonding.⁶ Acid red 17 (AR17, Figure 4-B) has two sulfonate groups at one side of the molecule, which allow the aromatic chromophore to approach the cellulose surface more closely than if they were on opposite sides of the molecule.

Dye-cellulose interactions similar to those described above may occur between cellulose and CB, which contains similar chemical moieties to these dyes (Figure 4-C).

⁵ Bird, J.; Brough, N.; Dixon, S.; Batchelor, S.N. *J. Phys. Chem. B* **2006**, *110*, 19557-19561.

⁶ *Stainsfile – Acid dyes*, URL <http://stainsfile.info/StainsFile/dyes/class/acid.htm>

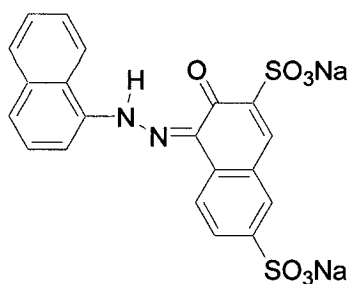


Figure 4-B. Molecular structure of Acid red 17 (AR17).

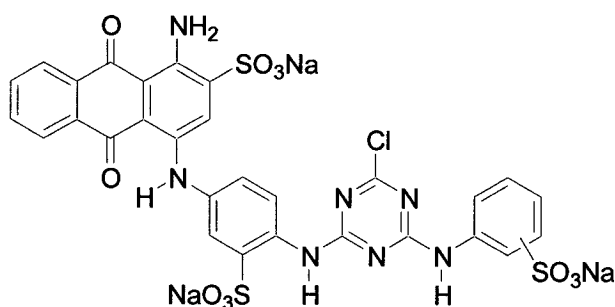


Figure 4-C. Molecular structure of Cibacron blue 3G-A (CB).

CB has been found to adsorb onto microcrystalline cellulose (MCC),⁷ which is a system that more closely resembles the cellulose nanocrystals we are studying than the typical macroscopic cellulose fibres used in such studies. However, its physical interaction with cellulose surfaces is much less studied. The adsorption enthalpy of CB may be weaker than that of CR, for example, as it contains three bulky sulfonate groups distributed throughout the molecule. The CB-cellulose interaction may be further reduced by the attached dextran polymer, which may hold the dye ligand in such a configuration as to

⁷ Stevenson, D.L.; Kennedy, J.F.; White, C.A. *Starch* **1988**, *11*, 433-437.

increase the distance between the conjugated aromatic chromophore and the cellulose nanocrystal surfaces.

Chapter 4

Induced Phase Separation in Low-Ionic-Strength Cellulose Nanocrystal Suspensions Containing High-Molecular-Weight Blue Dextrans

Reproduced with permission from
Beck-Candanedo, S.; Viet, D.; Gray, D.G. *Langmuir* **2006**, *22*, 8690-8695.
Copyright 2006 American Chemical Society.

4.1 INTRODUCTION

Phase separation phenomena occur in a wide range of systems containing highly anisotropic (rod-like) colloidal particles, as predicted by Onsager in 1949.¹ Neutral particles, such as sterically stabilized boehmite rods² or suspensions of polytetrafluoroethylene whiskers and surfactant,³ as well as charged particles, such as tobacco mosaic virus (TMV),⁴ chitin microcrystals^{5,6} and cellulose nanocrystals,^{5,7} spontaneously separate into anisotropic and isotropic phases when the particle concentration exceeds a critical value (e.g., 5 to 7 wt% for cotton cellulose nanocrystals⁷). This critical value is governed by several parameters, including particle dimensions (length L and diameter D), particle size polydispersity and surface charge of the particles.^{1,8} The critical number density of particles is proportional to $1/(L^2D)$.^{1,9} Charged particles can be modelled as hard rods with an effective diameter D_{eff} larger than the hard rod diameter D , which depends on the surface charge of the rod and the ionic properties of the solution.^{1,10} Increasing the ionic strength by adding salt to a suspension of charged particles increases the critical concentration at which the isotropic-nematic phase transition occurs.¹¹ Ions in the bulk solution screen the repulsive electrostatic double layer interactions; as the ionic strength increases, D_{eff} decreases and approaches the hard rod diameter D . The smaller value of D_{eff} shifts the phase transition to higher particle concentrations. The nature of the counterions also affects the phase transition behaviour of our cellulose suspension¹² due to the differing repulsive hydration forces;^{13,14} counterion type is known to affect electrostatic interactions such as ion exchange selectivity.¹⁵

Perhaps most interestingly, the addition of a nonadsorbing, spherical macromolecule can induce phase separation in anisotropic suspensions of rodlike particles. According to

Asakura and Oosawa,^{16,17} this so-called depletion-induced phase separation is based on the imbalance in osmotic pressure that results when a macromolecule is excluded from the region between two colloidal particles when they are separated by a distance smaller than the macromolecule diameter, giving rise to an effective attractive force between the colloids. This behaviour has been observed for the neutral system of polyisobutylene-grafted boehmite rods/polydimethyl siloxane in organic solvents,^{2,18} as well as aqueous ionic systems such as silica particles/carboxymethyl cellulose,¹⁹ TMV/polyethylene oxide²⁰ and filamentous *fd* virus/dextran.²¹

A previous study conducted in our laboratory on the effect of added polymer on the phase separation of colloidal cellulose nanocrystal suspensions used blue dextran (Dx) 2000 as an easily quantifiable non-adsorbing macromolecule.²² Blue dextran contains a sulfonated triazine dye, Cibacron blue 3G-A, which is bound to random hydroxyl groups on the dextran chain and has three charged sulfonate groups per molecule.²³ Blue dextran was added to completely anisotropic cellulose nanocrystal suspensions and phase separation into an upper isotropic and lower anisotropic phase occurred over a period of several days.²² Higher concentrations of blue dextran led to faster separation and larger volume fractions of isotropic phase. Although the exact mechanism by which the phase separation was induced was not discussed in detail, the introduction implied that depletion attractions due to the macromolecular dextran were the cause. This article further investigates the induced phase separation behaviour in anisotropic cellulose suspensions caused by blue dextrans of varying dye content and molecular weight.

4.2 EXPERIMENTAL METHODS

4.2.1 Chemicals

Dextrans T-110, T-500, T-2000 (\bar{M}_w 106 000, 532 000 and 2 000 000, respectively) and blue dextran 2000 ($\bar{M}_w \sim 2\,000\,000$) were purchased from Pharmacia Fine Chemicals. Cibacron blue 3G-A (CB, 55 % dye content) was purchased from Aldrich and used without further purification; see Figure 3.1 in Chapter 3 for the structure. Whatman ashless cotton cellulose powder was purchased from Cole-Parmer. Sulfuric acid (95–98 %) for hydrolysis was purchased from Fisher Scientific. Sodium hydroxide, sodium chloride, and sulfuric acid volumetric standards for conductometric titration were purchased from Aldrich. All water used was purified with a Millipore Milli-Q purification system.

4.2.2 Cellulose nanocrystal suspensions

Cellulose nanocrystal suspensions were prepared as described previously.^{7,24,25} Whatman ashless cotton cellulose powder (40 g) was hydrolyzed with sulfuric acid (700 mL, 64 wt%) at 45 °C for 45 minutes and then quenched by 10-fold dilution in cold distilled water. Samples were centrifuged and the precipitate washed once with distilled water and re-centrifuged. Excess acid was then removed from the precipitate by dialysis against distilled water until the suspension pH was between 5 and 7. The suspension was then sonified (Vibracell, Sonics & Materials, Inc., Danbury CT) in 500-mL batches for 3-minute intervals for a total of 15 minutes, taking care to ensure that the temperature did not exceed 40 °C. Well-dispersed suspensions displayed shear birefringence and no visible aggregates when viewed between crossed polars. The suspension was placed over a small amount of mixed bed ion-exchange resin (Sigma-Aldrich) for several hours with

gentle shaking in order to remove excess ionic materials, and the resin was removed by filtration and centrifugation if necessary. The initial dilute aqueous suspensions were around 1–2 % cellulose by weight.

The concentration of cellulose in the samples was determined by gravimetry. Conductometric titration was used to determine the quantity of sodium hydroxide required to neutralize the H^+ counterions associated with the sulfate ester groups on the nanocrystal surfaces. Sodium chloride (0.001 N, 100 mL) was added to the suspension samples (3–5 mL). A Contiburette $\mu 10$ (Ing. CAT, Staufen, Germany) was used for all titrations. Titrations were performed under a flow of nitrogen using an Orion conductivity cell 018010 (cell constant $K = 0.987 \text{ cm}^{-1}$) attached to a Fisher Scientific accumet pH meter 50. The suspension was then neutralized with sodium hydroxide. Finally, the suspension was concentrated by evaporation at ambient conditions to give a completely anisotropic cellulose suspension. A final concentration of 13.8 wt% cellulose was chosen, as the suspension viscosity is inconveniently high above this concentration.

4.2.3 Blue dextrans

Blue dextrans of various molecular weights and ligand densities (Table 4.1) were prepared using methods adapted from Mayes et al. (1990)²⁶ and Tang et al.(2004)²⁷ (see Figure 3.1 in Chapter 3). A typical preparation is as follows: A solution of 4 g dextran T-2000 in 120 mL water was mixed with solutions of 0.8 g Cibacron blue 3G-A (55 % dye content) in 40 mL water and 0.2 g Na_2CO_3 in 40 mL water. The mixture was shaken in a water bath at 45 °C. After around 75 h another 0.8 g CB was added. To precipitate the dextran-dye conjugate, an equal volume of ethanol was added to the mixture, which was allowed to stand at –20 °C for at least 60 min. The precipitate was then spun down and

rinsed with ethanol. Following resuspension in 40 mL water, the dextran was dialyzed (Spectrum Spectra/Por membrane, molecular weight cutoff 12 000–14 000 Da) against distilled water to remove any traces of unreacted dye and salt. Gel filtration indicated the absence of low-molecular-weight material of high absorbance. The final product was lyophilized and stored as a solid.

Table 4.1. Preparation conditions and ligand densities for blue dextrans.

Dextran	Reaction time (h)	Initial dye-dextran ratio (mol:mol)	[Na ₂ CO ₃] (M)	Ligand density (DS per AGU ^a , 10 ⁻⁴)
T-2000	24.0	280	0.100	3
	18.5	300	0.010	9
	21.5	300	0.010	16
	48.0	300	0.010	30
	96.5	300	0.010	36
	120.0	300	0.010	44
	144.5	300	0.010	56
	-- ^b	--	--	161
T-500	48.0	300	0.010	49
T-110	48.0	300	0.040	23

^a Degree of substitution per anhydroglucose repeat unit. ^b Commercial blue dextran 2000 (Pharmacia).

Moisture contents of the dextrans and dextran-dye conjugates were determined by thermogravimetric analysis (TA Instruments TGA Q500). The dextrans contained from 10.5–11.5 % water by mass, and the blue dextrans from 9–15 % water by mass.

The dye content of the dextran-dye conjugates was determined using UV-visible spectroscopy (Varian Cary 300 Bio spectrophotometer). Solutions of blue dextran 2000 (Pharmacia) were prepared with ligand concentrations below 5 μM to avoid dye stacking in solution²⁹ and a calibration curve prepared (see Appendix, Section 4.6). Ligand density was estimated from absorbance measurements at 609 nm for solutions of the conjugates, and calculated in terms of the degree of substitution per anhydroglucose repeat unit (AGU). It was assumed that the molar extinction coefficient of Cibacron blue 3G-A at this wavelength is not affected by its coupling to dextran.^{26,30} In this paper, the term “dye” refers to the free dye unless otherwise indicated, while “ligand” refers to the dye molecules covalently attached to the dextran, and “ionic group” refers to the charged sulfonate groups on the dye molecules or ligands.

4.2.4 Preparation of cellulose–dextran suspensions

Samples were prepared by adding solid dextran to aliquots of concentrated cellulose nanocrystal suspension and vortexing until homogeneous dispersion was achieved. Suspensions were allowed to equilibrate and monitored over a period of at least two weeks. The anisotropic and isotropic phase volume fractions, ϕ_{aniso} and ϕ_{iso} , were determined by measuring the heights of the anisotropic and isotropic phases in each vial.

The number density of the blue dextran and dextran molecules in the samples was calculated using equation 4.1:

$$C_i = \frac{N_i}{V_{\text{tot}}} = \frac{N_A \cdot m_i}{V_{\text{tot}} \cdot M_i}, \quad (4.1)$$

where N_i is the number of molecules of species i , V_{tot} is the volume of the sample, N_A is Avogadro’s number, m_i is the mass of species i , and M_i is the molar mass of species i . It should be noted that while number average molecular weight, \bar{M}_n , should be used in the

formula for number density, the molecular weights given for the dextrans are weight average, \bar{M}_w (supplier data). The polydispersity \bar{M}_w/\bar{M}_n of the dextrans decreases with decreasing molar mass (Table 4.1).³¹

4.3 RESULTS AND DISCUSSION

4.3.1 Dextrans

We prepared an initial series of anisotropic cellulose nanocrystal suspensions (13.8 wt%) to which we added dextrans T-2000, T-500 and T-110. The objective was to get a sense of the magnitude of phase separation induced by the different dextrans, particularly those of lower molecular weight, prior to using the blue dextrans, of which we had only limited quantities. However, phase separation was not observed in any of the samples; dextran T-2000 at volume fractions similar to those reported by Edgar and Gray for blue dextran 2000²² did not cause phase separation after a period of more than three weeks. This unexpected result led us to question the basis for the phase separation observed upon addition of blue dextran: were depletion attractions really the cause?

The range over which depletion forces act depends on the size of the added macromolecule;^{16,17} the influence of a macromolecule will be dependent not only on its size, but also on the geometry and spacing of the particles on which it acts. To obtain a rough estimate of the distances separating the cellulose nanocrystals in the ordered, concentrated suspension, we assume that each nanocrystal is a rectangular rod of square cross-section, measuring 120 by 10 by 10 nanometers (average dimensions from atomic force microscopy). The number density C_{cell} of the cellulose rods is given by equation 4.2:

$$C_{cell} = \frac{w}{[w + (100 - w)\rho] L h^2}, \quad (4.2)$$

where w is the weight percent cellulose concentration, ρ is the density of cellulose in water (assumed to be 1.6 g/cm^3), and L and h^2 are the length and the area of the square cross-section of the rods, respectively.³² A 13.8 wt% cellulose suspension thus has an approximate number density of $8 \times 10^{-6} \text{ nm}^{-3}$. If the rods are perfectly aligned in “pseudo-nematic” planes, and separated by equal distances d on all sides, calculation of the volume occupied by a rod and surrounding area (the “unit cell”) gives the average space between the particles $d \approx 20 \text{ nm}$ (Figure 4.1).

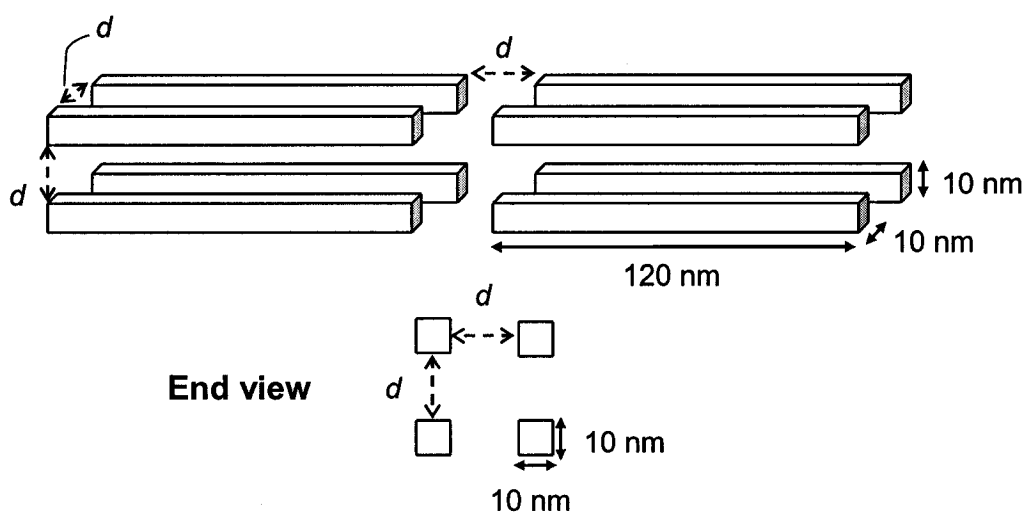


Figure 4.1. Schematic of idealized “nematic” nanocrystal distribution in the 13.8 wt% cellulose suspension. Separation between the cellulose rods $d \approx 20 \text{ nm}$.

Unmodified dextran molecules T-2000, T-500 and T-110 have radii of gyration of 34, 19.8 and 9.7 nm, respectively (Table 4.3 below). These values are of the same magnitude as the nanocrystal separation d , indicating that the dextran coils would not be able to fit into the chiral nematic structure of the cellulose nanocrystal suspension without some

distortion and loss of entropy associated with the individual coils. Since the suspension remains stable, this entropy loss is insufficient to drive an isotropic phase separation. On the other hand, blue dextrans prepared from dextrans T-2000, T-500 and T-110 will have radii of gyration larger than the values given above, due to the charges arising from the anionic dye ligands. Presumably, the dimensions and electrostatic charge on the chains increase the entropic cost of chain distortion necessary to fit into the concentrated anisotropic suspension, and phase separation occurs.

The answer to our initial question lies in the interactions between the colloidal cellulose rods and dextran in solution. For neutral colloids, the total interaction energy between a pair of colloidal particles in polymer solution is the sum of the van der Waals attraction, the hard core repulsion and the depletion attraction caused by the polymers. When sufficient macromolecule has been added such that the attraction dominates, the system will phase separate. The failure of neutral dextran T-2000 to induce phase separation in anisotropic cellulose suspensions, even at much higher number densities than the blue dextrans shown in Tables 4.2 to 4.4 (see below), may be explained by the fact that cellulose nanocrystals are negatively charged colloids, and therefore electrostatic forces must be taken into account. The total interaction potential between the negatively charged cellulose rods is thus a combination of the van der Waals attraction, hard core repulsion, and depletion attraction in addition to the repulsion between the electrostatic double layers. An exact description of the interaction potential is difficult to obtain, as the high cellulose concentration of the suspensions (colloidal, but not dilute) gives rise to complex interactions between the colloidal nanocrystals. For example, the distribution of counterions surrounding the cellulose crystallites is likely not uniform and may influence the interactions between the cellulose nanocrystals.³³ Because the cellulose suspensions

are of low ionic strength (“salt-free” conditions: the only counterions present are those associated with the sulfate ester groups on the nanocrystal surfaces: surface charge density $0.19 \text{ e/nm}^2 = 1.63 \times 10^{-4} \text{ mol OH}^- \text{ per gram cellulose} \approx 25 \text{ mM}$ ionic strength [i.e., equivalent to 25 mM NaCl] for a 14 wt% suspension), the range of the electrostatic repulsion may be large enough to dominate the effective depletion attraction due to the added dextran, stabilizing the suspension and preventing phase separation.

This phenomenon has been observed by Dogic et al. for an analogous system consisting of an aqueous mixture of charged semiflexible rods (fd virus) and neutral polymer (dextran T-500, $R_g = 19.8 \text{ nm}$).²¹ At low ionic strength ($I = 50 \text{ mM}$ added NaCl), added dextran T-500 did not affect the phase transition behaviour, while at high ionic strength ($I = 100\text{-}200 \text{ mM}$ added NaCl), it widened the isotropic-nematic coexistence region, with the polymer partitioning preferentially into the isotropic phase, as predicted by theory.³⁴ The experimental phase diagram obtained at low added ionic strength showed that addition of the polymer to a completely nematic suspension of the fd virus particles would not induce phase separation (a vertical line indicating increased polymer volume fraction drawn in the nematic region would not intersect the phase coexistence region).

Blue dextrans were added to anisotropic cellulose nanocrystal suspensions to verify our assumptions regarding the effect of molecular size/depletion forces and to determine the cause of the induced phase separation.

4.3.2 Blue dextrans of increasing number density

The depth of the attractive depletion potential depends on the concentration of macromolecule in solution.^{17,35} As shown in Table 4.2, we added blue dextrans of different ligand density to an anisotropic cellulose nanocrystal suspension such that the dextran number density increased while maintaining an equal total dye (ligand)

concentration in the samples. The volume fraction of isotropic phase at equilibrium was approximately equal for all samples, suggesting that depletion attractions are not effective at these conditions.

Table 4.2. Blue dextrans of increasing number density added to anisotropic suspension (13.8 wt% cellulose nanocrystals).

Sample	Ligand density (DS per AGU, 10^{-4})	C_{Dx} (10^{-6} nm^{-3})	I_{dye} (μM) ^a	ϕ_{iso} ^b
2000-A	30	4.86	1.45	0.26
2000-B	36	4.05	1.45	0.29
2000-C	56	2.68	1.45	0.29
2000-D	161	0.90	1.45	0.26

^a Ionic strength due to charged sulfonate groups on dye ligands attached to blue dextran.

^b Volume fraction of isotropic phase in sample vial.

4.3.3 Blue dextrans of increasing molecular weight

The range of the depletion potential is determined by the size of the added macromolecule, which is on the order of its diameter.^{16,17,35} At approximately equal ligand concentrations (Table 4.3), dextran molecular weight did not have a systematic effect on extent of phase separation. If depletion attractions were contributing to the observed phase separation, the molecular weight of the dextran should have an effect on the phase separation, with larger dextrans causing increased phase separation ($R_g = 0.66M_w^{0.43}$ over a MW range of 400 to 2,700 kDa; $a < 0.5$ due to dextran branching³⁶).³⁷ The absence of any molecular weight or size effect also suggests that depletion attractions do not induce phase separation in this system.

Table 4.3. Blue dextrans of increasing molecular weight added to anisotropic suspension (13.8 wt% cellulose nanocrystals).

Sample	Ligand density (DS per AGU, 10^{-4})	R_g (nm) 31,38,39	MW _{calc} (kDa)	C_{Dx} (nm ⁻³ , 10^6)	I_{dye} (μ M)	ϕ_{iso}
2000-I	30	34.0 ^a	2000	2.0	0.60	0.17
500-I	49	19.8 ^a	532	7.6	0.95	0.23
110-I	23	9.7 ^a	106	36.8	0.45	0.24
2000-II	30	34.0	2000	1.4	0.40	0.14
500-II	49	19.8	532	5.1	0.65	0.20
110-II	23	9.7	106	24.6	0.30	0.20

^a Radii of gyration determined by light scattering.

4.3.4 Blue dextrans of increasing dye ligand density

Blue dextrans of increasing dye ligand density were added to vials of completely anisotropic cellulose suspension (13.8 wt%), as shown in Table 4.4. After several hours to days, a dark blue upper phase and a lighter blue lower phase formed (Figure 4.1). Over a period of two weeks, the volume fraction of the upper phase increased and then leveled off. Higher initial rates of phase separation were observed for dextrans with the highest ligand density, the dextran with the lowest ligand density having a “lag time” of four days (Figure 4.2). The dextran with the highest ligand density (commercial blue dextran 2000) produced gelation in the suspension; no phase separation was observed.

Table 4.4. Blue dextrans 2000 of increasing ligand density added to anisotropic suspension (13.8 wt% cellulose nanocrystals).

Sample	Ligand density (DS per AGU, 10^{-4})	C_{Dx} (10^{-6} nm^{-3})	I_{dye} (μM)	ϕ_{iso}
2000-1	9	3.7	0.35	0.12
2000-2	16	3.7	0.60	0.13
2000-3	30	3.6	1.10	0.19
2000-4	36	3.7	1.35	0.26
2000-5	56	3.8	2.15	0.32
2000-6	161	3.7	6.00	-- ^a

^a Gelation of suspension prevented phase separation.

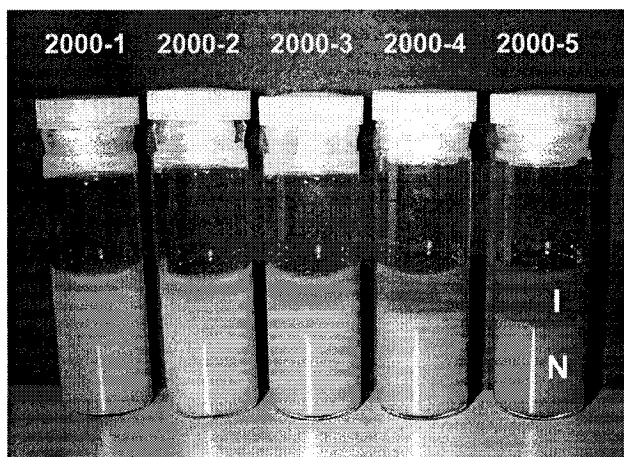


Figure 4.2. Induced phase separation caused by the addition of blue dextrans T-2000 of increasing ligand density to vials containing anisotropic cellulose nanocrystal suspension (13.8 wt%). Blue dextran partitions preferentially into the isotropic phase.

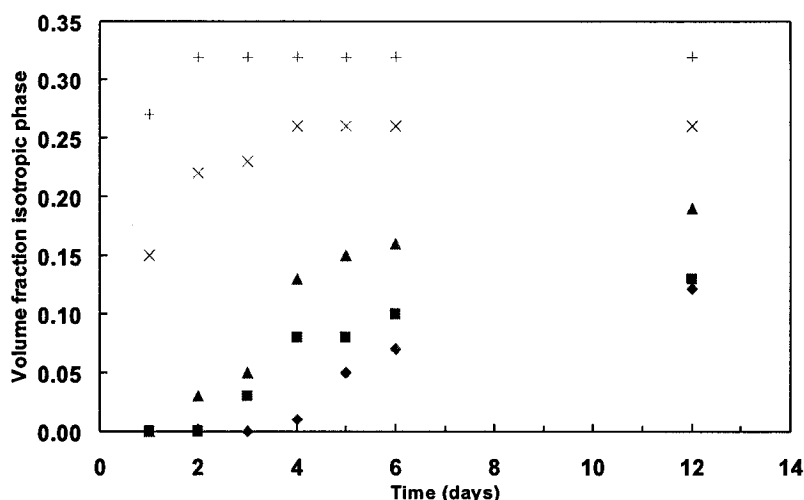


Figure 4.3. Volume fraction of upper isotropic phase as a function of time for phase separation of initially anisotropic samples (13.8 wt% nanocrystals) induced by adding blue dextrans 2000 with increasing ligand density. Samples: 2000-1 ◆; 2000-2 ■; 2000-3 ▲; 2000-4 ×; 2000-5 +.

The results shown in Figures 4.2 and 4.3 support the hypothesis that the phase separation is caused by the increase in ionic strength owing to the ionic dye ligands of the blue dextran. Depletion attraction may also be a contributing factor at higher ligand densities (see below). The higher rates of phase separation seen in Figure 4.3 at higher dye concentrations are similar to those observed previously,²² although the final volume fractions of isotropic phase are slightly larger in this case, despite lower total concentrations of dye. This may be attributed to the suspension properties, which vary from batch to batch and depend greatly on the concentration of cellulose rods, their surface charge and dimensions. The gelation of sample 2000-6 is likely caused by much higher ionic strength owing to the higher dye loading for commercial blue dextran 2000 (Table 4.4). Biphasic suspensions of cellulose nanocrystals are stable at ionic strengths up to about 50 mM;⁴⁰ higher ionic strengths screen the electrostatic repulsions between the

cellulose nanocrystals and lead to gelation or precipitation (salting-out effect).^{25,41} Because the effective ionic strength of sample 2000-6 is only 6.0 μM , the gelation is most likely due to the very high cellulose concentration of the suspension used. Ionic strength strongly influences the properties of systems consisting of charged colloids and polyelectrolytes.

4.3.5 Blue dextran and Cibacron blue 3G-A

Adding free Cibacron blue 3G-A dye to completely anisotropic cellulose suspensions also induced phase separation. Commercial dyes often contain stabilizing and diluent agents, as well as dispersants and anti-dusting agents.⁴² In the case of Cibacron blue 3G-A, the impurities are likely to be salts such as NaCl or Na₂SO₄, urea, and dodecyl alcohol.⁴³ Because the exact quantity of “ionic material” in each batch of dye is unknown, the final ionic strength of a solution of a given dye cannot be accurately calculated. However, simple ionic salts do not appear to have the same effect on the phase separation behaviour that the dye Cibacron blue 3G-A does: even at up to 1000 times the nominal ionic strength of the dye and blue dextran samples, added sodium chloride does not induce phase separation in cellulose nanocrystal suspension of the same concentration.⁴⁴ Figure 4.4 shows the phase separation for samples containing Cibacron blue 3G-A dye at concentrations resulting in ionic strengths equal to those in the blue dextran samples with increasing ligand density shown in Table 4.4. Increasing the total ligand concentration in suspension with constant dextran number density resulted in the formation of larger volume fractions of isotropic phase. At lower dye concentrations, the blue dextran and free dye result in approximately the same amount of phase separation, while at higher dye concentrations, the curves diverge, the blue dextran inducing more phase separation than the dye alone.

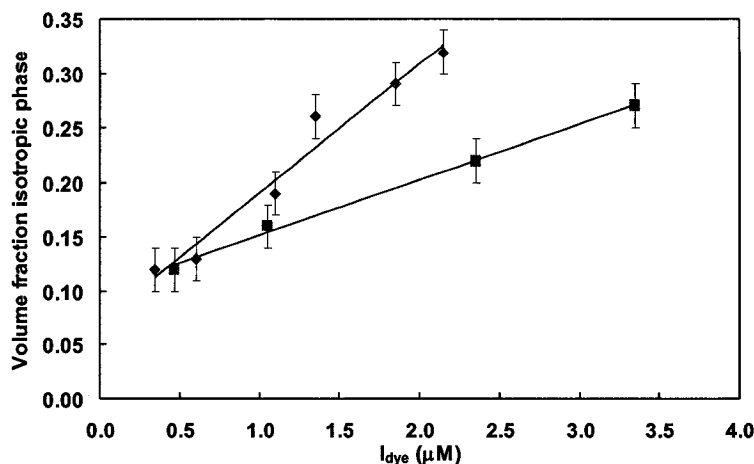


Figure 4.4. Volume fraction isotropic phase as a function of ionic strength due to sulfonate groups on dye ligands for blue dextran 2000 (\blacklozenge) and on Cibacron blue 3G-A (\blacksquare).

If depletion attractions were the only source of phase separation in this case (constant dextran number density), phase separation should increase with increasing concentration of dextran and not with increasing dye content. It is not unreasonable to assume that the charged dye ligands on the blue dextran screen some of the electrostatic repulsion between the charged cellulose rods, allowing depletion attractions to contribute to the phase separation in similar fashion to the system of Dogic et al. (2004).²¹ We can conclude that the phase separation caused by the blue dextran is in part due to the increase in critical cellulose concentration resulting from the higher ionic strength, and in part due to a contribution from the depletion attraction at higher dye concentrations, when the nanocrystal-nanocrystal electrostatic repulsion is screened enough by the ionic dye molecules. At low dye ligand concentrations, depletion effects are not present, and only the increased critical cellulose concentration causes phase separation, such that the free dye and blue dextran induce the same amount of phase separation. Additionally,

increasing ligand densities may result in significant increases in the dimensions of the blue dextran coil (as discussed above), leading to greater disruption of the ordered phase structure and increased depletion attraction forces.

Overall, the addition of anionic dye molecules attached to neutral dextran to an anisotropic suspension of negatively charged cellulose rods produces phase separation by: 1) shifting the critical cellulose concentration to a higher value, as previously observed,¹¹ and 2) screening the electrostatic repulsion between the particles allowing the depletion attraction to be effective, particularly at the higher concentrations of the dye ligand. In addition, the attractive depletion force between colloidal particles is known to be stronger and of longer range in solutions of macroions as compared to neutral macromolecules.^{16,17} However, particularly at low ionic strengths, the depletion interactions between macromolecules and colloids with like charges are complicated, and theories allowing computation of the behaviour of these systems have not been developed.⁴⁵

4.4 CONCLUSIONS

Adding blue dextran induces the separation of an isotropic phase in completely anisotropic cellulose nanocrystal suspensions, while no phase separation is observed on the addition of uncharged dextran. The anionic dye ligands attached to the dextran raise the ionic strength of the system, producing a two-fold effect: Initially, the critical cellulose concentration required for phase separation increases, shifting the phase equilibrium into the region of isotropic-chiral nematic phase coexistence. At higher ionic strengths, the electrostatic repulsions between the rods are sufficiently screened to allow depletion attractions from the dextran macromolecules to contribute to the phase separation.

4.5 REFERENCES

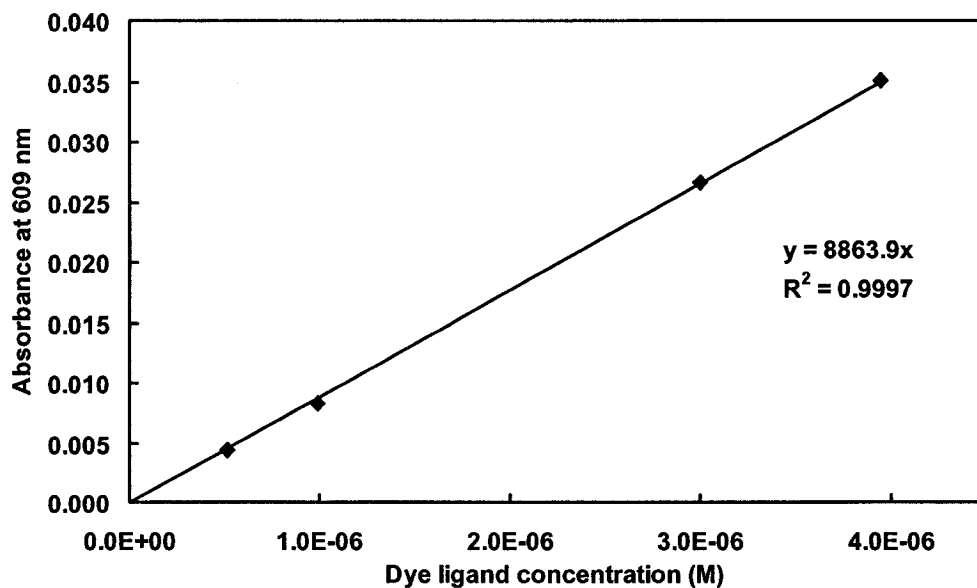
- (1) Onsager, L. *Ann. N.Y. Acad. Sci.* **1949**, *51*, 627-659.
- (2) Buitenhuis, J.; Donselaar, L.N.; Buining, P.A.; Stroobants, A.; Lekkerkerker, H.N.W. *J. Colloid Interface Sci.* **1995**, *175*, 46-56.
- (3) Folda, T.; Hoffmann, H.; Chanzy, H.; Smith, P. *Nature* **1988**, *333*, 55-56.
- (4) Bawden, F.C.; Pirie, N.W. *Proc. R. Soc. B.* **1937**, *123*, 274-320.
- (5) Marchessault, R.H.; Morehead, F.F.; Walter, N.M. *Nature* **1959**, *184*, 632-633.
- (6) Revol, J.-F.; Marchessault, R.H. *Int. J. Biol. Macromol.* **1993**, *15*, 329-335.
- (7) Dong, X.M.; Revol, J.-F.; Gray, D.G. *Cellulose* **1998**, *5*, 19-32.
- (8) Odijk, T. *Macromolecules* **1986**, *19*, 2313-2329.
- (9) Onsager, L. *Phys. Rev.* **1942**, *62*, 558.
- (10) Stroobants, A.; Lekkerkerker, H.N.W.; Odijk, T. *Macromolecules* **1986**, *19*, 2232-2238.
- (11) Dong, X.M.; Kimura, T.; Revol, J.-F.; Gray, D.G. *Langmuir* **1996**, *12*, 2076-2082.
- (12) Dong, X.M.; Gray, D.G. *Langmuir* **1997**, *13*, 2404-2409.
- (13) Pashley, R.M. *J. Colloid Interface Sci.* **1981**, *83*, 531-546.
- (14) Israelachvili, J.N. *Intermolecular & Surface Forces*; 2nd ed.; Academic Press Inc.: San Diego, CA, 1992.
- (15) Feitelson, J. *J. Phys. Chem.* **1962**, *66*, 1295-1298.
- (16) Asakura, S.; Oosawa, F. *J. Chem. Phys.* **1954**, *22*, 1255-1256.
- (17) Asakura, S.; Oosawa, F. *J. Polym. Sci.* **1958**, *33*, 183-192.

- (18) van Bruggen, M.P.B.; Lekkerkerker, H.N.W. *Macromolecules* **2000**, *33*, 5532-5535.
- (19) Snowden, M.J.; Williams, P.A.; Garvey, M.J.; Robb, I.D. *J. Colloid Interface Sci.* **1994**, *166*, 160-167.
- (20) Adams, M.; Fraden, S. *Biophys. J.* **1998**, *74*, 669-677.
- (21) Dogic, Z.; Purdy, K.R.; Grelet, E.; Adams, M.; Fraden, S. *Phys. Rev. E* **2004**, *69*, 051702-1 - 051702-9.
- (22) Edgar, C.D.; Gray, D.G. *Macromolecules* **2002**, *35*, 7400-7406.
- (23) Böhme, H.-J.; Kopperschlager, G.; Schulz, J.; Hofmann, E. *J. Chromatog.* **1972**, *69*, 209-214.
- (24) Revol, J.-F.; Bradford, H.; Giasson, J.; Marchessault, R.H.; Gray, D.G. *Int. J. Biol. Macromol.* **1992**, *14*, 170-172.
- (25) Revol, J.F.; Godbout, L.; Dong, X.M.; Gray, D.G.; Chanzy, H.; Maret, G. *Liq. Cryst.* **1994**, *16*, 127-134.
- (26) Mayes, A.G.; Moore, J.D.; Eisenthal, R.; Hubble, J. *Biotechnol. Bioeng.* **1990**, *36*, 1090-1096.
- (27) Tang, M.; Zhang, R.; Bowyer, A.; Eisenthal, R.; Hubble, J. *Biotechnol. Bioeng.* **2004**, *87*, 791-796.
- (28) Sigma-Aldrich, Blue Dextran Molecular Weight 2,000,000 Product No. D5751. Product Information, 1997.
- (29) Federici, M.M.; Chock, P.B.; Stadtman, E.R. *Biochemistry* **1985**, *24*, 647-660.
- (30) Mayes, A.G.; Eisenthal, R.; Hubble, J. *Biotechnol. Bioeng.* **1992**, *40*, 1263-1270.
- (31) Fishman, M.L.; Damert, W.C.; Phillips, J.G.; Barford, R.A. *Carbohydr. Res.* **1987**, *160*, 215-225.

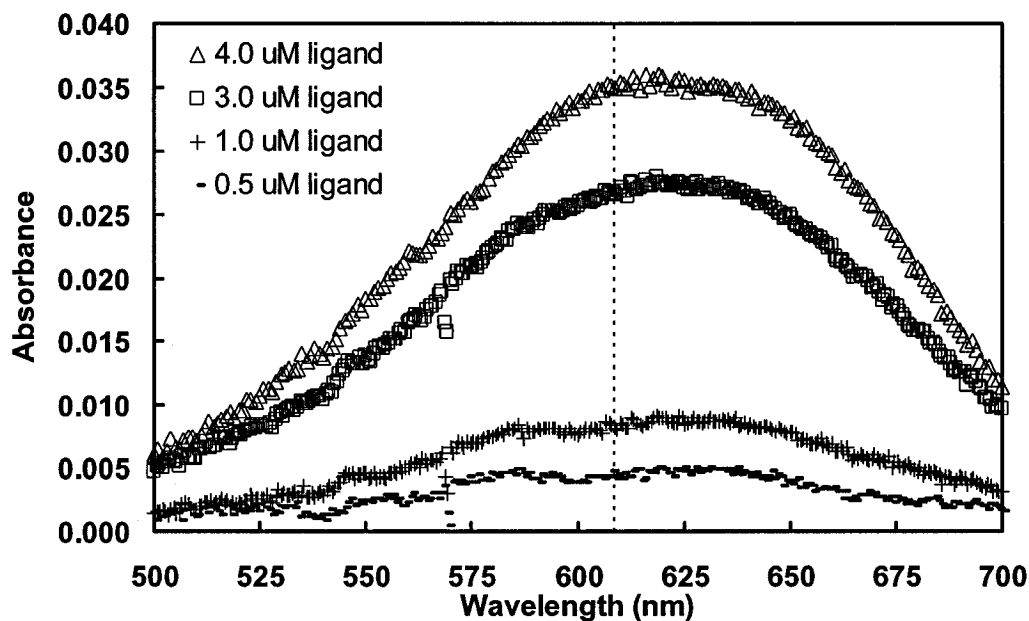
- (32) Dong, X.M. *Chiral Nematic Ordered Suspensions of Cellulose Microcrystallites*. Ph.D. thesis, McGill University: Montreal, 1997.
- (33) Manning, G.S. *J. Chem. Phys.* **1969**, *51*, 924-933.
- (34) Lekkerkerker, H.N.W.; Poon, W.C.-K.; Pusey, P.N.; Stroobants, A.; Warren, P.B. *Europhys. Lett.* **1992**, *20*, 559-563.
- (35) Ferreira, P.G.; Dymitrowska, M.; Belloni, L. *J. Chem. Phys.* **2000**, *113*, 9849-9862.
- (36) Senti, F.R.; Hellman, N.N.; Ludwig, N.H.; Babcock, G.E.; Tobin, R.; Glass, C.A.; Lamberts, B.L. *J. Polym. Sci.* **1955**, *27*, 527-546.
- (37) Frenkel, D. *Physica A* **2002**, *313*, 1-31.
- (38) Ioan, C.E.; Aberle, T.; Burchard, W. *Macromolecules* **2001**, *34*, 326-336.
- (39) Nordmeier, E.; Xing, H.; Lechner, M.-D. *Makromol. Chem.* **1993**, *194*, 2923-2937.
- (40) Revol, J.-F.; Godbout, L.; Gray, D.G. *J. Pulp Pap. Sci.* **1998**, *24*, 146-149.
- (41) Nishiyama, Y.; Kuga, S.; Wada, M.; Okano, T. *Macromolecules* **1997**, *30*, 6395-6397.
- (42) Kissa, E. in *The Analytical Chemistry of Synthetic Dyes*; Venkataraman, K., eds.; John Wiley & Sons: New York, 1977, pp. 519-553.
- (43) Lewis, D. 2006, *Personal communication*.
- (44) Beck-Candanedo, S.; Viet, D.; Gray, D.G. *Cellulose* **2006**, *13*, 629-635.
- (45) Tuinier, R.; Rieger, J.; de Kruifa, C.G. *Adv. Colloid Interface Sci.* **2003**, *103*, 1-31.

4.6 APPENDIX

The calibration curve for blue dextran 2000 at 609 nm and concentrations $< 5 \mu\text{M}$ dye is shown below.



Dye ligand concentrations correspond to blue dextran concentrations of 1–40 mg/mL. UV–visible spectra (in triplicate) of the blue dextrans used for the calibration curve are shown below.



Introduction to Partitioning in Biphasic Systems

The previous chapter discussed phase separation of cellulose nanocrystal suspensions caused by blue dextran. Figure 4.2 in Chapter 4 shows samples in which it is clear that the concentration of blue dextran in the upper isotropic phase is higher than in the lower liquid crystalline phase. The low surface tension between the phases (10^{-3} to 10^{-4} mN/m)¹ facilitates the partitioning and does not disturb the macromolecular structure. The equilibrium distribution of the components of a system is determined by the properties of the polymer and its physico-chemical interactions with itself, with any other species present (e.g., salts, cellulose nanocrystals), and with the solvent. The preferential partitioning of a solute between two phases is often the basis for the purification and separation of that species (e.g., from a solvent, from dissimilar contaminants or from other similar related species).

Different types of partitioning systems exploit different properties and interactions of the system components. Aqueous two-phase systems (ATPS) containing two or more dissolved polymers such as polyethylene glycol and dextran are widely used to partition biological materials such as proteins, DNA, cells and cell organelles.² These systems use the differences in solubility, polarity, particle size, and so forth to separate the system components and offer greater possibilities for fractionation and purification than conventional techniques. Phase-separated aqueous micellar systems are also used to partition proteins, based on excluded-volume interactions between nonionic surfactant micelles and biomolecules.³ Affinity partitioning, on the other hand, employs chemical and physicochemical interactions of the partitioned species with either non-specific

¹ Chen, W.; Gray, D.G. *Langmuir* **2002**, *18*, 633-637.

² Albertsson, P.-Å. *Partition of Cell Particles and Macromolecules*; 3rd ed.; Wiley-Interscience: New York, 1986, 323 pp.

³ For example: van Roosmalen, D. et al. *Biotechnol. Bioeng.* **2004**, *87*, 695-703.

ligands (e.g. triazine dyes such as blue dextran) or specific ligands (e.g. antibodies), which themselves are partitioned preferentially into one phase of the ATPS.⁴ Specific partitioning phenomena can even be used to determine the chemical nature of the species being partitioned by tailoring the partitioning system. In biphasic rod-coil or rod-sphere systems in which the difference in shape is the main difference (for example, sterically-stabilized boehmite rods and polystyrene in orthodichlorobenzene),⁵ partitioning of the rods and coils occurs due to excluded-volume interactions (i.e., entropy) and osmotic pressure effects.

The work in the following chapter is an extension of a preliminary study,⁶ in which we attempt to further understand the partitioning of blue dextran in cellulose nanocrystal suspensions by isolating and studying the effect of variables such as dye ligand density. The experimental partition coefficients are also compared with predictions using Sear's partitioning theory for coiled and rodlike polymers. It should be noted that this is one case in which it is important to characterize not only the cellulose nanocrystal suspension, but also the blue dextran macromolecule, as the theory is only applicable in the dilute regime for the coiled polymer.⁷

⁴ For example: Johansson, G.; Joelsson, M. *J. Chromatogr.* **1987**, *393*, 195-208.

⁵ Buitenhuis, J. et al. *J. Colloid Interface Sci.* **1995**, *175*, 46-56.

⁶ Edgar, C.D.; Gray, D.G. *Macromolecules* **2002**, *35*, 7400-7406.

⁷ Sear, R.P. *J. Phys. II* **1997**, *7*, 877-886.

Chapter 5

Partitioning of Charged and Neutral Dextran–Dye Derivatives in Biphasic Cellulose Nanocrystal Suspensions

5.1 INTRODUCTION

It is well-established that the drive to maximize entropy can cause ordering¹ and bulk demixing in systems containing components of sufficiently different physical properties, such as shape or flexibility.² The bulk demixing is predicted to give rise to phases enriched in one of the components of the system.^{1,3} Ordered phases of rodlike particles coexisting with random phases have been shown to exclude random coil polymers and spherical particles for several experimental systems,^{2,4-10} including cellulose nanocrystals and blue dextran.¹¹ Assuming only excluded-volume interactions between the components, Flory predicted the phase separation of a solution containing a rigid rod-like polymer and a flexible randomly coiled polymer and concomitant partitioning to give a rod-rich, coil-poor phase and a coil-rich, rod-poor phase.³ The phase separation is entropy-driven, based on depletion attractions observed in colloid-polymer systems.¹² The extent of the partitioning depends on the relative size and concentration of the two components as well as their chemical nature. This has been shown experimentally^{6,8,9} as well as theoretically.¹³

Preliminary results obtained in this laboratory for blue dextran in cellulose nanocrystal suspensions have shown that the partitioning behaviour is not affected by the nature of the phase separation, that is, whether the suspension concentration lies in the isotropic-chiral nematic (I-N) coexistence region, or whether phase separation is induced by the addition of a macromolecule to a completely ordered suspension.¹¹ This chapter further investigates the partitioning behaviour of blue dextrans in biphasic cellulose nanocrystal suspensions. It is our goal to clarify the factors driving the partitioning of such polyelectrolytic species, in particular the effect of the ionic charge due to the dye substituents on the partition coefficient.

5.2 EXPERIMENTAL METHODS

5.2.1 Materials

Whatman ashless cotton cellulose powder was purchased from Cole-Parmer. Sulfuric acid (95–98 %) for hydrolysis was purchased from Fisher Scientific. Cibacron blue 3G-A dye (CB, 55 % dye content, MW 840.12 Da), and sodium hydroxide, sodium chloride and sulfuric acid volumetric standards for conductometric titration were purchased from Sigma-Aldrich. Anhydrous sodium carbonate was purchased from Anachemia. Concentrated hydrochloric acid, ACS reagent grade, was purchased from ACP Chemicals. Methanol, HPLC grade, was purchased from Fisher Scientific. Blue dextran 2000 (nominal M_w 2 000 000 Da) and FITC-dextran 2000, 500 and 150 (M_w 2 000 000, 525 000, 130 000 and 77 000 Da, respectively) were purchased from Sigma-Aldrich. Dextran (Dx) T-2000, T-500, T-110 and T-70 (M_w 2 000 000, 532 000, 106 000 and 70 000 Da, respectively) were purchased from Pharmacia Fine Chemicals. All water used was purified using a Millipore Milli-Q purification system.

5.2.2 Cellulose nanocrystal suspensions

Suspensions of cellulose nanocrystals were prepared as described in Chapter 4.¹⁴⁻¹⁶ The aqueous suspensions, 0.5–2 % cellulose by weight, were evaporated with stirring at ambient conditions to obtain the desired final nanocrystal concentrations. Conductometric titration was used to determine the surface charge density of the cellulose nanocrystals associated with surface sulfate ester groups as described in Chapter 4. Equivalence points were used to calculate the amount of sodium hydroxide required to convert the suspensions to the sodium form (Na^+ counterions).

5.2.3 Preparation of blue dextrans

Blue dextrans of various molecular weights and ligand densities were prepared using methods adapted from Mayes et al.¹⁷ and Tang et al.¹⁸ (Figure 3.1 in Chapter 3), as described in previous publications.^{19,20}

5.2.4 Acid hydrolysis of dextran T-2000

To obtain fractions of dextran with molecular mass greater than 500 kDa, degradation of a high molecular weight dextran (T-2000) by acid hydrolysis was carried out according to starch hydrolysis methods^{21,22} adapted for dextran by Ioan et al.²³ Dextran T-2000 (1 g) was suspended in 4 mL of methanol to which various amounts of concentrated hydrochloric acid were added (0.02, 0.04, 0.06 and 0.09 mL, which yielded dextrans d1700, d1400, d1200 and d980, respectively). The suspensions were shaken for 4 days, at which point the limiting molar mass value was reached.²⁴ The degraded dextrans were neutralized with 1 M NaOH and washed with 1:1 methanol–water. The hydrolyzed dextran fractions were dialyzed against milliQ water to remove any traces of base or small dextran fragments, lyophilized and stored as solids. Following characterization (see below and Table 5.1), the solid dextrans were reacted with CB dye to give blue dextrans as mentioned above. It is important to note that the degradation is not fully random; the cleavage rate of the α -(1,6) bonds differs from that of the α -(1,3) bonds and leads to a change in the branching density which may affect the partitioning.²⁵

5.2.5 Characterization of blue dextrans

Moisture contents of the dextran–dye conjugates and degraded dextrans were determined by thermogravimetric analysis (TGA, TA Instruments TGA Q500).

The dye content of the dextran–dye conjugates was determined using UV–visible spectroscopy (Varian Cary 300 Bio spectrophotometer). A calibration curve was obtained

from solutions of commercially-available blue dextran 2000 and adherence to the Beer-Lambert law was established. The molar extinction coefficient for blue dextran 2000 at 609 nm was found to be $8865 \text{ M}^{-1}\text{cm}^{-1}$. The molar extinction coefficient at 620 nm was found to be $8966 \text{ M}^{-1}\text{cm}^{-1} = 0.823 \text{ g}^{-1}\text{dm}^3\text{cm}^{-1}$, which agrees well with the value of $0.812 \text{ g}^{-1}\text{dm}^3\text{cm}^{-1}$ found by Champ et al.²⁶ for commercially available blue dextran 2000. The ligand density was estimated from absorbance measurements at 609 nm for solutions of the dextran-dye conjugates, and calculated in terms of the degree of dye substitution (DS) per anhydroglucose repeat unit (AGU). Absorbance measurements in dilute aqueous solution and in 6 M HCl (aq)^{17,27} have shown that negligible intramolecular dye stacking occurs at dye ligand densities comparable to those reported in this chapter. It should be noted that the blue dye is bound randomly to the dextran backbone.²⁸

A combination of gel permeation chromatography (GPC) and static light scattering (SLS) was used to obtain molecular weights (\bar{M}_w, \bar{M}_n), and radii of gyration (R_g) for the hydrolyzed dextrans and for FITC-Dx 2000 (see Figure 5.3 for the structure). Dextrans (2 mg/mL) were dissolved in the eluent (pH 7, 0.2 M NaNO₃ and 0.01 M NaH₂PO₄ containing 0.2 % NaN₃) and filtered using 0.45- μm membranes. Samples (100 μL) were injected onto a GPC column (300 \times 75 mm PL aquagel-OH mixed 8 μm , 1×10^2 – 1×10^7 Da separation, Polymer Laboratories) at a flow rate of 1.0 mL/min using a Merck Hitachi AS-2000A autosampler and Waters 510 HPLC pump. The column was coupled to a Wyatt Optilab rEX IR detector (690 nm) and a Wyatt Technology Corporation DAWN EOS light scattering detector. Data were analyzed with Astra v5.3.0 18 software (Wyatt Technology Corporation).

Table 5.1. Properties of blue dextrans and FITC-dextrans.

Dextran–dye conjugate ^a	MW _{Dx} (kDa) ^b	MW (kDa) ^c	Dye ligand density (DS per AGU, 10 ⁻⁴)	R (nm) ^d
Blue dextran 2000 ₇	2000	2007	7	--
Blue dextran 2000 ₁₂	2000	2010	12	40.8 ± 1.0
Blue dextran 2000 ₁₆	2000	2017	16	37.9 ± 0.8
Blue dextran 2000 ₃₀	2000	2031	30	--
Blue dextran 2000 ₃₆	2000	2038	36	35.1 ± 1.1
Blue dextran 2000 ₅₆	2000	2058	56	36.9 ± 0.9
Blue dextran 2000 ₁₆₁	2000	2167	161	40.2 ± 0.8
Blue dextran 500 ₄₉	532	545	49	--
Blue dextran 500 ₁₁	532	535	11	18.4 ± 0.7
Blue dextran 110 ₁₄₃	106	114	143	--
Blue dextran 70 ₂₈₀	70	80.2	280	<10
Blue dextran 70 ₆₆	70	72.4	66	<10
Blue dextran d1700	1690 ± 10 ^e	1720	33	40.1 ± 0.4 ^e
Blue dextran d1400	1380 ± 10 ^e	1410	27	37.2 ± 0.4 ^e
Blue dextran d1200	1180 ± 10 ^e	1200	25	35.4 ± 1.4 ^e
Blue dextran d980	980 ± 20 ^e	1000	20	30.9 ± 2.8 ^e
FITC-dextran 2000	2000	2065	130	16
FITC-dextran 500	525	543	140	--
FITC-dextran 150	130	134	120	--
FITC-dextran 70	77	79.5	130	--

^a The designation “d” indicates dextrans prepared by acid degradation of dextran T-2000. ^b Supplier data, unless otherwise indicated. ^c Molecular weights calculated based on the DS per AGU obtained by UV–visible spectroscopy. ^d Hydrodynamic radius R_H , Beck-Candanedo et al.,²⁰ unless otherwise indicated. ^e Molecular weight M_w and radius of gyration R_g obtained by GPC coupled with SLS (see text).

5.2.6 Preparation of cellulose suspensions containing dextran–dye conjugate

Solid dextran–dye derivatives were added to samples of biphasic cellulose suspension, which were mixed and allowed to re-equilibrate for 24 to 48 hours. When phase separation was complete, samples were taken from the upper and lower phases and diluted prior to analysis to minimize scattering caused by the cellulose nanocrystals. Linear correlations between absorbance and concentration were observed for blue dextran 2000 and FITC-dextran 2000 in cellulose suspension. The volume fraction of the phases was determined by measuring the heights of the anisotropic and isotropic phases in each vial.

5.2.7 Determination of partition coefficients

UV–visible absorption spectra were taken and the absorbance measured at 609 nm for blue dextrans and 490 nm for FITC-dextrans. Suspensions of cellulose nanocrystals containing no dextran–dye conjugate, but otherwise identical to the sample suspensions, were used as references. Because calibration measurements showed that measured absorbance is proportional to the concentration of macromolecule, partition coefficients were calculated from the relative absorbance values of the two phases:

$$K_{\text{meas}} = A_{\text{iso}}/A_{\text{aniso}} \quad (5.1)$$

In this chapter, the partition coefficient is defined as the concentration in the isotropic phase divided by the concentration in the anisotropic phase.

The concentration of cellulose in the samples was determined by gravimetry. The number density of the dextran–dye conjugates and dextran molecules in the samples was calculated using equation 4.1, using the weight-average molecular weights of the dextrans as discussed in Chapter 4.²⁹

5.3 RESULTS AND DISCUSSION

5.3.1 Partition theory

The concentrations of hard core monodisperse rodlike particles in the isotropic and nematic phases are predicted to remain constant across the I–N coexistence region.¹ However, because the cellulose nanocrystals contain ionic sulfate groups on their surface, increasing the total cellulose concentration causes the particle densities in the isotropic and anisotropic phases to increase and diverge slightly due to the change in ionic strength in the aqueous medium, as previously observed for this system.^{11,30} Partitioning of the blue dextran coils between the coexisting isotropic and nematic or chiral nematic phases causes the rod densities in the phases to diverge further as more polymer coils are added.¹³ Because the concentration of coils is higher in the isotropic phase, adding blue dextran increases the osmotic pressure of the isotropic phase relative to the nematic phase. To compensate, the rod density decreases in the isotropic phase and increases in the nematic phase, resulting in a widening of the I–N coexistence region of the phase diagram.¹³

Sear has studied the phase behaviour of athermal lyotropic mixtures of rodlike and flexible polymers, obtaining an expression for the partition coefficient K of a flexible polymer:¹³

$$K = \frac{C_p^i}{C_p^a} \sim \exp \left[LD^{1/3} R_g^{5/3} (C_r^a - C_r^i) \right] \quad (5.2)$$

where C_p^i and C_p^a are the number densities of the polymer in the isotropic and the anisotropic (nematic) phases, respectively, L is the rod length, D is the rod diameter, R_g is

the radius of gyration of the polymer and C_r^i and C_r^a are the number densities of the rodlike polymer in the isotropic and anisotropic (nematic) phases.

The rodlike polymer is modelled as a hard rod with a diameter much smaller than the radius of the flexible coiled polymer, $D \ll R_g$. Interactions between the rods and coils are based on excluded volume; there are no attractive interactions between the rods, which is required for the suspension to be stable. The equation is valid in the dilute regime, that is, at small volume fractions of polymer.¹³ It predicts that polymers with larger radii of gyration will partition to a greater extent, while for a given radius of gyration, a larger difference in cellulose rod concentration between the two phases will increase partitioning (i.e., K increases with total cellulose concentration, as previously observed¹¹). This expression for K has been used previously to predict blue dextran partitioning in cellulose nanocrystal suspensions; despite the fact that the expression only provides an order of magnitude for K , it predicted an increase in partition coefficient with increasing blue dextran concentration.¹¹

The critical concentration C^* (at which the semi-dilute regime begins) for blue dextran 2000₁₆₁ is calculated to be around 73 mg/mL in 10 mM NaCl and 209 mg/mL in 200 mM NaCl.²⁰ Sear's theory is valid only in the dilute regime, where the volume fraction of polymers and colloidal rods is small.¹³ The dextran concentrations used in this study do not exceed 50 mg/mL; Sear's theory is therefore valid for our samples. However, although we are working in the dilute regime for the blue dextran, it should be noted that the cellulose nanocrystals also contribute to the sample viscosity; their volume fraction is fairly low (about 6.5 % for 10 wt% nanocrystals with $L = 120$ nm and $D = 10$ nm). Sear's theory also assumes constant rod concentration across the biphasic region, as predicted by

Onsager.¹ As stated above, this is not the case for suspensions of cellulose nanocrystals, which may contribute to any discrepancy between the theoretical predictions and experimental results.

The partition coefficient K of a macromolecule in a two-phase system can be expressed in general as

$$K_{\text{meas}} = K_{\text{hphob}} \cdot K_{\text{el}} \cdot K_{\text{size}} \cdot K_{\text{sol}} \cdot K_{\text{aff}} \cdot K_0, \quad (5.3)$$

where K_{hphob} , K_{el} , K_{size} , K_{sol} and K_{aff} represent the contributions to the total partition coefficient of the effects of hydrophobicity, electrostatic forces, size factors, solubility and affinity, respectively, and K_0 represents other effects on partitioning, such as the dimensions of the rodlike particles and their relative concentrations in the two phases.³¹ These factors may be competing with each other; their relative importance will depend on the composition of the biphasic system and the properties of the molecule being partitioned. The main contributions to K for blue dextran are likely to be K_{el} and K_{hphob} (the sulfonated triazine dye introduces both ionic and hydrophobic elements into the macromolecule). K_{size} is also expected to play a role for blue dextrans of different molecular weights. Because FITC-dextran is electrostatically neutral, K_{el} should not be an important factor in its partitioning behaviour; K_{hphob} may dominate due to the hydrophobic aromatic rings in the FITC dye.

5.3.2 Blue dextran partitioning

The effect of increasing blue dextran 2000₁₆₁ concentration on its partition coefficient is shown in Figure 5.1, which also contains data from a previous publication.¹¹ The agreement is good and the partition coefficient increases linearly with increasing blue dextran concentration.

The effect of the DS of blue dextran 2000 at constant AGU monomer concentration on its partition coefficient is shown in Table 5.2. The partition coefficients increased from around 1.3 to greater than 2 when the DS was increased from 7×10^{-4} to 1.61×10^{-2} . A two-fold increase in the AGU concentration did not have a significant effect on the partition coefficients.

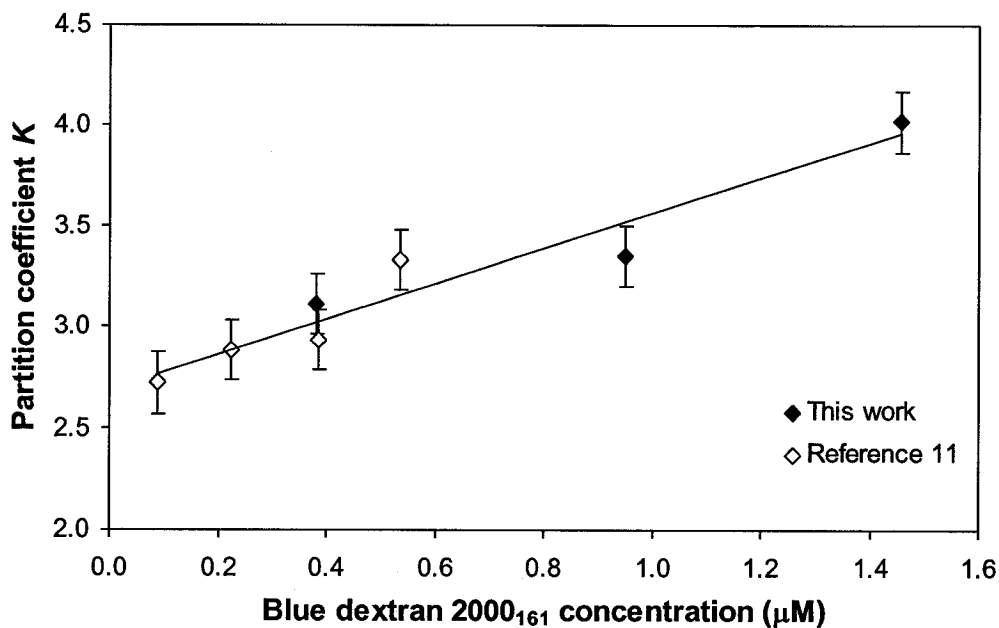


Figure 5.1. Partition coefficients for given total concentrations of blue dextran 2000₁₆₁ in ~ 10 wt% cellulose suspension. The line is the best fit to the data. Closed symbols were obtained in 10.1 wt% cellulose nanocrystal suspension; open symbols were obtained in 10.3 wt% cellulose nanocrystal suspension.

The effect of DS of blue dextran 2000 at constant dye concentration on its partition coefficient is shown in Table 5.3. The partition coefficients increased from 1.1 to greater than 3 when the DS increased from 1.60×10^{-3} to 1.61×10^{-2} . A 2.5-fold increase in the

total dye concentration did not have a significant effect on the partition coefficients (they increased slightly).

It can be concluded from the results in Tables 5.2 and 5.3 that increasing the DS results in larger K values for blue dextrans 2000 at constant AGU concentration and at constant dye concentration. The DS of the blue dextran 2000 thus determines the magnitude of K in this biphasic system; that is, the contribution of K_{el} , which increases with increasing DS, dominates K .

Table 5.2. Partition coefficients of blue dextrans 2000 in 10.1 wt% cellulose nanocrystal suspension at two constant total dextran anhydroglucose monomer concentrations.

Series	Dextran	DS per AGU, 10^{-4}	[AGU] (μM)	[Dye] (μM)	[Cellulose] (wt%)	K
I	Blue dextran 2000 ₁₆	16	18	29	10.1	1.46
	Blue dextran 2000 ₃₀	30	18	54	10.1	1.60
	Blue dextran 2000 ₃₆	36	18	65	10.1	1.72
	Blue dextran 2000 ₅₆	56	18	99	10.1	1.83
	Blue dextran 2000 ₁₆₁	161	18	290	10.1	4.02
II	Blue dextran 2000 ₇	7	40	29	10.1	1.28
	Blue dextran 2000 ₁₇	17	40	70	10.1	1.37
	Blue dextran 2000 ₃₀	30	40	121	10.1	1.47
	Blue dextran 2000 ₃₆	36	40	150	10.1	1.51
	Blue dextran 2000 ₅₆	56	40	228	10.1	1.55
	Blue dextran 2000 ₁₆₁	161	40	661	10.1	2.01

Table 5.3. Partition coefficients for blue dextrans 2000 in 10.1 wt% cellulose nanocrystal suspension at two constant dye concentrations.

Series	Dextran	DS per AGU, 10^{-4}	[AGU] (μM)	[Dye] (μM)	[Cellulose] (wt%)	K
III	Blue dextran 2000 ₁₆	16	123	197	10.1	1.10
	Blue dextran 2000 ₃₆	36	54	196	10.1	1.43
	Blue dextran 2000 ₅₆	56	35	193	10.1	1.41
	Blue dextran 2000 ₁₆₁	161	12	189	10.1	3.39
IV	Blue dextran 2000 ₁₆	16	47	78	10.1	1.23
	Blue dextran 2000 ₃₆	36	21	78	10.1	1.45
	Blue dextran 2000 ₅₆	56	13	76	10.1	1.54
	Blue dextran 2000 ₁₆₁	161	4.7	78	10.1	3.11

5.3.3 Effect of molecular weight on partition coefficient K

The partition coefficients for blue dextrans and FITC-dextrans of various molecular weights and DS are given in Table 5.4. In this case, it is particularly difficult to separate the effect of the DS of dye ligands (K_{el}) from the effect of the blue dextran molecular weight (K_{size}). For non-hydrolyzed blue dextrans with similar DS (shown in italics), K decreases from 1.48 to 1.12 when the molecular weight decreases from 2000 to 70 kDa. Partition coefficients for blue dextrans prepared from acid-hydrolyzed dextrans measured at similar AGU and dye concentrations (blue dextrans d1700–d980 contain 0.020 ± 0.001 g dye per g blue dextran) also decrease with decreasing dextran molecular weight. As shown in Figure 5.2, this is in qualitative agreement with Sear's partitioning

theory, in which K is proportional to $\exp(R_g^{5/3})$.¹³ It should be noted that the hydrolyzed dextrans are more polydisperse (Ip values for dextrans d1700, d1400, d1200 and d980 are 2.74, 2.98, 2.39 and 2.45, respectively) than the blue dextrans prepared from commercial dextrans, which have Ip values of around 1–1.25.²⁰ Lower molecular weight FITC-dextrans appear to partition more strongly into the anisotropic phase.

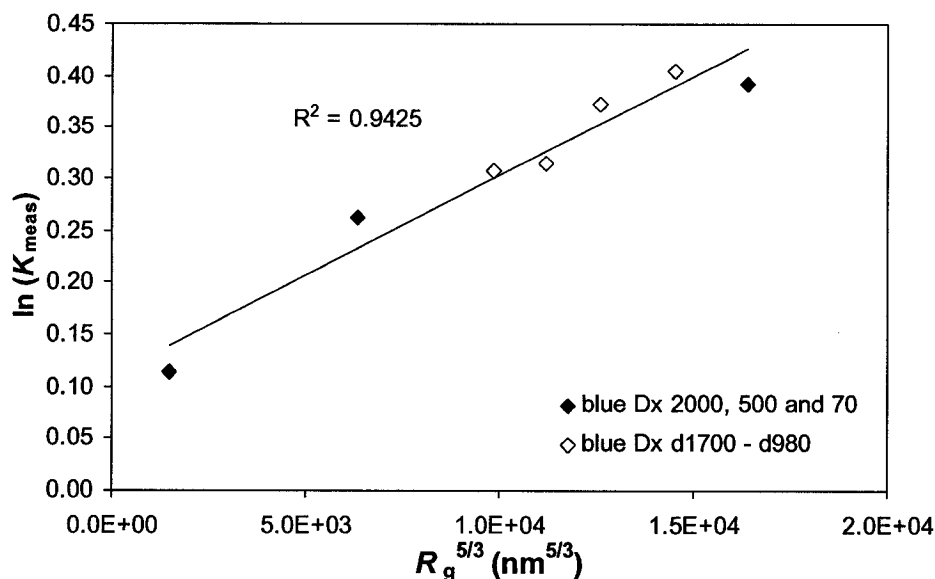


Figure 5.2. Natural logarithm of the measured partition coefficient K_{meas} as a function of $R_g^{5/3}$ for blue dextrans of different molecular weights. Radii of gyration of the dextrans were calculated using the equation $R_g = 0.66M_w^{0.43}$, which is valid over the M_w range 400 to 2,700 kDa.³²

Table 5.4. Partition coefficients for blue dextrans and FITC-dextrans of different molecular weight. Entries in italics denote blue dextrans of different molecular weights having similar DS values.

MW (kDa)	Dextran	DS per AGU, 10^{-4}	[Dye] (μ M)	[AGU] (μ M)	[Cellulose] (wt %)	<i>K</i>
2167	Blue dextran 2000 ₁₆₁	161	997	61700	10.1	3.38
2058	<i>Blue dextran 2000₅₆</i>	<i>56</i>	<i>344</i>	<i>61900</i>	<i>10.1</i>	<i>1.48</i>
2010	Blue dextran 2000 ₁₂	12	85	66000	10.1	1.39
2017	Blue dextran 2000 ₁₆	16	81	49700	10.1	1.13
1722	Blue dextran d1700	33	96	24400	9.8	1.50
1410	Blue dextran d1400	27	94	24200	9.8	1.45
1202	Blue dextran d1200	25	101	24000	9.8	1.37
1003	Blue dextran d980	20	97	24500	9.8	1.36
545	<i>Blue dextran 500₄₉</i>	<i>49</i>	<i>82</i>	<i>16600</i>	<i>10.1</i>	<i>1.30</i>
545	Blue dextran 500 ₄₉	49	86	17200	10.1	1.30
114	Blue dextran 110 ₁₄₃	143	79	5400	10.1	1.09
80.2	Blue dextran 70 ₂₈₀	280	55.0	1900	10.1	2.04
72.4	<i>Blue dextran 70₆₆</i>	<i>66</i>	<i>110</i>	<i>16100</i>	<i>10.1</i>	<i>1.12</i>
72.4	Blue dextran 70 ₆₆	66	110	12400	10.1	1.11
2065	FITC-dextran 2000	130	963	74000	9.8	0.98
543	FITC-dextran 500	140	256	18300	9.8	0.98
134	FITC-dextran 150	120	58	4800	9.8	0.88
79.5	FITC-dextran 70	130	36	2700	9.8	0.81

5.3.4 FITC-dextran partitioning

The partition coefficients for FITC-dextran in the same biphasic system were all around 0.8–1.0, indicating slight preferential partitioning into the lower anisotropic phase (Table 5.5). FITC-dextran is neutral at basic pH,³³ or at most slightly positive at the pH of 4–5 in the cellulose suspensions, but contains several hydrophobic aromatic rings, similarly to blue dextran (Figure 5.3).

Table 5.5. Partition coefficients for FITC-dextran.

Dextran	DS per AGU, 10 ⁻⁴	[AGU] (μ M)	[Dye] (μ M)	[Cellulose] (wt %)	<i>K</i>
Increasing FITC-dextran concentration					
FITC-dextran 2000	130	9000	117	9.8	1.05
	130	9900	129	9.8	0.90
	130	14900	194	9.8	1.07
	130	20400	265	9.8	1.02
	130	21000	272	9.8	1.02
	130	42500	552	9.8	0.91
	130	65000	846	9.8	0.91
	130	95400	1240	9.8	1.03
Increasing total cellulose nanocrystal concentration					
FITC-dextran 2000	130	27600	360	7.9	0.90
	130	21000	272	9.8	1.02
	130	27600	331	9.9	0.97
	130	27600	386	11.0	0.89

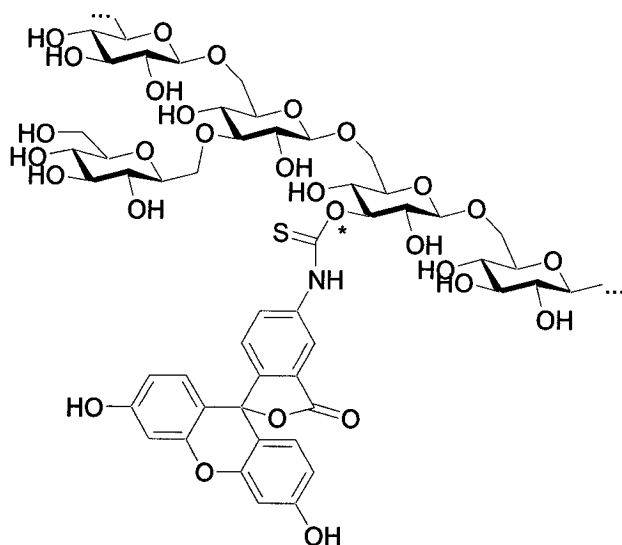


Figure 5.3. Structure of FITC-dextran. *FITC is assumed to associate randomly with any free hydroxyl group.³⁴

The observed partitioning behaviour of charged and neutral dye-labeled dextrans suggests that the blue dextran partitioning is partly electrostatic in nature, as mentioned above.

5.3.5 Increasing degree of dye substitution (DS)

Cibacron blue 3G-A dye has been found to adsorb onto the surface of microcrystalline cellulose (MCC, Avicel PH 102) in studies of the hydrolysis of amylose by CB-dyed amylases in the presence of MCC.³⁵ The adsorption of CB dye onto cellulose nanocrystals containing anionic surface sulfate esters was also verified by exhaustively dialyzing cellulose suspensions to which small amounts of CB dye were added. The absorption spectra of the resulting samples showed a peak in the range of 590–630 nm, indicating the presence of CB dye. Free CB dye was not found to partition in biphasic cellulose nanocrystal suspensions. Because CB contains three anionic sulfonate groups per molecule, it is soluble in water and it is therefore conceivable that many dye ligands

will be exposed on the surface of a blue dextran molecule in aqueous solution and be available to adsorb onto the surfaces of cellulose nanocrystals. This presumably occurs during the mixing and early equilibration stages of sample preparation. Upon formation of the anisotropic phase, the adsorbed blue dextrans may desorb and be expelled into the isotropic phase, as they are too large and interfere with the chiral nematic structure (excluded volume effect);¹⁹ the entropy gain and the associated reduction in free energy is greater than the reduction in free energy due to adsorption. The increase in K with increasing DS of the blue dextran may be caused by an electrostatic effect: the negatively-charged cellulose nanocrystals in the anisotropic phase may be more efficient at expelling the more highly-substituted blue dextrans which are more negatively-charged. This may explain why the observed blue dextran K values are much higher than predicted by Sear's theory (Figure 5.4),* which does not take electrostatic factors into account. Using surface charge density values measured by conductometric titration, the ratio of surface charge (and corresponding counterions) between the anisotropic and isotropic phases of 8.7 wt% and 9.8 wt% (total cellulose concentration) suspensions was calculated to be around 1.3 for both samples (which differed in nanocrystal surface charge density). There is therefore an electric potential difference between the phases, which may affect the partitioning behaviour of the negatively-charged blue dextrans. That is, blue dextrans with higher DS may be more strongly repelled by the negatively-charged nanocrystals, and prefer the more dilute isotropic phase. Thus, K_{el} increases with increasing blue dextran DS.³¹

* Although it only gives the order of magnitude for K .

5.3.6 Increasing blue dextran concentration

The divergence in the cellulose concentrations of the two phases (as predicted by Flory³ and observed by Edgar and Gray¹¹) caused by the increase in ionic strength from 0.4 to 7.3 μM due to the increasing concentration of blue dextran dye ligands is likely too small to affect K according to Sear's theory,¹³ as increasing the ionic strength from 0 to 2.5 mM was found to cause only a very slight divergence of the isotropic and anisotropic phase concentrations.³⁰ At low concentrations of dextran–dye conjugate, the mixing entropy dominates, resulting in a weak driving force for partitioning that increases with increasing polymer concentration. Increasing the total concentration of an ionic dextran–dye conjugate did not have an effect on the value of K in an aqueous two-phase system consisting of dextran and PEG, where such electrostatic and entropic (excluded volume) factors would not be present.³⁶

5.3.7 Nonionic FITC-dextran vs. anionic blue dextran

In the context of the above observations, the lack of preferential partitioning observed in the FITC-dextran samples is plausible. It has been found that in suspensions of rodlike fd virus suspensions at low ionic strength, neutral FITC-dextran has no effect on the coexistence concentrations of the I–N transition, and no partitioning is observed, in contrast to the strong partitioning predicted theoretically.³³ Dogic et al. explained this by stating that the depletion attraction caused by the polymer is screened by long-range electrostatic repulsion of the rods.³³ A similar phenomenon may be occurring here.

In addition, the nonionic FITC dye ligand is more hydrophobic than CB dye ligand due to its lack of charged groups, and is more likely to be found in the interior of the dextran coil, where it is not available to adsorb onto cellulose nanocrystals. Although free FITC dye has been found to adsorb somewhat onto cellulosic materials,^{37,38} there may be a high

concentration of nonadsorbed neutral FITC-dextran, which may be better tolerated in the anisotropic phase because it is more mobile and can fit in the defects (although blue dextran also fits in defects¹¹) and is not electrostatically repelled by the nanocrystals. If some FITC dye molecules are available for binding, they may not adsorb on cellulose to as great an extent as CB (the binding energy may be weaker for FITC than for CB dye); FITC-dextran with higher DS may possibly partition more strongly. FITC-dextran 2000 has a radius of gyration of around 16 nm (measured by GPC-LS in pH 7 0.20M NaNO₃ + 0.01 M NaH₂PO₄), which is significantly smaller than the radii obtained for blue dextrans 2000 (see Table 5.1). The smaller size of FITC-Dx is likely caused by its higher hydrophobicity and lack of intramolecular electrostatic repulsions (internal hydrophobic interactions of the aromatic rings cause the macromolecule to contract inwards). FITC-dextran partition coefficient values were found to be slightly lower than predicted theoretically (Figure 5.4).

Sear's theoretical calculation considers only the effect of the relative sizes of the rods and coils, in conjunction with the concentration of the rods in each phase, to predict K for a given system. The relative concentrations of the two species may also play a role in determining K , particularly in the case of electrostatically charged rods *and* coils, as in the case of blue dextran and cellulose nanocrystals. For blue dextrans, K_{el} (>1) appears to dominate the contribution to K_{meas} , while for FITC-Dx, the hydrophobic interactions ($K_{hphob} < 1$) of the dye ligands are of greater importance. The theoretical K values for both dextran-dye derivatives therefore lie on the same line (Figure 5.4), while their experimental values are very different.

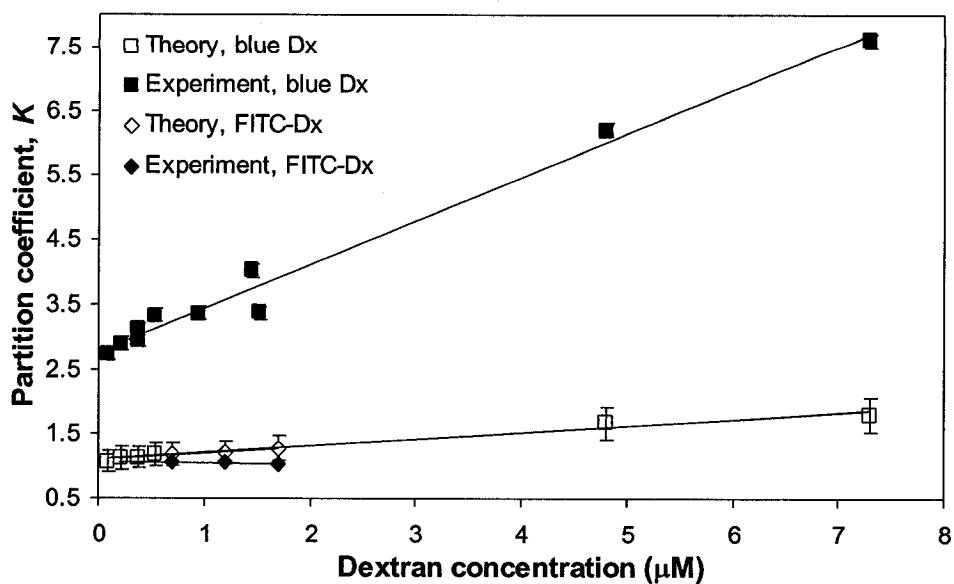


Figure 5.4. Theoretical and experimental K values for blue dextrans and FITC-dextrans in cellulose nanocrystal suspension. The error bars for experimental K values are on the order of the size of the data points.

5.4 CONCLUSIONS

The partitioning behaviour of blue dextrans and FITC-dextrans of high molecular weight in biphasic suspensions of negatively-charged cellulose nanocrystals was investigated. Increasing the total concentration of blue dextran increased the partition coefficient by causing a divergence in cellulose concentrations of the isotropic and nematic phases, in agreement with theory and previous experiments conducted in this laboratory. Increased blue dextran-nanocrystal electrostatic repulsions led to larger partition coefficients at higher degrees of CB dye substitution. The total concentration of anionic CB dye present in the sample and the DS per AGU affected the electrostatic and entropic contributions to the blue dextran partition coefficient in the cellulose suspension. For blue dextrans and hydrolyzed blue dextrans with similar DS at similar total dextran and dye concentrations, the natural logarithm of the partition coefficient varied linearly with $R_g^{5/3}$, in agreement with Sear's partition theory. Dextrans labeled with fluorescein isothiocyanate were found to have partition coefficients of around 1 in this system, possibly due to the lack of electrostatic repulsion and/or dye adsorption onto cellulose nanocrystals. Blue dextran partition coefficients were larger than predicted theoretically using a second virial coefficient approximation, while FITC-dextran partition coefficients were smaller.

5.5 REFERENCES

- (1) Onsager, L. *Ann. N.Y. Acad. Sci.* **1949**, *51*, 627-659.
- (2) Adams, M.; Dogic, Z.; Keller, S.L.; Fraden, S. *Nature* **1998**, *393*, 349-352.
- (3) Flory, P.J. *Macromolecules* **1978**, *11*, 1138-1141.
- (4) Takayanagi, M.; Ogata, T.; Morikawa, M.; Kai, T. *J. Macromol. Sci. Phys.* **1980**, *B17*, 591-615.
- (5) Hwang, W.-F.; Wiff, D.R.; Benner, C.L.; Helminiak, T.E. *J. Macromol. Sci. Phys.* **1983**, *B22*, 231-257.
- (6) Bianchi, E.; Ciferri, A.; Tealdi, A. *Macromolecules* **1982**, *15*, 1268-1272.
- (7) Adams, M.; Fraden, S. *Biophys. J.* **1998**, *74*, 669-677.
- (8) Inomata, K.; Ohara, N.; Shimizu, H.; Nose, T. *Polymer* **1998**, *39*, 3379-3386.
- (9) Ramzi, M.; Borgström, J.; Piculell, L. *Macromolecules* **1999**, *32*, 2250-2255.
- (10) Koenderink, G.H.; Vliegenthart, G.A.; Kluijtmans, S.G.J.M.; van Blaaderen, A.; Philipse, A.P.; Lekkerkerker, H.N.W. *Langmuir* **1999**, *15*, 4693-4696.
- (11) Edgar, C.D.; Gray, D.G. *Macromolecules* **2002**, *35*, 7400-7406.
- (12) Lekkerkerker, H.N.W.; Stroobants, A. *Il Nuovo Cimento* **1994**, *16D*, 949-962.
- (13) Sear, R.P. *J. Phys. II* **1997**, *7*, 877-886.
- (14) Dong, X.M.; Revol, J.-F.; Gray, D.G. *Cellulose* **1998**, *5*, 19-32.
- (15) Revol, J.-F.; Bradford, H.; Giasson, J.; Marchessault, R.H.; Gray, D.G. *Int. J. Biol. Macromol.* **1992**, *14*, 170-172.
- (16) Revol, J.F.; Godbout, L.; Dong, X.M.; Gray, D.G.; Chanzy, H.; Maret, G. *Liq. Cryst.* **1994**, *16*, 127-134.
- (17) Mayes, A.G.; Moore, J.D.; Eisenthal, R.; Hubble, J. *Biotechnol. Bioeng.* **1990**, *36*, 1090-1096.

- (18) Tang, M.; Zhang, R.; Bowyer, A.; Eissenthal, R.; Hubble, J. *Biotechnol. Bioeng.* **2004**, *87*, 791-796.
- (19) Beck-Candanedo, S.; Viet, D.; Gray, D.G. *Langmuir* **2006**, *22*, 8690-8695;
Chapter 4 of this thesis.
- (20) Chapter 3 of this thesis.
- (21) Ma, W.-P.; Robyt, J.F. *Carbohydr. Res.* **1987**, *166*, 283-297.
- (22) Fox, J.D.; Robyt, J.F. *Carbohydr. Res.* **1992**, *227*, 163-170.
- (23) Ioan, C.E.; Aberle, T.; Burchard, W. *Macromolecules* **2000**, *33*, 5730-5739.
- (24) Galinsky, G.; Burchard, W. *Macromolecules* **1995**, *28*, 2363-2370.
- (25) Ioan, C.E.; Aberle, T.; Burchard, W. *Macromolecules* **2001**, *34*, 3765-3771.
- (26) Champ, S.; Xue, W.; Huglin, M.B. *Macromol. Chem. Phys.* **2000**, *201*, 931-940.
- (27) Chambers, G.K. *Anal. Biochem.* **1977**, *83*, 551-556.
- (28) Sigma-Aldrich, Blue Dextran Molecular Weight 2,000,000 Product No. D5751.
Product Information, 1997.
- (29) Fishman, M.L.; Damert, W.C.; Phillips, J.G.; Barford, R.A. *Carbohydr. Res.* **1987**, *160*, 215-225.
- (30) Dong, X.M.; Kimura, T.; Revol, J.-F.; Gray, D.G. *Langmuir* **1996**, *12*, 2076-2082.
- (31) Albertsson, P.-Å. *Partition of Cell Particles and Macromolecules*; 3rd ed.; Wiley-Interscience: New York, 1986, 323 pp.
- (32) Senti, F.R.; Hellman, N.N.; Ludwig, N.H.; Babcock, G.E.; Tobin, R.; Glass, C.A.; Lamberts, B.L. *J. Polym. Sci.* **1955**, *27*, 527-546.
- (33) Dogic, Z.; Purdy, K.R.; Grelet, E.; Adams, M.; Fraden, S. *Phys. Rev. E* **2004**, *69*, 051702-1 - 051702-9.

- (34) Sigma-Aldrich, Fluorescein Isothiocyanate Dextran Product No. FD-2000S. Product Information, 1997.
- (35) Stevenson, D.L.; Kennedy, J.F.; White, C.A. *Starch* **1988**, *40*, 433-437.
- (36) Johansson, G.; Joelsson, M. *J. Chromatogr.* **1987**, *393*, 195-208.
- (37) Hildén, L.; Daniel, G.; Johansson, G. *Biotechnol. Lett.* **2003**, *25*, 553-558.
- (38) Pinto, R.; Carvalho, J.; Mota, M.; Gama, M. *Cellulose* **2006**, *13*, 557-569.

**Introduction to Triphase Equilibria
in Cellulose Nanocrystal + Dextran Systems**

The following two chapters, Chapters 6 and 7, deal with the spontaneous formation of a third (isotropic) phase when blue dextran and unmodified dextran are both added to a biphasic isotropic-nematic cellulose nanocrystal suspension. The initial observation of the I_1 - I_2 - N triphase equilibrium may be qualified as serendipitous: It is difficult to isolate the effects of dextran (i.e., AGU) and dye ligand concentration on the blue dextran partition coefficient (see Chapter 5) without having a series of blue dextrans with precisely-tailored dye loadings, which is near impossible to achieve, there being no easy way to monitor dye loading during synthesis. We attempted to measure the effect of dextran concentration by adding unmodified dextran to samples having identical concentrations of commercial blue dextran 2000. Rather unexpectedly, an equilibrium state containing three phases formed (Figure 6-A), sparking an investigation into the nature and properties of this new equilibrium.

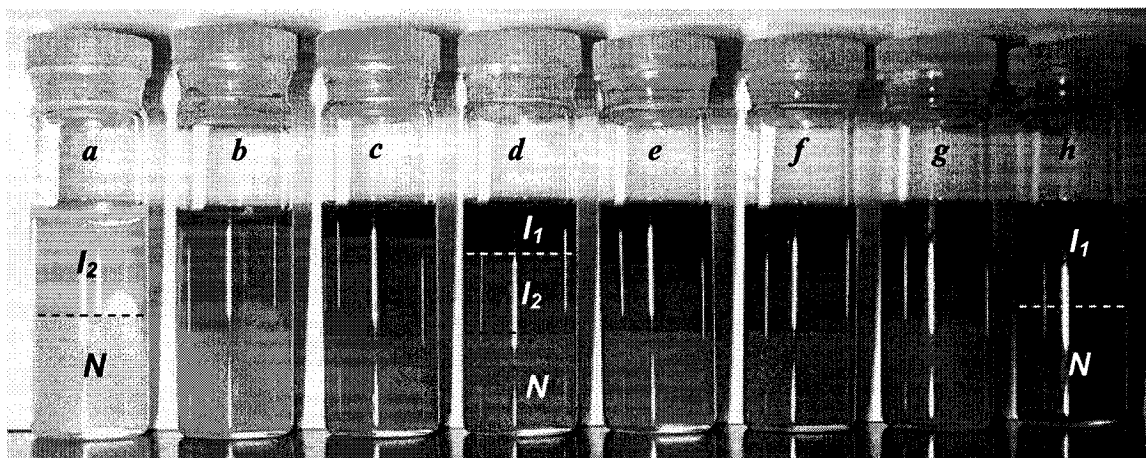


Figure 6-A. Cellulose nanocrystal suspensions containing identical concentrations of unmodified dextran T-2000 and blue dextran 2000 increasing in concentration from *b* to *h*. Sample *a* contains only dextran T-2000 and is designated I_2 - N ; sample *h* is designated I_1 - N .

In retrospect, however, the formation of a third phase should not have been entirely unexpected, as an examination of Gibbs' phase rule shows. Gibbs' phase rule (equation 6-A) states:¹

$$F = C + N - P \quad (6-A)$$

where F is the number of independent variables that can be changed independently without affecting the number of phases present (i.e., the degrees of freedom), C is the number of components (in this case, water, cellulose nanocrystals, blue dextran and dextran = 4), N is the number of non-compositional variables (generally, pressure and temperature, although for condensed systems the pressure is often negligible, and N = 1) and P is the number of phases. When we put P = 3, we have $F = 4 + 1 - 3 = 2$ degrees of freedom. This means that any two of the component concentrations can be independently changed within this region up to the phase boundaries. It also indicates that a four-phase equilibrium is also theoretically possible – although the concentrations at which we were working either did not lead to the fourth phase or it cannot be reached due to kinetic (i.e., viscosity) considerations.

¹ Gibbs, J.W. *Trans. Conn. Acad.* **Oct. 1875 – May 1876**, 3, 108-248; and **May 1877 – July 1878**, 3, 343-524.

Chapter 6

Triphase Equilibria in Cellulose Nanocrystal Suspensions Containing Neutral and Charged Macromolecules.

Reproduced with permission from
Beck-Candanedo, S.; Viet, D.; Gray, D.G. *Macromolecules* **2007**, *40*, 3429-3436.
Copyright 2007 American Chemical Society.

6.1 INTRODUCTION

The spontaneous phase separation of suspensions of rod- and plate-like colloidal particles to give isotropic and nematic liquid crystalline phases is well-known and was reported as early as the 1920s.¹⁻⁸ The isotropic-nematic phase transition is purely entropic in nature: although the orientational entropy of the system decreases due to alignment of the rods in the nematic phase, this loss is more than offset by the increase in positional or translational entropy of the system. In other words, the free volume available to individual rods increases as the rods align. Such systems can display rich phase behaviour; triphase isotropic-nematic-nematic (I-N-N) have been observed in suspensions of colloidal boehmite particles⁹ as well as in suspensions of tunicate cellulose whiskers.¹⁰

Widening of the biphasic coexistence region by the addition of coiled macromolecules, and their preferential partitioning into the isotropic phase, was predicted theoretically by Flory, who stated that the addition of a coiled polymer increases the volume fraction of rodlike particles in the anisotropic phase.¹¹ Non-interacting macromolecules thus create attractive depletion forces between rodlike colloids, inducing phase separation in anisotropic suspensions.¹²⁻¹⁴ The range of the depletion force depends on the size of the macromolecule, while the strength of the force depends on its concentration. Electrically charged macromolecules have been found to greatly increase the magnitude of the interaction.¹³ Depletion-induced phase separation has been studied experimentally and theoretically for a variety of colloid-polymer systems.^{5,15-19} Attractive depletion forces due to added macromolecules have been predicted to enrich the phase behaviour of

suspensions of rodlike particles, but the exact nature of the effect depends on the rod dimensions and polydispersity as well as the macromolecule concentration.²⁰⁻²²

Suspensions of electrostatically stabilized rodlike cellulose nanocrystals can be produced by acid hydrolysis of various types of cellulose, including bacterial, tunicate, cotton and wood cellulose.²³⁻²⁸ Within a narrow concentration range, these suspensions separate into isotropic and chiral nematic phases. Their phase separation behaviour depends on the nanocrystal dimensions and surface charge density and on the ionic strength of the suspension and the nature of the counterions.^{24,29-32} The addition of the polymer blue dextran 2000 has been shown to alter the phase separation behaviour of aqueous suspensions of cotton cellulose nanocrystals by inducing the separation of an isotropic phase from completely anisotropic suspensions.²⁷ Blue dextran 2000 consists of a non-adsorbing glucose polymer containing approximately 5% α -(1,3)-branching with a branched coil-like conformation.^{33,34} It contains a sulfonated triazine dye, Cibacron blue 3G-A (CB), is covalently bound to random hydroxyl groups on the dextran chain.³⁵ However, later work has found that equivalent concentrations of *unmodified* dextran T-2000 do *not* induce phase separation in similar suspensions.³⁶ If the phase separation were caused by attractive depletion forces induced by added macromolecules, blue and plain dextran of equivalent molar masses should have the same effect. The apparent inconsistency can be explained by the low ionic strength of the suspensions (no added salt), which allows the electrostatic repulsion between the nanocrystals to screen the attractive depletion forces caused by the neutral dextran. An analogous phenomenon has been observed by Dogic et al. for suspensions of fd virus containing the neutral polymer dextran T-500.¹⁸ Blue dextran contains anionic sulfonate groups as part of the dye

molecules, which increase the ionic strength when added to the suspension, thereby increasing the critical concentration required for phase separation, and at higher ionic strengths, masking the electrostatic repulsion sufficiently to allow depletion attraction to dominate.^{36,37}

Preferential partitioning of blue dextran into the isotropic phase has been measured for biphasic and initially anisotropic suspensions, and a widening of the isotropic-nematic (I-N) coexistence region was observed.²⁷ Greater partitioning occurred at higher blue dextran concentrations, in qualitative agreement with Sear's partitioning theory.³⁸ The effects of ionic strength (i.e., dye concentration) and macromolecule concentration being essentially inseparable when working with a particular blue dextran, increasing amounts of unmodified dextran were added to aliquots of biphasic cellulose suspension containing equal amounts of blue dextran in an attempt to measure the effect of only the dextran portion on the partitioning of blue dextran between the isotropic and chiral nematic phases. However, after mixing and equilibration, the samples unexpectedly displayed three phases: an upper isotropic (I_1) phase into which the blue dextran appears to partition preferentially, a middle isotropic (I_2) phase, and a lower chiral nematic (N) phase.

Triphase isotropic-isotropic-nematic (I-I-N) and isotropic-nematic-nematic (I-N-N) equilibria have been predicted theoretically for rodlike colloid and flexible polymer systems^{20,39} and have been observed in sterically-stabilized boehmite rod suspensions, both with⁵ and without⁹ added polymer. To our knowledge, triphase I-I-N equilibria in cellulose nanocrystal suspensions have not been reported in the literature. The present chapter describes the formation of the triphase equilibrium as well as the partitioning of

the dextrans among the phases. The following chapter examines the phase diagram for various dextran/blue dextran/nanocrystal compositions.⁴⁰

It should be noted that although the liquid crystalline phase of the cellulose suspensions is chiral nematic, the term nematic (N) will be used; the free energy difference between nematic and chiral nematic phases is much smaller than that between isotropic and anisotropic (whether nematic or chiral nematic).⁴¹ This allows results for systems containing chiral nematic phases to be compared with theories developed for nematic phases.

Unless otherwise specified, “dextran” refers to neutral, unmodified dextran and “blue dextran” refers to dextran with dye ligands attached.

6.2 EXPERIMENTAL METHODS

6.2.1 Chemicals

Dextrans T-110, T-500 and T-2000 (see Table 6.1) and blue dextran 2000 ($\bar{M}_w \approx 2\,000\,000$ with 0.1 mmol Reactive Blue 2 dye per gram of dextran bonded randomly via an ether linkage to the polymer backbone⁴²) were purchased from Pharmacia Fine Chemicals. Cibacron blue 3G-A (55% dye content) and fluorescein isothiocyanate-labelled dextran 2000 (FITC-dextran 2000) were purchased from Sigma-Aldrich and used without further purification. Whatman ashless cotton cellulose powder was purchased from Cole-Parmer. Sulfuric acid (95–98%) for hydrolysis was purchased from Fisher Scientific. Sodium hydroxide, sodium chloride, and sulfuric acid volumetric standards for conductometric titration were purchased from Aldrich. All water used was purified with a Millipore Milli-Q purification system.

Table 6.1. Molecular weights, polydispersities and radii of gyration of dextrans used.⁴³⁻⁴⁵

Dextran	\bar{M}_w (kDa)	\bar{M}_n (kDa)	Ip	R_g (nm)
T-2000	2000	--	--	34.0
T-500	532	183	2.91	19.8
T-110	106	80.9	1.31	9.7

6.2.2 Cellulose nanocrystal suspensions

Cellulose nanocrystal suspensions were prepared as described in Chapter 4.^{23,24,31} The final aqueous suspensions were 1–2 % cellulose by weight, determined by gravimetry. Conductometric titration was used to determine the surface charge density of the cellulose nanocrystals as described in Chapter 4. The suspension was then concentrated to 8.7 wt% by evaporation under ambient conditions.

6.2.3 Blue dextrans

Blue dextrans of various molecular weights and ligand densities (Table 6.2) were prepared using methods adapted from Mayes et al.⁴⁶ and Tang et al.⁴⁷, as described in Chapter 3.

6.2.4 Preparation of cellulose–dextran suspensions

Samples were prepared by adding solid dextran to aliquots of concentrated cellulose nanocrystal suspension and vortexing until homogeneous dispersion was achieved. Suspensions were allowed to equilibrate and monitored over a period of at least two weeks. The phase volume fractions were determined by measuring the heights of the anisotropic and isotropic phases in each vial.

Table 6.2. Preparation conditions and ligand densities of blue dextrans.

Blue dextran ^a	Reaction time (h)	Initial dye-dextran ratio (mol:mol)	[Na ₂ CO ₃] (M)	Ligand density (DS per AGU, 10 ⁻⁴)
2000 ₃₀	48	260	0.010	30
2000 ₁₆₁	-- ^b	-- ^b	-- ^b	161
500 ₄₉	48	300	0.010	49
110 ₁₃₀	120	300	0.45	130

^a Subscripts indicate dye ligand density. ^b Commercially available blue dextran 2000 (Pharmacia Fine Chemicals).

The number density, C_i , of the blue dextran and dextran molecules in the samples was calculated using equation 4.1:

$$C_i = \frac{N_i}{V_{tot}} = \frac{N_a \cdot m_i}{V_{tot} \cdot M_i}, \quad (4.1)$$

where N_i is the number of molecules of species i , V_{tot} is the volume of the sample, N_a is Avogadro's number, m_i is the mass of species i , and M_i is the molar mass of species i . It should be noted that while number average molecular weight, \bar{M}_n , should be used in the formula for number density, the molecular weights given for the dextrans are weight average, \bar{M}_w (supplier's data). The polydispersity \bar{M}_w/\bar{M}_n of the dextrans decreases with decreasing molar mass (Table 6.1).⁴³

6.2.5 Characterization methods

Photomicrographs of the three phases were taken using a polarized light microscope (Nikon Microphot-FXA). Pitch measurements were performed on microscope images of the chiral nematic (N) phase.

Moisture contents of the dextrans and dextran–dye conjugates were determined by thermogravimetric analysis (TA Instruments TGA Q500). The dextrans contained 10.5–11.5 % water by mass, and the blue dextrans contained 11.1–16.5 % water by mass. All dextran concentrations were calculated taking the moisture content into account.

The dye content of the dextran–dye conjugates was determined using UV–visible spectroscopy (Varian Cary 300 Bio spectrophotometer). A calibration curve was obtained from solutions of commercially-available blue dextran 2000 and adherence to the Beer-Lambert law was established. The ligand density was estimated from absorbance measurements at 609 nm for solutions of the dextran–dye conjugates, and calculated in terms of the degree of substitution (DS) per anhydroglucose (AGU) repeat unit (Table 6.2). According to convention, commercially available blue dextran 2000 purchased from Pharmacia will be referred to as “blue dextran 2000”, except where necessary for clarity.

The hydrodynamic radii of the blue dextran 2000 and dextran T-2000 (Table 6.3) were calculated using dynamic light scattering (DLS). Solutions of dextran and blue dextran were prepared in 0.200 M NaCl (aq). The solutions and solvents were clarified by filtration through a nylon filter of pore size 0.2 μm (Millipore); samples were filtered directly into the light scattering cells. Light scattering measurements were made at 21–22 °C on a Brookhaven Research BI-200SM laser light scattering goniometer and BI-2030AT digital correlator, using a polarized incident beam of wavelength 632.8 nm from a He-Ne laser (35 mW total power). DLS measurements were made at a 90° angle with sample times of 20 μsec over a duration of 30 seconds.

Table 6.3. Hydrodynamic radii of unmodified dextrans and blue dextrans in 0.200 M NaCl (aq) obtained by dynamic light scattering.

Dextran ^a	R_H (nm)
Dextran T-2000	37.7 ± 0.8
Blue dextran 2000 ₁₆₁	40.2 ± 0.8
Dextran T-500	17.8 ± 0.3
Blue dextran 500 ₁₁	18.4 ± 0.7
Dextran T-110	7.7 ± 1.2
Blue dextran 110 ₂₂	30.7 ± 3.1

^a Subscripts indicate dye ligand density (DS per AGU, 10^{-4}).

To measure the partitioning of blue dextran and FTIC-dextran among the phases of the suspensions, aliquots of each phase were carefully removed and diluted to minimize scattering by the cellulose nanocrystals. Concentrations of blue Dx 2000 and FITC-Dx 2000 in each phase were measured spectrophotometrically using dextran-free cellulose nanocrystal suspensions as the reference.

Tapping-mode atomic force microscopy (TM-AFM) images were obtained using an Asylum MFP 3D atomic force microscope (Asylum Research). Aliquots were taken from each phase of a triphasic sample (8.7 wt% cellulose nanocrystal suspension containing $C_{\text{blue Dx 2000}} = 4.42 \times 10^{-6} \text{ nm}^{-3}$ and $C_{\text{Dx T-2000}} = 4.80 \times 10^{-6} \text{ nm}^{-3}$), diluted to about 5×10^{-5} wt% concentration and dried down onto freshly cleaved mica, which was attached to a glass microscope slide. Samples were scanned under ambient conditions at 160 kHz with scan sizes ranging from 2–10 μm . Ultrasharp NSC 14/AIBS (MikroMasch) tips have a

nominal radius < 10 nm and a nominal force constant of 5 N/m, as given by the manufacturer. Nanocrystal length measurements were obtained from printouts of several height mode AFM images for each sample. The uncertainty in the AFM length measurements is approximately 10–15 nm.

6.3 RESULTS

6.3.1 Triphase equilibrium

When dextran and blue dextran are added to an 8.7 wt% biphasic cellulose nanocrystal suspension ($\phi_{\text{aniso}} = 0.40$), a three-phase coexistence develops (Figure 6.1). The appearance of the phases when viewed between partially crossed polarizers (Figure 6.1b) and using polarized light microscopy (Figure 6.2) suggests that the new phase is a dilute isotropic phase. No birefringence or “order” is visible in the upper phase, while the birefringence seen in the middle phase can be explained by a thin layer of nematic ordering on the surface of the glass (cf. Buitenhuis et al.⁵). Any tactoids are due to incomplete equilibration – it takes at least 24 hours for the phase separation to be distinct, and 2 to 3 days for it to near completion. In addition, the upper and middle phases mix more easily than the middle and lower phases upon gentle shaking, and the lower phase is barely disturbed. Based on its much larger volume fraction, the middle phase corresponds to the isotropic phase normally observed in biphasic cellulose nanocrystal suspensions. The three phases in equilibrium are designated, from top to bottom, as I_1 , I_2 and N.

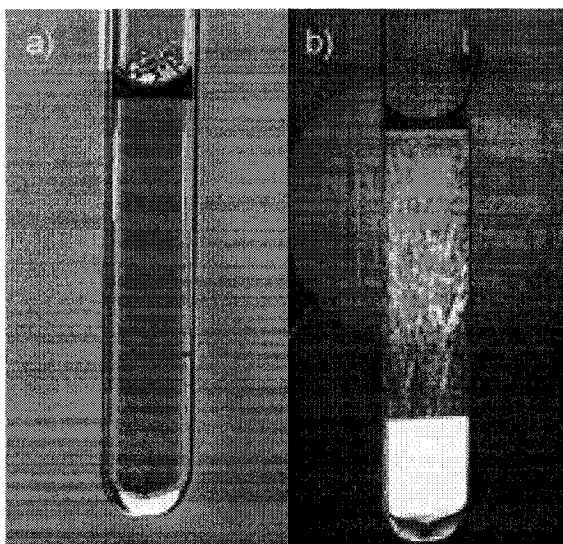


Figure 6.1. Sample of 8.7 wt% cellulose nanocrystal suspension containing blue dextran 2000 ($C_{\text{blue Dx}} = 8.3 \times 10^{-7} \text{ nm}^{-3}$) and dextran T-2000 ($C_{\text{Dx}} = 1.1 \times 10^{-5} \text{ nm}^{-3}$), showing separation into three phases: from top to bottom, I_1 , I_2 and N. Photos taken a) in incident light, and b) between partially crossed polarizers.

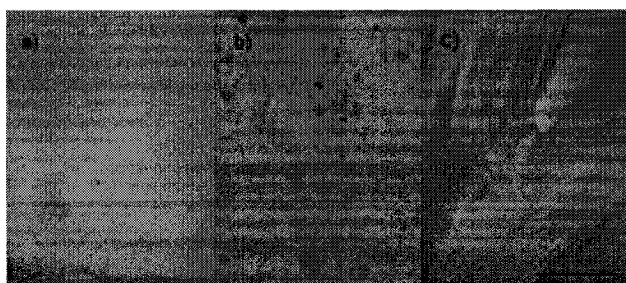


Figure 6.2. Photomicrographs of a) I_1 , b) I_2 and c) N phases of the sample in Figure 6.1. Taken at $10\times$ magnification between 90° crossed polars with 530 nm full-wave retardation plate. Streaks and droplets are visible in b) due to ordering at the surface of the glass. Characteristic chiral nematic fingerprint texture with approximately $38 \mu\text{m}$ pitch is visible in c). Scale bar = $250 \mu\text{m}$.

In cellulose nanocrystal suspensions, mixtures of blue dextran 2000 and dextran T-2000 induce triphase equilibria at number densities of around $4 \times 10^{-7} \text{ nm}^{-3}$ and $1 \times 10^{-6} \text{ nm}^{-3}$, respectively (Table 6.4). When mixtures of medium-molecular-weight dextrans (blue dextran 500₄₉ and dextran T-500) are used, three phases eventually form, but at such high dextran number densities that the samples are very viscous (equilibration times on the order of days to weeks), limiting the number of data points in the high-concentration regimes. When mixtures of low-molecular-weight dextrans (blue dextran 110₁₃₀ and dextran T-110) are used, no third phase is seen at similar number densities to those used for dextran 2000; before reaching concentrations favoring triphase equilibrium, the increasing viscosity and time required for macroscopic phase separation render the experiments impractical.

Table 6.4. Minimum number densities of blue and unmodified dextrans required to obtain triphase equilibria in 8.7 wt% cellulose suspension, for dextrans of equal molecular weight.

Blue dextran	Dextran	$C_{\text{blue Dx}} (\text{nm}^{-3}, 10^{-6})$	$C_{\text{Dx}} (\text{nm}^{-3}, 10^{-6})$	Phases
2000 ₁₆₁ ^a	T-2000	0.3–0.4	~1	I ₁ + I ₂ + N
500 ₄₉	T-500	~25	70–75	I ₁ + I ₂ + N
110 ₁₃₀	T-110	--	--	I ₂ + N ^b

^a Commercially available blue dextran 2000 (Pharmacia Fine Chemicals). ^b Dextran concentrations so high as to render the suspension too viscous for phase separation are reached prior to formation of triphase equilibrium in this system.

If the triphase equilibrium is caused by the interaction of bidisperse mixtures of spherical polymers of different diameter with the colloidal cellulose rods, then a

difference in polymer size would be expected to modify the phase behaviour. To test this premise, mixtures of blue dextrans and unmodified dextrans of different molecular weight were prepared (Table 6.5) and compared with the mixtures of blue dextran and unmodified dextrans of equal molecular weight in Table 6.4.

It can be seen in Tables 6.4 and 6.5 that the number densities of blue dextran 2000 and dextran T-500 required to obtain triphase equilibrium are similar to those needed when blue dextran 2000 and dextran T-2000 are mixed, whereas when blue dextran 500₄₉ and dextran T-2000 are used, around 30× as much blue dextran and around 15× as much plain dextran is required. In addition, triphase equilibrium is observed at much lower number densities (30× less blue dextran and 2× less unmodified dextran) when blue dextran 2000 is mixed with dextran T-500 than when blue dextran 500₄₉ is mixed with dextran T-2000. The molecular weight of the blue dextran species appears to be more important than that of unmodified dextran in determining the “onset” of three-phase coexistence.

Table 6.5. Minimum number densities of blue and unmodified dextrans required to obtain triphase equilibria in 8.7 wt% cellulose suspension, for dextrans of different molecular weight.

Blue dextran	Dextran	$C_{\text{blue Dx}} (\text{nm}^{-3}, 10^{-6})$	$C_{\text{Dx}} (\text{nm}^{-3}, 10^{-6})$	Phases
2000 ₁₆₁ ^a	T-500	0.2-0.4	4-6	I ₁ + I ₂ + N
500 ₄₉	T-2000	~ 10–15	~11–15	I ₁ + I ₂ + N
2000 ₁₆₁ ^a	T-110	1.6	200	I ₁ + I ₂ + N
110 ₁₃₀	T-2000	3.9	12	I ₂ + N

^a Commercially available blue dextran 2000 (Pharmacia Fine Chemicals).

Mixtures of blue dextran 2000 and dextran T-110 also give triphase equilibria at relatively high dextran volume fractions, but mixtures of blue dextran 110₁₃₀ and dextran T-2000 do not. These results suggest that the size of the blue dextran is a determining factor in inducing the triphase equilibrium. All the samples in Tables 6.4 and 6.5 have the same dye concentration; there are evidently complex interactions among the system components that lead to the triphasic equilibrium.

We prepared samples of similar ionic strength, *I*, and total number density of dextran as previous samples, but without using blue dextran. We also prepared a sample with the same total number density of dextran and the same dye concentration using only a blue dextran 2000 with a lower dye ligand density (Table 6.6). None of the samples formed three phases upon equilibration.

Table 6.6. Samples of 8.7 wt% cellulose suspension containing only unmodified dextran or only blue dextran, with dextran number density and ionic strength identical to those shown in Table 6.4.

Blue dextran	Dextran	$C_{Dx\ total} (nm^{-3}, 10^{-6})$	[dye] (mM)	<i>I</i> (M)	Phases
--	T-2000	5.7	--	0.0015 ^a	I + N
--	T-2000	6.2	--	0.0015 ^a	I + N
2000 ₃₀	--	6.2	0.37	0.0019	I + N

^a 10 μL of 0.45 M NaCl(aq) added to 3.00 mL of suspension.

It should be noted that dissolving blue dextran 2000 and dextran T-2000 in deionized water at concentrations similar to those used in the cellulose nanocrystal suspensions, as well as much higher concentrations, yielded only homogeneous isotropic solutions.

It can be concluded from these experiments that both polyelectrolytic blue dextran and neutral unmodified dextrans must be present for triphase equilibria to occur. The size of the blue dextran also appears to be a deciding factor.

6.3.2 Phase separation mechanism

The I_1 phase separation differs from the N- I_2 equilibration. To measure the phase separation kinetics, an 8.7 wt% cellulose nanocrystal suspension containing blue dextran and unmodified dextran is vortexed until homogeneity is achieved (t_0), and the initially uniform sample is allowed to equilibrate ($t > t_0$). As shown in Figure 6.3, the I_1 phase generally separates out within hours (macroscopic droplets move upwards), followed by the N and I_2 phases within two to four days, except at high dextran/blue dextran concentrations, when equilibration can take much longer (weeks to months) due to the high suspension viscosity.

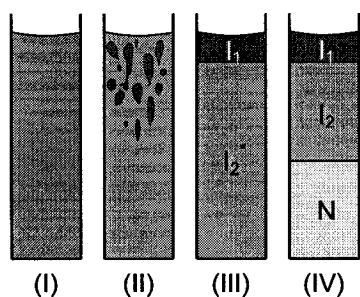


Figure 6.3. Schematic representation of the evolution of phase separation as typically observed in the three-phase coexistence region. (I) t_0 , initially uniform sample; (II) $t = 10\text{--}20$ min, droplets of I_1 phase moving upwards (bicontinuous structure of I_1 and I_2^* phases); (III) $t = 1\text{--}3$ hours, well-defined I_1 phase with metastable I_2^* phase; (IV) $t = 48\text{--}96$ hours, final $I_1\text{--}I_2\text{--}N$ coexistence.

Our observations are similar to those made by Poon et al. and Renth et al. for hard-sphere-like sterically stabilized polymethylmethacrylate (PMMA) particles and linear polystyrene (PS) in cis-decalin.⁴⁸⁻⁵⁰ The rapidity of the demixing of our I₁ phase suggests that the phase separation proceeds by a spinodal decomposition mechanism.⁴⁸

6.3.3 Cellulose nanocrystal fractionation

TM-AFM images of nanocrystals isolated by evaporation from the I₁, I₂ and N phases of a triphasic suspension are shown in Figure 6.4. Cellulose nanocrystal lengths L were measured for the I₂ and N phases. Nanocrystals in the I₁ phase could not be imaged because of the high polymer concentration coupled to the low nanocrystal concentration (see the Dextran partitioning section in the Discussion). Nanocrystals from the I₂ phase were less well-dispersed than those from the N phase (Figure 6.4), which contained the lowest polymer concentration and highest cellulose concentration. Length measurements were made on the isolated nanocrystals in the I₂ phase samples.

6.3.4 Dextran partitioning

Blue dextran is known to partition preferentially into the isotropic phase of an I–N biphasic cellulose suspension.²⁷ UV–visible spectroscopy was used to obtain partition coefficients for blue dextran in the three phases of one sample. Partition coefficients $K = c_i/c_a$ were calculated by dividing the absorbance due to blue dextran in the isotropic phases by the absorbance of blue dextran in the anisotropic phase (Table 6.7).⁵¹

Partition coefficients for the unmodified dextran cannot be measured directly by UV–visible spectroscopy due to the overlapping absorbance and scattering of the cellulose nanocrystals. In order to estimate the partition coefficient for undyed dextran, electrostatically neutral FITC-labelled dextran of molecular weight 2×10^6 Da was

substituted for the undyed dextran in a sample of cellulose nanocrystal suspension.¹⁸ The absorbance of the FITC-Dx 2000 was determined at $\lambda_{\text{max}} = 494 \text{ nm}$ by UV-visible spectroscopy (Table 6.8). FITC-Dx 2000 number densities were calculated assuming 10 wt% moisture and 0.009 moles of fluorescein isothiocyanate per mole anhydroglucose monomer.⁵² The structure of FITC-dextran is shown in Figure 5.3 in Chapter 5.

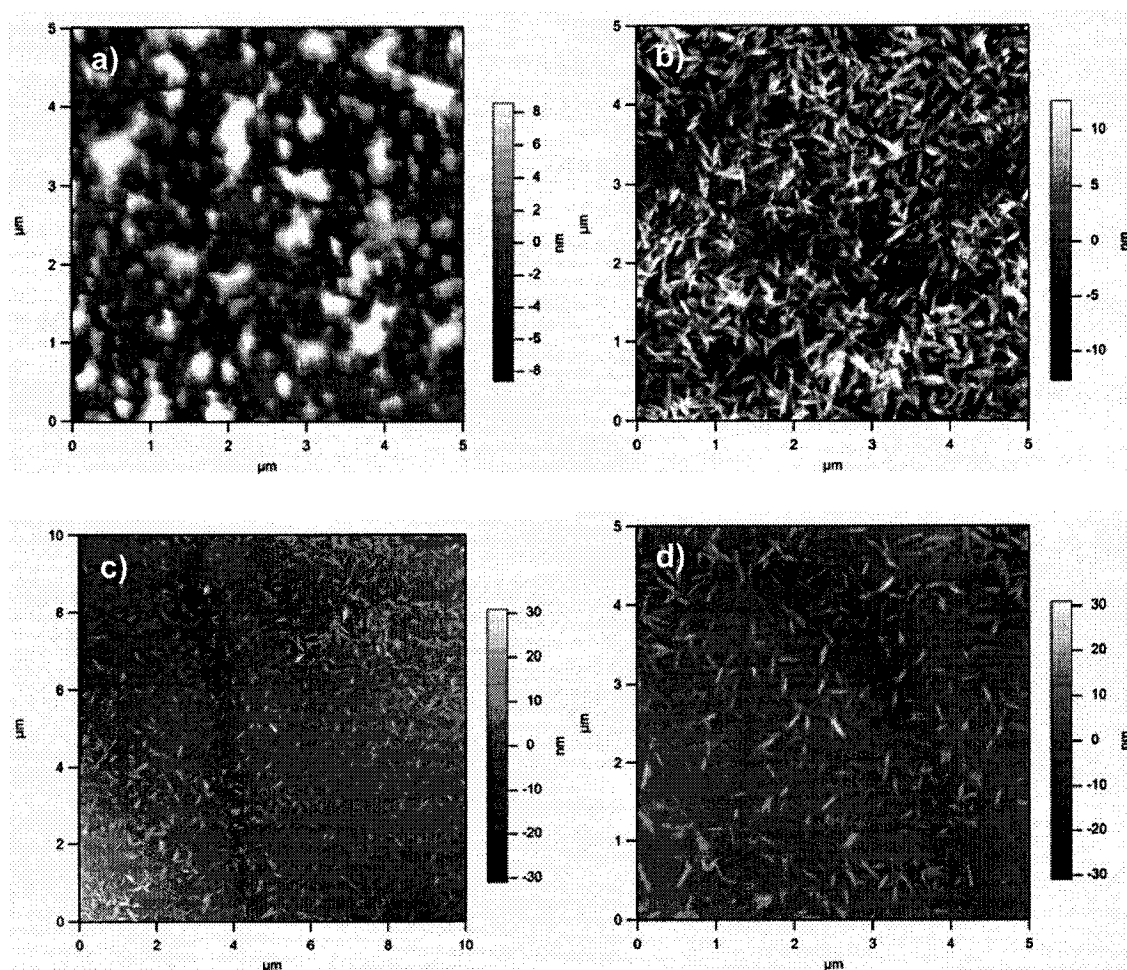


Figure 6.4. TM-AFM images (height mode) of dilute samples from a triphasic cellulose nanocrystal suspension containing blue dextran 2000 and dextran T-2000: a) I_1 phase showing polymer blobs on the mica; b) I_2 phase showing nanocrystals; c) and d) N phase showing well-dispersed nanocrystals.

Table 6.7. Partitioning of blue dextran in a triphasic 8.7 wt% cellulose nanocrystal suspension containing blue Dx 2000₁₆₁ ($C_{\text{blueDx } 2000} = 8.2 \times 10^{-7} \text{ nm}^{-3}$) and Dx T-2000 ($C_{\text{Dx T-2000}} = 1.1 \times 10^{-5} \text{ nm}^{-3}$).

Phase	ϕ_{phase}	Dilution factor	A_{609}^a	K_{blueDx}
I ₁	0.04	100	16.9	34.5
I ₂	0.69	24	2.02	4.1
N	0.27	20	0.49	-- ^b

^a Absorbances corrected for dilution. ^b Partition coefficients are relative to blue dextran 2000₁₆₁ concentration in the nematic N phase.

Cellulose concentrations in each phase were determined gravimetrically, subtracting the FITC-dextran and blue dextran concentrations found spectrophotometrically.

Table 6.8. Concentrations of FITC-dextran 2000 (total $C_{\text{FITC-Dx}} = 2.28 \times 10^{-6} \text{ nm}^{-3}$) and blue dextran 2000 (total $C_{\text{blue Dx}} = 2.72 \times 10^{-6} \text{ nm}^{-3}$) in the three phases of a triphasic cellulose nanocrystal suspension (8.7 wt% total cellulose concentration).

Phase	ϕ_{phase}	[FITC-Dx] (mg/mL)	[Blue Dx] (mg/mL)	[Cellulose] (wt %)	$C_{\text{cell}} (\text{nm}^{-3}, 10^{-6})$
I ₁	0.34	28	29	0.6	0.3
I ₂	0.15	2.2	2.5	8.4	4.8
N	0.51	1.2	1.1	14	8.3

6.4 DISCUSSION

6.4.1 Triphase equilibrium

Theoretical predictions and experimental evidence for dispersions of sterically stabilized boehmite rods and polystyrene in orthodichlorobenzene, a comparable system, suggest that the three phases in equilibrium are, from top to bottom, dilute isotropic (I_1), concentrated isotropic (I_2), and chiral nematic (N).^{5,9,20} The terms “dilute” and “concentrated” refer to the relative cellulose nanocrystal concentrations of the phases. A diagram of the dependence of the type of phase behaviour of rodlike colloid and flexible polymer mixtures on the size parameters of the components is shown in Figure 6.5. The theory is not limited to the second virial level and is therefore not restricted to very long rods and very low polymer concentrations.²⁰ When blue dextran 2000 and dextran T-2000 are used as the polymer, the parameters for our system are $L \approx 200$ nm, $D = 5\text{--}10$ nm, and $\sigma \approx R_g = 34$ nm. Thus, $L/D \approx 20\text{--}40$ and $\sigma/D \approx 6.8\text{--}13.6$. For blue dextran 500 and dextran T-500 ($R_g = 19.8$ nm), we obtain $\sigma/D \approx 4.0\text{--}8.0$. Our systems clearly lie in the $I_1\text{--}I_2\text{--}N$ region of the diagram. However, because the colloidal cellulose rods are electrostatically rather than sterically stabilized, their interactions will be complicated by repulsion between the charged species, so the diagram may not correspond quantitatively to our system. Additionally, the coil-to-polymer diameter ratio in our system is somewhat larger than those shown in Figure 6.5; this parameter also influences the phase behaviour. For example, the range of the depletion attraction is determined by the ratio of the radii of colloidal and polymer spheres.⁵

According to the literature, mixtures of relatively short rods and large polymers should produce $I_1\text{--}I_2\text{--}N$ phase behaviour,²⁰ but this does not explain why it appears only when a

combination of neutral undyed dextran and ionic blue dextran is added to cellulose nanocrystal suspensions. Similarly to mixtures of rods and coils, binary mixtures of rods (thin and thick or long and short) exhibit much richer phase behaviour than suspensions of monodisperse rods.^{9,53-55} Our system can be considered a ternary mixture of rods and two sizes of coils: because blue dextran is a polyelectrolyte, presumably it is more expanded in solution than the analogous plain dextran, owing to hydration and electrostatic repulsion⁵⁶ – as can be seen in Table 6.3, the hydrodynamic radii of blue dextrans are larger than those of unmodified dextrans of similar molecular weight.

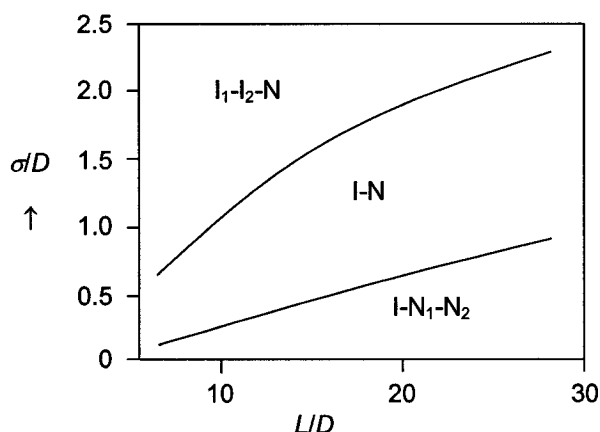


Figure 6.5. Type of phase behaviour shown by mixtures of rodlike colloids and flexible polymers as a function of the geometrical parameters L/D and σ/D .^{5,20} L is the rod length, D is the rod diameter and σ is the diameter of the polymer coil. “ I_1-I_2-N ” indicates a phase diagram with two isotropic phases and a nematic phase. Figure adapted from Lekkerkerker and Stroobants.²⁰

The triphase equilibrium may arise from the competition of demixing in the binary subsystems comprising the ternary cellulose-blue dextran-dextran system. Schmidt and Denton used density function theory to study the demixing behaviour of a model ternary system of hard colloidal spheres, ideal polymer spheres, and rigid vanishingly thin needles.⁵⁷ Neither the polymer spheres nor the needles interact with themselves; the colloidal spheres experience hard core repulsion. That is, the colloid-colloid potential energy $V_{CC} = 0$ if the interparticle distance exceeds $2R_C$; otherwise $V_{CC} = \infty$. The colloidal spheres interact with both the other components via excluded volume. When hard needle-polymer interactions are allowed, rich phase diagrams with three-phase coexistence and re-entrant demixing behaviour are predicted. The demixing behaviour is designated colloid-polymer (CP) and colloid-needle (CN). If the polymers are smaller than the colloids, e.g. $\sigma_P = \sigma_C/2$, a weaker depletion attraction is generated between the colloids at a given number density of polymers, and the needles are also long, $L = 2\sigma_C$, a stronger depletion is generated between the colloids, then the number density of needles required for demixing is reduced. Our system can be considered using the model of Schmidt and Denton if we take N as the cellulose nanocrystal “needles”, P as the blue dextran polymer and C as the plain dextran. Similarly to the conditions set by Schmidt and Denton, our cellulose needles have $L = 120\text{nm} > \sigma_C = 68\text{nm}$, and the polyelectrolytic blue dextran polymer has $\sigma_P > \sigma_C$ for plain dextran. The NP interaction of the cellulose “needles” with the blue dextran polymer due to repulsive electrostatic forces (instead of hard core interactions as modeled by Schmidt and Denton) is also likely to be stronger than the dextran-blue dextran CP interactions in this system. Schmidt and Denton also noted that,

“The ternary region ... grows solely out of the N-rich-poor coexistence, whereby CP coexistence is only a spectator, separated by mixed states.”⁵⁷

The theory Asakura and Oosawa devised to explain the depletion effect is a first-order approximation, as they assumed that no direct interaction existed between the colloidal particles and macromolecules (i.e., at low concentration).¹³ In reality, the depletion attraction is the short-range component of a more general effect caused by adding macromolecules to a suspension of colloidal particles.⁵⁸ When interactions between nonadsorbing macromolecules are taken into account, longer-range repulsions at higher depletant concentrations are observed.⁵⁸⁻⁶⁰ At lower depletant concentrations, flocculation or demixing is induced, whereas at higher concentrations, depletion stabilization prevents demixing.^{59,60} Higher-order concentration effects are particularly important for polyelectrolytes because of their larger effective volume fraction.⁶⁰

Experimentally and theoretically, the depletion interactions of polyelectrolyte species are not as well understood as those of neutral polymers.⁶¹ Any depletion attraction produced outside the depleted volume will be counteracted by repulsive double-layer interactions from within, leading to a complex net force that depends on the interstitial ionic structure.⁵⁸ Force balance studies of mixtures of like-charged colloids and flexible polymers (e.g., nanocrystals and blue dextran) have shown that the ion-averaged, screened coulombic repulsion between the particles magnifies the effective depletion interaction between them.^{22,58-60} Long-range electrostatic repulsion between particles is found to greatly increase the range and magnitude of the depletion interaction as compared to hard core interactions between neutral particles.^{12,13}

The effect of attractive depletion forces on the phase behaviour of rodlike particles

depends on the axial ratio L/D and polydispersity of the rods.^{20,21} Polydispersity always increases the range of the depletion interaction; at constant number density of neutral particles, increasing polydispersity increases the magnitude of depletion attraction, while the opposite effect is seen at constant volume fraction.²² For charged particles, the situation is reversed, with increasing polydispersity slightly decreasing the magnitude of the interaction at constant number density. The cellulose nanocrystals in our suspensions are quite polydisperse (see Figure 6.6), which may further increase the complexity of the interactions and phase behaviour.

6.4.1.1 Blue-to-plain dextran ratio required to obtain I_1 phase from I_2 -N equilibrium

Consistently, smaller amounts of blue dextran than undyed dextran are required to produce the formation of the I_1 phase (Tables 6.4 and 6.5), in agreement with the findings by Asakura and Oosawa for charged macromolecules.¹³ For the most part, the I_1 - I_2 -N and I_2 -N equilibria exist at blue-to-plain dextran number density ratios smaller than 1, while I_1 -N equilibrium exists at ratios greater than 1.

Similar ratios of blue to plain dextran are necessary to obtain formation of the I_1 phase for homogeneous mixtures of dextrans of molecular weights 2000 and 500 kDa (Table 6.4), suggesting that the ratio is independent of dextran molecular weight or size. The high viscosity of the 110-kDa-dextran samples prevents calculation of the ratio required for low-molecular-weight dextran.

6.4.1.2 Effect of dextran molecular weight on phase equilibrium

The data in Table 6.4 show that unmodified and blue dextrans of molecular weight 500 kDa are large enough ($R_H \approx 20$ nm) to induce formation of the I_1 phase. The range of depletion forces depends on the macromolecule size,¹³ so it is not surprising that,

compared to dextrans 2000 ($R_H \approx 40$ nm), higher concentrations of dextrans 500 are necessary to obtain the triphase equilibrium of a given suspension. In Figure 6.6, the σ/D ratio for dextrans 500 lies closer to the boundary separating phase diagrams with two isotropic phases from those with only one. Dextrans of molecular weight 110 kDa are apparently too small ($R_H \approx 10$ nm for unmodified dextran T-110) for the depletion forces to overcome the electrostatic forces at these dextran concentrations. Phase separation was very slow: the much higher ratios of blue dextran 110 to dextran T-110 that would be required to give triphase equilibrium would make the sample too viscous for phase separation.

The nature of the effect of dextran molecular weight on the phase equilibrium is not clear. It seems evident that if the triphase equilibrium were caused by the interaction with the colloidal cellulose rods of bidisperse mixtures of spherical polymers of different diameter, then an increase in the difference in polymer size would have a noticeable effect on the induction of triphase equilibria. However, this did not happen (see Tables 6.4 and 6.5), suggesting that the dextran molecular weight does not, in itself, play a deciding role in governing the phase equilibrium. However, differences in molecule *shape* as dictated by molecular weight, may play a role. It is known, for example, that as their molecular weight increases, dextran molecules become more symmetrical.^{33,62,63} The shape of the depletant greatly affects the interparticle potential energy; prolates with an axis ratio of 5 increase the depth of the secondary energy well, as compared to spheres (axis ratio = 1) at constant volume fraction. At constant number density, however, depletant shape does not have as strong an effect on the dispersion stability.⁶⁰ The lower symmetry of the smaller dextrans may therefore contribute to the complexity of

interparticle interactions.

6.4.2 Cellulose nanocrystal fractionation

The partitioning of longer particles into the anisotropic phase upon phase separation of a polydisperse suspension of rodlike colloids was first predicted by Onsager² and has been used to fractionate (i.e., obtain more monodisperse fractions) a variety of rodlike colloidal particles.^{29,31,53,64} Depletion attraction has been found to enhance size fractionation between coexisting phases of platelike colloids.¹⁹ Figure 6.6 shows that some partitioning of the longer nanocrystals into the N phase has occurred, the average length of the nanocrystals being significantly greater than that of those in the I₂ phase. No data was obtained regarding the length of the nanocrystals in the I₁ phase; it is assumed that they are shorter, as cotton cellulose nanocrystals produced under the hydrolysis conditions employed here average around 200 ± 30 nm in length,³¹ which is shorter than the overall average value found to be 222 ± 68 nm for all the nanocrystals measured in the I₂ and N phases. Cellulose nanocrystal concentrations differ among the phases in the triphase equilibrium, and are discussed in the next section.

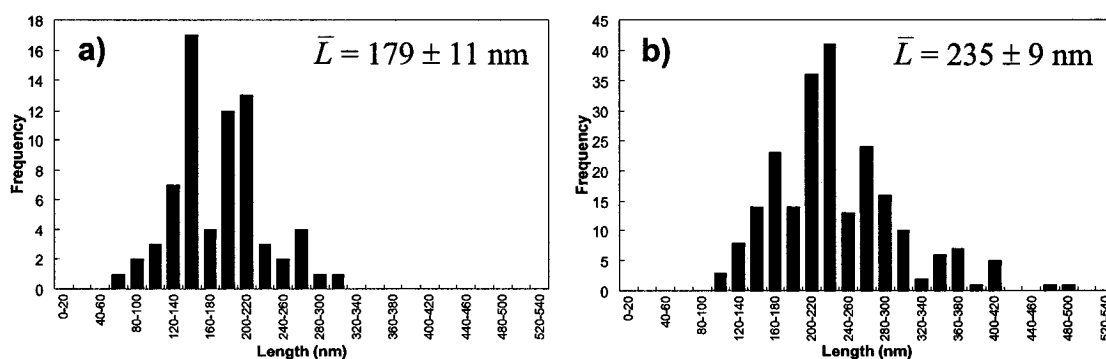


Figure 6.6. Distribution of particle length L of cellulose nanocrystals for the a) I₂ and b) N phases of a triphasic cellulose nanocrystal suspension containing blue dextran 2000 and dextran T-2000.

6.4.3 Dextran partitioning

Random coil polymers and spherical colloids tend to be excluded from an anisotropic phase made up of rodlike particles, in order to preserve its orientationally ordered structure. This phenomenon has been found to occur for numerous experimental systems, including *p*-benzamide and X-500,⁶⁵ TMV and PEO/BSA,⁶⁶ bacteriophage fd virus and polystyrene,¹⁶ and κ -carrageenan and dextran.⁶⁷ Blue dextran has been found to partition preferentially into the isotropic phases of the triphasic samples.²⁷ For a sample in the blue dextran 2000/dextran T-2000 system, the partition coefficients for partitioning of blue dextran between the N-I₁-and N-I₂ phases are $K_{N_I_1} = 34.5$ and $K_{N_I_2} = 4.1$, respectively (Table 6.9). Partitioning between the two isotropic phases is stronger even than partitioning between the N and I₂ phases ($K_{I_2I_1} \approx 8.5$), indicating a marked preference of the blue dextran for the dilute isotropic phase. Blue dextran 2000 partitioning from the N phase into the I₁ phase is much stronger than partitioning into the isotropic phase of biphasic I-N cellulose nanocrystal suspensions,²⁷ for which the partition coefficient ranges from 1.5 to 7.6. These values are comparable to the N-I₂ partition coefficients observed in this study.

Theoretical partition coefficients for blue dextran in cellulose suspensions have been calculated using equation 6.1³⁸

$$K = \exp(B_{rc}(C_a - C_i)) \quad (6.1)$$

where B_{rc} is the second virial coefficient of the rod-coil interactions (the order of magnitude of which is given by $B_{rc} \sim LD^{1/3}R_g^{5/3}$) and C_a and C_i are the number densities of the cellulose rods in the nematic and isotropic phases, respectively. Sear's theory³⁸ is

applicable to our system because the radius of gyration of the dextran is much greater than the diameter of the cellulose nanocrystals. Theoretical and experimental partition coefficient values for the FITC-dextran and blue dextran 2000 in a triphasic cellulose nanocrystal suspension are presented in Table 6.9.

Table 6.9. Theoretical and experimental values of the partition coefficients for FITC-dextran 2000 (total $C = 2.28 \times 10^{-6} \text{ nm}^{-3}$) and blue dextran 2000 (total $C = 2.72 \times 10^{-6} \text{ nm}^{-3}$) in triphasic 8.7 wt% cellulose nanocrystal suspension.

Phases	K_{theory}^a	$K_{\text{exp}} \text{ FITC-Dx}$	$K_{\text{exp}} \text{ blue Dx}$
I ₁ -N	2.1	24	28
I ₂ -N	1.4	1.9	2.3
I ₁ -I ₂	1.5	13	12

^a Parameters used to calculate K_{theory} : $R_g = 34 \text{ nm}$; $L = 200 \text{ nm}$; $D = 10 \text{ nm}$; $C_{\text{cell}}^N = 5.0 \times 10^{-6} \text{ nm}^{-3}$; $C_{\text{cell}}^{I_2} = 3.0 \times 10^{-6} \text{ nm}^{-3}$; and $C_{\text{cell}}^{I_1} = 0.2 \times 10^{-6} \text{ nm}^{-3}$.

Although the experimental partition coefficients are in general much larger than predicted by the theory, they follow the same trend, in that N-I₁ partition coefficient is largest, followed by I₂-I₁ and finally the N-I₂ partition coefficient. Sear's theory has previously been found to underestimate the partition coefficients, the discrepancy being due to the fact that the theory gives an order of magnitude only.²⁷

How are the three components (cellulose nanocrystals, dextran, and blue dextran) distributed among the three phases of a triphasic sample? According to Schmidt and Denton, when all the binary subsystems of a needle-colloid-polymer ternary mixture are

demixed, "...it is evident that the system will ultimately display coexistence between three phases, each one enriched by one of the components...".⁵⁷ Spectroscopic measurements tell us that the I₁ phase is (greatly) enriched in blue dextran compared to the other two phases. The nematic phase contains the highest cellulose concentration (14.3 wt%), the lowest cellulose concentration (0.6 wt%) being found in the least dense I₁ phase. Although the values found are reasonable, they are only accurate to about ± 2 wt%. The difference in the I₂ and N cellulose concentrations is larger than the difference observed in biphasic suspensions, which is explained by the presence of the second isotropic phase. Cellulose concentrations in the different phases also depend on the concentration of added macromolecule, as predicted by Flory¹¹ and observed for the blue dextran 2000-cellulose system.²⁷ The cellulose concentration of the I₂ phase (8.4 wt%), however, is only slightly lower than the total cellulose concentration of 8.7 wt%, similarly to the I phase in previous work on biphasic suspensions, which was about 0.3 to 1.3 wt% lower than the total concentration.²⁷ According to the theory of Schmidt and Denton,⁵⁷ the middle I₂ phase should be enriched in undyed dextran. However, FITC-dextran 2000 was found to be most abundant in the I₁ phase.

The exclusion of blue dextran 2000 from the nematic phase is not complete (non-zero absorbance at $\lambda_{\text{max CB}} = 609$ nm is observed for the nematic phase; see Tables 6.8 and 6.9). Some blue dextran coils are therefore able to be incorporated into the ordered structure of the liquid crystalline nematic phase. This behaviour has been seen by Adams et al. for the lamellar phase of bacteriophage fd virus and polystyrene,¹⁶ as well as by Edgar and Gray for blue dextran 2000 and cellulose nanocrystals,²⁷ where the lower

nematic phase showed distorted fingerprint textures and many disclinations relative to a dextran-free nematic phase.

6.5 CONCLUSIONS

Within certain concentration ranges, aqueous mixtures of blue dextrans, undyed dextrans and cellulose nanocrystals produce three-phase coexistence of a dilute isotropic (I_1), a concentrated isotropic (I_2) and a chiral nematic (N) phase. To the best of our knowledge, this represents the first triphasic equilibrium of cellulose nanocrystal suspensions to exhibit two isotropic phases. The separation of the I_1 phase appears to follow a spinodal decomposition mechanism. The molecular weight of the macromolecules, in particular that of the blue dextrans, has a significant effect on the macromolecule concentrations needed to produce the I_1 - I_2 -N phase behaviour. Partitioning of longer cellulose nanocrystals into the N phase relative to the I_2 phase is observed, in agreement with theoretical predictions. Blue dextran and FITC-dextran partition very strongly into the I_1 phase compared to the I_2 and N phases. While the interactions governing the equilibria are not clear, phase formation could result from the complex interplay of electrostatic and entropic forces.

6.6 REFERENCES

- (1) Zocher, H. *Z. Anorg. Allg. Chem.* **1925**, *147*, 91-110.
- (2) Onsager, L. *Ann. N.Y. Acad. Sci.* **1949**, *51*, 627-659.
- (3) Bawden, F.C.; Pirie, N.W. *Proc. R. Soc. London, Ser. B* **1937**, *123*, 274-320.
- (4) Folda, T.; Hoffmann, H.; Chanzy, H.; Smith, P. *Nature* **1988**, *333*, 55-56.
- (5) Buitenhuis, J.; Donselaar, L.N.; Buining, P.A.; Stroobants, A.; Lekkerkerker, H.N.W. *J. Colloid Interface Sci.* **1995**, *175*, 46-56.
- (6) Dogic, Z.; Fraden, S. *Langmuir* **2000**, *16*, 7820-7824.
- (7) de Sousa Lima, M.M.; Borsali, R. *Macromol. Rapid. Comm.* **2004**, *25*, 771-787.
- (8) Samir, M.; Alloin, F.; Dufresne, A. *Biomacromolecules* **2005**, *6*, 612-626.
- (9) Buining, P.A.; Lekkerkerker, H.N.W. *J. Phys. Chem.* **1993**, *97*, 11510-11516.
- (10) Kimura, F.; Kimura, T.; Tamura, M.; Hirai, A.; Ikuno, M.; Horii, F. *Langmuir* **2005**, *21*, 2034-2037.
- (11) Flory, P.J. *Macromolecules* **1978**, *11*, 1138-1141.
- (12) Asakura, S.; Oosawa, F. *J. Chem. Phys.* **1954**, *22*, 1255-1256.
- (13) Asakura, S.; Oosawa, F. *J. Polym. Sci.* **1958**, *33*, 183-192.
- (14) Vrij, A. *Pure Appl. Chem.* **1976**, *48*, 471-483.
- (15) Snowden, M.J.; Williams, P.A.; Garvey, M.J.; Robb, I.D. *J. Colloid Interface Sci.* **1994**, *166*, 160-167.
- (16) Adams, M.; Dogic, Z.; Keller, S.L.; Fraden, S. *Nature* **1998**, *393*, 349-352.
- (17) van Bruggen, M.P.B.; Lekkerkerker, H.N.W. *Macromolecules* **2000**, *33*, 5532-5535.

- (18) Dogic, Z.; Purdy, K.R.; Grelet, E.; Adams, M.; Fraden, S. *Phys. Rev. E* **2004**, *69*, 051702-1 - 051702-9.
- (19) van der Kooij, F.M.; Vogel, M.; Lekkerkerker, H.N.W. *Phys. Rev. E* **2000**, *62*, 5397-5402.
- (20) Lekkerkerker, H.N.W.; Stroobants, A. *Il Nuovo Cimento* **1994**, *16D*, 949-962.
- (21) Bolhuis, P.G.; Stroobants, A.; Frenkel, D.; Lekkerkerker, H.N.W. *J. Chem. Phys.* **1997**, *107*, 1551-1564.
- (22) Piech, M.; Walz, J.Y. *J. Colloid Interface Sci.* **2000**, *225*, 134-146.
- (23) Revol, J.-F.; Bradford, H.; Giasson, J.; Marchessault, R.H.; Gray, D.G. *Int. J. Biol. Macromol.* **1992**, *14*, 170-172.
- (24) Revol, J.F.; Godbout, L.; Dong, X.M.; Gray, D.G.; Chanzy, H.; Maret, G. *Liq. Cryst.* **1994**, *16*, 127-134.
- (25) Dong, X.M. *Chiral Nematic Ordered Suspensions of Cellulose Microcrystallites*. Ph.D. thesis, McGill University: Montreal, 1997.
- (26) Heux, L.; Chauve, G.; Bonini, C. *Langmuir* **2000**, *16*, 8210-8212.
- (27) Edgar, C.D.; Gray, D.G. *Macromolecules* **2002**, *35*, 7400-7406.
- (28) Grunert, M.; Winter, W.T. *J. Polym. Environ.* **2002**, *10*, 27-30.
- (29) Dong, X.M.; Kimura, T.; Revol, J.-F.; Gray, D.G. *Langmuir* **1996**, *12*, 2076-2082.
- (30) Dong, X.M.; Gray, D.G. *Langmuir* **1997**, *13*, 2404-2409.
- (31) Dong, X.M.; Revol, J.-F.; Gray, D.G. *Cellulose* **1998**, *5*, 19-32.
- (32) Araki, J.; Wada, M.; Kuga, S.; Okano, T. *Langmuir* **2000**, *16*, 2413-2415.

- (33) Senti, F.R.; Hellman, N.N.; Ludwig, N.H.; Babcock, G.E.; Tobin, R.; Glass, C.A.; Lamberts, B.L. *J. Polym. Sci.* **1955**, *27*, 527-546.
- (34) Ioan, C.E.; Aberle, T.; Burchard, W. *Macromolecules* **2000**, *33*, 5730-5739.
- (35) Böhme, H.-J.; Kopperschläger, G.; Schulz, J.; Hofmann, E. *J. Chromatogr.* **1972**, *69*, 209-214.
- (36) Beck-Candanedo, S.; Viet, D.; Gray, D.G. *Langmuir* **2006**, *22*, 8690-8695;
Chapter 4 of this thesis.
- (37) Beck-Candanedo, S.; Viet, D.; Gray, D.G. *Cellulose* **2006**, *13*, 629-635.
- (38) Sear, R.P. *J. Phys. II* **1997**, *7*, 877-886.
- (39) Lekkerkerker, H.N.W.; Poon, W.C.-K.; Pusey, P.N.; Stroobants, A.; Warren, P.B. *Europhys. Lett.* **1992**, *20*, 559-563.
- (40) Beck-Candanedo, S.; Viet, D.; Gray, D.G. *Macromolecules* **2007** *40*, 3429-3436;
and Chapter 7 of this thesis.
- (41) de Gennes, P.G.; Proust, J. *The Physics of Liquid Crystals*; 2nd ed.; Oxford University Press: Oxford, 1993, p. 110.
- (42) Sigma-Aldrich, Blue Dextran Molecular Weight 2,000,000 Product No. D5751. Product Information, 1997.
- (43) Fishman, M.L.; Damert, W.C.; Phillips, J.G.; Barford, R.A. *Carbohydr. Res.* **1987**, *160*, 215-225.
- (44) Nordmeier, E.; Xing, H.; Lechner, M.-D. *Makromol. Chem.* **1993**, *194*, 2923-2937.
- (45) Ioan, C.E.; Aberle, T.; Burchard, W. *Macromolecules* **2001**, *34*, 326-336.

- (46) Mayes, A.G.; Moore, J.D.; Eissenthal, R.; Hubble, J. *Biotechnol. Bioeng.* **1990**, *36*, 1090-1096.
- (47) Tang, M.; Zhang, R.; Bowyer, A.; Eissenthal, R.; Hubble, J. *Biotechnol. Bioeng.* **2004**, *87*, 791-796.
- (48) Poon, W.C.K.; Renth, F.; Evans, R.M.L.; Fairhurst, D.J.; Cates, M.E.; Pusey, P.N. *Phys. Rev. Lett.* **1999**, *83*, 1239-1242.
- (49) Poon, W.C.K.; Renth, F.; Evans, R.M.L. *J. Phys.: Condens. Matter* **2000**, *12*, A269-A274.
- (50) Renth, F.; Poon, W.C.K.; Evans, R.M.L. *Phys. Rev. E* **2001**, *64*, 031402-1 - 031402-9.
- (51) Hamad, E.Z.; Ijaz, W.; Ali, S.A.; Hastaoglu, M.A. *Biotechnol. Prog.* **1996**, *12*, 173-177.
- (52) Sigma-Aldrich, Fluorescein Isothiocyanate Dextran Product No. FD-2000S. Product Information, 1997.
- (53) Itou, T.; Teramoto, A. *Macromolecules* **1984**, *17*, 1419-1420.
- (54) Stroobants, A. *Journal of Physics Condensed Matter* **1994**, *6*, A285-A288.
- (55) Purdy, K.; Varga, S.; Galindo, A.; Jackson, G.; Fraden, S. *Phys. Rev. Lett.* **2005**, *94*, 057801-1 - 057801-4.
- (56) Budd, P.M. in *Polymer Characterization*; Booth, C.; Price, C., eds.; Pergamon Press: Oxford, 1989; Vol. 1, pp. 215-230.
- (57) Schmidt, M.; Denton, A.R. *Phys. Rev. E* **2002**, *65*, 021508-1 - 021508-8.
- (58) Sharma, A.; Walz, J.Y. *J. Chem. Soc. Faraday Trans.* **1996**, *92*, 4997-5004.
- (59) Walz, J.Y.; Sharma, A. *J. Colloid Interface Sci.* **1994**, *168*, 485-496.

- (60) Piech, M.; Walz, J.Y. *J. Colloid Interface Sci.* **2000**, *232*, 86-101.
- (61) Milling, A.J.; Kendall, K. *Langmuir* **2000**, *16*, 5106-5115.
- (62) Ogston, A.G. *Trans. Faraday Soc.* **1953**, *49*, 1481-1489.
- (63) Granath, K.A. *J. Colloid Sci.* **1958**, *13*, 308-328.
- (64) Sato, T.; Kakihara, T.; Teramoto, A. *Polymer* **1990**, *31*, 824-828.
- (65) Bianchi, E.; Ciferri, A.; Tealdi, A. *Macromolecules* **1982**, *15*, 1268-1272.
- (66) Adams, M.; Fraden, S. *Biophys. J.* **1998**, *74*, 669-677.
- (67) Ramzi, M.; Borgström, J.; Piculell, L. *Macromolecules* **1999**, *32*, 2250-2255.

Chapter 7

Triphase Equilibria in Cellulose Nanocrystal Suspensions Containing Neutral and Charged Macromolecules.

Phase Diagrams

Reproduced with permission from
Beck-Candanedo, S.; Viet, D.; Gray, D.G. *Macromolecules* **2007**, *40*, 3429-3436.
Copyright 2007 American Chemical Society.

7.1 INTRODUCTION

Within a narrow concentration range, suspensions of rodlike cellulose nanocrystals obtained by acid hydrolysis undergo entropically-driven phase separation based on the excluded volume effect¹⁻³ as predicted by Onsager for anisotropic colloidal particles.⁴ Such systems can display rich phase behaviour; triphase isotropic–nematic–nematic (I–N–N) equilibria have been observed in suspensions of colloidal boehmite particles^{5,6} as well as in suspensions of tunicate cellulose whiskers.⁷ It has been found that added particles or macromolecules of different shapes can further enrich the phase separation behaviour of such suspensions of rodlike colloidal particles, leading to the formation of multiple phases.⁸⁻¹¹ An isotropic–isotropic–nematic (I–I–N) phase equilibrium has been observed upon the addition of a combination of blue dextran and unmodified dextran of high molecular weight to cotton cellulose nanocrystal suspensions (Figure 7.1).¹² Blue dextran partitions strongly into the upper isotropic (I_1) phase, which is very dilute in cellulose nanocrystals; the lower nematic phase is enriched in cellulose but contains far less dextran. The middle isotropic (I_2) phase contains intermediate concentrations of both cellulose and polymer. To our knowledge, no I–I–N equilibrium has been previously reported in cellulose nanocrystal suspensions.

The present chapter examines the phase behaviour for various dextran/blue dextran/cellulose nanocrystal systems and investigates the effect of variables such as dextran molecular weight and degree of dye substitution, and cellulose concentration on the appearance of the associated phase diagrams. The previous chapter describes the formation of the triphase equilibrium as well as the partitioning of the dextrans among the phases.

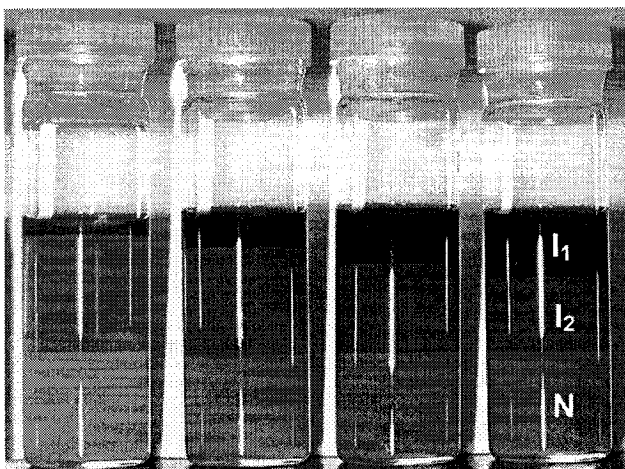


Figure 7.1. Vials of triphasic I_1 – I_2 – N cellulose nanocrystal suspension (8.7 wt%) containing blue dextran 2000 (from left to right, 0.45 to $2.50 \times 10^{-6} \text{ nm}^{-3}$) and dextran T-2000 ($5.3 \times 10^{-6} \text{ nm}^{-3}$). The preferential partitioning of blue dextran into the I_1 phase is evident. The volume fraction of the I_1 phase increases from left to right as more blue dextran 2000 is added.

7.2 EXPERIMENTAL METHODS

Dextrans T-110, T-500, T-2000 and blue dextran 2000 were purchased from Pharmacia Fine Chemicals. Cibacron Blue 3G-A (55 % dye content) was purchased from Sigma-Aldrich. Whatman ashless cotton cellulose powder was purchased from Cole-Parmer. Sulfuric acid (95–98 %) for hydrolysis was purchased from Fisher Scientific. All water used was purified using a Millipore Milli-Q purification system. Further samples of blue dextrans and cellulose nanocrystal suspensions were prepared and characterized, and their phase compositions were measured, as described previously.¹²

7.3 RESULTS AND DISCUSSION

7.3.1 Phase diagram

When a combination of high molecular weight dextran and blue dextran is added to a biphasic I–N cellulose suspension, a three-phase I₁–I₂–N coexistence develops.¹² Figure 7.2 presents a detailed diagram of the phase behaviour of cellulose nanocrystal suspensions containing blue dextran 2000 and dextran T-2000. All measurements were taken after several weeks to allow sufficient time for equilibration of the more viscous samples. The phase diagram is restricted to number densities below $4 \times 10^{-5} \text{ nm}^{-3}$ dextran and $1.2 \times 10^{-5} \text{ nm}^{-3}$ blue dextran; above these limits, the viscosity of the samples renders the phase separation kinetics impractical. Around 200 samples were prepared for the phase diagram in Figure 7.2.

For the ranges of dextran concentration used, the majority of the samples are triphasic. At low blue dextran concentrations, the suspensions remain I₂–N biphasic, while at higher blue dextran concentrations and low dextran concentrations, the suspensions become I₁–N biphasic. The boundary between the I₂–N and I₁–N coexistences (line indicated by * in Figure 7.2) is somewhat arbitrary, as no distinct transition was seen when adding blue dextran 2000 at low dextran T-2000 concentration. The designations I₂–N and I₁–N were assigned according to the relative volume fractions of the three phases upon reaching triphase equilibrium. For example, in Figure 7.4, the I₂ phase dominates the triphasic sample, so the initial and final biphasic samples are designated I₂–N; in contrast, the I₁ phase dominates the initial triphasic sample Figure 7.6. Using this nomenclature, there will be a continuous change from I₂–N to I₁–N coexistence, rather than a sharp boundary.

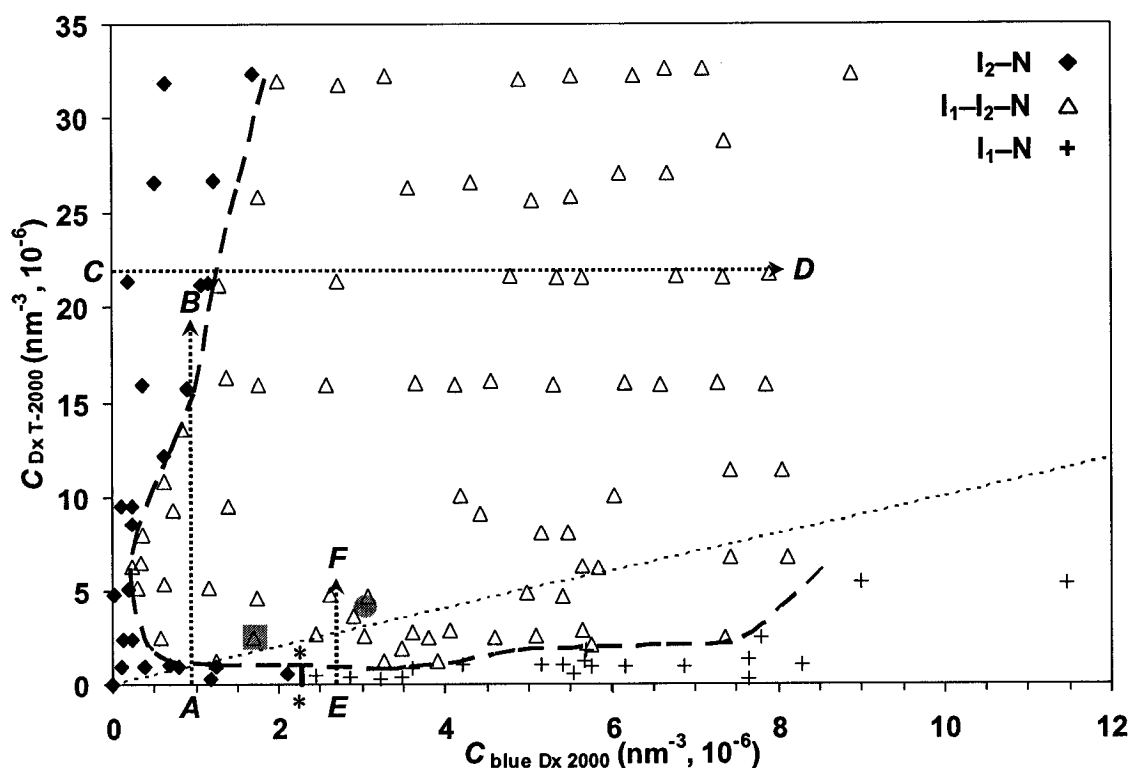


Figure 7.2. Phase diagram for 8.7 wt% cellulose nanocrystal suspension containing blue dextran 2000 and dextran T-2000. Dotted line indicates equal number densities of dextran and blue dextran. The boundaries between the regions of the phase diagram are intended as a guide to the eye. Some data points have been omitted for clarity. Compositions of phases along the arrows are shown in Figures 7.4 to 7.6 below. Shaded areas correspond to mixtures of blue dextrans of different DS; see text.

As described in Chapter 6, smaller amounts of polyelectrolytic blue dextran are necessary for the formation of the I_1 phase compared to undyed dextran.¹² The dotted line in Figure 7.2 indicates equal number densities of blue and unmodified dextran 2000; the I_1 - I_2 -N and I_2 -N equilibria mostly lie above the dotted line, while I_1 -N equilibrium lies below the line.

7.3.2 Re-entrant phase behaviour

An interesting feature of the phase diagram in Figure 7.2 is the re-entrant $I_2-N \rightarrow I_1-I_2-N \rightarrow I_2-N$ phase behaviour observed with increasing plain dextran concentration at low blue dextran concentration. The re-entrant portion of the phase diagram is shown at higher resolution in Figure 7.3. As dextran T-2000 is added to a suspension containing a given concentration of blue dextran 2000, the I_1 phase appears, increases in volume fraction, then decreases in volume fraction and disappears (Figure 7.4). At the same time, the N phase decreases in volume fraction.

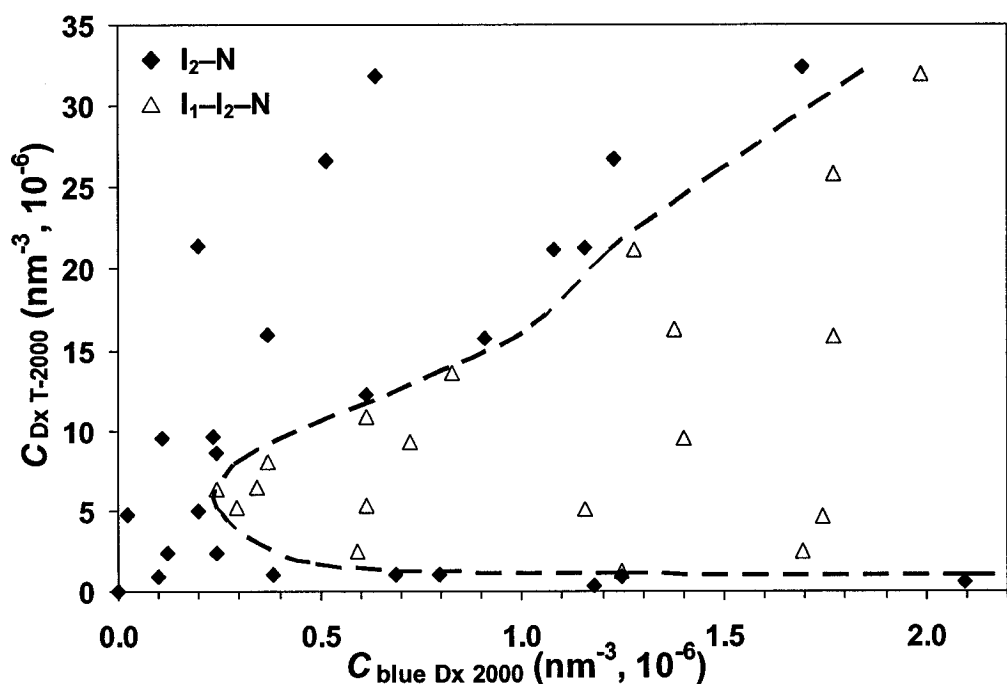


Figure 7.3. Area of phase diagram showing re-entrant $I_2-N \rightarrow I_1-I_2-N \rightarrow I_2-N$ phase behaviour for 8.7 wt% cellulose nanocrystal suspension containing blue dextran 2000 and dextran T-2000. The boundaries between the regions of the phase diagram are intended as a guide to the eye.

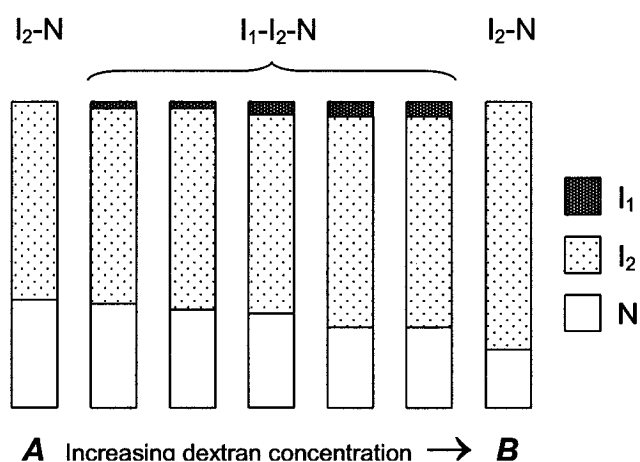


Figure 7.4. Example of re-entrant $I_2-N \rightarrow I_1-I_2-N \rightarrow I_2-N$ phase behaviour for 8.7 wt% cellulose nanocrystal suspension containing $8.2 \times 10^{-7} \text{ nm}^{-3}$ blue dextran 2000 and dextran T-2000 increasing from 0 to $2.0 \times 10^{-5} \text{ nm}^{-3}$ (concentrations correspond to arrow AB in Figure 7.2). As more dextran T-2000 is added, the N phase volume fraction decreases and the I_2 phase volume fraction increases; the I_1 phase increases and then decreases in volume fraction before disappearing.

Re-entrant phase behaviour has been observed in both thermotropic and lyotropic molecular liquid crystal systems.¹³ However, it is not well understood, particularly for lyotropic liquid crystalline systems. The only lyotropic liquid crystalline system in which the phenomenon is observed is the potassium laurate/decanol/water system,¹⁴ for which re-entrant isotropic-discotic nematic phase transition was first documented by Yu and Saupe in 1980.¹⁵

It should be noted that the “re-entrant” I_2-N biphasic suspension has a smaller volume fraction of N phase than the initial biphasic sample. This may be due to depletion attractions caused by the dextran; the ionic strength due to the sulfonate groups on the dye ligands and their sodium counterions is around $1.4 \text{ } \mu\text{M}$, comparable to values at

which blue dextran has been observed to induce greater phase separation than that produced in equal ionic strength suspension containing only free CB dye.¹⁶ A similar phenomenon was also reported by Dogic and Fraden for suspensions of fd virus containing dextran of molecular weight 500 kDa.¹⁷

7.3.3 Effect of increasing blue dextran concentration

Adding blue dextran 2000 to a biphasic I_2 -N cellulose nanocrystal suspension containing dextran T-2000 affects the phase coexistences as follows (Figure 7.5):

- a) Initially, the I_2 phase volume fraction increases while the N phase volume fraction decreases. Eventually the I_1 phase forms.
- b) The I_2 phase volume fraction continues to decrease, eventually disappearing, while the I_1 phase increases in volume fraction. The N phase also increases in volume fraction.
- c) Finally, the I_1 phase volume fraction continues to increase while the N phase again decreases in volume fraction (not shown in Figure 7.5).

The phase coexistences corresponding to a), b) and c) are I_2 -N, I_1 - I_2 -N and I_1 -N, respectively.

Adding blue dextran to a biphasic I_2 -N cellulose suspension containing a fixed quantity of undyed dextran results in the development of the triphase I_1 - I_2 -N equilibrium, followed by the I_1 -N equilibrium. The blue dextran concentration is fairly low at the first formation of triphase equilibrium, as shown in Figure 7.2, arrow CD. The initial increase in I_2 phase volume fraction with a corresponding decrease in N phase volume fraction probably results from a combination of (1) the higher ionic strength due to the charged dye ligands on the blue dextran and the resulting increase in critical cellulose

concentration required for phase separation, and (2) destabilizing attractive depletion forces, both of which would tend to favor the formation of I_2 phase.

Once the I_1 phase appears, the decrease in volume fraction of the I_2 phase with increasing blue dextran concentration indicates that the I_1 phase is more favorable than the I_2 phase. Increasing blue dextran appears to favor demixing to give the I_1 phase: The stability of the N - I_1 equilibrium is enhanced relative to that of the N - I_2 equilibrium as the blue dextran concentration increases.

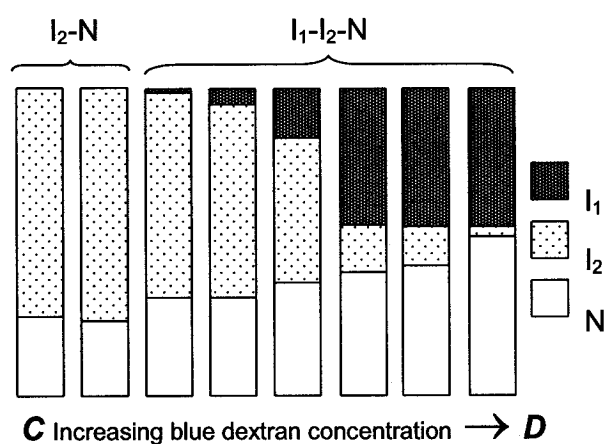


Figure 7.5. Example of phase behaviour for 8.7 wt% cellulose nanocrystal suspension with dextran T-2000 number density = $2.2 \times 10^{-5} \text{ nm}^{-3}$ and increasing blue dextran 2000 number density (concentrations correspond to arrow CD in Figure 7.2).

The observed decrease in N phase volume fraction as the blue dextran number density continues to increase is most likely due to the increasing ionic strength due to the dye ligands. Depletion attraction is also a possibility, as *oscillatory* interactions which depend on the interparticle distance between the depletants (and hence on their concentration),

have been seen¹⁸ but we cannot verify the occurrence of this phenomenon in our samples, as the sample viscosity becomes prohibitive at such high blue dextran concentrations.

7.3.4 Effect of increasing dextran concentration

At blue dextran concentrations favoring re-entrant phase behaviour, adding increasing quantities of dextran T-2000 to a mixture of cellulose nanocrystal suspension and blue dextran 2000 causes the I_1 phase to appear, increase in volume fraction, then decrease and disappear, while the I_2 phase increases slightly in volume fraction and the volume fraction of the N phase decreases somewhat overall (see Figure 7.4).

At blue dextran concentrations lying in the I_1 -N \rightarrow I_1 - I_2 -N region of the phase diagram (i.e., at $C_{\text{blue Dx}} \geq 2 \times 10^{-6} \text{ nm}^{-3}$), increasing the dextran concentration leads to a decrease in the volume fraction of the I_1 phase and formation of the I_2 phase as the triphase equilibrium is reached. The volume fraction of the N phase also decreases, as would be expected due to depletion-induced phase separation. Figure 7.6 shows the phase behaviour of samples with $C_{\text{blue Dx}} = 2.7 \times 10^{-6} \text{ nm}^{-3}$. Because the volume fraction of I_1 phase decreases with increasing dextran concentration, it is likely that the I_2 -N coexistence region would be reached at higher dextran concentrations if sample viscosity permitted.

Increasing the concentration of the electrostatically neutral dextran should theoretically increase the magnitude of the depletion attraction.¹⁹ However, the presence of polyelectrolytic blue dextran may complicate the situation even though its number density is held constant for these experiments. Phase behaviour in the re-entrant I_2 -N \rightarrow I_1 - I_2 -N \rightarrow I_2 -N region of the phase diagram may be an example of this interplay between the attractive depletion and repulsive electrostatic forces.

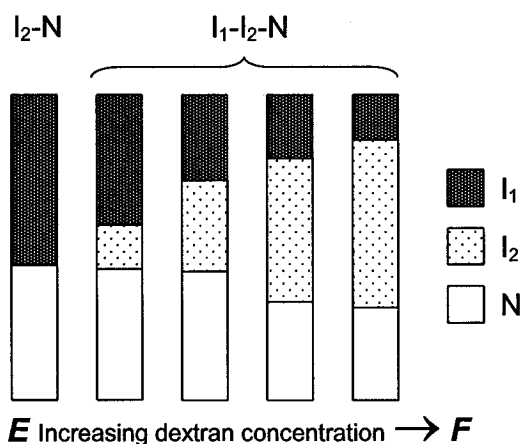


Figure 7.6. Example of phase behaviour for 8.7 wt % cellulose nanocrystal suspension at blue dextran 2000 number density = $2.7 \times 10^{-6} \text{ nm}^{-3}$ and increasing dextran T-2000 number density (concentrations correspond to arrow EF in Figure 7.2).

7.3.5 Effect of cellulose nanocrystal concentration

A series of samples was prepared using a cellulose suspension of lower concentration (6.3 wt% cellulose; $\phi_{\text{aniso}} = 0.29$). The nematic phase almost disappears upon addition of dextran T-2000, leaving mostly I_2 phase (Figure 7.7). The phase diagram in Figure 7.8 shows that, in comparison with Figure 7.2, more blue dextran 2000 is needed to obtain triphase equilibrium when the suspension is more dilute.

In order to determine whether triphase equilibrium was attainable starting from a monophasic suspension, two series of dilute (completely isotropic) suspensions with increasing cellulose concentration were prepared and dextran T-2000 and blue dextran 2000 were added (Table 7.1). The dextran concentrations were comparable to those used in the 8.7 wt% cellulose suspensions, as were the blue-to-plain dextran ratios used (0.3 and 0.5 in Series I and II, respectively).

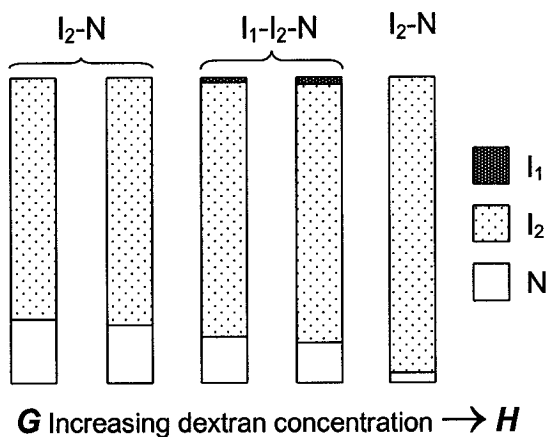


Figure 7.7. Relative volume fractions of the phases obtained when blue dextran 2000 and dextran T-2000 were added to a dilute nanocrystal suspension containing 6.3 wt% cellulose with $\phi_{\text{aniso}} = 0.29$. The number density of blue dextran is $8.3 \times 10^{-7} \text{ nm}^{-3}$ and the dextran T-2000 number density increases from 0 to $1.3 \times 10^{-5} \text{ nm}^{-3}$ (concentrations correspond to arrow GH in Figure 7.8).

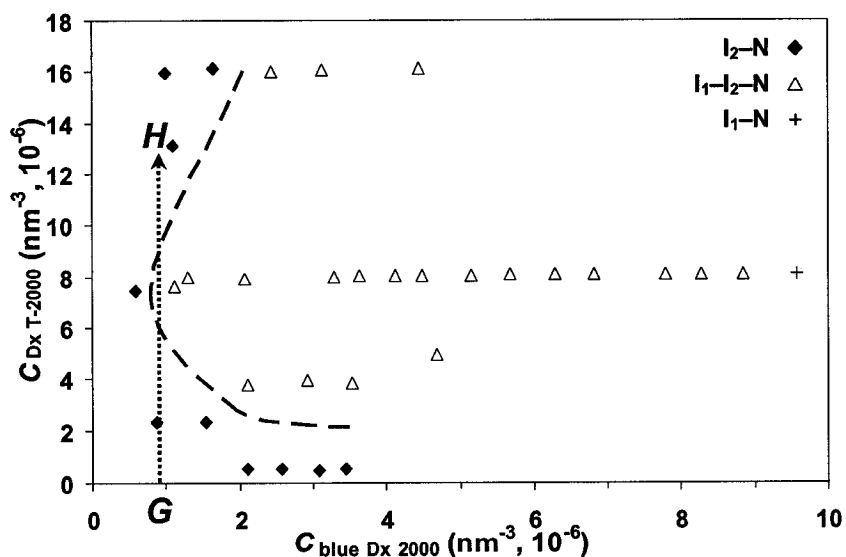


Figure 7.8. Partial phase diagram for dilute biphasic (6.3 wt%; $\phi_{\text{aniso}} = 0.29$) cellulose suspension. The boundary between the regions of the phase diagram is intended as a guide to the eye.

At the dextran concentrations used in the first series, it can be seen that triphase equilibrium was not obtained until the cellulose concentration reached 6 wt%. The second series showed triphase equilibrium in all but the most dilute cellulose suspension, which was biphasic I₁-N, because of the higher dextran concentrations (Figure 7.9). In both series, it is evident that the number density ratio of (total) dextran to cellulose necessary for triphase equilibrium increases with decreasing cellulose concentration.

Table 7.1. Effect of cellulose nanocrystal concentration on dextran and cellulose number densities required to obtain triphase equilibrium.

Series	[Cellulose] (wt%)	Phases	C_{blueDx}^a	C_{Dx}^a	C_{cell}^a	$C_{\text{blueDx}}/C_{\text{Dx}}$	$C_{\text{Dxtot}}/C_{\text{cell}}$
I	2.0	I ₂	1.6	5.5	1.1	0.3	6.5
	2.5	I ₂	1.6	5.4	1.4	0.3	5.0
	3.0	I ₂	1.6	5.5	1.7	0.3	4.2
	3.5	I ₂	1.6	5.4	2.0	0.3	4.3
	4.0	I ₂	1.6	5.3	2.3	0.3	3.0
	6.0	I ₁ -I ₂ -N	1.6	5.6	3.4	0.3	2.1
II	2.0	I ₁ -N	5.9	11.5	1.1	0.5	15.8
	2.5	I ₁ -I ₂ -N	5.9	11.5	1.4	0.5	12.8
	3.0	I ₁ -I ₂ -N	5.9	11.5	1.6	0.5	10.9
	3.5	I ₁ -I ₂ -N	5.9	11.5	1.9	0.5	9.2
	4.0	I ₁ -I ₂ -N	5.9	11.5	2.2	0.5	7.9

^a Number density in nm⁻³, 10⁻⁶.

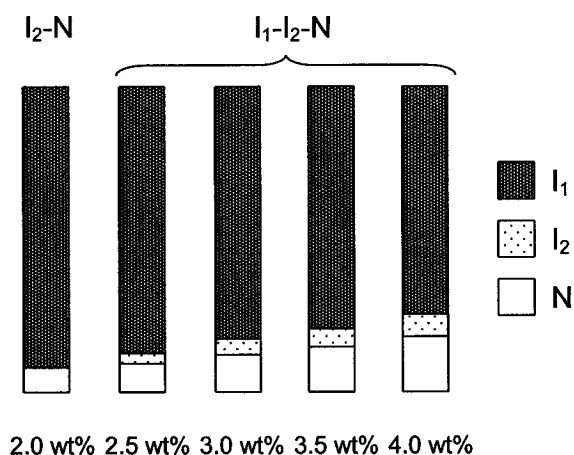


Figure 7.9. Relative volume fractions of the phases obtained when blue dextran 2000 and dextran T-2000 ($C_{\text{blue D}_x} = 6.0 \times 10^{-6} \text{ nm}^{-3}$ and $C_{\text{D}_x} = 1.2 \times 10^{-5} \text{ nm}^{-3}$) were added to dilute cellulose suspensions (concentrations in wt% indicated).

The cellulose nanocrystal suspension evidently does not have to be biphasic for triphase equilibria to occur, since isotropic suspensions at cellulose concentrations well below the I–N transition show triphase equilibria upon addition of dextran and blue dextran. This is similar to experimental evidence found by Koenderink et al.,²⁰ who observed a depletion-induced phase transition in a mixture of colloidal silica spheres and silica-coated boehmite rods at rod concentrations well below the isotropic-nematic transition. Anisotropic rods give rise to larger attractions than equivalent volume fractions of spheres because of the much higher rod number density,²¹ which may explain the ability of the dilute suspensions to phase separate. As the cellulose suspension becomes more dilute, however, a higher total dextran-to-cellulose ratio is required to obtain three-phase coexistence (Table 7.1).

It is known that electrostatic interactions stabilize mixtures of charged colloids and polymers against depletion-induced phase separation, and that increasing the range of the

electrostatic interactions enhances the stabilization.^{22,23} The more dilute cellulose suspensions contain fewer total surface sulfate groups and their associated counterions in solution, and therefore have lower ionic strengths, which reduces the screening of electrostatic interactions between charged macromolecules. This has a weakening effect on the (neutral or charged) polymer depletion-induced attraction between cellulose nanocrystals, ultimately resulting in increased stability toward demixing. In addition, since the nanocrystals themselves are farther apart in dilute suspensions, higher concentrations of macromolecular depletant would be needed to increase the strength of the depletion attraction to the point where phase separation occurs. (We can also predict that molecular weight effects will be stronger in the dilute suspensions, because the range of depletion attraction is dependent on this variable; if the nanocrystals are farther apart, the equilibrium will be more sensitive to the range of the attraction force.)

7.3.6 Blue-to-plain dextran ratio required to obtain I_1 phase from I_2 -N biphasic equilibrium

The ratio of blue dextran to plain dextran appears to have an important effect on the phase equilibria observed. As the concentration of added plain dextran increases, the ratio of blue dextran 2000 to plain dextran T-2000 required for the initial formation of the triphase equilibrium decreases greatly, starting at about 2.00 and leveling off at 0.06 (Figure 7.10).

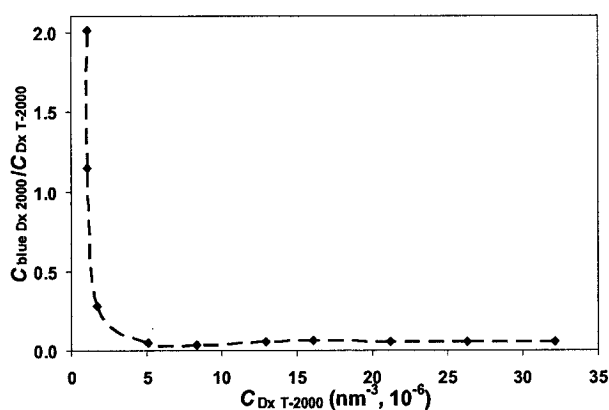


Figure 7.10. Blue-dextran-to-dextran ratio required for the formation of I_1 – I_2 –N equilibrium in 8.7 wt% cellulose nanocrystal suspension.

7.3.7 Effect of dextran molecular weight

Phase diagrams for mixtures of medium molecular weight dextrans are shown in Figure 7.11. The triphase coexistence region for mixtures of blue dextran 500 and dextran T-500 (Figure 7.11a) is shifted to higher number densities of both blue dextran and plain dextran relative to mixtures of blue dextran 2000 and dextran T-2000 (Figure 7.2). In contrast, mixtures of blue dextran 2000 and dextran T-500 (Figure 7.11b) are shifted only slightly toward higher number densities of plain dextran. Finally, mixtures of blue dextran 500 and plain dextran T-2000 are shifted to higher number densities for both types of dextran (Figure 7.11c), although not to as great an extent as for the “homogeneous” dextran 500 mixture in Figure 7.11a. As mentioned above and in Chapter 6, the molecular weight of the blue dextran used seems to dominate the phase behaviour, determining when the formation of the triphase equilibrium occurs. Undyed dextran also has an effect, but to a much lesser degree. The phase diagrams in Figure 7.11 are not complete, owing to the difficulty of working at the necessary higher dextran concentrations (higher sample viscosities).

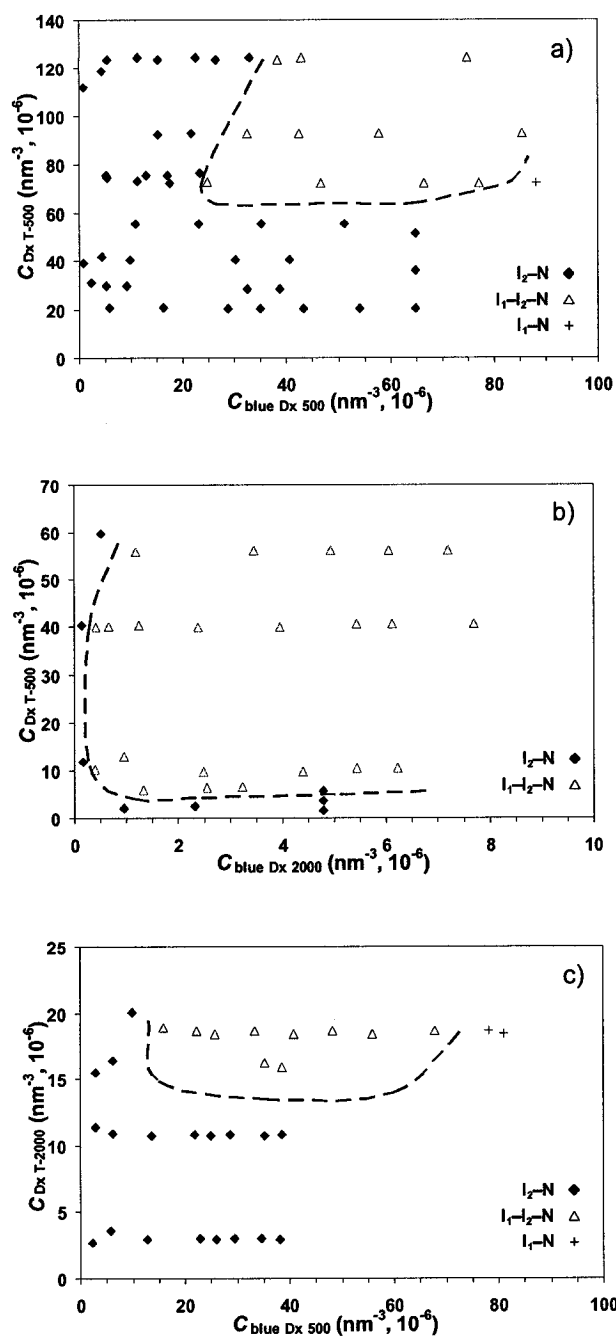


Figure 7.11. Phase diagrams for 8.7 wt% cellulose nanocrystal suspension containing a) blue dextran 500 and dextran T-500; b) blue dextran 2000 and dextran T-500; and c) blue dextran 500 and dextran T-2000. The boundaries between the regions of the phase diagram are intended as a guide to the eye. Note: the phase diagrams are not on identical scales.

The previous chapter shows that dextrans of high and medium molecular weights (500–2000 kDa) induce formation of the I_1 phase, while dextrans of low molecular weight (110 kDa) do not induce formation of the I_1 phase in the concentration range studied. Higher concentrations of the smaller dextrans are required, as the range of depletion forces depends on the macromolecule size.¹⁹ These differences are reflected in the phase diagrams in Figure 7.11.

7.3.8 Effect of blue dextran charge density

Blue dextrans 2000 having low ligand densities (blue Dx's 2000₁₆, 2000₁₈, 2000₃₆ and 2000₅₆) were used instead of unmodified dextran T-2000 in mixtures with highly-substituted commercial blue dextran 2000₁₆₁ and 8.7 wt% cellulose nanocrystal suspension at two different number density combinations. For comparison with the blue Dx 2000₁₆₁/Dx T-2000 system, the number density combinations are indicated by shaded areas in Figure 7.2. At dextran concentrations corresponding to the shaded square, triphase equilibrium was observed only when blue dextran 2000₁₆ was used, the other blue dextrans with higher degrees of substitution all yielding biphasic I–N suspensions. However, at higher blue dextran/dextran concentrations corresponding to the shaded circle in Figure 7.2, all the samples showed triphase equilibrium. It can be concluded that a minimum difference in charge density between the two blue dextrans is necessary for triphase equilibrium to occur at a given number density of each polymer species. In other words, the triphase coexistence regions of the phase diagrams for combinations of blue dextrans shift to higher concentrations of each macromolecular component as the difference in their charge density diminishes. This phenomenon may also partially explain the shift to higher concentrations between the phase diagrams when unmodified

dextran T-2000 is used (cf. Figures 7.2 and 7.11c), as blue dextran 500₄₉ has a smaller DS and therefore smaller charge density than commercial blue dextran 2000₁₆₁.

7.4 CONCLUSIONS

Within certain concentration ranges, aqueous mixtures of blue dextrans, undyed dextrans and cellulose nanocrystals produce a three-phase I_1 - I_2 -N coexistence. To the best of our knowledge, this represents the first triphasic equilibrium of cellulose nanocrystal suspensions to exhibit two isotropic phases. The molecular weight of the macromolecules, in particular that of the blue dextrans, appears to govern the macromolecule concentrations needed to produce the I_1 - I_2 -N phase behaviour. Re-entrant I_2 -N \rightarrow I_1 - I_2 -N \rightarrow I_2 -N phase behaviour as well as regions of I_2 -N and I_1 -N biphasic coexistence are seen. For mixtures of blue dextrans with different levels of dye substitution, there exists a threshold difference in charge density above which the triphase equilibrium develops. Triphase equilibrium is also obtained upon addition of unmodified and blue dextrans to dilute (isotropic) cellulose suspensions. While the interactions governing the equilibria are not clear, phase formation could result from the complex interplay of electrostatic and entropic forces.

7.5 REFERENCES

- (1) Revol, J.F.; Godbout, L.; Dong, X.M.; Gray, D.G.; Chanzy, H.; Maret, G. *Liq. Cryst.* **1994**, *16*, 127-134.
- (2) Dong, X.M.; Kimura, T.; Revol, J.-F.; Gray, D.G. *Langmuir* **1996**, *12*, 2076-2082.
- (3) Dong, X.M.; Revol, J.-F.; Gray, D.G. *Cellulose* **1998**, *5*, 19-32.
- (4) Onsager, L. *Ann. N.Y. Acad. Sci.* **1949**, *51*, 627-659.
- (5) Buitenhuis, J.; Donselaar, L.N.; Buining, P.A.; Stroobants, A.; Lekkerkerker, H.N.W. *J. Colloid Interface Sci.* **1995**, *175*, 46-56.
- (6) Buining, P.A.; Lekkerkerker, H.N.W. *J. Phys. Chem.* **1993**, *97*, 11510-11516.
- (7) Kimura, F.; Kimura, T.; Tamura, M.; Hirai, A.; Ikuno, M.; Horii, F. *Langmuir* **2005**, *21*, 2034-2037.
- (8) Lekkerkerker, H.N.W.; Stroobants, A. *Il Nuovo Cimento* **1994**, *16D*, 949-962.
- (9) Bolhuis, P.G.; Stroobants, A.; Frenkel, D.; Lekkerkerker, H.N.W. *J. Chem. Phys.* **1997**, *107*, 1551-1564.
- (10) Piech, M.; Walz, J.Y. *J. Colloid Interface Sci.* **2000**, *225*, 134-146.
- (11) Adams, M.; Dogic, Z.; Keller, S.L.; Fraden, S. *Nature* **1998**, *393*, 349-352.
- (12) Beck-Candanedo, S.; Viet, D.; Gray, D.G. *Macromolecules* **2007** *40*, 3429-3436; and Chapter 6 of this thesis.
- (13) Barois, P. in *Handbook of Liquid Crystals*; Demus, D.; Goodby, J.; Gray, G.W.; Speiss, H.-W., eds.; Wiley-VCH: New York, 1998; Vol. 1, p. 306.
- (14) Moldovan, R.; Tintaru, M.; Puica, M.R.; Beica, T.; Zgura, I. *Rom. J. Phys.* **2004**, *49*, 625-630.

- (15) Yu, L.J.; Saupe, A. *Phys. Rev. Lett.* **1980**, *45*, 1000-1003.
- (16) Beck-Candanedo, S.; Viet, D.; Gray, D.G. *Langmuir* **2006**, *22*, 8690-8695;
Chapter 4 of this thesis.
- (17) Dogic, Z.; Purdy, K.R.; Grelet, E.; Adams, M.; Fraden, S. *Phys. Rev. E* **2004**, *69*,
051702-1 - 051702-9.
- (18) Henderson, D.; Lozada-Cassou, M. *J. Colloid Interface Sci.* **1986**, *114*, 180-183.
- (19) Asakura, S.; Oosawa, F. *J. Polym. Sci.* **1958**, *33*, 183-192.
- (20) Koenderink, G.H.; Vliegenthart, G.A.; Kluijtmans, S.G.J.M.; van Blaaderen, A.;
Philipse, A.P.; Lekkerkerker, H.N.W. *Langmuir* **1999**, *15*, 4693-4696.
- (21) Piech, M.; Walz, J.Y. *J. Colloid Interface Sci.* **2000**, *232*, 86-101.
- (22) Belloni, L.; Ferreira, P.G. *Phil. Trans. R. Soc. Lond. A* **2001**, *359*, 867-877.
- (23) Denton, A.R.; Schmidt, M. *J. Chem. Phys.* **2005**, *122*, 244911-1 - 244911-7.

Chapter 8

General Conclusions

CONCLUSIONS

It has been the objective of this thesis to gain a better understanding of the interactions between colloidal rods and polymer coils and the macroscopic phase behaviour which results from them. To this end, an in-depth examination of phase separation phenomena in cellulose nanocrystal suspensions containing dextran–dye derivatives has been carried out. The dextran polymer was chosen to have monomer segments which chemically resembled the surface of the cellulose nanocrystals. Incorporation of the relatively small number (10^{-3} – 10^{-2} per dextran monomer) of anionic aromatic dye units into the polymer chain produced significant effects that impacted the results in almost every chapter. While electrostatic effects were dominant, hydrophobic interactions were also important, as were the generalized rod-coil mixing effects that were the initial motivation for this work.

Softwood and hardwood pulps yield similar nanocrystals in terms of dimensions and surface charge density when hydrolyzed with sulfuric acid under identical conditions. Increasing the hydrolysis time and acid-to-pulp ratio measurably affects the nanocrystal length distributions and suspension phase separation behaviour (e.g., the critical concentration for formation of anisotropic phase), which depend particularly on the acid-to-pulp ratio, increasing with greater amounts of acid. The chiral nematic pitch of the anisotropic phase decreases with increasing hydrolysis time and acid-to-pulp ratio, indicating an increase in chiral interactions, possibly due to higher surface charge density. Surface charge density of cellulose nanocrystals is not as sensitive to hydrolysis conditions and may be controlled by other factors.

The physico-chemical properties and polyelectrolytic nature of blue dextran were established by various characterization methods; blue dextrans have significantly different properties from their unmodified counterparts. Increasing the solvent ionic strength causes a decrease in the intrinsic viscosity of solutions of blue dextrans. The ionic dye ligands cause the specific refractive index increment to increase relative to the values for unmodified dextrans, and also lead to an increase in molecular weight, as shown by UV-visible spectroscopy and GPC-LS measurements. The polymer coil dimensions of blue dextrans are also increased by the ligands, although the simultaneous hydrophobic and ionic natures of the dye are at odds with each other.

The separation of an isotropic phase from completely anisotropic cellulose nanocrystal suspensions upon addition of blue dextran is attributed to the anionic dye ligands attached to the dextran. The ionic strength of the suspension increases, raising the critical cellulose concentration required for phase separation and screening inter-rod electrostatic repulsions, thereby allowing depletion attractions caused by dextran macromolecules to dominate.

Blue dextran partitions preferentially into the isotropic phase of biphasic, isotropic-chiral nematic cellulose nanocrystal suspensions. The partition coefficient K varies with the total blue dextran concentration and the degree of dye substitution, as well as the size (R_g) of the dextran, in agreement with theoretical predictions. That is, K_{el} appears to dominate the partitioning behaviour of blue dextran. Nonionic FITC-dextran does not partition preferentially in this system, presumably due to lack of ionic groups on the dye ligand.

Within certain concentration ranges, aqueous mixtures of blue dextrans, undyed dextrans and cellulose nanocrystals produce a three-phase I_1 - I_2 -N coexistence. To the best of our knowledge, this represents the first triphasic equilibrium of cellulose nanocrystal suspensions to exhibit two isotropic phases (one dilute and one concentrated). The molecular weight of the macromolecules, in particular that of the blue dextrans, has a significant effect on the macromolecule concentrations needed to produce the triphase equilibrium. In addition, the difference in the charge density (determined by the degree of dye substitution, DS) of two blue dextrans also determines the component concentrations at which triphase equilibrium develops, larger differences favouring the formation of I_1 phase. Re-entrant I_2 -N \rightarrow I_1 - I_2 -N \rightarrow I_2 -N phase behaviour as well as regions of I_2 -N and I_1 -N biphasic coexistence are seen. While the interactions governing the equilibria are not clear, phase formation must result from the complex interplay of electrostatic and entropic forces.

ORIGINAL CONTRIBUTIONS TO KNOWLEDGE

- (1) An addition to the knowledge base on the effect of hydrolysis conditions on the dimensions and surface charge density of cellulose nanocrystals deriving from wood pulp, in particular from black spruce and eucalyptus, was made.
- (2) A range of physico-chemical properties (viscosity behaviour, radii of gyration and hydrodynamic radii, specific refractive index increments) for a selection of blue dextrans of variable molecular weights and dye loading were measured for the first time, there being no in-depth studies in the literature.
- (3) The polyelectrolytic nature of blue dextran turned out to be an important factor in induced phase separation and partitioning, as the ionic groups have significant and

somewhat unexpected consequences for the phase behaviour of cellulose nanocrystal suspensions to which this macromolecule is added. The experiments in Chapter 4 reveal that, contrary to the initial belief, blue dextran cannot be treated simply as neutral “nonadsorbing”, “noninteracting” macromolecules when added to cellulose nanocrystal suspensions. The increased ionic strength of the suspension drives the phase separation (and partitioning).

- (4) The partitioning of blue dextran in cellulose nanocrystal suspensions has been found to have a significant electrostatic contribution; the partitioning does not depend solely on entropic (depletion) factors.
- (5) Triphase isotropic-isotropic-nematic equilibria were observed for the first time in cellulose nanocrystal suspensions. It was determined that the addition of blue dextran and unmodified dextran in certain proportions to cellulose nanocrystal suspensions yields this triphase equilibrium. The molecular weight and relative degree of dye substitution of the blue dextrans appears to strongly affect the onset of the triphase equilibria. Phase diagrams for several systems were constructed. The concentration of cellulose nanocrystals determines the relative volume fractions of the three phases at a given concentration of blue dextran and dextran.

SUGGESTIONS FOR FUTURE WORK

Further physico-chemical characterization of blue dextran should be carried out in order to clarify the hydrophobic and ionic contributions of dye ligands to the hydrophobic and polyelectrolytic character of blue dextran.

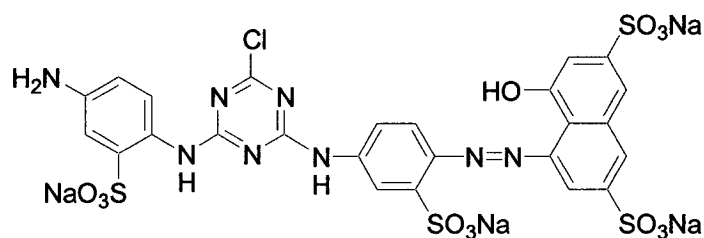
This will lead to a better understanding of the behaviour of cellulose nanocrystal suspensions containing the macromolecule. In particular, more in-depth viscosimetric studies should be performed in solvents of varying ionic strength and counterion type.

To study the effective depletion attraction caused by the dextran portion of the blue dextran macromolecule, the electrostatic repulsion of the cellulose nanocrystals should be screened by an excess of a simple ionic salt, such as NaCl, KCl, CsCl, etc. The difficulty lies in finding a range of “added” ionic strength which will not excessively increase the suspension viscosity or cause gelation of the suspension. Once this range is found, dextran and blue dextran may be added to completely anisotropic suspensions of varying “added ionic strengths” and their effect on the induced phase separation determined. The effect of the total ionic strength of the (biphasic) suspension on the partition coefficient of the blue dextran should also be measured.

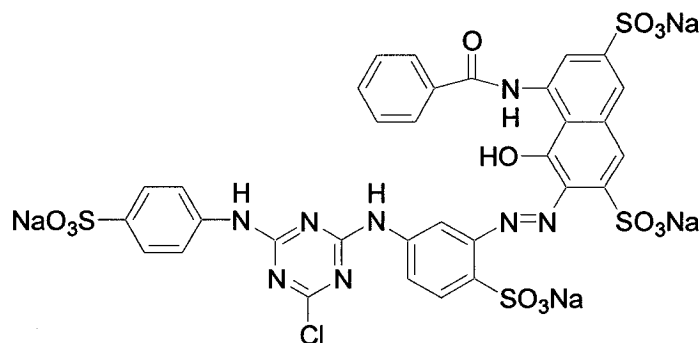
In view of the effect of blue dextran DS on the triphase equilibria in cellulose nanocrystal suspensions, the effect of the surface charge density of cellulose nanocrystals on the induced phase separation behaviour and partitioning of blue dextrans should be studied. To elucidate the contribution of electrostatic repulsions (K_{el}) to the partitioning of blue dextrans, nanocrystal suspensions of varying surface charge densities can be prepared by varying the hydrolysis conditions under which they are produced. Similarly, the effect of nanocrystal length on phase separation and partitioning can also be studied (for example, tunicate whiskers, which have a much greater axial ratio, could be used).

Different dextran–dye derivatives can be produced, including Dx–Reactive green 19, Dx–Reactive red 4 and Dx–Rhodamine B isothiocyanate (see below), all of which are sold by Sigma-Aldrich. These dextrans can also, presumably, be prepared from the dyes

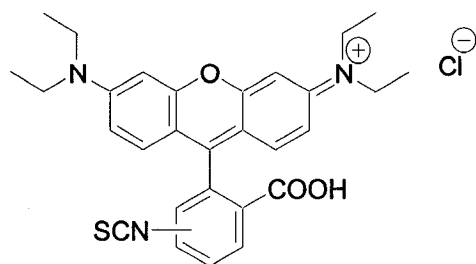
and unmodified dextrans according to the procedures given in this thesis. While CB has three anionic sulfonate groups, Reactive green 19 and Reactive red 4 both have four. In addition, they may be able to adsorb differently onto the cellulose nanocrystals because their structure is different from CB. Rhodamine B isothiocyanate may be particularly interesting because it is positively-charged, which may make it bind more strongly or even irreversibly to the nanocrystals. These dextran derivatives may be used to measure the effect of the charge on the dye ligands, both on partitioning and induced phase separation. For example, the extent to which K_{el} controls the partitioning may be studied by synthesizing and using dextran-dye derivatives with very low DS. Hydrophobically modified polyelectrolytic dextrans are another interesting possibility which may permit the hydrophobic association to be studied, if different dyes, some with small chromophores and some much larger with many aromatic groups, are used to colour the dextrans.



Reactive green 19



Reactive red 4



Rhodamine B isothiocyanate

To study in greater detail and with greater precision the effect of dextran size on the extent of its partitioning, blue dextrans of different molecular weight with *identical dye loadings* (assuming random distribution of dye) should be used. Assuming the dye ligand will not bind to the enzyme, dextranases may be used to “cut up” blue dextrans into different sizes. Partitioning and induced phase separation can then be studied and the results compared to theoretical predictions.

A broader view of the effects of polyelectrolytes on the phase behaviour of cellulose nanocrystal suspensions should be obtained. Polymers which do not contain bulky, hydrophobic/ionic dye ligands and varying charge density could be used. The suspension pH could be altered to vary the charge density on the polymers (although this also affects the suspension phase separation behaviour, so co-polymers with different contents of the charged monomers could also be used). The effect of charge density on partitioning and induced phase separation could then be studied. These experiments may also elucidate the role of the bulky aromatic dye group in the experiments performed in this thesis.

The most promising area for future in-depth study is the triphase equilibrium observed when blue and undyed dextrans are added to cellulose nanocrystal suspensions. Three-dimensional phase diagrams having axes defined by blue dextran, dextran and cellulose

nanocrystal concentrations would provide more detailed information, particularly regarding the one-phase (isotropic) region at low cellulose nanocrystal concentration. A detailed systematic investigation of the role of dextran molecular weight should be carried out with acid-hydrolyzed dextrans and blue dextrans. Different polyelectrolytes may also be used as described above to further determine the role of polymer charge density as well as polymer. In addition, the effect of cellulose nanocrystal charge density should be investigated in conjunction with its effect on phase separation and partitioning as described above. Finally, microscopy and laser light scattering studies can be used to determine the kinetics and mechanism of phase separation, as well as the nature and morphology of the phases.

